CATALOGED BY ASTIA
AS AD No. 254905

GALCIT SM 61-8

FINAL REPORT-GALCIT 101
Thiokol Subcontract No. RS-69752

FUNDAMENTAL STUDIES RELATING TO SYSTEMS ANALYSIS OF SOLID PROPELLANTS

February 1961

ASTIA
JUN 2 1961

Guggenheim Aeronautical Laboratory
California Institute of Technology
Pasadena, California

XEROX

FUNDAMENTAL STUDIES RELATING TO SYSTEMS ANALYSIS OF SOLID PROPELLANTS

N O T I C E

THIS DOCUMENT HAS BEEN REPRODUCED FROM THE BEST COPY FURNISHED US BY THE SPONSORING AGENCY. ALTHOUGH IT IS RECOGNIZED THAT CERTAIN PORTIONS ARE ILLEGIBLE, IT IS BEING RELEASED IN THE INTEREST OF MAKING AVAILABLE AS MUCH INFORMATION AS POSSIBLE.

GALCIT SM 61-5

FINAL REPORT -- GALCIT 101
Subcontract No. R-69752

FUNDAMENTAL STUDIES RELATING TO SYSTEMS ANALYSIS OF SOLID PROPELLANTS

M. L. Williams
P. J. Blatz
R. A. Schapery

February 1961

This program was supported by Thiokol Chemical Corporation, Redstone Division as a portion of the scope-of-work required under Contracts DA-01-021-ORD-11919 (780), DA-01-021-ORD-5314, Mod. 7, and AF 33(600) 36514. This final report on Subcontract R-69752 is being circulated to all designated to receive phase reports under the above contracts and is designated Thiokol Report No. 23-61.

Guggenheim Aeronautical Laboratory
California Institute of Technology
Pasadena, California

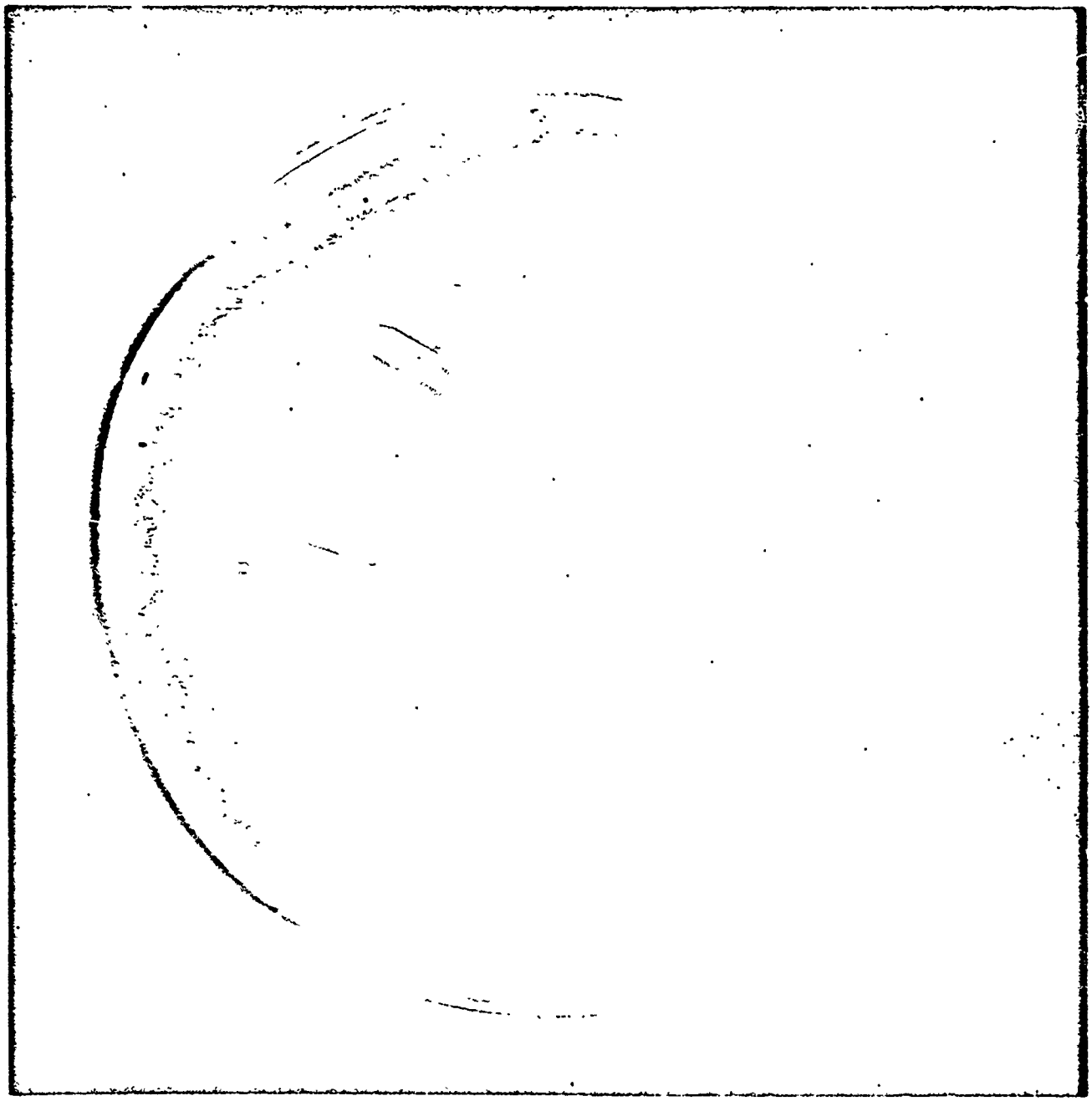

The above photograph, taken by R. R. Parmerter and M. E. Fourney (GALCIT), shows a photoelastic specimen of a solid rocket grain subjected to a simulated internal pressure when viewed in a white light polariscope.

FOREWORD

Over the last several years, the solid propellant rocket has received increasing attention, based primarily upon its generally increased reliability and state of readiness, although not to the exclusion of alternate propulsion means such as the liquid propellant rocket. During the design of the solid rocket motor system certain structural problems immediately arise, with two of the more common ones being high temperature nozzle design and the fabrication of ultra-high strength metal cases to contain the burning motor. As an outgrowth of a meeting in 1958 of the Physical Properties Panel, which is a technical group sponsored by the joint services through the Solid Propellant Information Agency at the Applied Physics Laboratory of the Johns Hopkins University, it appeared advisable to direct increased attention toward another class of problems; namely, evaluating the structural integrity of the rocket grain or viscoelastic solid fuel itself. The physical and technical behavior of the fuel, in contrast to most solids in engineering use, is significantly affected by relatively small changes in temperature and characteristic time scale under consideration. For this reason, less commonly employed structural analysis methods must be used in order to assess quantitatively the behavior of the grain under pressure, temperature, and environmental loadings.

During the aforementioned meeting, Dr. F. J. Lavacot expressed the hope that it would be possible to collect certain interdisciplinary information, cutting across the fields of chemistry, internal ballistics and structural design which would permit the design engineer to make more accurate assessments of rocket performance. This suggestion led, among other things, to establishing a project late that year at the Guggenheim Aeronautical Laboratory of the California Institute of Technology (GALCIT) in support of certain work of the Thiokol Chemical Corporation, Redstone Division. The results of various phases of this program have been subsequently reported in six quarterly progress reports through June 1960. This final report is not necessarily a compendium of these previous reports[1.1 - 1.6], although it leans heavily upon them, but is rather an attempt to describe comprehensively the type of structural complications introduced by a viscoelastic material and provide certain background information to assist the analyst in evaluating the structural integrity of a solid propellant rocket grain.

From the engineering standpoint, the problem areas have been separated into three catagories: (i) characterization of material properties; (ii) analysis procedures; and (iii) failure criteria. As is true with the conventional engineering materials, these areas are intimately related, but with the underlying new feature being the viscoelastic character of the solid fuel itself. Emphasis has been placed primarily upon engineering application as an end aim, and for this reason many interesting scientific excursions have been deliberately by-passed.

It is a pleasure to acknowledge the cooperation of the Thiokol Chemical Corporation, and especially Dr. W. F. Arendale, during the course of this study. The authors also wish to thank innumerable members of the solid rocket industry at large and in particular the Physical Properties Panel for the many discussions relating to the interplay of chemical and structural factors. Within GALCIT, many members of staff and graduate students have contributed to the subject matter of this project, and the secretarial assistance of Mrs. Beth Berry has been invaluable in the editing and preparation of the progress and final reports. We also wish to acknowledge our appreciation of the technical contributions of W. G. Knauss and L. D. Stimpson.

TABLE OF CONTENTS

APPENDICES

1. INTRODUCTION

1.1 Basic Assumptions

In preparing to analyze a solid propellant rocket grain, it is necessary as well as expedient to establish the assumptions under which the analysis will be conducted. Notwithstanding certain glaring deficiencies which will be discussed later, particularly in connection with failure theory, it is proposed to consider the medium as isotropic, homogeneous, and continuous. The practical objections to these assumptions are based upon the fact that the viscoelastic elastomer, which consists of the order of 20 percent by volume, is merely a binder in which are imbedded various considerably harder particles. Thus basically one does not have a homogeneous, nor perhaps an isotropic, medium. One must perforce only assume that there does exist, on the average macroscale, an equivalent medium of this type. For many analyses this approximation will be satisfactory, certainly at the present stage, although the assumption can be seriously in error in fracture or tearing where the origin of failure begins on the microscale. Next, the assumption of continuity is not always fulfilled because it implies that there is always a bond between the various solid filler elements and the elastomeric binder. Actually the pullaway effect is well established, wherein excessive tensile stress will cause the filler-binder adhesion to part. On the other hand the bond will still exist between those surfaces in compression, which therefore leads to (non-continuum) load induced isotropy. Nevertheless, in order to conduct present analyses it is customary, and at least temporarily appropriate, to assume an isotropic, homogeneous continuum.

The second assumption is that the strains will be sufficiently small that infinitesimal deformations can be assumed. Actually for the loads and geometries used in present motors, strains of 30 percent are frequently computed from infinitesimal theory, which certainly pushes the limit of validity for this assumption. On the other hand, finite strain analysis, even without viscoelastic effects, is far from simple. Considering the widespread knowledge of infinitesimal deformation theory and its relative ease of application, it is considered appropriate, pending some later qualifications, to begin at this point.

As a third assumption, it is appropriate to neglect inertia forces, due to straining, during ordinary viscoelastic deformations. They are usually highly damped and exponentially decaying, although in certain cases, such as possible stress wave propagation through the grain due to burning phenomena, this particular assumption might have to be reevaluated.

The final assumption, which is chosen for analytical simplicity, relates to the geometries chosen for investigation. This one is not in principle as restrictive, depending primarily upon the time the analyst can afford to devote to analysis which already incorporates certain simplifying assumptions. Thus one is not surprised to find the majority of examples confined to thick-walled right circular cylinders or spheres. On the other hand such a n approach is not unreasonable; it follows the engineer's usual approach of developing his intuition by a careful study of idealized situations which then permit him to make judicious and considered extrapolation to situations where analysis is hopeless or uneconomical.

In summary then, the assumptions currently to be considered are:

1. the viscoelastic medium is isotropic, homogeneous, and continuous;
2. deformations are sufficiently small to be considered infinitesimal;
3. inertia forces, due to straining, are neglected; and
4. idealized geometries are considered for which analytical solutions may be obtained.

1.2 Review of Elastic Analysis

As a point of departure, let us collect the appropriate relations used in formulating the governing field equations for stress in the theory of infinitesimal elasticity in rectangular coordinates[1.7], where u (or v, w) is the small displacement in the x (or y, z) direction.

Equations of stress equilibrium:

$$\begin{aligned} \frac{\partial \sigma_x}{\partial x} + \frac{\partial \tau_{xy}}{\partial y} + \frac{\partial \tau_{xz}}{\partial z} + X = 0 \\ \frac{\partial \tau_{xy}}{\partial x} + \frac{\partial \sigma_y}{\partial y} + \frac{\partial \tau_{yz}}{\partial z} + Y = 0 \\ \frac{\partial \tau_{xz}}{\partial x} + \frac{\partial \tau_{yz}}{\partial y} + \frac{\partial \sigma_z}{\partial z} + Z = 0 \end{aligned} \qquad (1.2.1)$$

Strain-displacement relations:

$$\begin{aligned} \epsilon_x = \frac{\partial u}{\partial x} \quad , \qquad \gamma_{xy} = \frac{\partial u}{\partial y} + \frac{\partial v}{\partial x} \\ \epsilon_y = \frac{\partial v}{\partial y} \quad , \qquad \gamma_{yz} = \frac{\partial v}{\partial z} + \frac{\partial w}{\partial y} \\ \epsilon_z = \frac{\partial w}{\partial z} \quad , \qquad \gamma_{xz} = \frac{\partial w}{\partial x} + \frac{\partial u}{\partial z} \end{aligned} \qquad (1.2.2)$$

Stress-strain relations:

$$
\begin{aligned}
E\epsilon_x &= \sigma_x - \nu(\sigma_y + \sigma_z) \\
E\epsilon_y &= \sigma_y - \nu(\sigma_x + \sigma_z) \\
E\epsilon_z &= \sigma_z - \nu(\sigma_x + \sigma_y) \\
\mu\,\gamma_{xy} &= \tau_{xy} \\
\mu\,\gamma_{yz} &= \tau_{yz} \\
\mu\,\gamma_{xz} &= \tau_{xz}
\end{aligned}
\qquad (1.2.3)
$$

The preceding equations are seen to form a set of 15 equations in 15 unknowns, where it is important to recognize that only the last set --those connecting stress and strain--contains or are influenced by the material properties Young's modulus, E, and Poisson's ratio, ν . These equations may be formally simplified to give three equations in the displacements,

$$
\begin{aligned}
&\frac{\partial}{\partial x}\left[\frac{\partial u}{\partial x}+\frac{\partial v}{\partial y}+\frac{\partial w}{\partial z}\right]+(1-2\nu)\left[\frac{\partial^2 u}{\partial x^2}+\frac{\partial^2 u}{\partial y^2}+\frac{\partial^2 u}{\partial z^2}\right]+\frac{1-2\nu}{\mu}X=0 \\
&\frac{\partial}{\partial y}\left[\frac{\partial u}{\partial x}+\frac{\partial v}{\partial y}+\frac{\partial w}{\partial z}\right]+(1-2\nu)\left[\frac{\partial^2 v}{\partial x^2}+\frac{\partial^2 v}{\partial y^2}+\frac{\partial^2 v}{\partial z^2}\right]+\frac{1-2\nu}{\mu}Y=0 \\
&\frac{\partial}{\partial z}\left[\frac{\partial u}{\partial x}+\frac{\partial v}{\partial y}+\frac{\partial w}{\partial z}\right]+(1-2\nu)\left[\frac{\partial^2 w}{\partial x^2}+\frac{\partial^2 w}{\partial y^2}+\frac{\partial^2 w}{\partial z^2}\right]+\frac{1-2\nu}{\mu}Z=0
\end{aligned}
\qquad (1.2.4)
$$

by solving (1.2.3) to give the stresses in terms of strains and inserting the results into (1.2.1) which become strain equations of equilibrium. Then (1.2.2) is substituted to give the three displacement equations. Alternately the equations can be formulated solely in terms of stress by inserting (1.2.3) into (1.2.2) to give stresses in terms of displacements; by carrying out various cross derivatives, the displacements can be eliminated to give the equations of compatibility, viz

$$
\begin{aligned}
&(1+\nu)\nabla^2\sigma_x+\frac{\partial^2\theta}{\partial x^2}=0 \quad , \qquad (1+\nu)\nabla^2\tau_{yz}+\frac{\partial^2\theta}{\partial y\partial z}=0 \\
&(1+\nu)\nabla^2\sigma_y+\frac{\partial^2\theta}{\partial y^2}=0 \quad , \qquad (1+\nu)\nabla^2\tau_{xz}+\frac{\partial^2\theta}{\partial x\partial z}=0 \\
&(1+\nu)\nabla^2\sigma_z+\frac{\partial^2\theta}{\partial z^2}=0 \quad , \qquad (1+\nu)\nabla^2\tau_{xy}+\frac{\partial^2\theta}{\partial x\partial y}=0
\end{aligned}
\qquad (1.2.5)
$$

where $\nabla^2=\frac{\partial^2}{\partial x^2}+\frac{\partial^2}{\partial y^2}+\frac{\partial^2}{\partial z^2}$ and $\theta=\sigma_x+\sigma_y+\sigma_z$. The choice of

which system of equations to be used depends usually upon whether the boundary conditions are given in terms of displacements or stresses. (Corresponding equations can also be given for cylindrical coordinates, see Section 3. 3. 2).

As a matter of philosophy, the analyst must usually inquire as to whether he is mainly interested in stress (strain) or displacement, and in order that he be able to solve the appropriate equations, he needs only to (1) run laboratory tests to determine the material properties E and ν , (2) solve the governing field equations for determining the stress everywhere as a function of applied load--and thus its maximum value, and (3) using an appropriate failure criterion, e.g., maximum stress, deduce the applied load at which this maximum stress is reached.

The purpose of the following sections is to illustrate how the equivalent steps are carried out when the material is viscoelastic.

REFERENCES

1.1 Schapery, R. A.; Stimpson, L. D.; Williams, M. L.: Fundamental Studies Relating to Systems Analysis of Solid Propellants. California Institute of Technology GALCIT 101 Progress Report No. 1, January 1959.

1.2 Schapery, R. A.; Stimpson, L. D.; Williams, M. L.: Fundamental Studies Relating to Systems Analysis of Solid Propellants. California Institute of Technology GALCIT 101 Progress Report No. 2, April 1959.

1.3 Schapery, R. A.; Stimpson, L. D.; Williams, M. L.: Fundamental Studies Relating to Systems Analysis of Solid Propellants. California Institute of Technology GALCIT 101 Progress Report No. 3, July 1959.

1.4 Schapery, R. A.; Stimpson, L. D.; Williams, M. L.: Fundamental Studies Relating to Systems Analysis of Solid Propellants. California Institute of Technology GALCIT 101 Progress Report No. 4, October 1959.

1.5 Blatz, P. J.; Knauss, W. G.; Schapery, R. A.; Stimpson, L. D.; Williams, M. L.: Fundamental Studies Relating to Systems Analysis of Solid Propellants. California Institute of Technology GALCIT 101 Progress Report No. 5 January 1960.

1.6 Blatz, P. J.; Knauss, W. G.; Schapery, R. A.; Williams, M. L.: Fundamental Studies Relating to Systems Analysis of Solid Propellants. California Institute of Technology GALCIT 101 Progress Report No. 6, June 1960.

1.7 Timoshenko, S.; Goodier, J. N.: Theory of Elasticity, McGraw-Hill Book Company, Inc., New York, 1951.

2. MATERIAL CHARACTERIZATION

In order to predict the response of viscoelastic materials to applied stress, it is necessary to know the elastic and viscous parameters of the material as a function of time, rate, and temperature. In principle these parameters may all be combined into a generalized stress-strain law such that the strain (stress) may be calculated or deduced for an applied stress (strain) as a function of these parameters. When it is justified to assume this behavior is of linear form, based upon experimental evidence, one can view this association between stress and strain as a transfer function having the property that when it is multiplied by a linear functional of strain (stress), it generates the associated linear functional of stress (strain). We proceed to consider first the more familiar behavior of metals.

2.1 Operational Concept for Stress-Strain Relations

When a uniaxial steel tensile specimen at a moderate temperature is stretched, it is observed that the instantaneous strain is very nearly proportional to the applied stress up to the yield point; and that if the bar is unloaded the same law is followed. Consequently, we say the material obeys Hooke's law in tension up to the yield point and write

$$\sigma = E\epsilon \qquad (2.1.1)$$

in which σ and ϵ are based on the original specimen dimensions as in the usual engineering sense. The proportionality constant, E, which represents the slope of the stress-strain curve, is called Young's modulus or the tensile modulus*. This law can also be written in the inverse form

$$D\sigma = \epsilon \qquad (2.1.2)$$

The proportionality constant D is then commonly referred to as the tensile compliance. It has been found experimentally that the above law holds for many materials, particularly metals, as long as the strains are small.

---

* Poisson's ratio, ν, the ratio of transverse to longitudinal strain, is customarily measured by resistance strain gages.

It is evident that if a material which obeys Hooke's law is held at a constant strain, the stress also remains unchanged with time. However, when a viscoelastic tensile specimen at room temperature is stretched and held at a constant strain ϵ_o (stress relaxation test), the stress $\sigma(t)$ necessary to maintain this elongation decays with time. In other words, the tensile relaxation modulus, $E(t) = \sigma(t)/\epsilon_o$, decreases. This situation is illustrated in Figure 2.1a; behavior at constant stress is shown in Figure 2.1b.

In addition to strong time dependence, the mechanical properties are greatly affected by temperature. Below a temperature, T_g, defined as the glass transition temperature, the propellant is glassy and behaves as a brittle body obeying Hooke's law. Above this temperature, however, the response is time dependent and varys considerably with temperature. This behavior leads one to formulate a general functional relationship between tensile stress and strain which includes both time and temperature dependence for temperatures greater than T_g. However, it has been found for many polymers, particularly plastics and rubbers, that these two variables can be considered separately if the temperature range is not too great. For example, if certain material constants are known at one temperature, it is possible to predict behavior at another temperature by simply shifting the time scale. Since composite propellants are filled rubbers or filled plastics and double-base propellants are plastics, it is expected that the same rule should hold. On this basis therefore, only the time dependent behavior at a fixed temperature will be discussed, but will be followed in later sections by an explanation of the method used to change to a different temperature.

Expanding now the simple stress-strain relation given by (2.1.1) for a simple elastic behavior to a more general time dependent behavior one can write

$$O_1[\sigma(t)] = O_2[\epsilon(t)] \qquad (2.1.3)$$

where O_1 and O_2 represent algebraic and differential operations on $\sigma(t)$ and $\epsilon(t)$. For example, when Hooke's law (2.1.1) applies, the operators are the simple constants $O_1 = 1$ and $O_2 = E$. It is important to note, however, that these operators are not always linear. Indeed for large deformations of some metals, a more realistic elastic is for example

$$\sigma = \equiv (1 - 2\nu\epsilon) \ln (1+\epsilon) \qquad (2.1.4)$$

where ν is Poisson's ratio. In this instance O_2 is a non-linear algebraic operator.

A simple time dependent extension of Hooke's law is to consider stress proportional to both strain and strain rate. For this case, (2.1.3) becomes

$$\sigma(t) = \eta_v \frac{d\epsilon(t)}{dt} + E_v \epsilon(t) \qquad (2.1.5)$$

in which E_v and η_v are proportionality constants. An important implied property of the differential operator is that it is linear and therefore obeys many of the ordinary rules of algebra, such as association, commutation, and superposition. This allows us to write

$$\sigma(t) = \left[\eta_v \frac{d}{dt} + E_v \right] \epsilon(t) \qquad (2.1.6)$$

and hence identify

$$O_1 = 1 \quad ; \quad O_2 = \eta_v \frac{d}{dt} + E_v \qquad (2.1.7)$$

If we now consider a creep test in which a constant uniaxial stress, σ_o, is applied to a material following (2.1.5), the resulting axial strain can be calculated simply by integration. Assuming the specimen to be unstressed and unstrained at time $t = 0$, we obtain

$$\epsilon(t) = \frac{\sigma_o}{E_v}\left(1 - e^{-\frac{t}{\tau_v}}\right) \qquad (2.1.8)$$

where it is convenient to define a retardation time, τ_v, such that

$$\tau_v = \frac{\eta_v}{E_v} \qquad (2.1.9)$$

the creep compliance D(t) is therefore

$$D(t) = \frac{\epsilon(t)}{\sigma_o} = E_v^{-1}\left(1 - e^{-\frac{t}{\tau_v}}\right) = D_v\left(1 - e^{-\frac{t}{\tau_v}}\right) \qquad (2.1.10)$$

A schematic plot of D(t) is shown in Figure 2.2. It is seen that D(t), given by equation (2.1.10), is qualitatively similar to the creep compliance shown in Figure 2.1 for an actual propellant.

Following the general evaluation technique as applied in this example, we see that: (a) the material was characterized by (2.1.5); (b) the stress analysis was made, in this uniaxial case $\sigma = P/A$, or load divided by initial area; and (c) a failure criteria must next be applied. If for example, fracture occurs when a critical rupture strain ϵ_R is reached, the time to failure for an applied stress σ_o is easily computed from (2.1.10) as

$$t_R = -\tau_v \ln\left[1 - \frac{\epsilon_R E_v}{\sigma_o}\right] \qquad (2.1.11)$$

and the analysis is completed.

Unfortunately however, the stress analysis is usually not this simple, nor is it possible to describe accurately the complete stress and displacement behavior of propellant by such a simple relation; it is therefore necessary to go to more complicated operators. It turns out that if the degree of complication is such that the actual stress-strain response (2.1.3) can be adequately described by more general linear operators of the form (2.1.6), the mathematics involved in solving stress problems is greatly simplified. This important fact therefore provides the impetus for investigating possible representations of the mechanical behavior by linear operators and their associated mechanical models.

2.2 Linear Viscoelastic Representation

We now define a special generalization of (2.1.3) such that O_1 and O_2 are taken to be linear differential operators. In the literature such a stress-strain law is called a linear viscoelastic representation*, and for a simple tensile test is written

$$\left[p_n \frac{d^n}{dt^n} + \cdots + p_1 \frac{d}{dt} + p_o\right]\sigma(t) = \left[q_m \frac{d^m}{dt^m} + \cdots + q_1 \frac{d}{dt} + q_o\right]\epsilon(t) \qquad (2.2.1)$$

or more compactly

$$[P'']\sigma(t) = [Q'']\epsilon(t) \qquad (2.2.2)$$

where P'' and Q'' stand for the bracketed operators O_1 and O_2 respectively. d^i/dt^i is a linear operator that represents the ith derivative with respect to time, and p_i and q_i are experimental material constants which are obtained by methods to be discussed subsequently.

---

* If a time dependent stress produces an associated time dependent strain, then if doubling the magnitude of the stress holding the mode shape of the time variation the same also doubles the strain magnitude without changing the shape of its time dependence, the material is said to be linearly viscoelastic.

The relation (2.2.1) has been verified experimentally for small strains over a wide temperature range for many unfilled polymers. Even though composite propellants are essentially highly filled polymers, it is nevertheless expected that they would exhibit more or less of a linear viscoelastic behavior depending upon the specific composition.

Before discussing various specializations of (2.2.1), it should be remarked that the same form of a stress-strain law is found to hold for hydrostatic pressure and volume change, and for shear stress and shear strain in a simple shear test. Thus, the response of an element subjected to hydrostatic pressurization is represented by

$$[P']\,\sigma_p(t) = [Q']\,\frac{\Delta V(t)}{V_o} \qquad (2.2.3)$$

where $V(t)/V_o$ is the volume change per unit undeformed volume due to the hydrostatic pressure $\sigma_p(t)$. Similarly, write

$$[P]\,\tau(t) = [Q]\,\gamma(t) \qquad (2.2.4)$$

in which $\tau(t)$ is a shear stress and $\gamma(t)$ the corresponding shear strain. P, Q, P', Q' are of the general form of P'' and Q'' shown in (2.2.1), but, of course, with different experimental material constants. Equations (2.2.2), (2.2.3), and (2.2.4) are analogous to the elastic stress-strain laws, since for an <u>elastic</u> body undergoing small deformations we can write

simple uniaxial tension:	$\sigma = E\epsilon$;	(E = Young's modulus)	
hydrostatic pressurization:	$\sigma_p = K\frac{\Delta V}{V_o}$;	(K = bulk modulus)	(2.2.5)
shear:	$\tau = \mu\gamma$;	(μ = shear modulus)	

Similarly for a linear viscoelastic material we have

simple uniaxial tension:	$\sigma(t) = \frac{Q''}{P''}\,\epsilon(t)$	
hydrostatic pressurization:	$\sigma_p(t) = \frac{Q'}{P'}\cdot\frac{\Delta V(t)}{V_o}$	(2.2.6)
shear:	$\tau(t) = \frac{Q}{P}\,\gamma(t)$	

where the association of E with Q''/P'', etc., is obvious*.

---

* This operational notation, e.g. Q''/P'', is purely formal and represents an implied form of integration. Its actual significance will be explained in the subsequent section on models.

It may be remarked that a purely mathematical approach to linear theory does not restrict the form of the P, Q operators. However, Biot[2.1] has used irreversible thermodynamics to show that the coefficients are restricted in such a way that the ratios Q''/P'', Q'/P', and Q/P must be identical with the transfer functions for mechanical models consisting of springs and dashpots. Since the operator ratios in (2.2.6) are restricted to be of a definite form, it is often convenient to retain this form rather than multiplying all terms out and separating P and Q. Therefore, defining $p = d/dt$, we shall generally write $E(p)$, $K(p)$ and $\mu(p)$ in place of Q''/P'', Q'/P', Q/P and thus maintain this analogy between the viscoelastic and elastic problems in our notation.

When it comes to actually computing the stresses and displacements in a linear viscoelastic body, use will be made of this analogy by working out an associated elastic solution in terms of the associated operator form of the material representation. For the present, however, we shall continue with a discussion of the material characterization.

It can be shown that when a three dimensional elastic body is isotropic and homogeneous there can exist no more than two independent elastic constants[2.2]. In their natural form, they are the bulk modulus, K, governing the stress-strain proportionality for (hydrostatic) dilatation acting alone, and the shear modulus, μ, governing distortion alone. Similarly, as a result of geometric symmetry, only two independent operator relations can exist for an isotropic, homogeneous, linear viscoelastic material. Specifically we have from (2.2.5) and (2.2.6) the analogy

$$\mu \rightarrow \mu(P) \tag{2.2.7}$$

$$K \rightarrow K(P) \tag{2.2.8}$$

Engineering analysts frequently find it convenient to solve elastic problems in terms of Young's modulus and Poisson's ratio which are related to K and μ, and the viscoelastic associations by

$$E = \frac{9\mu K}{3K+\mu} \rightarrow \frac{9\mu(P)K(P)}{3K(P)+\mu(P)} = E(P) \tag{2.2.9}$$

$$\nu = \frac{3K-2\mu}{6K+2\mu} \rightarrow \frac{3K(P)-2\mu(P)}{6K(P)+2\mu(P)} \tag{2.2.10}$$

The choice of the various alternate forms depend upon which operators are known from experiments. We turn now to specific representations of viscoelastic media and their associated operator equations.

2.3 Model Representation

As previously mentioned, Biot[2.1] has shown that the operator equations (2.2.6), which define the stress-strain behavior of a linear viscoelastic material, can be represented diagrammatically by mechanical models that exhibit the same macroscopic behavior[2.3]. It is important to emphasize that these models will give a description only of the phenomenological behavior of a material, and usually tell nothing of the complex molecular processing causing this behavior. However, they are useful for illustrating the physical significance of an operator equation and are a convenient means for constructing an operator in order to approximate observed viscoelastic behavior.

2.3.1 Finite element models

The simplest models are those which can be constructed by arranging a few spring and dashpot elements in different ways to generate various characteristic responses.

Hookean model. - The simplest model representation of an elastic body has already been mentioned. This Hookean model consisting of a spring is shown in Figure 2.3. If we denote the spring constant by a modulus, m, the applied force by stress, σ, and the extension by strain, ϵ, we have a model, following (2.2.6) which can be used to represent either tension, shear, or bulk behavior.

Newtonian model. - Another simple model may be used when the stress is a function only of strain rate, as in a fluid. Here the constant of proportionality is represented by the viscosity, η, of a dashpot as shown in Figure 2.4. It is characteristic of this model that with a constant stress the strain is unbounded with time, i.e. unlimited flow.

Now since the response in shear, tension, and bulk is assumed to be linearly viscoelastic, the stress, σ, and strain, ϵ, used with the models will, for convenience, be usually assumed to represent any one of these three types of loading*.

* When applying the operator expressions relating σ and ϵ to experimental data or to the solving of a stress problem, different symbols should be used for tension, bulk and shear. We shall use the symbols proposed by the Committee on Nomenclature of the Society of Rheology (H. Leaderman, Trans. Soc. Rheology, I, 213, 1957) in this report (with the exception of the shear modulus), which is given in the following table:

Type of Deformation	Modulus ($= \sigma/\epsilon$)	Compliance ($= \epsilon/\sigma$)
unspecified	m	k
simple tension	E	D
bulk	K	B
shear	μ	J

However, there is an exception which must be noted for certain models, depending upon the loading condition. Specifically, when a simple shear stress is applied to an uncross-linked polymer element, its deformation increases indefinitely. However if this same polymer is subjected to a hydrostatic pressure the volume cannot decrease in an unlimited manner, but must approach an equilibrium value. Consequently, a model that evinces unlimited flow behavior cannot be used to define an operator equation relating hydrostatic pressure (stress) and relative volume change (strain). In contrast, a cross-linked polymer specimen subjected to a shear stress will always reach an equilibrium deformation. We therefore have the rule that in describing tension, bulk, and shear response for a cross-linked polymer, or bulk response for an uncross-linked polymer, a model should be used that does not exhibit unlimited flow under stress.

Voigt model. - Turning now to the first of the combined element models, consider a spring and a dashpot arranged in parallel as shown in Figure 2.5. In order to derive the appropriate operator equation for the model, write an equation of stress equilibrium in which the applied stress is balanced by the internal stresses on the elements, as shown in Figure 2.5a, and then relate the overall strain (or extension) ϵ of the element to the internal strains. For the Voigt model, this step is trivial since the overall strain is the same as in the dashpot and spring. It is seen that equation (2.1.5), discussed previously, is represented by this model.

The behavior in standard tests is shown in Figures 2.5b and 2.5c. In a creep test, the equation for strain is found by integrating the operator equation in which the applied stress is constant. The initial condition needed to determine the constant of integration is $\epsilon = 0$ when $t = 0$. It should be noted that there is no instantaneous strain, whereas an actual propellant does deform immediately (neglecting inertia effects). The recovery equation of strain is obtained by integrating the operator equation with the stress set equal to zero, and the initial condition $\epsilon = \epsilon_1$, when $t = t_1$. The curve shows that the model completely recovers to its original length as $t \to \infty$.

The reason for defining previously the ratio η_v/m_v as retardation time τ_v, as in (2.1.9), is seen by the creep behavior. Here, τ_v represents a quantity with the dimensions of time and has the effect of shifting the time scale in regards to the delayed action of the material. More specifically, it is the time needed for the instantaneous unattained compliance $(D_e - D)$ to be reduced to $(1/e)$ of the total unattained compliance D_e. For example, when τ_v is large, the strain is retarded so that it increases slowly; whereas if τ_v is small, the curve shifts to the left and the equilibrium strain is approached quite rapidly with very little retardation.

When this model is held at a constant strain, as in a stress relaxation test, the stress remains constant since no flow occurs in the dashpot. Thus, the Voigt model does not exhibit stress relaxation, while a propellant does. With a constant strain rate, Figure 2.5c, the stress immediately jumps to a finite value and then increases linearly. This behavior also is not representative of a propellant since the stress in a real material increases continuously from zero at a decreasing rate.

Maxwell model. - The other possible two element arrangement consists of arranging the spring and dashpot in series. The operator equation is obtained by noting that the stress in the dashpot is the same as that in the spring, and equating the overall strain to the strain in the dashpot plus that in the spring. The behavior is summarized in Figure 2.6*.

The integrated expression for strain in a creep test (Figure 2.6b) shows that deformation occurs immediately, and that unlimited flow occurs, i.e. the strain does not approach an upper limit. If the stress is removed, there is an immediate recovery to a finite strain which remains as a permanent deformation.

This model shows stress relaxation behavior in a manner similar to uncross-linked polymers, in that the stress decays to zero at a decreasing rate. For this model, the time constant is defined as $\tau_m = \eta_m / m_m$ in which τ_m is called the relaxation time. It has the dimensions of time and represents the time for the stress to fall to (1/e) of its original value in a relaxation test. It is, therefore, a measure of the rate at which the relaxation occurs; for example, if the relaxation time, τ_m, is small, the stress decays to zero almost immediately. If the model is strained at a constant rate, the stress-time curve in Figure 2.6d shows a response qualitatively similar to that of a propellant (Figure 2.1).

Three element model (Maxwell element plus spring). - As the Voigt or Maxwell models by themselves usually possess insufficient generality to represent propellant behavior, it is necessary to form combinations of these basic units in order to approximate actual linear viscoelastic response. This is usually done by adding Voigt models in a series or Maxwell models in parallel to form an array of

---

* The operational notation that is shown has a two-fold significance. First, the expression

$$\sigma = \frac{m_m \frac{d\epsilon}{dt}}{\frac{d}{dt} + \frac{1}{\tau_m}} \equiv \frac{m_m p \epsilon}{p + \frac{1}{\tau_m}} \qquad \text{(a)}$$

with $p \equiv d/dt$, can be interpreted as an implied form of integration by the method of partial fractions. The integral is found by recognizing that σ is the solution to the first order differential equation

$$\frac{d\sigma}{dt} + \frac{\sigma}{\tau_m} = m_m \frac{d\epsilon}{dt} \qquad (b)$$

in which τ_m and m_m are constant if the material's temperature is constant; however, when the temperature is transient these parameters will generally be functions of time because of their temperature dependence. In the general case of time dependent parameters $\tau_m(t)$, $m_m(t)$, integration of (b) yields

$$\sigma = m_m e^{-\int^t \frac{du}{\tau_m(u)}} \left[\int_0^t e^{\int^v \frac{du}{\tau_m(u)}} \frac{d\epsilon(v)}{dv} dv + C_1 \right] \equiv \frac{m_m p \epsilon}{p + \frac{1}{\tau_m}} \qquad (c)$$

where C_1 is a constant to be determined from initial conditions ($C_1 = 0$ for initially zero). With constant coefficients, (c) simplifies to

$$\sigma = m_m e^{-\frac{t}{\tau_m}} \left[\int_0^t e^{\frac{v}{\tau_m}} \frac{d\epsilon(v)}{dv} dv + C_1 \right] \equiv \frac{m_m p \epsilon}{p + \frac{1}{\tau_m}} \qquad (d)$$

A second interpretation of notation (a) is associated with the Laplace transform method, which can be conveniently used when the material constants are independent of time. The Laplace transform of a function $y(t)$ is defined as

$$\bar{y}(p) = \int_0^\infty e^{-pt} y(t)\, dt \qquad (e)$$

where the symbol p now represents the complex transform parameter (whose real part must be positive for convergence of the integral (e)). Operating on the differential equation (b) with this transform yields

$$\int_0^\infty e^{-pt} \left[\frac{d\sigma}{dt} + \frac{\sigma}{\tau_m} = m_m \frac{d\epsilon}{dt} \right] dt = p\bar{\sigma} + \frac{\bar{\sigma}}{\tau_m} = m_m p \bar{\epsilon} \qquad (f)$$

in which we have integrated $d\sigma/dt$ and $d\epsilon/dt$ by parts and assumed, for simplicity, that σ and ϵ are initially zero. Thus, it is seen that a second interpretation of (a) is that it is the transfer function relating transformed stress $\bar{\sigma}$ and strain $\bar{\epsilon}$ if properties are constant and the stress and strain are initially zero; namely, with p as the Laplace transform parameter,

$$\frac{m_m p}{p + \frac{1}{\tau_m}} = \frac{\bar{\sigma}}{\bar{\epsilon}} \qquad (g)$$

If stress (or strain) is given as a function of time, then the time dependent stress (or strain) can usually be found with standard transform tables which associate functions of p with time dependent functions, and thereby eliminate the need for formal integration. When the operator equation consists of a sum of partial fractions, as it does if additional elements are added to the model, then each term can be interpreted by means of (c) or (g).

springs and dashpots. The mathematical relations developed for these models will serve as a useful guide in designing experiments for the testing of propellants. The first of these, shown in Figure 2.7, consists of a spring in parallel with a Maxwell element*.

It will be recalled that the Maxwell model behaves qualitatively like an uncross-linked polymer in that unlimited flow (or strain) occurs under a continuously applied stress. In order to describe the behavior of a cross-linked polymer, a spring is attached in parallel as shown in Figure 2.7a. The modulus of a spring in parallel with one or more Maxwell elements is denoted by m_e, the equilibrium modulus. Its physical significance can be seen in Figure 2.7c, since it represents the long-time modulus of the model under constant strain. In addition, this spring provides complete recovery as shown in Figure 2.7b. Another significant parameter is the glass modulus m_g. It is the effective elastic modulus for very short loading times and also corresponds to the effective modulus at temperatures below the glass transition temperature.

Response to the various types of loading shown in Figure 2.7b, 2.7c, and 2.7d is readily obtained, as before, by integration of the operator equation (or by the Laplace transform method) for creep, stress relaxation and constant strain rate conditions.

Five element model - two Maxwell elements plus spring. - The last finite element model to be discussed explicitly permits one to fit experimental data over a wider time range than that covered by a three element model. The effect of this additional flexibility is illustrated in Figure 2.8. In this case, while a second order differential equation relates stress and strain**, the response for creep, relaxation, and constant strain rate is seen to be very similar to that of the three element model.

The intermediate case of a four element model, which is used for uncross-linked polymers, was not discussed since it can be readily obtained from the five element model by setting $m_e = 0$. In addition, composite propellants are usually crosslinked so that the more common condition requires passing directly to five elements.

---

* Previously, the series arrangement of a spring and dashpot was referred to as a Maxwell model, however when it comprises only part of a more general model, it will be called a Maxwell element.

** It is important to realize that this does not reflect inertia effects since the roots of the operator equation are always real, which results from having used a model that includes only springs and dashpots.

In concluding this section on finite element model representations, it is expected that the foregoing models will provide a reasonable flexibility to approximate propellant response over a limited time interval to the desired accuracy of a one to five parameter curve fit of experimental data as represented by the spring and dashpot material constants.

2.3.2 Infinite element models

While the finite element models permit reasonable representation of experimental data over a limited time range, to the extent of the number of unknown material constants or parameters available, it may happen that the time range of interest is too broad to be represented by a model with just a few elements. Hence to hold the desired accuracy, but simultaneously to extend the time interval of data representation, the only recourse is to add additional elements which, as a practical matter, is frequently impractical for stress analysis*. However, it is useful to consider the limit situation of an infinite number of elements which will yield (mathematically) perfect accuracy over the entire time spectrum.

Wiechert or generalized Maxwell model. - The first of two infinite combinations, which will be shown later to possess certain reciprocity features, consists of an infinite number of Maxwell elements in parallel with a spring which is used to represent a cross-linked polymer possessing an equilibrium modulus. Characteristically this type of model is used when the strain is imposed as an input by the experimental set-up, and the stress output is measured. The behavior is illustrated in Figure 2.9 where the operator equation has been developed from a (large) finite number of Maxwell elements which has subsequently been increased to infinity thus converting a finite summation to an integral representation. The limit is taken such that the stress remains finite, as indicated in the figure.

Instead of having a finite number of discrete parameters, we now have introduced an arbitrary function, $H(\tau)$, usually called the relaxation spectrum. If $H(\tau)$ and m_e are known, the stress-strain law is completely defined for all types of loading. The techniques used to determine $H(\tau)$ from experimental data will be discussed subsequently, but they amount essentially to:(a) imposing a known strain, $\epsilon(t)$, e.g. ϵ_0; (b) measuring the stress, $\sigma(t)$ response experimentally and fitting the data with an analytical curve; (c) substituting into the stress-strain relation (see Figure 2.9) for $\sigma(t)$ and $\epsilon(t)$; and (d) solving this integral equation analytically or numerically for $H(\tau)$.

* Various proposals have been advanced to use electrical analog techniques (e.g. Blizard[2.4] and Gross[2.5]) with only limited success.

Integration of the general operator equation for the constant strain case may still be carried out through the usual procedure for partial fractions or application of the Laplace transform, even though there is not a finite sum of terms. With this latter method, the solution for zero initial conditions is obtained immediately, which gives the relaxation modulus in terms of the relaxation spectrum*. This modulus evaluated at $t = 0$ is defined as the glass modulus, m_g, in accordance with the previous definition when finite element models were considered. The equilibrium modulus m_e takes on the same significance as before.

For constant strain rate, stress can also be easily determined by means of the Laplace transform. The result is seen to be similar to the relaxation modulus. In fact a very interesting relation is shown to exist, namely that the slope of the stress-strain curve is a constant strain rate test, $\dot{\epsilon}(t) = R$ is equal to the stress relaxation modulus evaluated at (ϵ/R). This relation is independent of the relaxation spectrum and thus depends only on the assumption of linear springs and dashpots. Indeed, this same correspondence exists for the models with a finite number of elements. Such a relation is very useful since data from these two types of tests can be used to check the assumption of linearity.

---

* This will be shown to illustrate an application of the transform method to the integral representation. In accordance with the previous footnote, the transformed equation (equation (i), Figure 2.9) is

$$\bar{\sigma}(p) = \left[m_e + \int_0^\infty \frac{H(\tau)p}{p+\tau^{-1}} \cdot \frac{d\tau}{\tau} \right] \bar{\epsilon}(p) \qquad \text{(a)}$$

in which p is the transformation variable and all conditions are taken as zero for $t \leq 0$. Even though this is the transform of an integral expression rather than a finite sum of terms, the standard procedure can be used; the only additional restriction is that the integral converge uniformly. For constant strain input, ϵ_0, its transform is $\bar{\epsilon}(p) = \epsilon_0/p$ and the transformed equation becomes

$$\bar{\sigma}(p) = \left[\frac{m_e}{p} + \int_0^\infty \frac{H(\tau)}{p+\tau^{-1}} \cdot \frac{d\tau}{\tau} \right] \epsilon_0 \qquad \text{(b)}$$

The inverse transform is found using the relation

$$\frac{H(\tau)}{p+\tau^{-1}} \cdot \frac{d\tau}{\tau} = \overline{\left[\frac{H(\tau) e^{-t/\tau}}{\tau} d\tau \right]} \qquad \text{(c)}$$

which yields the time dependent relaxation modulus

$$m(t) \equiv \frac{\sigma(t)}{\epsilon_0} = \left[m_e + \int_0^\infty \tau^{-1} H(\tau) e^{-t/\tau} d\tau \right]$$

(see also Figure 2.9)

Experimental data is obtained for the relaxation modulus, $\sigma(t)/\epsilon_0$, and the equilibrium modulus is estimated at long times from the same data. Thus, in principle everything is known except $H(\tau)$, for which the integral equation is solved analytically or numerically.

Kelvin or generalized Voigt model. - The other infinite element model can be generated as shown in Figure 2.10 by arranging a large number of Voigt elements and a spring in series. In fact, it turns out that the linear viscoelastic behavior generated by the Wiechert model can also be defined equivalently by the Kelvin model*. Therefore, in principle, only one method of representation is actually needed to solve stress problems, although both are sometimes used for experimental reasons and cross-checking of data. Also, the Kelvin model is customarily used when the input function for the experiment is stress and the measured output is strain.

For example, reference to Figure 2.10 shows that when stress is given, as in a strain retardation or creep test, the strain is a relatively simple function of the model parameters if the Kelvin model is used. Conversely a Wiechert representation is natural and simpler for a stress relaxation experiment.

Because of the close correspondence between the Wiechert and Kelvin models, the latter will not be discussed in detail. However, some simple correspondences are evident. It is seen for example that spring constants are written in terms of compliances, k_i, rather than their reciprocals, m_i; similarly, the dashpots are defined by fluidity, ϕ_i, instead of the reciprocal η_i. This choice of nomenclature exemplifies the similarity in the corresponding mathematical representations of the two models. Thus one may see that $1/k_g \equiv m_g$ and $1/m_e \equiv k_e$. Many other more involved expressions relating the infinite element models can be found in the literature on linear viscoelasticity[2.5]. They are particularly useful in checking the

---

* The equivalence of the Wiechert and Kelvin models can be shown when they have either a finite or infinite number of elements. However, there are a couple of conditions which must be satisfied in order to do this. One is that the finite and infinite element models must both have the same basic behavior in regards to limited or unlimited strain. In particular, if $m_e \neq 0$ in the Wiechert model, then the equivalent Kelvin model must have a spring adjacent to all the dashpots. Similarly, if the Wiechert model represents uncross-linked material ($m_e \equiv 0$), then the equivalent Kelvin model must have a free dashpot in series with the spring k_g. The other condition is that the number of elements in each model must be the same.

To prove that the finite element models are equivalent, it is necessary and sufficient to show, as will be carried out later, that the operator equation for each can be written in identical form. That is, the same derivatives must appear in both numerators and in both denominators. The coefficients of the derivative terms d^n/dt^n will, of course, consist of different parameters. However, by equating the coefficients of the same derivative terms in each model, relations between the parameters of the models are obtained. With an integral representation, the correspondence between model parameters is obtained in the form of integral equations (see equations 2.4.15 and 2.4.16).

theory by comparing data from various types of tests. It is important to note, however, that such simple relations between the short and long time limit moduli generally do not hold between the time dependent quantities of the models. For example, it is not generally true that the relaxation modulus is the reciprocal of the creep compliance.

Ladder model. - There is another particularly useful arrangement of spring and dashpot elements which does not exactly fall into the previous categories. For years, rheologists have been compounding elements into arrays analogous to electric circuits, with little thought to the implications of polymer molecule kinematics. Because of the intrinsic awkwardness of these models, it has been necessary to achieve adequate material representation through the use of broad distribution functions or at best four or more element networks.

In 1948, Blizard[2.4] proposed what has come to be known as a realistic network representation of an array of polymer molecules. He suggested that, since a segment of a polymer molecule is actually imbedded in a medium of average viscosity, the viscous forces or dashpots be distributed uniformly along the chain, represented by a long elastic spring. Furthermore, he assumed that all segments are equally elastic and contribute equally to sharing the stress reaction (affine behavior). Thus he was able to arrive at a model based on only three parameters which provides an excellent representation of material behavior; this is known as the ladder model (see insert).

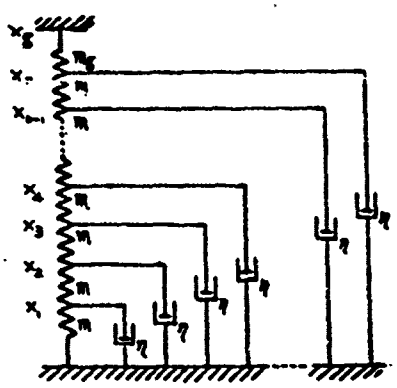

x_i is the coordinate of the tail of the ith stretched element.

ℓ_o is the length of an unstretched element

$\tau = \eta/m$ is the retardation time of the viscous stresses

ℓ_g is the unstretched length of the glassy segment

m_g is the modulus of the glassy segment

The following kinematic relations stem from the topology of the network:

$$\frac{x_k - x_{k-1}}{l_o} + \tau \frac{\dot{x}_k}{l_o} = \frac{x_{k+1} - x_k}{l_o} \; ; \quad k = 1, 2, \cdots n-1 \qquad (2.3.1)$$

$$\frac{x_n - x_{n-1}}{l_o} + \tau \frac{\dot{x}_n}{l_o} = \frac{m_g}{m} \cdot \frac{x_g - x_n}{l_g} = \frac{\sigma}{m} \qquad (2.3.2)$$

$$\epsilon = \frac{x_g - x_o}{n l_o + l_g} \qquad (2.3.3)$$

These equations may be solved by the usual methods applicable to difference equations to yield the transfer function of the network, which is the ratio of the Laplace transforms of the stress output to the strain input,

$$\frac{\bar{\sigma}}{\bar{\epsilon}} = \frac{m_e}{\frac{m_e}{m_c} + \left(1 - \frac{m_e}{m_c}\right) \frac{\tanh \sqrt{p \tau_o}}{\sqrt{p \tau_o}}} \qquad (2.3.4)$$

In arriving at this solution, it is assumed that $n \tau_o^{\frac{1}{2}} \rightarrow \tau_o^{\frac{1}{2}}$ and $n \cdot l_o \rightarrow L$ for large n. Finally, m, L, and m_g are eliminated by the introduction of m_e and m_G, the overall rubbery and glassy moduli of the network. Note that $m_g \neq m_G$, because the strain of the network is referred to $(n l_o + l_g)$, whereas the strain of the glassy element is referred to l_g.

The importance of (2.3.4) lies in the fact that this simple function, based on only one parameter besides the usual limiting moduli, i.e. τ_o, provides an excellent representation of actual data in many cases. On the other hand, the presence of an essential singularity in the denominator makes all analytic inversions intractable. The associated creep and relaxation functions are being calculated numerically at the National Bureau of Standards.

2.3.3 The dynamic behavior of models.

In the previous sections, the operation equations and the operational moduli and compliances were presented for various models which implicitly related stress to strain. In addition, time dependent solutions were given for certain simple loading conditions such as the variation of strain with time when a constant load was applied, or variation of stress under constant applied strain. The former, for example, was called a creep test, and the ratio of strain $\epsilon(t)$ to stress σ_o was defined as the creep compliance, k(t).

Now in addition to the use of this kind of loading, there is another convenient method of determining model parameters by using complex (or dynamic) moduli and compliances that relate sinusoidal time-dependent stress and strain. They are obtained by formally substituting $i\omega$ (ω = frequency, $i = \sqrt{-1}$) for the time derivative symbol $p = d/dt$ in the operator equations given in Figures 2.5 to 2.10 and separating the real and imaginary parts. The symbols will be similar to those used previously in the general presentation, except that complex quantities will be starred such that m^* will denote complex modulus, and k^* complex compliance. When these are used for a particular propellant, it will be necessary, of course, to indicate whether they represent simple tension, bulk, or shear behavior. For example, the complex shear compliance is denoted by $J^*(\omega)$, and the complex shear modulus by $\mu^*(\omega)$.

For simplicity, complex notation is used, e.g. sinusoidal stress is written as $\sigma_o e^{i\omega t}$ and sinusoidal strain as $\epsilon_o e^{i\omega t}$. If stress is given, σ_o is considered to be a real constant representing the maximum amplitude of the sine wave, and ϵ^*_o is a complex function of frequency, ω. For $\sigma_o = 1$, ϵ^*_o is identically the dynamic compliance k^*. Similarly, with strain given, ϵ_o is real and σ_o^* is a complex function of frequency which is identical with the dynamic or complex modulus when $\epsilon_o = 1$. As another matter of notation, it is convenient to represent the modulus by its real and imaginary components $m'(\omega)$ and $m''(\omega)$; thus

$$m^*(\omega) = m'(\omega) + i\,m''(\omega) = \frac{\sigma}{\epsilon} = \frac{\sigma_o^* e^{i\omega t}}{\epsilon_o e^{i\omega t}} = \frac{\sigma_o^*}{\epsilon_o} \qquad (2.3.5)$$

and the compliance by its real and imaginary components $k'(\omega)$ and $-k''(\omega)$:

$$k^*(\omega) = k'(\omega) - i\,k''(\omega) = \frac{\epsilon}{\sigma} = \frac{\epsilon_o^* e^{i\omega t}}{\sigma_o e^{i\omega t}} = \frac{\epsilon_o^*}{\sigma_o} \qquad (2.3.6)$$

Because of viscosity, there is a phase angle between stress and strain which is

$$\zeta = \tan^{-1}\frac{m''(\omega)}{m'(\omega)} = \tan^{-1}\frac{k''(\omega)}{k'(\omega)} \qquad (2.3.7)$$

The strain lags behind the stress so that $m'(\omega)$, $m''(\omega)$, $k'(\omega)$, $k''(\omega)$ are all positive functions of frequency. These complex quantities may also be written in the form

$$m^*(\omega) = |m^*| e^{i\delta} \qquad (2.3.8)$$
$$k^*(\omega) = |k^*| e^{-i\delta}$$

where

$$|m^*| = \sqrt{(m')^2 + (m'')^2} \qquad (2.3.9)$$

$$|k^*| = \sqrt{(k')^2 + (k'')^2} \qquad (2.3.10)$$

Since

$$m^*(\omega) = \frac{\sigma}{\epsilon} = \frac{1}{k^*} \quad \text{or} \quad m^*(\omega) k^*(\omega) = 1 \qquad (2.3.11)$$

it follows that

$$|m^*||k^*| = 1 \qquad (2.3.12)$$

which is useful in converting data from compliances to moduli or visa versa.

In order to illustrate the procedure for determining the complex moduli and compliances from operational expressions, consider as an example the Voigt model. From Figure 2.5a, the operator equation gives

$$m(p) = m_v(\tau_v p + 1) \qquad (2.3.13)$$

Letting $p = i\omega$ gives the complex modulus

$$m^*(\omega) = m_v + i\omega m_v \tau_v \qquad (2.3.14)$$

from which the real (m') and imaginary (m'') components are

$$m' = m_v \qquad (2.3.15)$$

$$m'' = m_v \tau_v \omega \qquad (2.3.16)$$

This representation thus produces a real part of the modulus which is constant, and the imaginary part which is linear in frequency.

The operational compliance is the reciprocal of the modulus, namely

$$k(p) = \frac{1}{m(p)} = \frac{1}{m_v(\tau_v p + 1)} = \frac{k_v}{\tau_v p + 1} \qquad (2.3.17)$$

Again, letting $p = i\omega$

$$k^*(\omega) = \frac{k_v(1 - i\omega\tau_v)}{(1 + \omega^2\tau_v^2)} \qquad (2.3.18)$$

one finds

$$k' = \frac{k_v}{(1 + \omega^2\tau_v^2)} \qquad (2.3.19)$$

$$k'' = \frac{\omega\tau_v k_v}{(1 + \omega^2\tau_v^2)} \qquad (2.3.20)$$

where we have defined $k_v = 1/m_v$.

Complex moduli and compliances for several models have been computed and are given in Figures 2.11 - 2.15. It was mentioned previously that when model response is to be related to test data, it is most convenient to use models consisting of Voigt elements in series if stress is given; while if strain is given, models consisting of Maxwell elements in parallel should be used. Similarly, it is desirable to represent the dynamic behavior of Voigt type models by complex compliances and dynamic behavior of Maxwell type models by complex moduli. Except in the case of the basic two-element models, this rule is followed in presenting the dynamic moduli and compliances.

2.4 Spectral Distribution Functions

We have seen that there are several ways of characterizing a viscoelastic material. It may be represented by various forms of finite models, or by a spectral distribution of the relaxation times associated with a Wiechert, Kelvin or ladder model. The distribution function may be thought of as an unknown transfer function by which the stress and strain are related. If a known stress (strain) is imposed and the strain (stress) response is measured, then the third unknown element--the transfer function connecting them--can be deduced.

Since the choice of model used to represent a given mechanical behavior is arbitrary, it follows that the various models must be related, both topologically and analytically. The topology of network models is an as yet unexplored area, which will be continually pursued as an important development phase of linear

viscoelasticity. The analytic nature of network model representation by distribution functions permits a mathematical investigation of the character of the interrelation.

One of the most direct ways of determining the spectral distribution functions is to apply a constant strain input, ϵ_o, measure the uniaxial stress response, $\sigma(t)$ (and hence the relaxation modulus $E(t) = \sigma(t)/\epsilon_o$), and solve analytically or numerically for the resulting transfer function, or explicitly, the integral equation for $H(\tau)$ in the Wiechert model. In particular, from Figure 2.9, we have

$$\sigma(t) = \left[E_e + \int_0^\infty \frac{H(\tau)\, d\tau}{\left(\frac{d}{dt} + \frac{1}{\tau}\right)} \frac{d}{dt} \right] \epsilon(t) \qquad (2.4.1)$$

which for the case of constant strain, ϵ_o, gives

$$E(t) = \frac{\sigma(t)}{\epsilon_o} = E_e + \int_0^\infty \tau^{-1} H(\tau) e^{-t/\tau} d\tau \qquad (2.4.2)$$

with the normalizing condition (Figure 2.9)

$$E_g - E_e = \int_0^\infty \tau^{-1} H(\tau) d\tau \qquad (2.4.3)$$

An alternate approach for determining the distribution function is to apply a constant stress, σ_o, measure the uniaxial strain response $\epsilon(t)$ (and hence the creep compliance $D(t) = \epsilon(t)/\sigma_o$), and solve analytically or numerically for the resulting transfer function, or explicitly, the integral equation for $L(\tau)$ in the Kelvin model. In particular, from Figure 2.10, we have

$$\epsilon(t) = \left[D_g + \int_0^\infty \frac{L(\tau) d\tau}{\left(\frac{d}{dt} + \frac{1}{\tau}\right) \tau^2} \right] \sigma(t) \qquad (2.4.4)$$

which for the case of constant stress, σ_o, gives

$$D(t) = \frac{\epsilon(t)}{\sigma_o} = D_g + \int_0^\infty \tau^{-1} L(\tau)(1 - e^{-t/\tau}) d\tau \qquad (2.4.5)$$

with the normalizing condition (Figure 2.10)

$$D_e - D_g = \int_0^\infty \tau^{-1} L(\tau) d\tau \qquad (2.4.6)$$

Inasmuch as either of these analytical representations of the distribution functions apply to the same material, it follows that one may convert the analytical representation of one transfer function, say $\bar{\sigma}(p)/\bar{\epsilon}(p)$, into the other, $\bar{\epsilon}(p)/\bar{\sigma}(p)$, which must be the reciprocal. The subsequent section discusses these relations

2.4.1 Model interrelationships.

The relation of the distribution functions $H(\tau)$ and $L(\tau)$ is easily established in principle by using relationships between the Laplace transforms. Specifically, the transforms of (2.4.1) and (2.4.4) are, respectively

$$\frac{\bar{\sigma}(p)}{\bar{\epsilon}(p)} = E_e + \int_0^\infty \frac{pH(\tau)}{p+\tau^{-1}} \frac{d\tau}{\tau} \equiv E_e + (E_g - E_e)\int_0^\infty \frac{pH'(\mu)}{p+\mu} \frac{d\mu}{\mu} \qquad (2.4.7)$$

$$\frac{\bar{\epsilon}(p)}{\bar{\sigma}(p)} = D_g + \int_0^\infty \frac{L(\tau)}{p+\tau^{-1}} \frac{d\tau}{\tau^2} \equiv D_g + (D_e - D_g)\int_0^\infty \frac{L'(\mu)}{p+\mu} d\mu \qquad (2.4.8)$$

where the change of variable $\tau = 1/\mu$ has been employed along with the definitions

$$H(\tau) = H\left(\frac{1}{\mu}\right) \equiv (E_g - E_e)\, H'(\mu) \qquad (2.4.9)$$

$$L(\tau) = L\left(\frac{1}{\mu}\right) \equiv (D_e - D_g)\, L'(\mu) \qquad (2.4.10)$$

which requires in the normalizing functions (2.4.3) and (2.4.6) that

$$\int_0^\infty H'(\mu)\, d(\ln\mu) = 1 \quad ; \quad \int_0^\infty L'(\mu)\, d(\ln\mu) = 1 \qquad (2.4.11)$$

Multiplying (2.4.7) and (2.4.8) together gives the relation

$$\left[E_e + (E_g - E_e)\int_0^\infty \frac{pH'(\mu)}{p+\mu} \frac{d\mu}{\mu}\right]\left[D_g + (D_e - D_g)\int_0^\infty \frac{L'(\mu)}{p+\mu}\, d\mu\right] = 1 \qquad (2.4.12)$$

which, using (2.4.11), is equivalent to the more symmetrical form

$$\left[E_g - (E_g - E_e)\int_0^\infty \frac{H'(\mu)}{p+\mu}\, d\mu\right]\left[D_g + (D_e - D_g)\int_0^\infty \frac{L'(\mu)}{p+\mu}\, d\mu\right] = 1 \qquad (2.4.13)$$

Note that from a limit check at large and small p, respectively, one deduces

$$E_e D_e = 1 \quad ; \quad E_g D_g = 1 \qquad (2.4.13a)$$

so that it is obvious that if either $H(\tau)$ or $L(\tau)$ is known, the other can be calculated*.

---

* By way of detail in carrying out the preceding calculation, note that if we have two Laplace transforms defined by the relations

$$g(p) = \int_0^\infty f(t) e^{-pt} dt \qquad (a)$$

$$h(s) = \int_0^\infty g(p) e^{-ps} dp \qquad (b)$$

then

$$h(s) = \int_0^\infty \frac{f(t)}{s+t}\,dt \qquad \text{(c)}$$

The iterated Laplace transform (c) is known as a Stieltje transform, and has rather simple inversion properties. If (a) exists and converges, then h(s) is analytic in the entire s-plane except the negative real axis, where it has a branch point at the origin. Use may be made of this cut in the principal Riemann sheet to invert (c). First note that

$$h(ne^{-i\pi}) = \lim_{\delta\to 0} \int_0^\infty \frac{f(t)\,dt}{t-n-i\delta} \qquad ; \text{ with } s=-n-i\delta,\ n>0$$

$$= \lim_{\delta\to 0} \int_0^\infty \frac{f(t)(t-n+i\delta)}{(t-n)^2+\delta^2}\,dt$$

$$= \lim_{\delta\to 0} \int_0^\infty \frac{f(t)(t-n)\,dt}{(t-n)^2+\delta^2} + i \lim_{\delta\to 0} \delta \int_0^\infty \frac{f(t)\,dt}{(t-n)^2+\delta^2}$$

$$= \int_0^\infty \frac{f(t)\,dt}{t-n} \qquad \lim_{\delta\to 0} \delta \int_{-\pi}^{0} \frac{f(n+\delta\tan\theta)\,\delta\sec^2\theta}{\delta^2\sec^2\theta}\,d\theta$$

using $(t-n) = \delta\tan\theta$

$$= \int_0^\infty \frac{f(t)\,dt}{t-n} + i\pi \lim_{\delta\to 0} f(n+\delta\tan\theta)$$

$$= \int_0^\infty \frac{f(t)\,dt}{t-n} + i\pi f(n) \qquad \text{(d)}$$

Similarly

$$h(ne^{i\pi}) = \int_0^\infty \frac{f(t)\,dt}{t-n} - i\pi f(n) \qquad \text{(e)}$$

The integral in (d) and (e) is the principal value. The difference between equations (d) and (e) is known as the jump, given by

$$h(ne^{-i\pi}) - h(ne^{i\pi}) = 2\pi i f(n) \qquad \text{(f)}$$

Thus, the inversion of (c) is accomplished simply by calculating the jump of the function $h(s)/2\pi i$. Hence using the definitions (2.4.14), (2.4.17), and (2.4.18) in (2.4.13), one may deduce that

$$S_L(p) = \frac{\beta S_u(p)}{1-(1-\beta)S_u(p)} \qquad \text{(g)}$$

which, using (f), yields (2.4.15) or (2.4.16).

After using (2.4.13a) and defining

$$\frac{E_e}{E_g} = \frac{D_g}{D_e} \equiv \beta \tag{2.4.14}$$

it is found that

$$L'(\mu) = \frac{\beta H'(\mu)}{\left[1-(1-\beta)\left\{\frac{H'(\xi)d\xi}{\xi-\mu}\right]^2 + (1-\beta)^2\pi^2\left[H'(\mu)\right]^2\right.} \tag{2.4.15}$$

and also

$$H'(\mu) = \frac{\beta^{-1} L'(\mu)}{\left[1-(1-\beta^{-1})\left\{\frac{L'(\xi)d\xi}{\xi-\mu}\right]^2 + (1-\beta^{-1})^2\pi^2\left[L'(\mu)\right]^2\right.} \tag{2.4.16}$$

where it is frequently convenient to have defined the integrals

$$S_L(p) = \int_0^\infty \frac{L'(\mu)}{p+\mu} d\mu \tag{2.4.17}$$

$$S_H(p) = \int_0^\infty \frac{H'(\mu)}{p+\mu} d\mu \tag{2.4.18}$$

We are now concerned with the problem of specifying the various useful types of stress inputs and strain inputs and defining the relations among them. The subsequent table lists the most important inputs.

Strain input	Associated stress behavior	Transform
$\epsilon(t)$	generalized relaxation	$\overline{E}(p)$
ϵ_0	relaxation	ϵ_0/p
$\epsilon_0 e^{i\omega t}$	dynamic response to sinusoidal strain input	$\epsilon_0/(p-i\omega)$
$\epsilon_0 \sin\omega t$	imaginary part of dynamic response	$\epsilon_0\omega/(p^2+\omega^2)$
Rt	tensile stress (at constant rate of strain)	R/p^2
Stress input	**Associated strain behavior**	**Transform**
$\sigma(t)$	generalized creep	$\overline{\sigma}(p)$
σ_0	creep	σ_0/p
$\sigma_0 e^{i\omega t}$	dynamic response to sinusoidal stress input	$\sigma_0/(p-i\omega)$
$\sigma_0 \sin\omega t$	imaginary part of dynamic response	$\sigma_0\omega/(p^2+\omega^2)$

Among these sets the most easily procured data is creep, and the most precise is dynamic response to sinusoidal stress input. It is important to establish relations which enable one to convert one set of data to the other for the purpose of rapidly predicting physical behavior.

The relation between relaxation at constant strain and tensile stress at constant rate of strain. - It may be noted incidentally that there is no parallel with retardation, since equipment for testing at constant rate of stress rise is not ordinarily applied to polymeric materials. The ratio of the transforms of the strain inputs is given by

$$\frac{\bar{\epsilon}_{tens.}}{\bar{\epsilon}_{rel.}} = \frac{R}{\epsilon_0 p} = \frac{\bar{\sigma}_{tens.}}{\bar{\sigma}_{rel.}} \qquad (2.4.19)$$

where the constant strain rate is designated as R. Since the transfer function is independent of the strain input, the ratio of the linear functionals of the stress outputs is equal to the ratio of the same quantities for the strain inputs. Equation (2.4.19) may be recast as

$$\frac{\bar{\sigma}_{rel.}}{\epsilon_0} = \bar{E}_{rel.}(p) = \frac{p}{R}\bar{\sigma}_{tens.} \qquad (2.4.20)$$

and remembering that the stress at zero time is taken to be zero, the inversion yields

$$\frac{\sigma_{rel.}}{\epsilon_0} = E_{rel.}(t) = \frac{1}{R}\frac{d\sigma_{tens.}}{dt} = \left.\frac{d\sigma_{tens.}}{d\epsilon}\right|_{\epsilon=Rt} \qquad (2.4.21)$$

Equation (2.4.21) shows that the relaxation modulus at $t = \epsilon/R$ is the slope of the tensile stress curve at ϵ. Conversely, relaxation data can be integrated, in the framework of linear viscoelastic theory, to generate tensile stress data.

The relation between relaxation at constant strain and creep at constant stress. - From (2.4.8) and (2.4.17), it follows that

$$\frac{\bar{\epsilon}_{crp.}}{\sigma_0} = \bar{D}_{crp.} = \frac{1}{p}\left[D_g + (D_e - D_g)S_L(p)\right] \qquad (2.4.22)$$

Likewise from (2.4.7) and (2.4.18)

$$\frac{\bar{\sigma}_{rel.}}{\epsilon_0} = \bar{E}_{rel.} = \frac{1}{p}\left[E_g - (E_g - E_e)S_H(p)\right] \qquad (2.4.23)$$

Multiplication of these latter two equations, using footnote equation (g) and (2.4.14) yields

$$\bar{D}_{crp.}\,\bar{E}_{rel.} = \frac{1}{p^2} \qquad (2.4.24)$$

which may be recast as

$$\overline{D}_{crp.}(p) = \frac{1}{p} \cdot \frac{1}{E_g - (E_g - E_e) S_u(p)} \tag{2.4.25}$$

No general inversion can be given for $\overline{D}_{crp}(p)$; but if $\overline{E}_{rel}(p)$ is representable by a simple analytical function, then the inversion can often be effected analytically. If, as is often the case, the analytical representation of $\overline{E}_{rel}$ is quite complex, then the following numerical formula[2.6] may be used for inversion. Let

$$g(p) = \int_0^\infty f(t) e^{-pt} dt \tag{2.4.26}$$

then,

$$f(t) = \lim_{n \to \infty} \frac{(-1)^n}{n!} \left[p^{n+1} \frac{d^n}{dp^n} g(p) \right]_{p=\frac{n}{t}} \tag{2.4.27}$$

Also useful, for inversion of the Stieltje transform[2.6], is the following: Let

$$h(s) = \int_0^\infty \frac{f(t)}{s+t} dt = \int_0^\infty g(p) e^{-sp} dp \tag{2.4.28}$$

then

$$f(t) = \lim_{m \to \infty} \frac{(-1)^{m-1}}{m!(m-2)!} \cdot \frac{d^m}{dt^m} \left[t^{2m-1} \frac{d^{m-1}}{dt^{m-1}} h(t) \right] \tag{2.4.29}$$

Sinusoidal and constant inputs. - Consider now the relation between responses to sinusoidal strain input. Similar relations may also be developed relating sinusoidal and constant stress input. The constant strain input results in an output defined by (2.4.23), and may be inverted to

$$\frac{\sigma_{rel.}}{\epsilon_o} = E_{rel.} = E_g - (E_g - E_e) \int_0^\infty H'(\mu)(1 - e^{-\mu t}) d(\ln \mu) \tag{2.4.30a}$$

$$= E_e + (E_g - E_e) \int_0^\infty H'(\mu) e^{-\mu t} d(\ln \mu) \tag{2.4.30b}$$

The imaginary part of the sinusoidal input results in

$$\frac{\overline{\sigma}_{sin.}}{\epsilon_o} = \overline{E}_{sin.} = \frac{\omega}{p^2 + \omega^2} \left[E_g - (E_g - E_e) S_u(p) \right] \tag{2.4.31}$$

$$\frac{\sigma_{sin.}}{\epsilon_o} = E_{sin.} = E_g \sin \omega t - (E_g - E_e) \int_0^\infty H(\mu) \frac{\omega e^{-\mu t} + \mu \sin \omega t - \omega \cos \omega t}{\omega^2 + \mu^2} d\mu \tag{2.4.32}$$

As $t \to \infty$, the measured sinusoidal stress becomes steady. This actually occurs in a very short time, and is represented by

$$\frac{\sigma_{sin.st.}}{\epsilon_o} = E_{sin.st.} = \left[E_g - (E_g - E_e)\int_0^\infty \frac{\mu^2}{\mu^2+\omega^2} H'(\mu)\, d(\ln\mu)\right]\sin\omega t$$

$$+\left[(E_g - E_e)\int_0^\infty \frac{\mu\omega}{\mu^2+\omega^2} H'(\mu)\, d(\ln\mu)\right]\cos\omega t \qquad (2.4.33)$$

$$\equiv E'\sin\omega t + E''\cos\omega t$$

Similarly, the real part results in

$$\frac{\bar{\sigma}}{\epsilon_o} = \bar{E}_{cos} = \frac{p}{p^2+\omega^2}\left[E_g - (E_g - E_e)S_e(p)\right] \qquad (2.4.34)$$

$$\frac{\sigma_{cos.st.}}{\epsilon_o} = E_{cos.st.} = E'\cos\omega t - E''\sin\omega t \qquad (2.4.35)$$

Referring to the sinusoidal strain input cited in the table above, we have

$$\epsilon^* = \epsilon_o e^{i\omega t} = \epsilon_o\cos\omega t + i\epsilon_o\sin\omega t \qquad (2.4.36)$$

so that

$$\sigma^* = \sigma_{cos\,st.} + i\sigma_{sin.st.} = \epsilon_o(E_{cos.st.} + iE_{sin.st}) = \epsilon_o e^{i\omega t}(E' + iE'') \qquad (2.4.37)$$

$$\frac{\sigma^*}{\epsilon^*} = E^* = E' + iE'' \qquad (2.4.38)$$

Similarly, it can be easily shown that

$$\frac{\epsilon^*}{\sigma^*} = D^* = D' - iD'' \qquad (2.4.39)$$

from which it follows that

$$E^*D^* = 1 = (E' + iE'')(D' - iD'') = (E'D' + E''D'') + i(E''D' - E'D'') \qquad (2.4.40)$$

or

$$1 = E'D' + E''D'' \qquad (2.4.41a)$$

$$E''D' = E'D'' \qquad (2.4.41b)$$

Thus, the transfer function for dynamic strain and stress inputs are reciprocal.

Before completing the relations between static and dynamic moduli, it is convenient to note that the inverse Fourier-sine transform of a unit step function is a pure sine wave

$$1(t) = \frac{1}{\pi}\int_0^\infty \frac{\sin\omega t}{\omega}\,d\omega + \frac{1}{2} \qquad (2.4.42)$$

This suggests that the Fourier transform of relaxation data must generate dynamic data, and we have (as is verified by direct substitution):

$$-E_e + E' = \omega\int_0^\infty [E_{rel.}(t) - E_e]\sin\omega t\,dt \qquad (2.4.43)$$

$$E'' = \omega\int_0^\infty [E_{rel.}(t) - E_e]\cos\omega t\,dt \qquad (2.4.44)$$

$$E^* - E_e = i\omega\int_0^\infty [E_{rel.}(t) - E_e]e^{i\omega t}\,dt \qquad (2.4.45)$$

$$E^* = \left[p\,\overline{E}_{rel.}(p)\right]_{p=i\omega} \qquad (2.4.46)$$

Inversion of these transforms results in

$$E_{rel.}(t) - E_e = \frac{2}{\pi}\int_0^\infty \frac{E_g - E'}{\omega}\sin\omega t\,d\omega \qquad (2.4.47)$$

$$E_{rel.}(t) - E_e = \frac{2}{\pi}\int_0^\infty \frac{E''}{\omega}\cos\omega t\,d\omega \qquad (2.4.48)$$

from which it follows that E' and E'' must be related. The reciprocal relations between them are known as the Kronig-Kramers integrals[2.7] (principal values indicated by cuts in integral signs):

$$\frac{E_g - E'}{\omega} = \frac{2}{\pi}\int_0^\infty \frac{E''(\beta)}{\beta}\cdot\frac{\omega}{\omega^2 - \beta^2}\,d\beta \qquad (2.4.49)$$

$$\frac{E''}{\omega} = \frac{2}{\pi}\int_0^\infty \frac{E_g - E'(\beta)}{\beta^2 - \omega^2}\,d\beta \qquad (2.4.50)$$

In summary, equation (2.4.40) relates outputs produced by sinusoidal strain input and sinusoidal stress input. Equations (2.4.42) - (2.4.48) relate the real and imaginary parts of the dynamic modulus to the relaxation modulus and equations (2.4.49) and (2.4.50) relate the real and imaginary parts of the dynamic modulus, one to another. Similar relations hold for compliances.

2.4.2 Power law distribution function.

Before examining viscoelastic test data in detail, it is appropriate to inquire into the general character of creep and relaxation data. The first observation is that most materials behave such that if the relaxation modulus is plotted against time on log-log paper, a nearly straight line results. Furthermore, if the compliance data is plotted in a similar way, again a straight line arises--of approximately the same slope but reversed sign. Then if unit time is located at the inflection point, creep behaves as relaxation at reciprocal time, and of course, visa versa. Such observations lead to the selection of a trial distribution function which, when inserted into the integral expressions (2.4.2) or (2.4.4), will integrate out to give essentially a log-log straight line in the physical time plane.

The first function chosen is a simple power law ($\mu \equiv \tau^{-1}$)

$$H(\tau) = C\tau^{-n} \equiv C\mu^{n} \tag{2.4.51}$$

and we wish to compute its associated relaxation modulus from (2.4.2) allowing for the normalization (2.4.3) which fixes the constant, C, i.e.

$$E_g - E_e = \int_0^{\mu_m} C\mu^{n-1} d\mu = C\mu_m^n/n \tag{2.4.52}$$

so that*

$$C = (E_g - E_e)n/\mu_m^n \tag{2.4.53}$$

and thus, incorporating (2.4.9),

$$H'(\mu) = n\left(\frac{\mu}{\mu_m}\right)^n \quad ; \qquad 0 \le \mu \le \mu_m \tag{2.4.54}$$

$$= 0 \quad ; \qquad \mu > \mu_m$$

---

* In order to normalize (2.4.52), it is necessary to assume an upper limit for μ, say μ_m, equivalent to a lower limit, say τ_m, for τ. In practice, this lower limit is so small that neglecting $\tau < \tau_m$ has little observable effect upon measured data. This is why this approximation is frequently called the cutoff power law distribution.

With the constant determined, we calculate the relaxation modulus in a tensile specimen (Figure 2.16) as

$$E_{rel.}(t) = E_e + (E_g - E_e)\int_0^{\mu_m} n\left(\frac{\mu}{\mu_m}\right)^{n-1} e^{-\mu t} d\mu$$

$$= E_e + (E_g - E_e)\frac{n\Gamma(n, \mu_m t)}{(\mu_m t)^n} \qquad (2.4.55)$$

which as soon as $\mu_m t = t/\tau_m \geq 3$, $\Gamma(n, \mu_m t) \to \Gamma(n)$, a constant, the log-log straight line slope desired is therefore actually obtained over most of the time range, i.e.

$$\log \frac{E_{rel}(t) - E_e}{E_g - E_e} = \log \Gamma(1+n) - n \log (\mu_m t) \qquad (2.4.56)$$

The straight line portion usually begins after a few microseconds or so, and hence to use this approximate distribution function:

1. Plot the experimental relaxation modulus, $\sigma(t)/\epsilon_o$ versus time on log-log paper and determine the slope of the straight line portion of the curve, this calculation fixes n.
2. Read off this curve the best values of the long and short time moduli, E_e and E_g.
3. Pick an experimental point, $E_r(t_1)$, near the center of the straight line part of the curve at a particular time, t_1. Knowing the two moduli (E_g and E_e) and n, calculate μ_m from (2.4.56) at the time, t_1.
4. The distribution function is now determined.

Following the discussion in connection with the Wiechert model, and Figure 2.9, the stress during a constant strain rate test ($\epsilon = Rt$) may be easily computed by integrating (2.4.55) with respect to time and evaluating the result at $t = \epsilon/R$, i.e., $d\sigma/d\epsilon = d\sigma/d(Rt) = E_{rel}(t)$ and

$$\sigma_{term.}(t) = R\int_0^{\frac{\epsilon}{R}} E_{rel.}(t)dt = \left[E_e + (E_g - E_e)\frac{\Gamma(1+n)}{(1-\gamma_1)}\left(\frac{R}{\mu_m \epsilon}\right)^n\right]Rt \qquad (2.4.57)$$

where the connection with the relaxation modulus may be noted, namely

$$\sigma_{term.}(t) = \epsilon\left[E_e + \left(\frac{E_{rel.}(t) - E_e}{1-n}\right)_{t=\frac{\epsilon}{R}}\right] \qquad (2.4.58)$$

In order to calculate the creep compliance from the relaxation modulus, it is necessary to proceed via the Laplace transforms:

$$\overline{E}_{rel.} = \frac{E_e}{p} + (E_g - E_e)\frac{n}{p}\left(\frac{p}{\mu_m}\right)^n B_{\frac{\mu_m}{p+\mu_m}}(n, 1-n) \simeq \frac{E_e}{p} + (E_g - E_e)\frac{p^{n-1}}{\mu_m^n}\cdot\frac{n\pi}{\sin n\pi} \quad (2.4.59)$$

where, using (2.4.24), we have

$$\overline{D}_{crp.} = \frac{1}{p^2}\,\frac{1}{\left[\frac{E_e}{p} + (E_g - E_e)\frac{p^{n-1}}{\mu_m^n}\frac{n\pi}{\sin n\pi}\right]} \quad (2.4.60)$$

In order to effect the inversion, it is necessary at this point to assume $E_e \ll E_{rel}$; this approximation, along with the previous one of assuming $\mu_m/p \ll 1$ limits the application of the resulting formula to the transition region, sufficiently removed from the rubbery and glassy limits to make the approximations valid. With this restriction then, it follows that

$$\overline{D}_{crp.} \simeq \frac{\mu_m^n \sin n\pi}{E_g p^{1+n} n\pi} \quad (2.4.61)$$

$$D_{crp.} \simeq \frac{(\mu_m t)^n}{E_g \Gamma(1+n)}\cdot\frac{\sin n\pi}{n\pi} \quad (2.4.62)$$

This leads to another simple relation, observed between creep and relaxation; namely

$$D_{crp.} \cdot E_{rel.} \simeq \frac{\sin n\pi}{n\pi} \quad (2.4.63)$$

The complex modulus and compliance are easily obtained (see 2.4.46)

$$E^* = E' + iE'' = E_e + (E_g - E_e)\frac{n\pi}{\sin n\pi} e^{in\frac{\pi}{2}}\left(\frac{\omega}{\mu_m}\right)^n; \quad \frac{\omega}{\mu_m} \ll 1 \quad (2.4.64)$$

$$D^* = \frac{1}{E_e + (E_g - E_e)\frac{n\pi}{\sin n\pi} e^{in\frac{\pi}{2}}\left(\frac{\omega}{\mu_m}\right)^n} \simeq D_g \frac{\sin n\pi}{n\pi} e^{-in\frac{\pi}{2}}\left(\frac{\mu_m}{\omega}\right)^n; \frac{\omega}{\mu_m} \ll 1 \quad (2.4.65)$$

It remains to connect the distributions $H'(\mu)$ and $L'(\mu)$. Since the exact relations involving the cutoff functions are mathematically quite involved, one can gain some insight to the relation by using (2. 4. 30b) with $E_e \ll E_g$ and (2. 4. 56):

$$E_{rel.} \simeq E_g \int_0^\infty \frac{H'(\mu)}{\mu} e^{-\mu t} d\mu = E_g \frac{\Gamma(1+n)}{(\mu_m t)^n} \tag{2. 4. 66}$$

$$\overline{E}_{rel.} \simeq E_g \frac{\Gamma(1+n)\Gamma(1-n)}{\mu_m^n p^{1-n}} \tag{2. 4. 67}$$

$$\overline{D}_{crp.} \simeq \frac{D_g \mu_m^n}{\Gamma(1+n)\Gamma(1-n)\, p^{1+n}} = \frac{D_g \mu_m^n}{p^{1+n}} \cdot \frac{\sin n\pi}{n\pi} \tag{2. 4. 68}$$

$$D_{crp.} = D_e - (D_e - D_g) \int_0^\infty L(\mu) e^{-\mu t} d(\ln \mu) \tag{2. 4. 69}$$

$$\overline{D}_{crp.} \simeq \frac{D_e}{p} - (D_e - D_g) \int_0^\infty \frac{L(\mu) d\mu}{\mu(p+\mu)} = \frac{D_g}{p} + \frac{D_e - D_g}{p} S_L(p) \tag{2. 4. 70}$$

$$\overline{D}_{crp.} \simeq \frac{D_e}{p} S_L(p) \tag{2. 4. 71}$$

$$S_L \simeq \frac{p}{D_e} \overline{D}_{crp.} = \frac{D_g \mu_m^n \sin n\pi}{D_e p^n \, n\pi} \tag{2. 4. 72}$$

and hence finally using (a), (b), and (c) in the previous footnote

$$L'(\mu) \simeq \frac{D_g \mu_m^n}{D_e n \mu^n} \cdot \frac{1}{[\Gamma(n)\Gamma(1-n)]^2} = \frac{D_g \mu_m^n \sin^2 n\pi}{D_e n \mu^n \, \pi^2} \tag{2. 4. 73}$$

Comparison of (2. 4. 51) and (2. 4. 73) leads to a simple relation between the distribution functions, namely

$$H'(\mu) \cdot L'(\mu) \simeq \frac{D_g}{D_e} \cdot \frac{\sin^2 n\pi}{\pi^2} = \beta \frac{\sin^2 n\pi}{\pi^2} \tag{2. 4. 74}$$

using (2. 4. 14).

It is reiterated that the preceeding relations, (2.4.61) to (2.4.74) are valid only in the transition region. Finally it is to be noted that, in this region, both distribution functions are directly proportional to the associated relaxation and creep data, at the corresponding relaxation and retardation times. Thus the creep curve traces out, as it were, the retardation spectrum. And similarly the relaxation curve traces out the relaxation spectrum.

Turning now to relations governing the complex moduli, (see Section 2.3.3) we have

$$\frac{E'-E_e}{E_g-E_e}=\frac{n}{2}\left(\frac{\omega}{\mu_m}\right)^n B_{\frac{\mu_m^2}{\omega^2+\mu_m^2}}\left(\frac{n}{2},1-\frac{n}{2}\right)\simeq\left(\frac{\omega}{\mu_m}\right)^n\frac{n\frac{\pi}{2}}{\sin n\frac{\pi}{2}}\ , \tag{2.4.75}$$

The middle term of (2.4.75) contains the factor $B_x(p,1-p)$, the incomplete Beta function, which very rapidly becomes approximated by the complete Beta function:

$$B_x(p,1-p)\simeq B(p,1-p)\equiv\frac{\Gamma(p)\Gamma(1-p)}{\Gamma(1)}\equiv\frac{\pi}{\sin\pi p} \tag{2.4.76}$$

Based on the observation that plots of relaxation moduli versus time and the real part of dynamic modulus versus frequency are practically superimposeable, one can equate $E_{rel.}\equiv E'$:

$$\frac{\Gamma(1+n)}{(\mu_m t)^n}=\left(\frac{\omega}{\mu_m}\right)^n\frac{n\frac{\pi}{2}}{\sin n\frac{\pi}{2}} \tag{2.4.77}$$

which gives

$$\omega t=\left[\frac{2}{\pi}\sin\frac{n\pi}{2}\,\Gamma(n)\right]^{\frac{1}{n}} \tag{2.4.78}$$

Note that for $n\equiv 1,\ \omega t\equiv 2/\pi$
$n\equiv\frac{1}{2},\ \omega t\equiv 2/\pi$ $\Big\}\equiv 0.637$
$n\equiv 0,\ \omega t\equiv e^{-\gamma}\equiv 0.560$

so that (cf. Figure 2.17), in general, ωt is well approximated by a value of 0.6.

The imaginary part of dynamic modulus is calculated to be

$$\frac{E''}{E_g-E_e}=\frac{n}{2}\left(\frac{\omega}{\mu_m}\right)^n B_{\frac{\mu_m^2}{\omega^2+\mu_m^2}}\left(\frac{1+n}{2},\frac{1-n}{2}\right)\simeq\left(\frac{\omega}{\mu_m}\right)^n\frac{n\frac{\pi}{2}}{\cos\frac{n\pi}{2}} \tag{2.4.79}$$

which leads to another simple relation

$$\frac{E''}{E'-E_e}\simeq\tan\frac{n\pi}{2} \tag{2.4.80}$$

2.4.3 Modified power law distribution function.

An alternate way of guaranteeing normalization of the power-law distribution without introducing an artificial cutoff at τ_m is by multiplying in an exponential whose argument is approximately zero in the transition region. Thus (2.4.51) is arbitrarily changed to

$$H(\tau) = C\tau^{-n} e^{-\frac{\tau_o}{\tau}} \equiv C\mu^n e^{-\frac{\mu}{\mu_o}} \qquad (2.4.81)$$

where the constant of proportionality, now over the entire time range, is determined from (2.4.3) as

$$C = \frac{E_g - E_e}{\Gamma(n)} \tau_o^n \qquad (2.4.82)$$

leading therefore to

$$H(\tau) = \frac{E_g - E_e}{\Gamma(n)} \left(\frac{\tau}{\tau_o}\right)^{-n} e^{-\frac{\tau_o}{\tau}} \qquad (2.4.83)$$

This function, compared with others in Figure 2.18, has first of all some very interesting analytical properties. The mean reciprocal relaxation time is given by

$$\langle \mu \rangle = \int_0^\infty \frac{\mu^n e^{-\mu}}{\mu} d\mu = \Gamma(n) \qquad (2.4.84)$$

at which value ($\langle \tau \rangle \equiv \Gamma(n)^{-1}$) the maximum of the curve $H(\mu)$ versus μ occurs.

Following now the same order as before, we calculate the associated relaxation function as*

$$E_{rel.} = E_e + \frac{(E_g - E_e)}{\Gamma(n)} \int_0^\infty \left(\frac{\mu}{\mu_o}\right)^{n-1} e^{-\frac{\mu}{\mu_o}} e^{-\mu t} d\left(\frac{\mu}{\mu_o}\right) = E_e + \frac{E_g - E_e}{(1+\mu_o t)^n} \qquad (2.4.85)$$

which also has the property that when $t/\tau_o > 1$, it generates a straight line in log-log coordinates.

As before, the tensile stress during a constant strain, $\epsilon = Rt$, is obtained by integration

$$\frac{\sigma_{tens.}}{\epsilon} = E_e + \left(\frac{E_g - E_e}{1-n}\right)\left(\frac{R}{\mu_o \epsilon}\right)\left[\left(1 + \frac{\mu_o \epsilon}{R}\right)^{1-n} - 1\right] \qquad (2.4.86)$$

---

* A similar form can be fit to compliance data, see equation 4.1.3.

The last item is the relation of the spectra, $H^s(\mu)$ to $L^s(\mu)$. The Laplace transform of (2. 4. 85) gives

$$p\bar{E}_{rel.} = E_e + (E_g - E_e)p^n e^p \Gamma(1-n, p) \tag{2.4.87}$$

so that

$$S_u(p) = 1 - p^n e^p \Gamma(1-n, p) \tag{2.4.88}$$

A complete analytical representation of (2. 4. 88) is given by

$$\begin{aligned} S_u(p) &= 1 - e^p p^n \Gamma(1-n) + e^p p^n \sum_{m=0}^{\infty} \frac{(-1)^m}{m!} \cdot \frac{p^{m+1-n}}{m+1-n} \\ &= 1 - e^p p^n \Gamma(1-n) + \sum_{m=1}^{\infty} \frac{\Gamma(1-n)\, p^m}{\Gamma(m+1-n)} \end{aligned} \tag{2.4.89}$$

And for large p, the asymptotic expansion becomes

$$S_u(p) \simeq -\sum_{m=1}^{M-1} \frac{\Gamma(m+n)}{\Gamma(n)(-p)^m} + O(|p|^{-M}), \quad \begin{matrix} p \to \infty \\ -\frac{3\pi}{2} < \arg p < \frac{3\pi}{2} \\ M = 1, 2, \ldots \end{matrix} \tag{2.4.90}$$

Making use of (2. 4. 15), it is possible to evaluate the retardation function:

$$L'(\mu) = \frac{\beta H'(\mu)}{\left[1 - (1-\beta)\left\{1 - H'(\mu)\pi \operatorname{ctn} n\pi + \sum_{m=1}^{\infty} \frac{\Gamma(1-n)(-\mu)^m}{\Gamma(m+1-n)}\right\}\right]^2 + (1-\beta)^2\pi^2\left[H'(\mu)\right]^2} \tag{2.4.91a}$$

or asymptotically,

$$L'(\mu) = \frac{\beta H'(\mu)}{\left[1 - (1-\beta)\left\{1 - H'(\mu)\pi \operatorname{ctn} n\pi - \sum_{m=0}^{M-1} \frac{\Gamma(m+n)}{\Gamma(n)\mu^n}\right\}\right]^2 + (1-\beta)^2\pi^2\left[H'(\mu)\right]^2} \tag{2.4.91b}$$

Figure 2. 19 compares the retardation and relaxation functions for the particular case when $n = 0.5$ and $\beta = 10^{-3}$. The real and imaginary parts of the complex dynamic modulus are obtained by letting $p = i\omega$ in (2. 4. 87), namely

$$\frac{E' - E_e}{E_g - E_e} = \omega^n \cos\left(\omega + \frac{n\pi}{2}\right)\Gamma(1-n) - \sum_{m=1}^{\infty} \frac{\Gamma(1-n)(-\omega^2)^m}{\Gamma(2m+1-n)} \tag{2.4.92a}$$

$$\frac{E''}{E_g - E_e} = \omega^n \sin\left(\omega + \frac{n\pi}{2}\right)\Gamma(1-n) - \sum_{m=1}^{\infty} \frac{\Gamma(1-n)\,\omega^{2m-1}(-1)^m}{\Gamma(2m-n)} \tag{2.4.92b}$$

The associated asymptotic expansions are:

$$\frac{E'-E_e}{E_s-E_e} = \sum_{m=0}^{M-1} \frac{\Gamma(2m+n)(-1)^m}{\Gamma(n)\left(\frac{\omega}{\omega_0}\right)^{2m+1}} \qquad (2.4.93a)$$

$$\frac{E''}{E_s-E_e} = \sum_{m=0}^{M-2} \frac{\Gamma(2m+1+n)(-1)^m}{\Gamma(n)\left(\frac{\omega}{\omega_0}\right)^{2m+1}} \qquad (2.4.93b)$$

Figure 2.20 is a Nyquist diagram which shows the relation between the magnitude and phase of the complex modulus. Note that for low frequency ($\omega \to 0$), the phase relation is given by

$$\frac{E''}{E'-E_e} = \tan\frac{n\pi}{2} \qquad (2.4.94)$$

which is identical with (2.4.80) for the cutoff power law distribution.

2.4.4 The Cole distribution function.

A third distribution function which has proved useful in fitting dynamic data is given by

$$H'(\mu) = \frac{2\sin\frac{n\pi}{2}}{\pi\left[2\cos\frac{n\pi}{2} + \mu^n + \mu^{-n}\right]} = \frac{\sin\frac{n\pi}{2}}{\pi\left[\cos\frac{n\pi}{2} + \cosh n\ln\mu\right]} \qquad (2.4.95)$$

Figure 2.18, the so-called Cole distribution function[2.8] is compared with the smoothed power law function. Note that on the log scale the Cole function is symmetrical about the point $\mu = 1$, whereas the smoothed power law parallels only the left-hand branch of the Cole. Furthermore, the Cole function has a maximum at $\mu/\mu_o = 1$, the value of which is equal to

$$H'(\mu)\Big|_{max.} = \frac{\tan\frac{n\pi}{4}}{\pi} \qquad (2.4.96)$$

whereas the smoothed function has a maximum at $\mu/\mu_o = n$, the value of which is equal to

$$H'(\mu)\Big|_{max.} = \frac{n^n e^{-n}}{\Gamma(n)} \qquad (2.4.97)$$

Note that for:	$H'(\mu)\|_{max.}$ — COLE	$H'(\mu)\|_{max.}$ — SMOOTHED POWER LAW
$n = 1$	$\frac{1}{\pi} = 0.32$	$\frac{1}{e} = 0.37$
$n = \frac{1}{2}$	$\frac{\sqrt{3-2\sqrt{2}}}{\pi} = 0.18$	$\frac{1}{\sqrt{2e}\,\Gamma(1/2)} = 0.24$
$n = \epsilon$	$\frac{\epsilon}{4}$	ϵ

so that the Cole distribution always peaks at a lower value than the smoothed power law function.

The Cole function has the merit of casting the dynamic modulus into a rather simple form, namely:

$$\frac{E_g - E'}{E_g - E_e} = \int_0^\infty \frac{2\sin\frac{n\pi}{2}}{\pi} \frac{u^2}{(u^2+\omega^2)} \frac{d\ln u}{\left[2\cos\frac{n\pi}{2} + \left(\frac{u}{u_o}\right)^n + \left(\frac{u}{u_o}\right)^{-n}\right]}$$

$$= \frac{1}{2\pi i}\int_0^\infty \frac{dv}{v+\left(\frac{\omega}{u_o}\right)^2}\left[\frac{1}{1+(ve^{-i\pi})^{\frac{n}{2}}} - \frac{1}{1+(ve^{i\pi})^{\frac{n}{2}}}\right] = \frac{u_o^n}{\omega^n + u_o^n} \qquad (2.4.98)$$

Note that the operation involved in transducing the terminal equality of (2.4.98) is the inverstion of a Stieltje transform (cf. (f), earlier). Figure 2.21 shows the excellent straight line obtained in the rectification of dynamic data obtained for glass-bead filled polyurethane binders[2.9].

The associated expressions for E_{rel}, σ_{tens}, E'', $L(t)$, and D_{crp} involve quadratures which cannot be reduced to simpler analytical representations. Thus, also the Cole distribution provides an excellent representation of dynamic compliance data, although it does not lend itself to generating simple associated representations. For this reason, more attention was paid to the more tractable smoothed power law.

2.5 Temperature-time Shift Phenomena.

Up to this point, little or nothing has been said about the effect of temperature upon viscoelastic processes represented by tensile, creep, relaxation, and dynamic data. In order to gain insight into the mechanism by which temperature influences viscous processes, let us examine a typical creep data obtained on a polyurethane binder filled with 60% ammonium perchlorate (Figure 2.22), in which compliance is plotted versus time on log-log coordinates for various temper-

atures. Note that the individual curves suggest that a displacement along the absicissa in the appropriate direction will bring any two into conjunction. This is equivalent to stating that the curves obtained at the higher temperatures can be brought into conjunction with the one obtained at the lowest temperature merely by dividing their time scales by a set of fractional numbers, one for each temperature. The resulting master curve is shown in Figure 2.23. The associated temperature dependence of this shift factor for each curve, according to its temperature, is given in Figure 2.24.

This so-called superposition process has been shown to hold for many types of viscoelastic data. It reveals itself, for example, in the dynamic data of Landel[2.9] used in Figure 2.21. It was first used by Tobolsky in reducing relaxation data[2.10], and since then has been used by many authors, notably T. L. Smith, who has reduced ultimate stress and strain data from GRS rubber[2.11]. Workers in the solid propellant field have also applied this scheme to the ultimate stress and strain properties of various propellants and Figures 2.25, 2.26, and 2.27 show such typical data for a polyurethane, a polybutadiene-acrylic acid, and a plastisol binder, respectively.

The fact that this scheme works so well for polymeric materials suggests that there is something rather simple in the nature of flow processes of polymer molecules. It was first shown by Leaderman[2.12] that the solution viscosity of polymer molecules above a certain minimum chain length is independent of chain length and dependent only on temperature. Secondly, it was shown by Rouse[2.13] that the distribution of relaxation times governing solution viscosity is strictly a function of chain length distribution. Zimm[2.14] then extended these statements to bulk viscosity. It follows therefore that a given relaxation time, τ_i, characteristic of any one element on a mechanical model, or of the ith flow segment in a polymer chain, must depend separately on temperature and on chain length,

$$\tau_i = A_i f(T) \qquad (2.5.1)$$

where we shall arbitrarily associate the time dimension with the temperature dependent factor.

To understand the implications of (2.5.1), consider the expression which represents the relaxation of a discrete model in uniaxial tension

$$E_{rel.} = E_e + \sum E_i e^{-\frac{t}{\tau_i}} \qquad (2.5.2a)$$

After introducing (2.5.1), we have

$$E_{rel.} = E_e + \sum E_i \, e^{-\left[\frac{t}{f(T)}\right]\left[\frac{1}{A_i}\right]} \qquad (2.5.2b)$$

and, neglecting the linear dependence of the spring or non-flow se[illegible] upon the absolute temperature, it becomes immediately obvious that there will be no change of the relaxation modulus with temperature, providing that the physical time, t, is divided by a temperature dependent shift factor. The behavior is thus reflected solely in a reduced time parameter, t/f(T). This example illustrates the general principle of temperature-time equivalence.

At this point there is some arbitrariness in a precise specification of f(T), and there are various more or less equivalent ways to remove it. The various curves, each at a constant temperature, may be shifted so as to coincide with any one other curve, having its associated temperature, say T_{ref}. This is equivalent to saying that after the curves are all superimposed, a shift bodily one way or the other over the temperature range of interest (-60°F to +160°F) does not affect their superposing into the same curve. Furthermore, one may proceed to divide the physical time by the arbitrarily selected shift factors to obtain the reduced time plot versus t/f(T), anticipated from (2.5.2). Depending now upon how the scale of the abscissae is fixed, one can obtain different characterizations of the reduced time parameter which affects the convenience of data presentation.

One such convenient representation stems from Tobolsky's[2.10] suggestion that a good analytical representation of relaxation data may be obtained using the fact that a plot on probability paper of

$$\frac{\log E_{rel.} - \log E_e}{\log E_g - \log E_e} \quad \text{vs.} \quad \log \frac{t}{K(T)}$$

yields the straight line

$$\frac{\log E_{rel.} - \log E_e}{\log E_g - \log E_e} = \frac{1}{2}\left[1 - \operatorname{erf}\left(h \log \frac{t}{K(T)}\right)\right] \qquad (2.5.3a)$$

where K(T) is taken to be that value of f(T) at which t/f(T) equals unity. The value of h is the reciprocal of $\sqrt{2}$ times the standard deviation and for most polymers is of the order of 0.4. With this provision, t/K(T) = 1 corresponds to the inflection in the relaxation curve at which point

$$\left.\frac{\log E_{rel.} - \log E_e}{\log E_g - \log E_e}\right|_{\frac{t}{K}=1} = \frac{1}{2} \qquad (2.5.3b)$$

In other words, at the inflection point the relaxation modulus assumes its geometric mean value

$$\bar{E}_{rel.} = \sqrt{E_g E_e} \qquad (2.5.4)$$

Tobolsky has furthermore shown that at this particular value the shift factor where $t/f(T) = 1$, the curve of $K(T)$ versus T has an inflection point which he specified as the distinctive temperature T_d. This particular value of T_d and $K(T_d) \equiv K_d$ is of no immediate interest to stress analysts, but does have some meaning to rheologists interested in polymer mechanics. As a point of fact, however, T_d is usually not more than $10^{\circ}F$ above the glass transition temperature. Nevertheless, it develops that the portion of the shift factor curve which does concern engineering analysis, generally at temperatures above T_d, can be well approximated by (Figure 2.28)

$$\log \frac{K(T)}{K_d} = \frac{-16(T-T_d)}{100+T-T_d} \qquad (2.5.5)$$

where T is expressed in degrees Fahrenheit. For example, $T_d \simeq -80^{\circ}F$ for an unfilled polyurethane binder and $T_d \simeq 0^{\circ}F$ for one type of polyurethane propellant. The shift factor for most polymeric materials is $K_d \simeq 2$ minutes.

A second convenient representation scheme for reducing data[2.15] casts the shift factor $f(T) \rightarrow a_T$ in terms of a temperature, T_s, which is arbitrarily fixed at $50^{\circ}C$ above the glass transition temperature. In this way one arrives at another near universal temperature dependence for most polymers,

$$\log a_T = \frac{-8.86(T-T_s)}{101.8+T-T_s} \qquad (2.5.6)$$

where T is expressed in degrees Centigrade. The use of this shift factor tends to place the glassy behavior of the relaxation modulus at unit reduced time scale $t/a_T = 1$, whereas the Tobolsky scheme places unit reduced time, $t/K(T)=1$, in the transition region.

Returning now for a moment to the relaxation data, we may now proceed to identify the arbitrary constant, μ_0, in the power law representation of the data. We [illegible] (2.4.85)

$$\frac{E_{rel.}-E_e}{E_g-E_e} = (1+\mu_0 t)^{-n} \qquad (2.5.7)$$

where it is now evident that it can be associated with a temperature shift factor, $\mu_o = 1/f(T)$. Now near the center of the transition region where $E_e \ll E_{rel} \ll E_g$, we have the approximation

$$E_{rel.} \doteq E_g (\mu_o t)^{-n} \tag{2.5.8}$$

On the other hand, when the argument of the error function in (2.5.3) is near unity, which implies $1/30 < K < 30$, we have the approximation

$$\frac{\log E_{rel.} - \log E_e}{\log E_g - \log E_e} \doteq \frac{1}{2}\left[1 - \frac{2h}{\sqrt{\pi}} \log \frac{t}{K(T)}\right]$$

and thus

$$E_{rel.} \doteq \sqrt{E_e E_g}\left(\frac{t}{K}\right)^{-\frac{h}{\sqrt{\pi}} \log \frac{E_g}{E_e}} \tag{2.5.9}$$

A comparison of (2.5.8) and (2.5.9) indicates that the log-log slope similarity requires

$$n = \frac{h}{\sqrt{\pi}} \log \frac{E_g}{E_e} \tag{2.5.10}$$

and for $t \to K$, the relaxation moduli will be the same if

$$E_g [\mu_o K(T)]^{-n} = \sqrt{E_g E_e}$$

or

$$\mu_o(T) = \frac{(E_g/E_e)^{\frac{1}{2n}}}{K(T)} \tag{2.5.11}$$

which thus specifically identifies the heretofore arbitrary constant.

Note that since $\log (E_g/E_e)$ is approximately three for most unfilled polymeric materials, it follows from (2.5.10) and $h \simeq 0.4$ that $n \simeq 0.7$, whereas in filled materials $\log (E_g/E_e) \simeq 2$, then $n \simeq 0.5$. These values have been generally substantiated.

In conclusion, it may be remarked that the existence of a temperature-time shift correlation is important in making an engineering analysis. Under certain conditions to be discussed more fully in the following section, it is possible to make some progress in answering the question: At what temperatures and loading times will it be sufficiently accurate to treat the propellant material as essentially elastic, allowing possibly for a linear variation of the spring or non-flow elastic glassy or rubbery moduli with temperature, and when must the full viscoelastic analysis be employed. This problem becomes particularly difficult when combined heat flow rates and mechanical loading rates result in strain rates falling within the transition region.

2.6 Mechanical Property Determination

We shall discuss in this section what might be called the minimum amount of information needed to calculate viscoelastic stresses and strains in complex geometries, for which the temperature is spacewise and timewise constant. First, the minimum test requirements will be reviewed, and then we shall show how data obtained from these tests can be used to determine model parameters, i.e. the constants in the operational moduli or compliances. The previous Section 2.4 dealt with the problem of determining operator equations which represent actual material response quite accurately over the entire time or frequency scale through the use of distribution functions. However, we shall restrict outselves here to simple finite element models which are capable of representing actual behavior over only a limited time or frequency scale. It will be shown later in the Engineering Analysis, Section 3.2, that the stress analysis is often greatly simplified if it is possible to use an approximate model with only a few elements--usually no more than four or five. These models will probably be sufficient for calculation of strains induced by ignition pressures; however, it is not clear at the present time that they are adequate for the long-time environmental slump problem. Indeed, with the inclusion of temperature variations, the complete distribution function may be needed (or some other equivalent method of representing the stress-strain behavior over the entire time scale, such as using convolution type integrals with relaxation moduli[2.16]). At this stage, however, convenient analysis techniques have not been developed which can be applied to this long-time thermal problem. Therefore, model fitting methods will be discussed here which are directly applicable to the short-time ignition problem.

2.6.1 Minimum test requirements

The determination of mechanical properties for standard engineering metals has been reduced to more or less of a standard procedure where reference may be made to various publications of the American Society for Testing Materials (ASTM). Without attempting to infer that these tests are always simple, common usage has caused them to become well known and standardized. It is customary to determine the Young's modulus from the slope of the stress-strain curve and Poisson's ratio by orthogonal strain gage measurements on a tensile specimen. Viscoelastic materials, and rubbers in particular, are characterized by relative softness and large extensions before fracture. In the first place, normal strain measuring devices such as wire resistance gages and mechanical extensometers do not work. Second, the large extensions also usually exceed the range of common indicators. For this

reason, optical tracking of bench marks or crystals and the use of birefringent coatings has frequently been employed, although data reduction and analysis is further complicated by the necessity to accumulate time histories of the stress and strain.

For these and other reasons the customary test used in deducing propellant properties is a uniaxial tensile specimen stretched in a controlled displacement machine which simultaneously records the applied force. The standardized specimen is shown in Figure 2.29. From these remarks it is seen that the basic data is thus force and displacement. The former can be easily converted to stress by dividing by initial cross sectional area, A_o, for small strains or the local area, A, if the strains are large, providing the Poisson's ratio is known. In the case of uniaxial tensile specimens, the transverse strains, $\epsilon_x = \epsilon_y = -\nu\epsilon_z$, can be used to compute the local cross sectional area as $A = A_o(1+\epsilon_x)^2 = A_o(1-\nu\epsilon_z)^2$, from which the true stress, $\bar{\sigma}$, becomes

$$\bar{\sigma} = \frac{P}{A_o(1-\nu\epsilon_z)^2} = \frac{\sigma}{(1-\nu\epsilon_z)^2}$$

For most propellants, it is often permissible to assume incompressibility ($\nu = \frac{1}{2}$) in which the true stress for non-infinitesimal strains becomes

$$\bar{\sigma} = \frac{\sigma}{(1-\frac{1}{2}\epsilon_z)^2} \cong \frac{\sigma}{1-\epsilon_z} \cong \sigma(1+\epsilon_z) = \sigma\lambda_z$$

where the definition of extension ratio $\lambda = 1 + \epsilon$ has been used.

The determination of the local strain corresponding to the calculated stress however is another matter in the absence of direct measurement. If the elongation measured during the test is divided by the nominal gage length of two inches (see Figure 2.29), a poor determination of strain is deduced because it has been found that there is a flow of material in from the jaw area which tends to increase the gage length to an effective length of approximately 2.7 inches. In addition, there is the viscous deformations contributed by the flow near the jaws which tends to confuse the accuracy. Some recent work incorporating square flat ended specimens bonded to metal plates has been reported[2.17] which may tend to eliminate much of the effective gage length controversy, providing satisfactory bonds can be made for all the propellants of interest.

For the time being however, unfortunate as it may be, the analyst will generally have at his disposal only force-displacement data to work with, from which a nominal or true stress-strain curve is deduced. Of course, when more accurate data becomes available, it should be utilized for determining the mechanical properties.

One other preliminary point must be covered. It has been mentioned that the various operator equations, with certain physical restrictions, may be used to represent either bulk (dilitation) or shear (distortion) behavior. As a practical matter, at the present state of the art, it is usually sufficient to assume the propellant to be incompressible, or at most elastic. In either case, whether the bulk modulus $K \to \infty$ or K is finite, the dilitation behavior is non-viscoelastic by assumption. Hence, only the determination of a viscoelastic operator in distortion, $\mu(p)$ (or its inverse J(p)), or in simple tension, E(p) (or its inverse D(p)) is required, along with perhaps measuring the elastic bulk modulus. If this assumption is adopted, any test which yields $\mu(p)$ or E(p), will suffice. In particular, if $K \to \infty$ or is even large compared to the shear modulus, (2.2.9) indicates that $\mu(p) = E(p)/3$ so that the tensile test is sufficient to deduce the desired properties.

By way of review, then, the present minimum requirements call for:

1. Measuring an elastic bulk modulus, or assuming incompressibility ($K = \infty$); and
2. Measuring the uniaxial viscoelastic tensile modulus, using the best available stress-strain measurements in order to determine the shear characteristics of the propellant.

Even though the simple relaxation test is the one most commonly used, data obtained from this test is not necessarily the easiest to use for model fitting and stress analysis. But the data which often fits most naturally into well-established techniques, and is most accurate with small strains, is procured from dynamic tests*: namely, measurement of displacement (or load) when a steady-state sinusoidal load (or displacement) is applied to a specimen in simple tension or shear. We shall not consider the details of this test, or others, since comprehensive presentations of viscoelastic testing methods can be found in the literature, especially reference (2.18). However, if one does not have dynamic data available, it is possible, in principle, to calculate the dynamic modulus or compliance from other tests by using the appropriate expressions given in Section 2.4. This procedure will probably yield less accurate results than obtained through direct dynamic measurement, but the advantages of Fourier analysis methods which can be used with dynamic data may be sufficient to warrant this data conversion.

---

* It will be seen later in this section that a simple graphical scheme can be used with dynamic data to determine the parameters in a four-element model. Also in Section 3, it will be shown that dynamic data can be used directly in the Fourier inversion integral to calculate strains and stresses, wherein neither an analytical representation of the data nor models are needed.

We shall now consider some specific methods that can be used to determine the spring and dashpot constants in simple models from relaxation and dynamic data.

2.6.2 Fitting simple models to relaxation data.

As we shall presently show, the response of simple models can be made to agree closely with experimental data only over a very limited portion of the time scale, so that it is necessary to first specify this time interval. This is dictated by the loading time history (and the temperature of the body) assigned to the particular stress analysis problem. For example, if it is desired to determine a model for the calculation of stresses in a grain induced by ignition pressures, then one would assume a time, say t_f, beyond which failure is not expected. Model parameters would then be found by curve fitting model relaxation response (or creep response) to experimental values over the time interval, $0 \leq t \leq t_f$*.

---

* The material in a pressurized grain is not strained step-wise in time, but generally has a strain-time history which is not only quite different from that realized in a relaxation test, but also it varies from point to point in the grain; hence, it is not obvious that a good fit of model relaxation behavior for $0 \leq t \leq t_f$ implies a good approximation to ignition response for the same time interval. However, that it does, follows from the fact that stress response to arbitrary straining can be written in terms of an integral of the relaxation modulus. This representation can be derived very easily with transform theory. Assuming zero initial conditions, the transformed stress-strain law is

$$\bar{\sigma}(p) = m(p)\bar{\epsilon}(p) \qquad \text{(a)}$$

which can also be written in terms of the transformed relaxation modulus $\bar{m}_{rel}(p) = m(p)/p$,

$$\bar{\sigma}(p) = \bar{m}_{rel.}(p)\, p\bar{\epsilon}(p) \qquad \text{(b)}$$

This is inverted for arbitrary straining by using the well-known convolution theorem, which yields

$$\sigma(t) = \int_0^t m_{rel.}(t-\xi)\frac{d\epsilon(\xi)}{d\xi}\,d\xi \qquad \text{(c)}$$

This is also known as the Duhamel representation of the viscoelastic stress-strain law. It is clear from (c) that knowledge of the relaxation modulus for $0 \leq t \leq t_f$ completely specifies the stress-strain behavior over the same time interval.

As a simple example, let us now fit a two-element Maxwell model (Figure 2.6) over an interval $0 \leq t \leq t_f$ by matching its tensile relaxation modulus to experimental values E(t) at two intermediate times, t_1 and t_2. The two-parameter system with material constants E_m and τ_m yields

$$E(t_1) \equiv E_1 = E_m e^{-\frac{t_1}{\tau_m}} \qquad (2.6.1)$$

$$E(t_2) \equiv E_2 = E_m e^{-\frac{t_2}{\tau_m}} \qquad (2.6.2)$$

from which it is easy to calculate that

$$\tau_m = (t_2 - t_1) \ln \frac{E_1}{E_2} \qquad (2.6.3)$$

$$E_m = E_1 \exp\left[t_1 \ln\left(\frac{E_1}{E_2}\right)/(t_2 - t_1)\right] \qquad (2.6.4)$$

so that the tensile stress-strain relation becomes

$$\frac{1}{E_1 \exp\left[t_1 \ln\left(\frac{E_1}{E_2}\right)/(t_2 - t_1)\right]}\left[\frac{d\sigma(t)}{dt} + \frac{\ln \frac{E_1}{E_2}}{t_2 - t_1}\sigma(t)\right] = \frac{d\epsilon(t)}{dt} \qquad (2.6.5a)$$

and the operational Young's modulus is

$$E(p) = \frac{E_1 \exp\left[t_1 \ln\left(\frac{E_1}{E_2}\right)/(t_2 - t_1)\right] p}{\left[p + \ln\left(\frac{E_1}{E_2}\right)/(t_2 - t_1)\right]} \qquad (2.6.5b)$$

If the range 0 to t_f is excessive, the fit will not be good and additional elements must be added.

This collocation procedure is straightforward, but rapidly becomes algebraically complicated with an increasing number of elements because of the transcendental character of the simultaneous equations. Other procedures could be used, such as minimizing the square error between model and experimental relaxation moduli, but one still has to solve transcendental equations to determine the parameters. Nevertheless, in order to illustrate the difference between simple model response and experimental data, and to show the effect of adding elements, we shall compare the relaxation moduli of three and five element models to experimental data (represented analytically by means of the distribution function for the Wiechert model). The material used is polyisobutylene (PIB) whose relaxation spectrum in tension can

be represented quite well by a modified power law for the glass-to-rubber transition region[2.19]*.

$$H(\tau) = \frac{E_g - E_e}{\Gamma(n)} \left(\frac{\tau_o}{\tau}\right)^n e^{-\frac{\tau_o}{\tau}} \qquad (2.6.6)$$

where $n = 0.68$, and τ_o is a known reference constant. The relaxation modulus corresponding to this distribution function is (see equation 2.4.83)

$$E_{rel_u}(t) = E_e + (E_g - E_e)\left(1 + \frac{t}{\tau_o}\right)^{-n} \qquad (2.6.7)$$

The relaxation modulus for the three-element model is, from Figure 2.7

$$E_{rel_3}(t) = E_e + (E_g - E_e) e^{-\frac{t}{\tau_a}} \qquad (2.6.8)$$

and for the five element, Figure 2.8, is

$$E_{rel_5}(t) = E_e + E_1 e^{-\frac{t}{\tau_1}} + (E_g - E_1 - E_e) e^{-\frac{t}{\tau_2}} \qquad (2.6.9)$$

The comparison shown in Figure 2.30 is presented assuming that the glassy modulus, E_g, is the same for all the models, and further that $E_e \ll E_g$. This latter assumption allows us to neglect E_e/E_g in the foregoing expressions as long as we consider only the short time response. The arbitrary parameters of the three and five element models (which are reduced to two and four element models by neglecting E_e/E_g) were chosen in order to fit the polyisobutylene modulus for $0 \leq t/\tau_o \leq 10$. The particular values used are

$$\frac{1}{\tau_a} = \frac{0.30}{\tau_o}\ , \quad \frac{1}{\tau_1} = \frac{2.11}{\tau_o}\ , \quad \frac{1}{\tau_2} = \frac{0.20}{\tau_o}\ , \quad \frac{E_1}{E_g} = 0.25 \qquad (2.6.10)$$

---

* Polyisobutylene is uncross-linked, so that it does not have a true equilibrium modulus. However, molecular entanglements provide an apparent equilibrium modulus which maintains a relatively constant stress for some time after the stress has relaxed from its initial glassy value. But after a sufficient amount of time elapses (this time depends on the molecular weight) the stress again falls off and approaches zero. Thus, the value E_e in (2.6.6) represents this apparent equilibrium modulus. But we shall later neglect E_e when fitting models to the very short time relaxation modulus since $E_e/E_g \ll 1$.

Stresses in a constant strain rate test are also compared in Figure 2.30. The pertinent equations, obtained from Figures 2.9, 2.7d, and 2.8d are:

$$\text{Wiechert:}\quad \frac{\sigma}{RE_g\tau_o} = \frac{1}{\beta-1} + \frac{\left(1+\frac{t}{\tau_o}\right)^{1-\beta}}{1-\beta} \qquad (2.6.11)$$

$$\text{Three element:}\quad \frac{\sigma}{RE_g\tau_m} = \frac{t}{\tau_m}\cdot\frac{E_e}{E_g} + \left(1-\frac{E_e}{E_g}\right)\left(1-e^{-\frac{t}{\tau_m}}\right) \qquad (2.6.12)$$

$$\text{Five element:}\quad \frac{\sigma}{RE_g\tau_1} = \frac{t}{\tau_1}\cdot\frac{E_e}{E_g} + \frac{E_1}{E_g}\left(1-e^{-\frac{t}{\tau_1}}\right) + \frac{\tau_2}{\tau_1}\left(1-\frac{E_1}{E_g}-\frac{E_e}{E_g}\right)\left(1-e^{-\frac{t}{\tau_2}}\right) \qquad (2.6.13)$$

The comparison clearly shows that a few elements are insufficient to describe the behavior of PIB over a broad time scale; such a conclusion has also been found to apply to propellants.

Now that the model parameters (2.6.10) are specified, we are in a position to make a viscoelastic stress analysis by using the operational modulus of either the two or four element models (we have neglected E_e for short time response). If it has been determined that it is necessary to take $t_f = 10\ \tau_o$, for example, then four elements will probably suffice; if the stress analysis is made using only the Maxwell model, large errors may be introduced in the solution due to the poor fit shown in Figure 2.30. On the other hand, if we take $t_f = 20\ \tau_o$, then it is not clear that even four elements are enough to obtain a reasonably accurate solution. In view of this uncertainty regarding the error, as well as not knowing a priori which portions of the relaxation curve should be weighted most heavily in fitting the models, we will present another method which does not contain these shortcomings, and which makes use of the more accurate dynamic data.

2.6.3 Fitting simple models to dynamic data.

Spectral analysis of the loading. - A method employing the complex frequency dependent moduli or compliances has been proposed by Lee[2.20] for fitting the data, which we shall illustrate by applying it to the grain ignition problem. As the response of finite-element models can be made to correspond approximately to actual behavior only over a narrow frequency band, it is first necessary to determine the range of interest by making a Fourier analysis of the loading function. The example will eventually be carried through to the calculation of strains in a pressurized case-bonded grain. At this point, however, only the characteristics of the pressure loading need be defined; the geometry will not enter in until after model parameters are calculated.

A pressure pulse is transient rather than periodic so that it cannot be represented exactly by a series of discrete frequency components; rather it must be given by a Fourier integral in which frequency is a continuous variable. Nevertheless, for practical purposes, it is sufficient to consider the grain to be loaded by periodic pulses spaced far enough apart that most of the strain introduced by one pulse relaxes out before the next one is applied. Clearly, then, the response to each of the widely separated pulses is very nearly the same as for the transient load. Consequently the important frequencies in a transient pulse can be determined if we consider not only the time scale of interest in regard to the possibility of mechanical failure, but also the viscous properties of the propellant.

For our example, it will be assumed that pressure $p_i(t)$ increases linearly with time from $p_i = 0$ to $p_i = p_o$ at $t = t_1$, and then remains constant. In addition we will assume that from the standpoint of failure, response only up to $t = 3t_1 = t_f$ need be considered. Thus, the periodic function shown in Figure 2.31 will be used in the analysis. Symmetrical waves are indicated since they lead to a simpler series than obtained if the pressure is removed instantaneously. The number of terms required to represent the function sufficiently well by a finite Fourier series will now be found. We have chosen the ratio of root mean square error between the series $s_m(t)$ and the exact function $p_i(t)$ to the pressure averaged over its time of application as a criterion of accuracy. This is indicated by α_m in the figure. α_m can be calculated quite readily as a function of t_1/T_F and m by the relation (2.21):

$$\frac{1}{T}\int_0^T \left[P_i(t) - S_m(t)\right]^2 dt = \frac{1}{T}\int_0^T P_i^2(t)\,dt - \frac{1}{2}\sum_{n=1,3,\cdots}^{m} a_n^2 \qquad (2.6.14)$$

where a_n are the Fourier coefficients in the cosine series

$$S_m(t) = \sum_{n=1,3,\cdots}^{m} a_n \cos\frac{2n\pi t}{T_F}$$

where

$$a_n = \frac{4P_o T_F}{\pi^2 t_1}\frac{1}{n^2}\sin\frac{n\pi t_1}{T_F}\sin\frac{3n\pi t_1}{T_F}$$

From symmetry, (2.6.14) can be written as

$$\frac{4}{T_F}\int_0^{\frac{T_F}{4}} \left[P_i(t) - S_m(t)\right]^2 dt = \frac{4}{T_F}\int_0^{\frac{T_F}{4}} P_i^2(t)\,dt - \frac{1}{2}\sum_{n=1,3,\cdots}^{m} a_n^2 \qquad (2.6.15)$$

yielding for α_m

$$\alpha_m^2 = \frac{256}{27}\left(\frac{t_1}{T_F}\right)\left[1 - \frac{3}{2\pi^4}\left(\frac{T_F}{t_1}\right)^3 \sum_{n=1,3,\cdots}^{m}\frac{1}{n^4}\sin^2\frac{n\pi t_1}{T_F}\sin^2\frac{3n\pi t_1}{T_F}\right] \qquad (2.6.16)$$

which is plotted in Figure 2.31.

We now choose the value of t_1/T_F such that the time between the end of one pulse and the start of the next is twice the total length of a single pulse ($4t_1$). Subsequently, when the solution to the strain analysis problem is obtained, a check must be made to see if the time between pulses ($8t_1$) is sufficient for most of the strain to relax out. Thus, we take

$$\frac{T_F}{2} = 4t_1 + 8t_1 = 12t_1$$

or

$$\frac{t_1}{T_F} = \frac{1}{24}$$

In addition, we assume that when $\alpha_m \leq 0.05$ the function is given accurately enough by a finite series terminating with $n = m$. From Figure 2.31, we take $m = 13$. The lowest frequency (f) in the series is $f = 1/T_F$, the highest is $f = 13/T_F$. In terms of t_1

$$\frac{1}{24t_1} \leq f \leq \frac{13}{24t_1} \qquad (2.6.17a)$$

A typical value of 0.01 seconds will be used for t_1, so that

$$4 \text{ cps.} \leq f \leq 52. \text{ cps.} \qquad (2.6.17b)$$

Graphical determination of model parameters. - In view of the present lack of appropriate data on propellants, the analysis will be carried out using the dynamic shear data in Figure 2.32, which was obtained by Landel[2.9] and is for NBS polyisobutylene (PIB) filled with 36.7% (vol.) glass beads. This idealized filled material exhibits the same qualitative behavior as a typical composite propellant, so that the results should be very useful in evaluating the model fitting technique when applied to propellants.

The complex compliance is represented in Figure 2.32 by its real and imaginary components as functions of reduced frequency. ω is the frequency in terms of radians per second, while a'_T represents the temperature shift factor which is discussed in Section 2.5*. This factor is defined to be unity at 12.5°C, so that the master curves in Figure 2.32 give the actual complex compliance frequency dependence when the material is at 12.5°C. If the material is at temperatures other than this value, it is necessary to compute the corresponding values of a'_T in order to determine the frequency dependence.

---

* The shift factor is now designated as a'_T, rather than a_T, since the temperature at which it is defined to be unity is not the standard reference temperature (T_s=-23°C for PIB with 36.7% filler). This different normalization was used because the original data was given at 12.5°C. The two shift factors are proportional to each other, with the relation being:

$$a'_T = \frac{a_T(T)}{a_T(12.5°)}$$

For our example, it is desirable to choose the temperature such that PIB responds to pressure with a large time effect. It was found that a temperature of $-35^{\circ}F$ ($a'_T = 10^4$) gives the desired result if $t_1 = 0.01$ seconds. (With a highly filled propellant, the time effect is often quite significant at temperatures on the order of $+40^{\circ}F$ due to the compactness of the filler).

The frequency shift, being exponential in temperature, is much more important than the linear shift in the ordinate indicated in reference 2.9; so for simplicity we will consider only the effect of temperature on the frequency scale given by a'_T. This allows us to use the master curve drawn at $12.5^{\circ}C$ directly for $-35^{\circ}F$ because

$$\text{Log } \omega = \text{Log } \omega a'_T - \text{Log } a'_T = \text{Log } \omega a'_T - 4 \qquad (2.6.18)$$

That is, by subtracting four from the abscissa values, the actual compliance frequency curve is obtained for use in the example. Since frequency on the master curve is in terms of radians, it will be convenient to express the frequency range given in (2.6.17) in terms of $\omega = 2\pi f$:

$$1.4 \leq \text{Log } \omega \leq 2.5$$

or

$$5.4 \leq \text{Log } \omega a'_T \leq 6.5 \qquad (2.6.19)$$

Now that the frequency range of interest and temperature are specified, the model parameters can be determined using a method described by Bland and Lee[2.22] It is shown in their paper that a simple graphical scheme may be used if the model contains no more than four elements; i.e. two dashpots and two springs. Therefore we will use the four-element model in Figure 2.13a and, as special cases, the two-element Voigt and Maxwell models in Figure 2.11. It should be remarked that the models can often be chosen independently of whether the material is cross-linked or uncross-linked. It will be recalled that an uncross-linked polymer strains indefinitely under a constant load; and that, in principle, this should be accounted for by a free dashpot such as in Figure 2.11b. However, when the frequency band does not include $\omega = 0$ such behavior does not appear. In addition, if the material is enclosed in a case under constant internal pressure, unlimited ... prohibited due to the presence of a bulk modulus which causes the strain to approach a definite limiting value.

The complex compliance of the four-element model is obtained from Figure 2.13a; however shear behavior is to be represented by the model so we let $k \to J$ and write the real and imaginary components as

$$J'(\omega) = J_g + \frac{J_1}{\omega^2\tau_1^2+1} \tag{2.6.20}$$

$$J''(\omega) = \frac{1}{\omega\eta} + \frac{\omega\tau_1 J_1}{\omega^2\tau_1^2+1} \tag{2.6.21}$$

In order to make a strain analysis of a case-bonded grain, it is usually necessary to know two different moduli or compliances. Thus, in addition to the complex shear compliance, the bulk modulus K will be used. A reasonable assumption is that bulk response is elastic so that K is constant. A typical value for K is 2×10^6 psi or 13.8×10^{10} dynes/cm^2. With this in mind, it will be convenient to consider the nondimensional compliance KJ^*. Defining

$$\begin{gathered}\phi'(\omega) = KJ'(\omega), \quad \phi''(\omega) = KJ''(\omega) \\ B_g = KJ_g, \quad B_1 = KJ_1, \quad B_2 = \frac{K\tau_1}{\eta}\end{gathered} \tag{2.6.22}$$

the compliances (2.6.20) and (2.6.21) become

$$\phi'(\omega) = B_g + \frac{B_1}{\omega^2\tau_1^2+1} \tag{2.6.23}$$

$$\phi''(\omega) = \frac{B_2}{\omega\tau_1} + \frac{B_1\omega\tau_1}{\omega^2\tau_1^2+1} \tag{2.6.24}$$

ϕ' and ϕ'' can be combined to yield

$$\omega\,\phi''(\omega) = -\frac{1}{\tau_1}\phi'(\omega) + \frac{B_1+B_2+B_g}{\tau_1} \tag{2.6.25}$$

which is the equation of a straight line if $\omega\,\phi''(\omega)$ is plotted against $\phi'(\omega)$. The slope is $-1/\tau_1$ and the intercept on the $\omega\,\phi''(\omega)$ axis is $(B_1 + B_2 + B_g)/\tau_1$. Hence by plotting the experimental data of Figure 2.32 using $\omega\,\phi''$ and ϕ' as coordinates, the model parameters τ_1 and $B_1 + B_2 + B_g$ are determined by a best straight line fit in the previously estimated frequency band. This is done in Figure 2.33, and the parameters are found graphically to be

$$B_1 + B_2 + B_g = 66$$
$$\tau_1 = 0.925 \times 10^{-2} \text{ sec.}$$

Now that τ_1 is known, it can be used to plot experimental values of ϕ' against $(\omega^2\tau_1^2 + 1)^{-1}$. It is seen from equation (2.6.23) that the four element model is again represented by a straight line, but now with slope B_1 and with B_g as the ϕ' intercept. Carrying out this, we find from Figure 2.34 that $B_1 = 50$, $B_g = 6.5$, and $B_2 = 9.5$.

The parameters in the two-element models of Figure 2.11 will now be determined. In terms of shear behavior, the complex compliance for the Voigt model is given by

$$J'(\omega) = \frac{J_v}{\omega^2 \tau_v^2 + 1} \tag{2.6.26}$$

$$J''(\omega) = \frac{\omega \tau_v J_v}{\omega^2 \tau_v^2 + 1} \tag{2.6.27}$$

Defining

$$\phi'(\omega) = K J'(\omega), \quad \phi''(\omega) = K J''(\omega), \quad B_v = K J_v \tag{2.6.28}$$

the nondimensional compliances for the Voigt model are

$$\phi'(\omega) = \frac{B_v}{\omega^2 \tau_v^2 + 1} \tag{2.6.29}$$

$$\phi''(\omega) = \frac{\omega \tau_v B_v}{\omega^2 \tau_v^2 + 1} \tag{2.6.30}$$

These are the same as ϕ' and ϕ'' for the four-element model if we set $B_2 = B_g = 0$, $B_v = B_1$, and $\tau_v = \tau_1$. Thus, the straight line equation (2.6.25) reduces to

$$\omega \phi''(\omega) = -\frac{1}{\tau_v} \phi'(\omega) + \frac{B_v}{\tau_v} \tag{2.6.31}$$

B_v and τ_v are given immediately from Figure 2.33 as

$$B_v = 66 \quad , \quad \tau_v = 0.925 \times 10^{-2} \text{ sec.}$$

Figure 2.11 provides us with the complex compliance of the Maxwell model

$$\phi'(\omega) = B_m \tag{2.6.32}$$

$$\phi''(\omega) = \frac{1}{\omega B} \tag{2.6.33}$$

where

$$\phi'(\omega) = K J'(\omega), \quad \phi''(\omega) = K J''(\omega), \quad B_m = K J_m, \quad \frac{1}{B} = \frac{K J_m}{\tau_m} \tag{2.6.34}$$

B_m and B are determined numerically such that ϕ' and ϕ'' take on the experimental values approximately half-way between the frequency limits, indicated in Figure 2.33. as

$$B_m = 30 \quad , \quad B = \frac{1}{3200} = 0.312 \times 10^{-3} \text{ sec.}$$

The four element model can be reduced immediately to the three element model in Figure 2.12a by setting $\eta = \infty$, and by definition this requires that $B_2 = 0$ in equations (2.6.23) and (2.6.24). It is observed that with three elements

$$B_1 + B_g = 66$$

and further, from (2.6.23) and (2.6.24) that when $(\omega^2\tau_1^2 + 1) = 1$,

$$B_1 + B_g = 66 = \phi'$$

Reference to Figure 2.34 shows that a straight line passing through $\phi' = 66$ at $(\omega^2\tau_1^2 + 1) = 1$ fits the experimental curve best if the ϕ' intercept is zero. This requires $B_g = 0$, thereby reducing the model to the Voigt. Thus, four elements must be used to obtain a better fit than offered by two which justifies omission of the three-element model in the strain analysis problem.

The nondimensional compliances ϕ' and ϕ'' are plotted in Figure 2.35 for all three models and compared with the experimental data. In addition, the compliances for the four-element model are shown in Figure 2.32 in order to clearly illustrate how the model response compares with the entire experimental master curves. It is interesting to note that both ϕ' and ϕ'' for four elements are reasonably close to the actual response. However, with the Maxwell model, ϕ' is in considerable error, while ϕ'' is somewhat better. Conversely, with the Voigt model, ϕ' is satisfactory while ϕ'' deviates considerably from the experimental values.

In Section 3.2, all three models will be used to carry out a strain analysis of a case-bonded grain in order to compare their respective responses.

REFERENCES

2.1 Biot, M.A.: Theory of Stress-Strain Relations in Anisotropic Viscoelasticity and Relaxation Phenomena. Journal of Applied Physics, Vol. 25, p. 1385, 1954.

2.2 Sokolnikoff, I.S.: Mathematical Theory of Elasticity. Chapter 3, p. 65, McGraw-Hill Book Company, Inc., New York, 1956.

2.3 Eirich, F.R.: Rheology. Vol. I, Chapter 11, 1956, and Vol. II, Chapter 1, 1958. Academic Press, Inc., New York.

2.4 Blizard, R.B.: Viscoelasticity of Rubber. Journal of Applied Physics, Vol. 22, p. 730, 1951.

2.5 Gross, B.: Mathematical Structure of the Theories of Viscoelasticity. Hermann, Paris, 1953.

2.6 Widder, D.V.: Laplace Transform. Princeton University Press, 1941.

2.7 Kronig, R.L. Theory of Dispersion of X-Rays. Optical Society of America, Vol. 12, p. 547, 1926.

2.8 Cole, R.; Davidson, D.W.: Dielectric Relaxation in Glycerin. Journal of Chemical Physics, Vol. 18, p. 1417, 1950.

2.9 Landel, R.F.: The Dynamic Mechanical Properties of a Model Filled System: Polyisobutylene-Glass Beads. Trans. Society of Rheology, Vol. 2, pps 53-75, 1958.

2.10 Tobolsky, A.V.: Stress Relaxation Studies of the Viscoelastic Properties of Polymers. Journal of Applied Physics, Vol. 27, p. 673, July 1956.

2.11 Smith, T.L.: Elastomeric-Binder and Mechanical Property Requirements for Solid Propellants. California Institute of Technology, Jet Propulsion Laboratory Memorandum No. 20-178, January 7, 1959.

2.12 Leaderman, H.; Smith, R.; Jones, R.: Rheology of Polyisobutylene. II. Low Molecular Weight Polymers. Journal of Polymer Science, Vol. 14, p. 47, 1954.

2.13 Rouse, P.; Sittel, K.: Viscoelastic Properties of Dilute Polymer Solutions. Journal of Applied Physics, Vol. 24, p. 690, 1953.

2.14 Zimm, B.: Dynamics of Polymer Molecules in Dilute Solution: Viscoelasticity, Flow Birefringence Dielectric Loss. Journal of Chemical Physics, Vol. 24, p. 269, 1956.

2.15 Williams, M.L.; Landel, R.F.; Ferry, J.D.: The Temperature Dependence of Relaxation Mechanisms in Amorphous Polymers and Other Glass-Forming Liquids. Journal of American Chemical Society, Vol. 77, pps 3701-3707, 1955.

2.16 Hunter, S.C.: Possible Equation to Describe Transient Stress, Strain, and Temperature Fields in Viscoelastic Solids. Brown University Technical Report No. 2, NOrd 18594, January 1960.

2.17 Baldwin, J.B.; Cooper, M.H.: Preliminary Report on a Bonded Tensile Specimen. Bulletin 19th Meeting of JANAF Physical Properties Panel, September 1960. p. 151.

2.18 Eirich, R.F.: Rheology, Vol. II, Chapter 11, Academic Press, Inc., New York, 1958.

2.19 Smith, T.L.: California Institute of Technology, Jet Propulsion Laboratory (Personal communication.)

2.20 Lee, E.H.: Viscoelastic Stress Analysis. Brown University, NR-064-406, July 1958.

2.21 von Karman, T.; Biot, M.A.: Mathematical Methods in Engineering. McGraw-Hill Book Company, Inc., New York, p. 333, 1940.

2.22 Bland, D.R.; Lee, E.H.; On Fitting a Four Element Visco-Elastic Model to Measured Complex Compliance Functions. Brown University, Technical Report No. 13, NOrd 11496, June 1955.

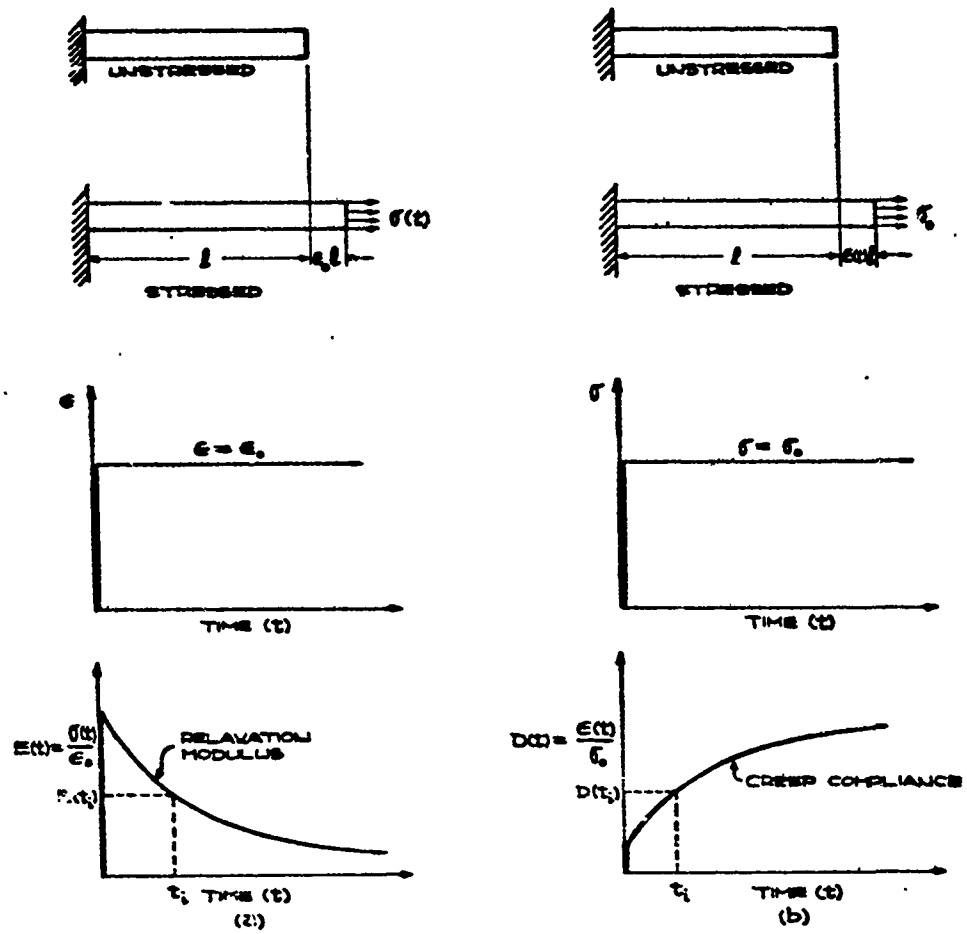

FIG. 2.1. TYPICAL PROPELLANT BEHAVIOR.
(a) RELAXATION TEST
(b) CREEP TEST

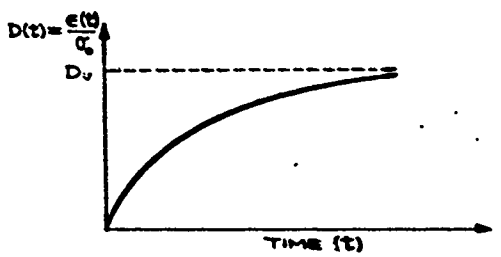

FIG. 2.2. CREEP COMPLIANCE FOR STRESS STRAIN LAW: $\sigma(t) = \left[E_v + \eta_v \frac{d}{dt}\right]\epsilon(t)$

$\sigma = \eta\varepsilon$

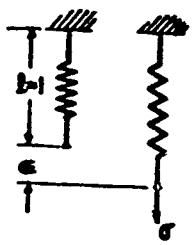

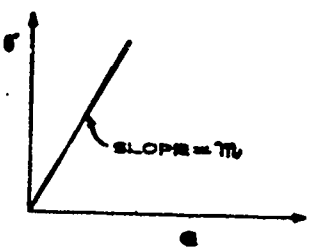

FIG. 2.3. HOOKEAN MODEL

$\sigma = \eta \frac{d\varepsilon}{dt}$

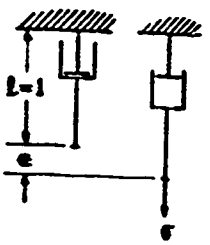

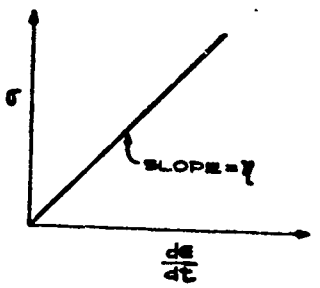

FIG. 2.4. NEWTONIAN MODEL

$\sigma = \sigma_d + \sigma_s$

WHERE $\sigma_d = \eta_v \frac{d\epsilon}{dt}$

$\sigma_s = m_v \epsilon$

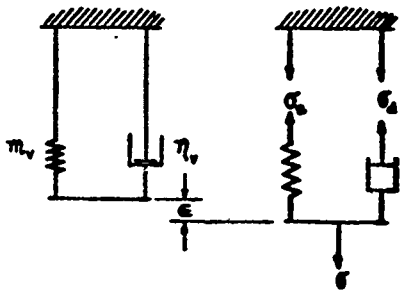

OPERATOR EQUATION:

$$\sigma(t) = \left(\eta_v \frac{d}{dt} + m_v\right)\epsilon(t) = \tau_v m_v \left(\frac{d}{dt} + \frac{1}{\tau_v}\right)\epsilon(t)$$

(a) MODEL

$\sigma = \sigma_0$; $\epsilon(t) = \frac{\sigma_0}{m_v}\left(1 - e^{-\frac{t}{\tau_v}}\right)$: FOR $0 < t \leq t_1$

$\sigma = 0$; $\epsilon(t) = \epsilon_1 e^{-\frac{(t-t_1)}{\tau_v}}$: FOR $t > t_1$

WHERE $\tau_v = \frac{\eta_v}{m_v}$

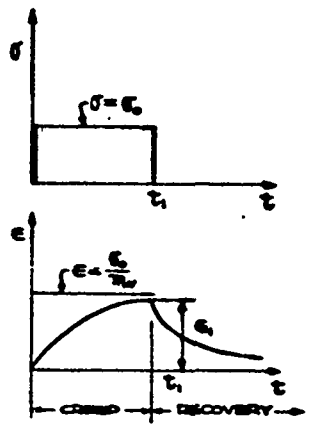

(b) CREEP & RECOVERY

$\epsilon = Rt$ (R = STRAIN RATE)

$\sigma = Rm_v[t + \tau_v]$

(C) CONSTANT STRAIN RATE

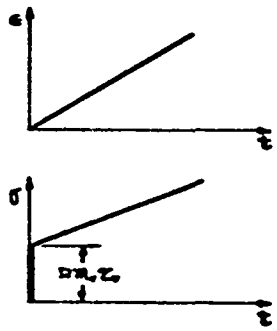

FIG. 2.5. TWO ELEMENT VOIGT MODEL

$$\epsilon = \epsilon_e + \epsilon_d$$

OR $$\frac{d\epsilon}{dt} = \frac{d\epsilon_e}{dt} + \frac{d\epsilon_d}{dt}$$

WHERE $$\frac{d\epsilon_e}{dt} = \frac{1}{m_m}\frac{d\sigma}{dt}$$

$$\frac{d\epsilon_d}{dt} = \frac{1}{\eta_m}\sigma$$

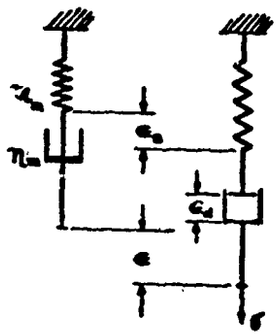

OPERATOR EQUATION:

$$\sigma(t) = m_m \frac{d\epsilon(t)}{dt} \Big/ \left(\frac{d}{dt} + \frac{1}{\tau_m}\right)$$

WHERE $\tau_m = \frac{\eta_m}{m_m}$

(a) MODEL

$\sigma = \sigma_0$; $\epsilon(t) = \frac{\sigma_0}{m_m}\left(1 + \frac{t}{\tau_m}\right)$: FOR $0 < t \le t_1$

$\sigma = 0$; $\epsilon(t) = \frac{\sigma_0}{m_m}\frac{t_1}{\tau_m}$; FOR $t > t_1$

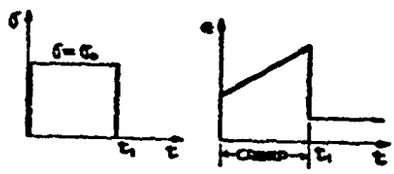

(b) CREEP

$\epsilon = \epsilon_0$; $\sigma(t) = \epsilon_0 m_m e^{-\frac{t}{\tau_m}}$: FOR $t > 0$

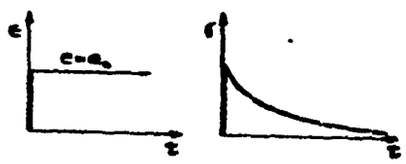

(c) RELAXATION

$\epsilon = Rt$ (R = STRAIN RATE)

$\sigma = R\tau_m m_m (1 - e^{-\frac{t}{\tau_m}})$

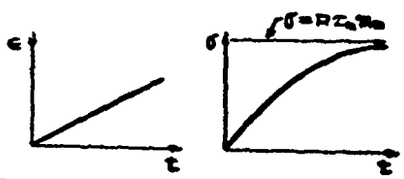

(d) CONSTANT STRAIN RATE

FIG. 2.6. TWO ELEMENT MAXWELL MODEL

$$\epsilon = \epsilon_e + \epsilon_d$$

$$\sigma = \sigma_e + \sigma_m$$

WHERE $\dfrac{d\epsilon_e}{dt} = \dfrac{1}{m_m}\dfrac{d\sigma_m}{dt}$

$$\frac{d\epsilon_d}{dt} = \frac{\sigma_m}{\eta_m}$$

$$\epsilon = \frac{\sigma_e}{m_e}$$

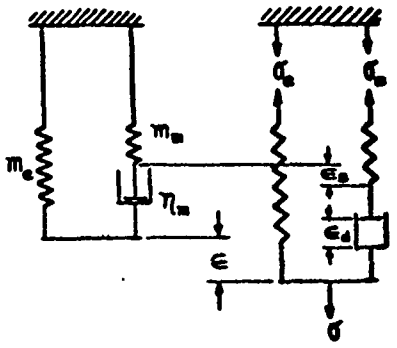

OPERATOR EQUATION:

$$\sigma(t) = \left[m_e + \frac{m_m \frac{d}{dt}}{\left(\frac{d}{dt} + \frac{1}{\tau_m}\right)} \right] \epsilon(t) \quad \text{OR} \quad \sigma(t) = \frac{m_g\left(\frac{d}{dt} + \frac{m_e}{m_g}\frac{1}{\tau_m}\right)}{\left(\frac{d}{dt} + \frac{1}{\tau_m}\right)} \epsilon(t)$$

WHERE $\tau_m = \dfrac{\eta_m}{m_m}$; $\quad m_m + m_e = m_g$

(a) MODEL

$$\epsilon = \left[1 - \left(1 - \frac{m_e}{m_g}\right) e^{-\frac{m_e}{m_g}\frac{t}{\tau_m}}\right] \frac{\sigma_o}{m_e} \quad : \text{FOR } 0 < t \le t_1$$

$$\epsilon = \left[\epsilon_1 - \frac{\sigma_o}{m_g}\right] e^{-\frac{m_e}{m_g}\frac{(t-t_1)}{\tau_m}} \quad : \text{FOR } t > t_1$$

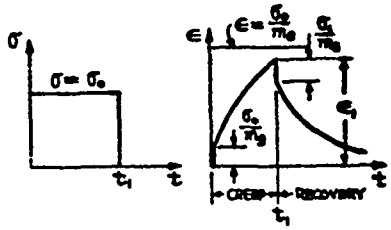

(b) CREEP & RECOVERY

$$\sigma = \left[1 + \left(\frac{m_g}{m_e} - 1\right) e^{-\frac{t}{\tau_m}}\right] m_e \epsilon_o \quad : \text{FOR } t > 0$$

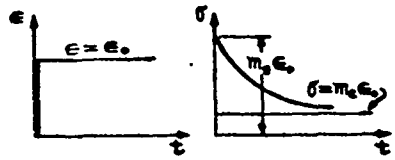

(c) RELAXATION

$$\epsilon = Rt \quad (R = \text{STRAIN RATE})$$

$$\sigma = \left[\frac{t}{\tau_m} + \left(\frac{m_g}{m_e} - 1\right)\left(1 - e^{-\frac{t}{\tau_m}}\right)\right] R m_e \tau_m$$

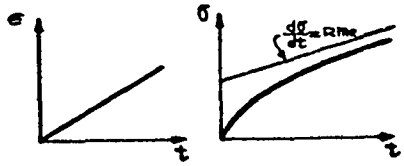

(d) CONSTANT STRAIN RATE

FIG. 2.7. THREE ELEMENT MODEL : MAXWELL + SPRING

$$\epsilon = \epsilon_{e_1} + \epsilon_{d_1} = \epsilon_{e_2} + \epsilon_{d_2}$$

$$\sigma = \sigma_e + \sigma_1 + \sigma_2$$

WHERE

$$\frac{d\epsilon}{dt} = \left[\frac{1}{m_1}\frac{d}{dt} + \frac{1}{\eta_1}\right]\sigma_1$$

$$= \left[\frac{1}{m_2}\frac{d}{dt} + \frac{1}{\eta_2}\right]\sigma_2$$

$$\epsilon = \frac{\sigma_e}{m_e}$$

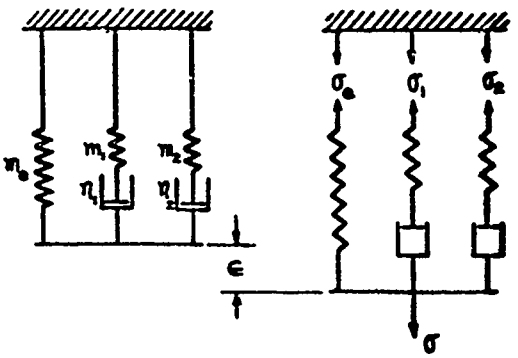

OPERATOR EQUATION:

$$\sigma(t) = \left[m_e + \frac{m_1\frac{d}{dt}}{\left(\frac{d}{dt}+\frac{1}{\tau_1}\right)} + \frac{m_2\frac{d}{dt}}{\left(\frac{d}{dt}+\frac{1}{\tau_2}\right)}\right]\epsilon(t) \text{ OR } \sigma(t) = \frac{m_3\left[\frac{d^2}{dt^2} + \left(\frac{m_e}{m_3}+\frac{m_1}{m_3}+\frac{m_2}{m_3}\right)\frac{d}{dt} + \frac{m_e}{m_3}\right]}{\left[\frac{d^2}{dt^2} + \left(\frac{1}{\tau_1}+\frac{1}{\tau_2}\right)\frac{d}{dt} + \frac{1}{\tau_1\tau_2}\right]}\epsilon(t)$$

WHERE $\tau_1 = \frac{\eta_1}{m_1}$; $\tau_2 = \frac{\eta_2}{m_2}$; $m_3 = m_e + m_1 + m_2$

(a) MODEL

$$\epsilon = \left[\frac{a_0}{\alpha\beta} - \frac{\alpha^2 - a_1\alpha + a_0}{\alpha(\beta-\alpha)}e^{-\alpha t} - \frac{\beta^2 - a_1\beta + a_0}{\beta(\alpha-\beta)}e^{-\beta t}\right]\frac{\sigma_0}{m_3} \text{ : FOR } t>0$$

WHERE

$$a_0 = \frac{1}{\tau_1\tau_2} \; ; \quad a_1 = \frac{1}{\tau_1} + \frac{1}{\tau_2}$$

AND α & β ARE FOUND FROM THE FOLLOWING EQUATIONS:

$$\alpha+\beta = \left[\frac{\frac{m_2}{m_3}+\frac{m_1}{m_3}}{\tau_2} + \frac{\frac{m_e}{m_3}+\frac{m_2}{m_3}}{\tau_1}\right]; \quad \alpha\beta = \frac{\frac{m_2}{m_3}}{\tau_1\tau_2}$$

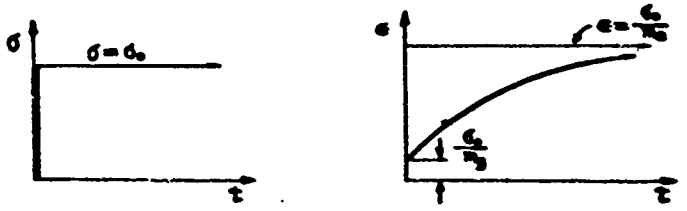

(b) CREEP

FIG. 2.8 FIVE ELEMENT MODEL : TWO MAXWELL ELEMENTS + SPRING

$$\sigma = \left[1 + \frac{m_1}{m_e} e^{-\frac{t}{\tau_1}} + \frac{m_2}{m_e} e^{-\frac{t}{\tau_2}}\right] m_e \epsilon_0 \quad : \text{FOR} \quad t > 0$$

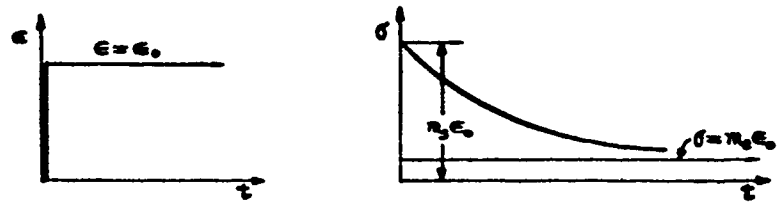

(C) RELAXATION

$$\epsilon = Rt$$

$$\sigma = \left[\frac{t}{\tau_1} + \frac{m_1}{m_e}\left(1 - e^{-\frac{t}{\tau_1}}\right) + \frac{\tau_2}{\tau_1}\frac{m_2}{m_e}\left(1 - e^{-\frac{t}{\tau_2}}\right)\right] R m_e \tau_1$$

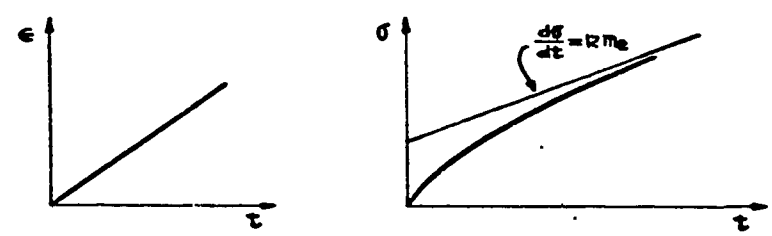

(d) CONSTANT STRAIN RATE

FIG. 2.8. FIVE ELEMENT MODEL : TWO MAXWELL ELEMENTS + SPRING (Continued)

$$\epsilon = \epsilon_{e_i} + \epsilon_{d_i} \qquad (a)$$

$$\sigma = \sigma_e + \sum_{i=1}^{n} \sigma_i \qquad (b)$$

WHERE $$\frac{d\epsilon}{dt} = \left[\frac{1}{m_i}\frac{d}{dt} + \frac{1}{\eta_i}\right]\sigma_i \qquad (c)$$

$$\epsilon = \frac{\sigma_e}{m_e} \qquad (d)$$

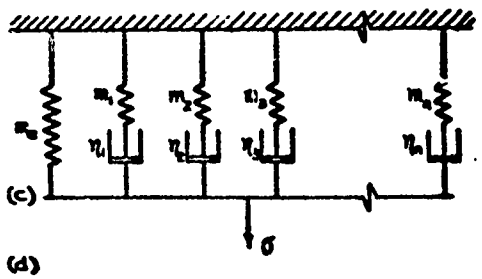

OPERATOR EQUATION:

$$\sigma(t) = \left[m_e + \sum_{i=1}^{n} \frac{m_i}{\left(\frac{d}{dt} + \frac{1}{\tau_i}\right)}\left(\frac{d}{dt}\right)\right]\epsilon(t) \; ; \qquad (e), \text{ USING (c), (d) IN (b).}$$

WHERE $$\tau_i = \frac{\eta_i}{m_i} \; ; \quad m_g - m_e = \sum_{i=1}^{n} m_i \qquad (f)$$

TO OBTAIN INTEGRAL REPRESENTATION, LET

$$m_i = H(\tau_i)\frac{\Delta_i \tau}{\tau_i} \qquad (g)$$

AND TAKE THE LIMIT:

$$\lim_{\substack{n\to\infty \\ \Delta_i\tau\to 0 \\ 0<\tau<\infty}} \sum_{i=1}^{n} \frac{H(\tau_i)\Delta_i\tau}{\left(\frac{d}{dt} + \frac{1}{\tau_i}\right)\tau_i} = \int_0^{\infty} \frac{H(\tau)}{\left(\frac{d}{dt} + \frac{1}{\tau}\right)\tau} d\tau \qquad (h)$$

OPERATOR EQUATION FOR AN INFINITE NUMBER OF ELEMENTS:

$$\sigma(t) = \left[m_e + \int_0^{\infty} \frac{H(\tau)}{\left(\frac{d}{dt} + \frac{1}{\tau}\right)\tau} d\tau \left(\frac{d}{dt}\right)\right]\epsilon(t) \qquad (i)$$

$H(\tau) \equiv$ RELAXATION SPECTRUM

FIG. 2.9. WIECHERT MODEL

RELAXATION:

$\epsilon = \epsilon_0$: FOR $t>0$

$$\sigma(t) = \left[m_e + \int_0^\infty \frac{H(\tau) e^{-\frac{t}{\tau}}}{\tau} d\tau\right] \epsilon_0 \quad , \quad \text{USING FIG. 2.6C FOR } \sigma_t \text{ IN (b), OR SEE FOOTNOTE IN TEXT.}$$

$$\left[m_e + \int_0^\infty \frac{H(\tau) e^{-\frac{t}{\tau}}}{\tau} d\tau\right] \equiv m(t) \equiv \text{RELAXATION MODULUS}$$

WHERE $$m_g - m_e = \int_0^\infty \frac{H(\tau)}{\tau} d\tau$$

BECAUSE THE STRESS RESPONDS TO THE GLASSY MODULUS AT ZERO TIME, I.E. $\sigma(0) = \left[m_e + \int_0^\infty \frac{H(\tau)}{\tau} d\tau\right] \epsilon_0 = m_g \epsilon_0$.

CONSTANT STRAIN RATE:

$\epsilon = Rt$

$$\sigma(t) = \left[m_e t + \int_0^\infty H(\tau)(1 - e^{-\frac{t}{\tau}}) d\tau\right] R$$

DIFFERENTIATING THIS EQUATION WITH RESPECT TO TIME YIELDS:

$$\frac{d\sigma}{dt} = R\, m(t) \qquad \text{OR} \qquad \frac{d\sigma}{d\epsilon} = m\left(\frac{\epsilon}{R}\right)$$

WHERE

σ = STRESS IN CONSTANT STRAIN RATE TEST

FIG. 2.9. WIECHERT MODEL (Continued)

$$\epsilon = \epsilon_g + \sum_{i=1}^{n} \epsilon_i \qquad (a)$$

$$\sigma = \sigma_{s_i} + \sigma_{d_i} \qquad (b)$$

WHERE $\dfrac{d\epsilon_i}{dt} = \phi_i \sigma_{d_i}$ (c)

$$\epsilon_i = k_i \sigma_{s_i} \qquad (d)$$

$$\sigma = \left[\frac{1}{\phi_i}\frac{d}{dt} + \frac{1}{k_i}\right]\epsilon_i \qquad (e)$$

$$\epsilon_g = k_g \sigma \qquad (f)$$

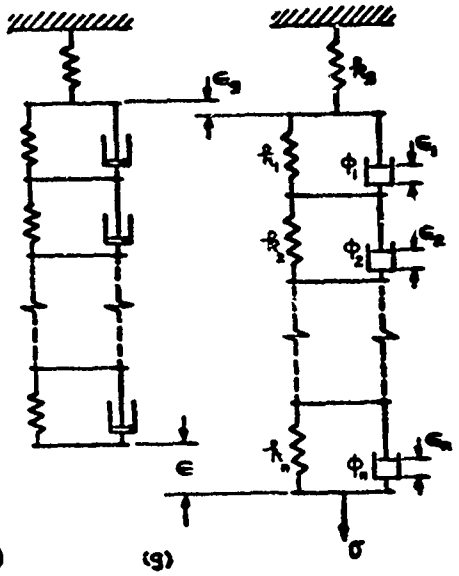

OPERATOR EQUATION:

$$\epsilon(t) = \left[k_g + \sum_{i=1}^{n} \frac{k_i}{\tau_i\left(\frac{d}{dt} + \frac{1}{\tau_i}\right)}\right]\sigma(t) \qquad (g)$$

WHERE $\tau_i = \dfrac{k_i}{\phi_i}$; $k_e - k_g = \sum_{i=1}^{n} k_i$ (h)

TO OBTAIN INTEGRAL REPRESENTATION, LET

$$k_i = L(\tau_i)\frac{\Delta_i \tau}{\tau_i} \qquad (i)$$

AND TAKE THE LIMIT:

$$\lim_{\substack{n\to\infty \\ \Delta_i\tau\to 0 \\ 0<\tau<\infty}} \sum_{i=1}^{n} \frac{L(\tau_i)\Delta_i\tau}{\tau_i\left(\frac{d}{dt} + \frac{1}{\tau_i}\right)\tau_i} = \int_0^\infty \frac{L(\tau)}{\left(\frac{d}{dt} + \frac{1}{\tau}\right)\tau^2}\, d\tau \qquad (j)$$

OPERATOR EQUATION FOR AN INFINITE NUMBER OF ELEMENTS:

$$\epsilon(t) = \left[k_g + \int_0^\infty \frac{L(\tau)}{\left(\frac{d}{dt} + \frac{1}{\tau}\right)\tau^2}\, d\tau\right]\sigma(t) \qquad (k)$$

$L(\tau) \equiv$ RETARDATION SPECTRUM

FIG. 2.10. KELVIN MODEL

CREEP:

$\sigma = \sigma_0$: FOR $t > 0$

$$\epsilon(t) = \left[k_g + \int_0^\infty \frac{L(\tau)(1 - e^{-\frac{t}{\tau}})}{\tau} d\tau \right] \sigma_0$$

$$\left[k_g + \int_0^\infty \frac{L(\tau)(1 - e^{-\frac{t}{\tau}})}{\tau} d\tau \right] \equiv k(t) \equiv \text{CREEP COMPLIANCE}$$

WHERE

$$k_e - k_g = \int_0^\infty \frac{L(\tau)}{\tau} d\tau$$

BECAUSE THE STRAIN RESPONDS TO THE EQUILIBRIUM COMPLIANCE AT INFINITE TIME, I.E. $\epsilon(\infty) = \left[k_g + \int_0^\infty \frac{L(\tau) d\tau}{\tau} \right] \sigma_0 = k_e \sigma_0$

CONSTANT STRESS RATE:

$\sigma = Rt$

$$\epsilon(t) = \left\{ kt + \int_0^\infty L(\tau) \left[\frac{t}{\tau} - (1 - e^{-\frac{t}{\tau}}) \right] d\tau \right\} R$$

DIFFERENTIATING THIS EQUATION WITH RESPECT TO TIME YIELDS:

$$\frac{d\epsilon}{dt} = R k(t) \quad \text{OR} \quad \frac{d\epsilon}{d\sigma} = k\left(\frac{\sigma}{R}\right)$$

WHERE

ϵ = STRAIN IN CONSTANT STRESS RATE TEST

FIG. 2.10. KELVIN MODEL (Continued)

OPERATIONAL COMPLIANCE: $k(p) = \frac{k_v}{\tau_v p + 1}$

COMPLEX COMPLIANCE: $k^*(\omega) = k'(\omega) - i\,k''(\omega)$

$$k'(\omega) = \frac{k_v}{\omega^2 \tau_v^2 + 1}$$

$$k''(\omega) = \frac{\omega \tau_v k_v}{\omega^2 \tau_v^2 + 1}$$

OPERATIONAL MODULUS: $m(p) = m_v(\tau_v p + 1)$

COMPLEX MODULUS: $m^*(\omega) = m' + i\,m''(\omega)$

$$m' = m_v$$

$$m''(\omega) = m_v \tau_v \omega$$

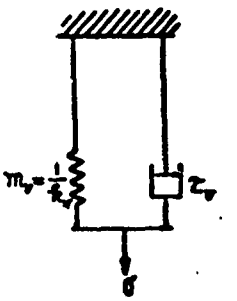

(a) VOIGT MODEL

OPERATIONAL COMPLIANCE: $k(p) = \frac{1}{k_m} + \frac{k_m}{\tau_m p}$

COMPLEX COMPLIANCE: $k^*(\omega) = k'(\omega) - i\,k''(\omega)$

$$k' = k_m$$

$$k''(\omega) = \frac{k_m}{\omega \tau_m}$$

OPERATIONAL MODULUS: $m(p) = \frac{m_m \tau_m p}{\tau_m p + 1}$

COMPLEX MODULUS: $m^*(\omega) = m'(\omega) + i\,m''(\omega)$

$$m'(\omega) = \frac{\omega^2 \tau_m^2 m_m}{\omega^2 \tau_m^2 + 1}$$

$$m''(\omega) = \frac{\omega \tau_m m_m}{\omega^2 \tau_m^2 + 1}$$

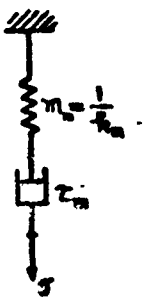

(b) MAXWELL MODEL

FIG. 2.11. DYNAMIC BEHAVIOR OF TWO-ELEMENT MODELS

OPERATIONAL COMPLIANCE: $k(p) = k_g + \frac{k_1}{\tau_1 p + 1}$

COMPLEX COMPLIANCE: $k^*(\omega) = k'(\omega) - i\,k''(\omega)$

$$k'(\omega) = k_g + \frac{k_1}{\omega^2 \tau_1^2 + 1}$$

$$k''(\omega) = \frac{\omega \tau_1 k_1}{\omega^2 \tau_1^2 + 1}$$

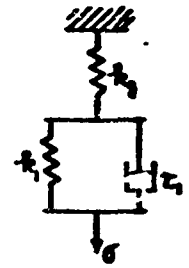

(a) VOIGT ELEMENT IN SERIES WITH GLASSY SPRING

OPERATIONAL MODULUS: $m(p) = m_e + \frac{m_1 \tau_1 p}{\tau_1 p + 1}$

COMPLEX MODULUS: $m^*(\omega) = m'(\omega) + i\,m''(\omega)$

$$m'(\omega) = m_e + \frac{\omega^2 \tau_1^2 m_1}{\omega^2 \tau_1^2 + 1}$$

$$m''(\omega) = \frac{\omega \tau_1 m_1}{\omega^2 \tau_1^2 + 1}$$

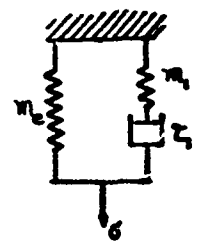

(b) MAXWELL ELEMENT IN PARALLEL WITH EQUILIBRIUM (RUBBERY) SPRING

FIG. 2.12. DYNAMIC BEHAVIOR OF EQUIVALENT THREE-ELEMENT MODELS

OPERATIONAL COMPLIANCE: $k(p) = k_0 + \frac{1}{\eta p} + \frac{k_1}{\tau_1 p + 1}$

COMPLEX COMPLIANCE: $k^*(\omega) = k'(\omega) - i\,k''(\omega)$

$$k'(\omega) = k_0 + \frac{k_1}{\omega^2 \tau_1^2 + 1}$$

$$k''(\omega) = \frac{1}{\omega \eta} + \frac{\omega \tau_1 k_1}{\omega^2 \tau_1^2 + 1}$$

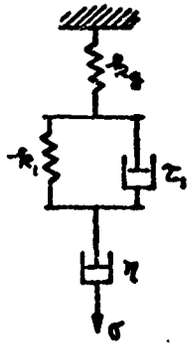

(a) VOIGT ELEMENT IN SERIES WITH MAXWELL ELEMENT

OPERATIONAL MODULUS: $m(p) = \frac{m_1 \tau_1 p}{\tau_1 p + 1} + \frac{\eta_2 \tau_2 p}{\tau_2 p + 1}$

COMPLEX MODULUS: $m^*(\omega) = m'(\omega) + i\,m''(\omega)$

$$m'(\omega) = \frac{\omega^2 \tau_1^2 m_1}{\omega^2 \tau_1^2 + 1} + \frac{\omega^2 \tau_2^2 m_2}{\omega^2 \tau_2^2 + 1}$$

$$m''(\omega) = \frac{\omega \tau_1 m_1}{\omega^2 \tau_1^2 + 1} + \frac{\omega \tau_2 m_2}{\omega^2 \tau_2^2 + 1}$$

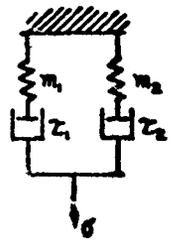

(b) TWO MAXWELL ELEMENTS IN PARALLEL

FIG. 2.13. DYNAMIC BEHAVIOR OF EQUIVALENT FOUR-ELEMENT MODELS

OPERATIONAL COMPLIANCE: $k(p) = k_g + \frac{k_1}{\tau_1 p + 1} + \frac{k_2}{\tau_2 p + 1}$

COMPLEX COMPLIANCE: $k^*(\omega) = k'(\omega) - i\,k''(\omega)$

$$k'(\omega) = k_g + \frac{k_1}{\omega^2 \tau_1^2 + 1} + \frac{k_2}{\omega^2 \tau_2^2 + 1}$$

$$k''(\omega) = \frac{\omega \tau_1 k_1}{\omega^2 \tau_1^2 + 1} + \frac{\omega \tau_2 k_2}{\omega^2 \tau_2^2 + 1}$$

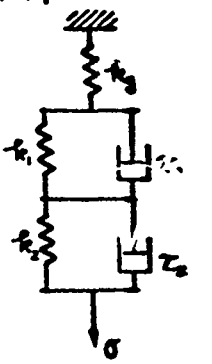

(a) TWO VOIGT ELEMENTS IN SERIES WITH GLASSY SPRING

OPERATIONAL MODULUS: $m(p) = m_e + \frac{m_1 \tau_1 p}{\tau_1 p + 1} + \frac{m_2 \tau_2 p}{\tau_2 p + 1}$

COMPLEX MODULUS: $m^*(\omega) = m'(\omega) + i\,m''(\omega)$

$$m'(\omega) = m_e + \frac{\omega^2 \tau_1^2 m_1}{\omega^2 \tau_1^2 + 1} + \frac{\omega^2 \tau_2^2 m_2}{\omega^2 \tau_2^2 + 1}$$

$$m''(\omega) = \frac{\omega \tau_1 m_1}{\omega^2 \tau_1^2 + 1} + \frac{\omega \tau_2 m_2}{\omega^2 \tau_2^2 + 1}$$

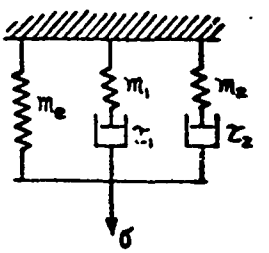

(b) TWO MAXWELL ELEMENTS IN PARALLEL WITH EQUILIBRIUM SPRING

FIG. 2.14. DYNAMIC BEHAVIOR OF EQUIVALENT FIVE-ELEMENT MODELS

OPERATIONAL COMPLIANCE: Finite n; $\bar{k}(p) = k_g + \sum_{i=1}^{n} \frac{k_i}{\tau_i p + 1}$

$$n = \infty; \quad \bar{k}(p) = k_g + \int_0^\infty \frac{L(\tau)}{(\tau p + 1)} \frac{d\tau}{\tau}$$

COMPLEX COMPLIANCE: $\bar{k}^*(\omega) = \bar{k}'(\omega) - i\bar{k}''(\omega)$

Finite n; $\bar{k}'(\omega) = k_g + \sum_{i=1}^{n} \frac{k_i}{\omega^2\tau_i^2 + 1}$, $\bar{k}''(\omega) = \sum_{i=1}^{n} \frac{\omega\tau_i k_i}{\omega^2\tau_i^2 + 1}$

$$n = \infty; \quad \bar{k}'(\omega) = k_g + \int_0^\infty \frac{L(\tau)\, d\tau}{(\omega^2\tau^2 + 1)\tau}, \quad \bar{k}''(\omega) = \int_0^\infty \frac{\omega\tau L(\tau)\, d\tau}{(\omega^2\tau^2 + 1)\tau}$$

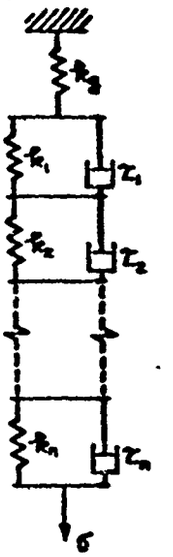

(a) n VOIGT ELEMENTS IN SERIES WITH GLASSY SPRING (KELVIN)

OPERATIONAL MODULUS: Finite n; $\bar{m}(p) = m_e + \sum_{i=1}^{n} \frac{m_i \tau_i p}{\tau_i p + 1}$

$$n = \infty; \quad \bar{m}(p) = m_e + \int_0^\infty \frac{H(\tau)\tau p}{(\tau p + 1)} \frac{d\tau}{\tau}$$

COMPLEX MODULUS: $\bar{m}^*(\omega) = \bar{m}'(\omega) + i\bar{m}''(\omega)$

Finite n; $\bar{m}'(\omega) = m_e + \sum_{i=1}^{n} \frac{\omega^2\tau_i^2 m_i}{\omega^2\tau_i^2 + 1}$

$$\bar{m}''(\omega) = \sum_{i=1}^{n} \frac{\omega\tau_i m_i}{\omega^2\tau_i^2 + 1}$$

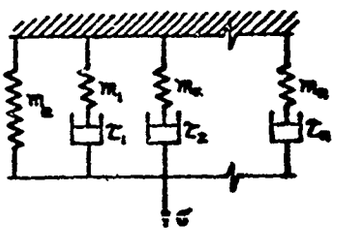

$$n = \infty; \quad \bar{m}'(\omega) = m_e + \int_0^\infty \frac{\omega^2\tau^2 H(\tau)\, d\tau}{(\omega^2\tau^2 + 1)\tau}; \quad \bar{m}''(\omega) = \int_0^\infty \frac{\omega\tau H(\tau)\, d\tau}{(\omega^2\tau^2 + 1)\tau}$$

(b) n MAXWELL ELEMENTS IN PARALLEL WITH EQUILIBRIUM SPRING (WIECHERT)

FIG. 2.15. DYNAMIC BEHAVIOR OF EQUIVALENT KELVIN AND WIECHERT MODELS

OPERATIONAL COMPLIANCE: Finite n; $k(p)=k_g+\frac{1}{\eta p}+\sum_{i=1}^{n}\frac{k_i}{\tau_i p+1}$

$n=\infty$; $k(p)=k_g+\frac{1}{\eta p}+\int_0^{\infty}\frac{L(\tau)}{(\tau p+1)}\frac{d\tau}{\tau}$

COMPLEX COMPLIANCE: $k^*(\omega)=k'(\omega)-i\,k''(\omega)$

Finite n; $k'(\omega)=k_g+\sum_{i=1}^{n}\frac{k_i}{\omega^2\tau_i^2+1}$

$k''(\omega)=\frac{1}{\eta\omega}+\sum_{i=1}^{n}\frac{\omega\tau_i k_i}{\omega^2\tau_i^2+1}$

$n=\infty$; $k'(\omega)=k_g+\int_0^{\infty}\frac{L(\tau)}{(\omega^2\tau^2+1)}\frac{d\tau}{\tau}$

$k''(\omega)=\frac{1}{\eta\omega}+\int_0^{\infty}\frac{\omega\tau L(\tau)}{(\omega^2\tau^2+1)}\frac{d\tau}{\tau}$

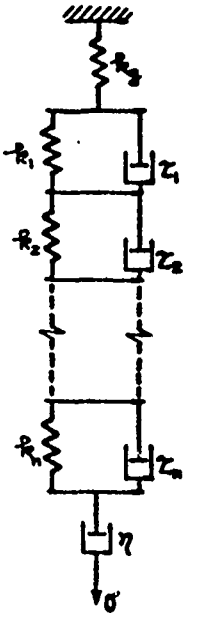

(a) n VOIGT ELEMENTS IN SERIES WITH MAXWELL ELEMENT (KELVIN)

OPERATIONAL MODULUS: Finite n; $m(p)=\sum_{i=1}^{n+1}\frac{m_i\tau_i p}{\tau_i p+1}$

$n=\infty$; $m(p)=\int_0^{\infty}\frac{H(\tau)\tau p}{(\tau p+1)}\frac{d\tau}{\tau}$

COMPLEX MODULUS: $m^*(\omega)=m'(\omega)+i\,m''(\omega)$

Finite n; $m'(\omega)=\sum_{i=1}^{n+1}\frac{\omega^2\tau_i^2 m_i}{\omega^2\tau_i^2+1}$

$m''(\omega)=\sum_{i=1}^{n+1}\frac{\omega\tau_i m_i}{\omega^2\tau_i^2+1}$

$n=\infty$; $m'(\omega)=\int_0^{\infty}\frac{\omega^2\tau^2 H(\tau)}{(\omega^2\tau^2+1)}\frac{d\tau}{\tau}$; $m''(\omega)=\int_0^{\infty}\frac{\omega\tau H(\tau)}{(\omega^2\tau^2+1)}\frac{d\tau}{\tau}$

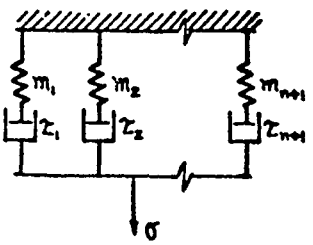

(b) (n+1) MAXWELL ELEMENTS IN PARALLEL (WIECHERT)

FIG. 2.15. DYNAMIC BEHAVIOR OF EQUIVALENT KELVIN AND WIECHERT MODELS (CONT.)

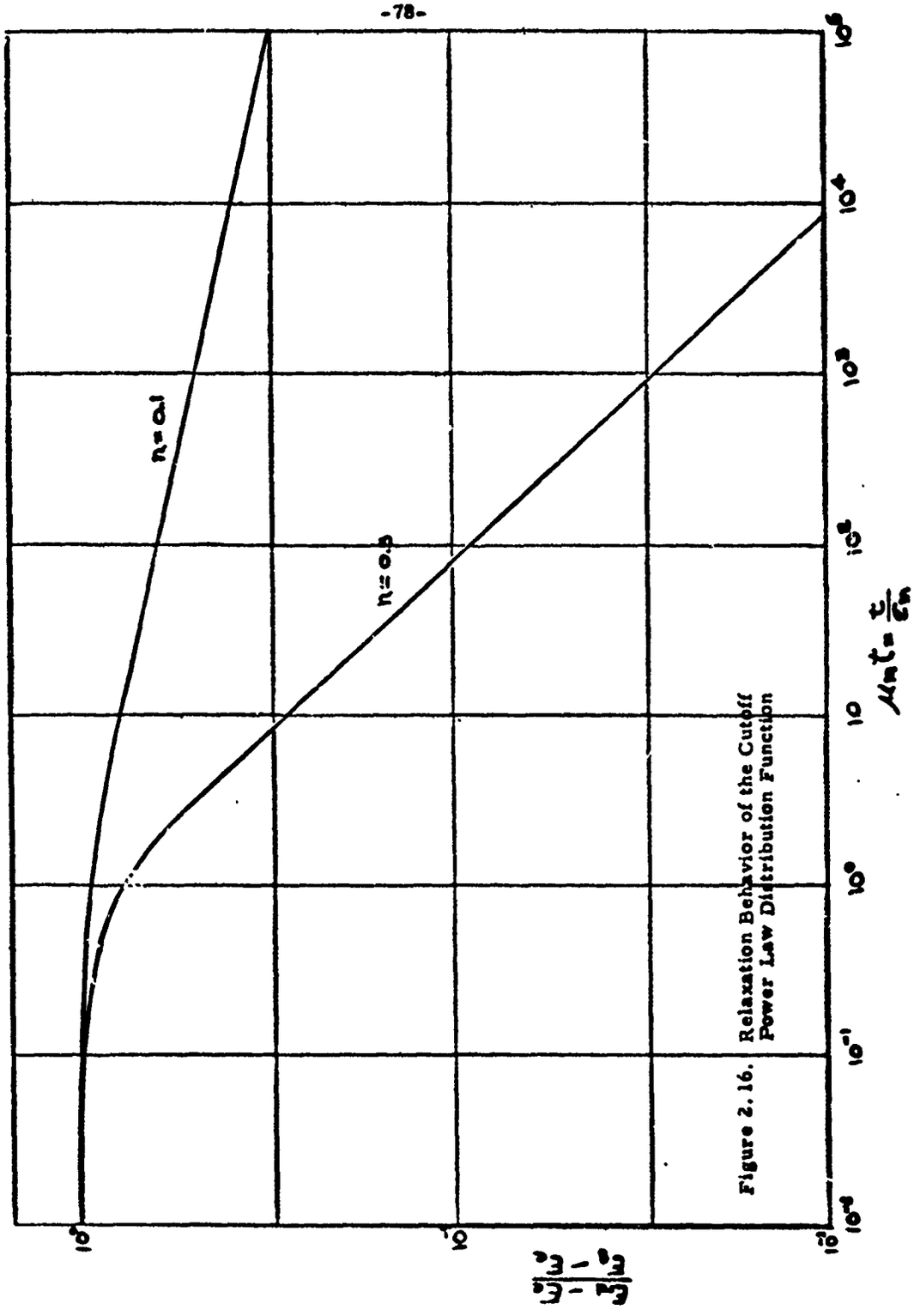

Figure 2.16. Relaxation Behavior of the Cutoff Power Law Distribution Function

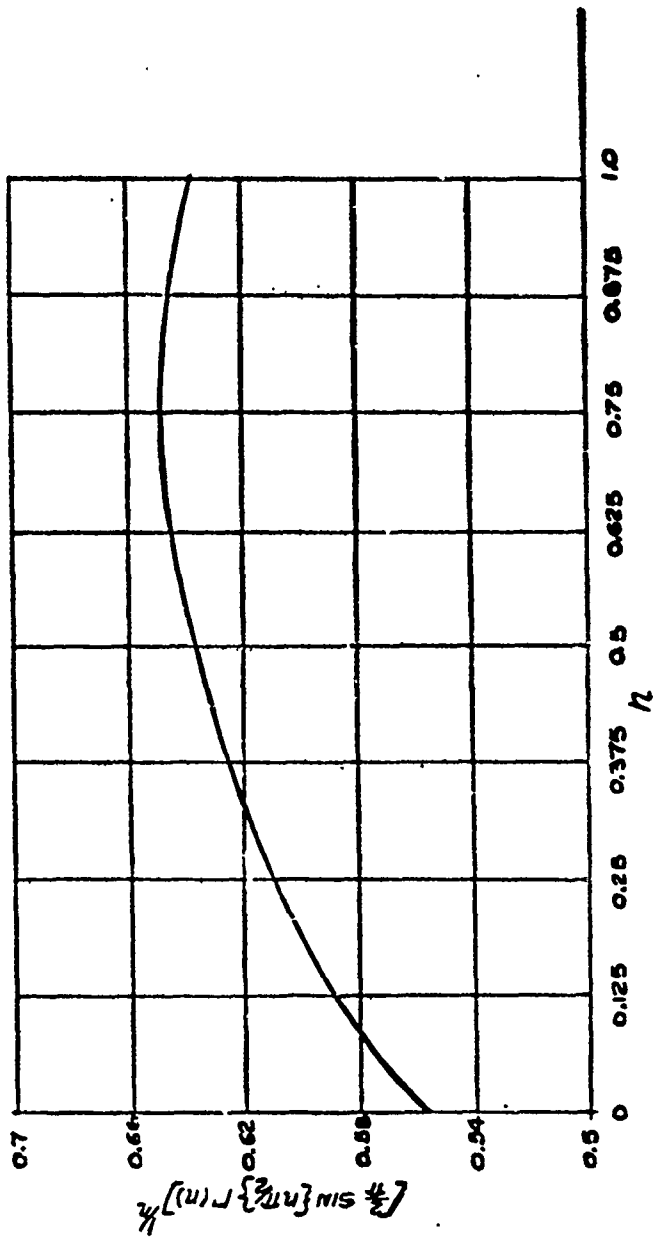

Fig. 2.17 The Product ωt as a Function of n, the Log-Log Slope of Relaxation Data.

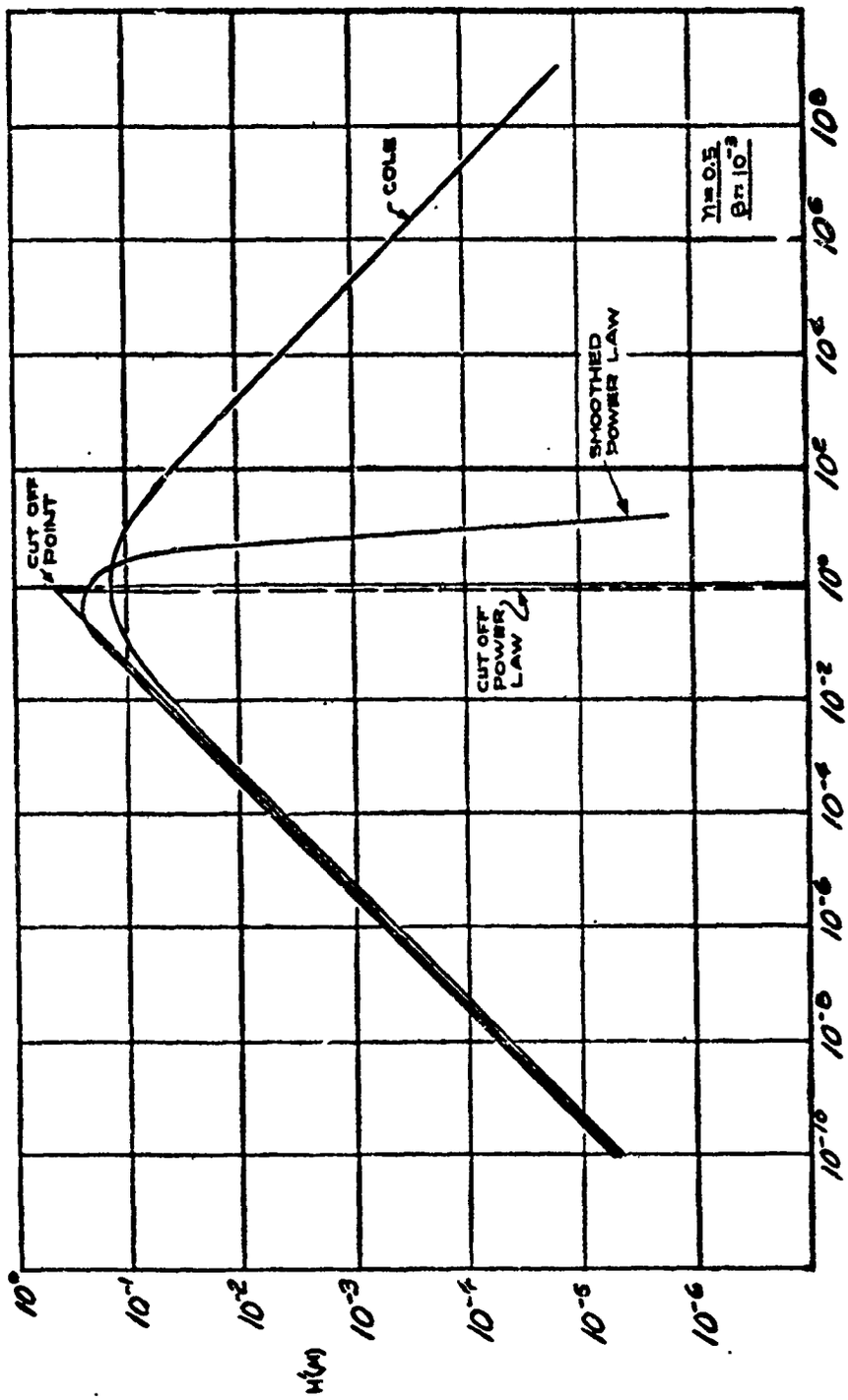

Fig. 2.18-a. A Comparison of the Cole and Smoothed Power Law Distribution Functions.

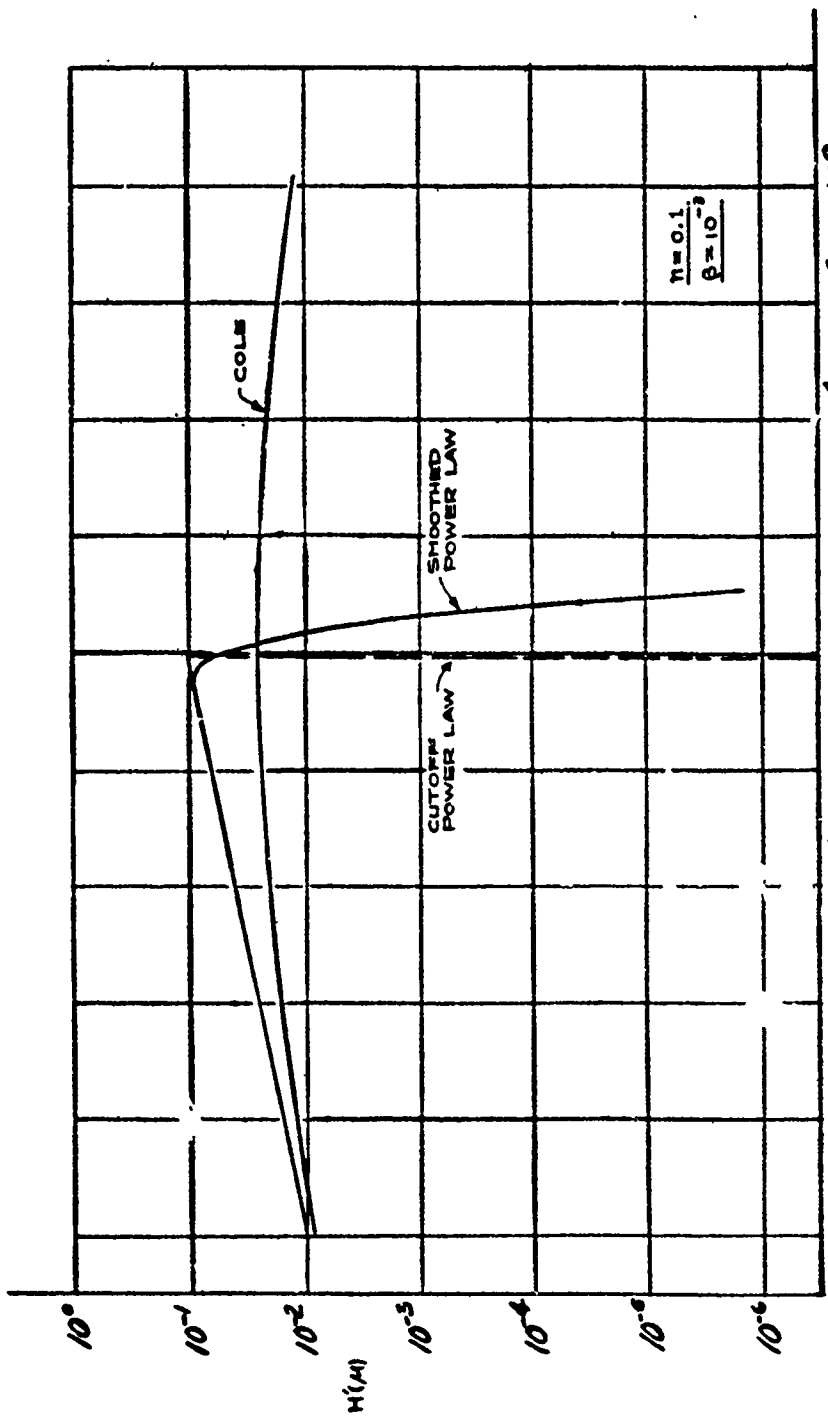

Fig. 2.18-b. Comparison of the Cole, Smoothed Power Law, and Cut-off Power Law.

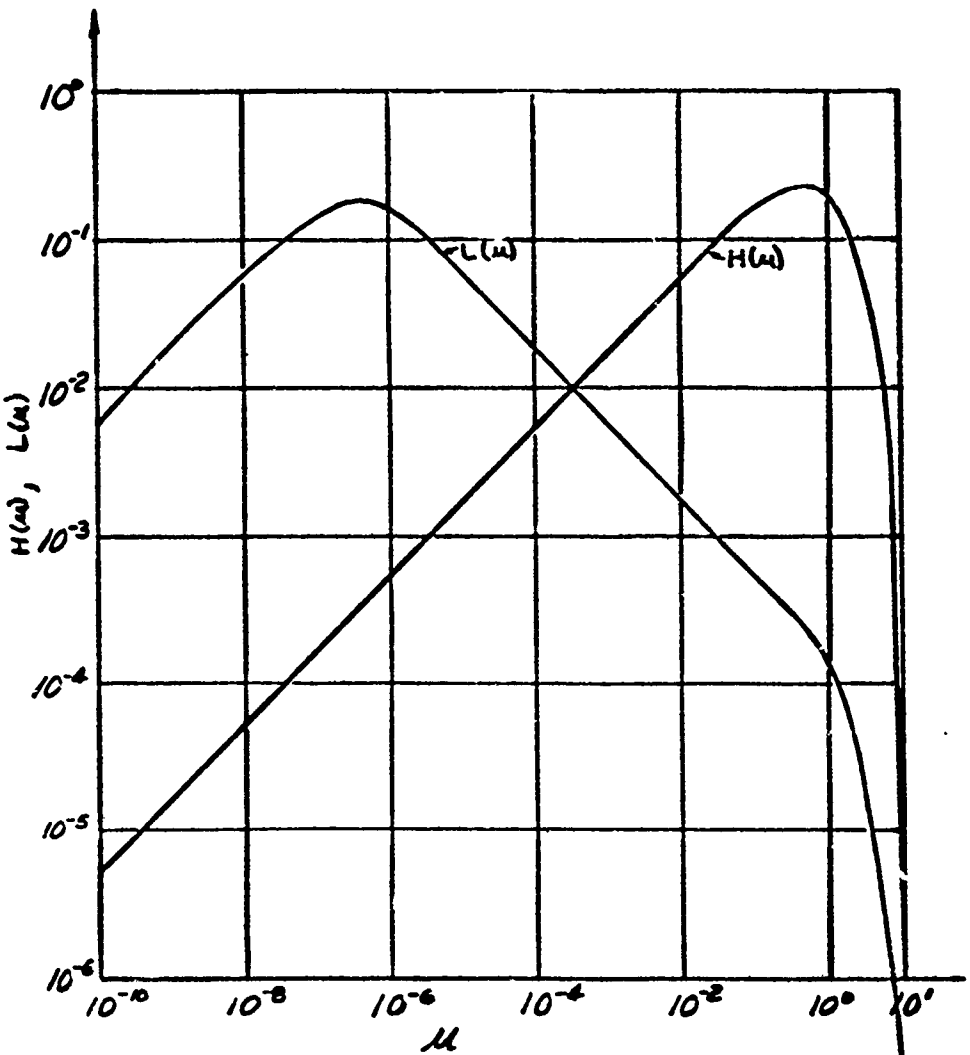

Fig. 2.19. A Comparison of the Smoothed Power Law Relaxation Spectrum and its Associated Retardation Spectrum for n = 0.5.

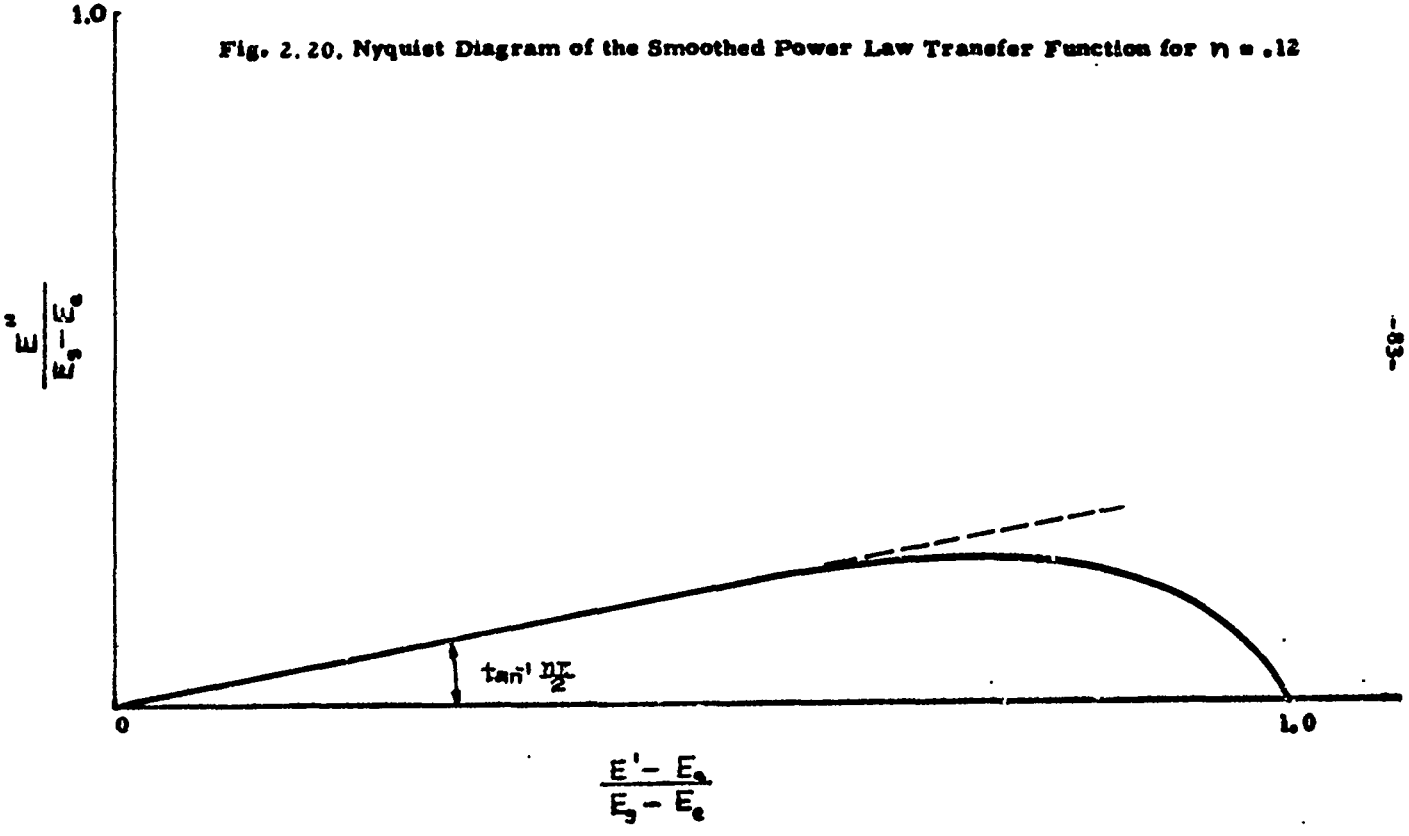

Fig. 2.20. Nyquist Diagram of the Smoothed Power Law Transfer Function for $n = .12$

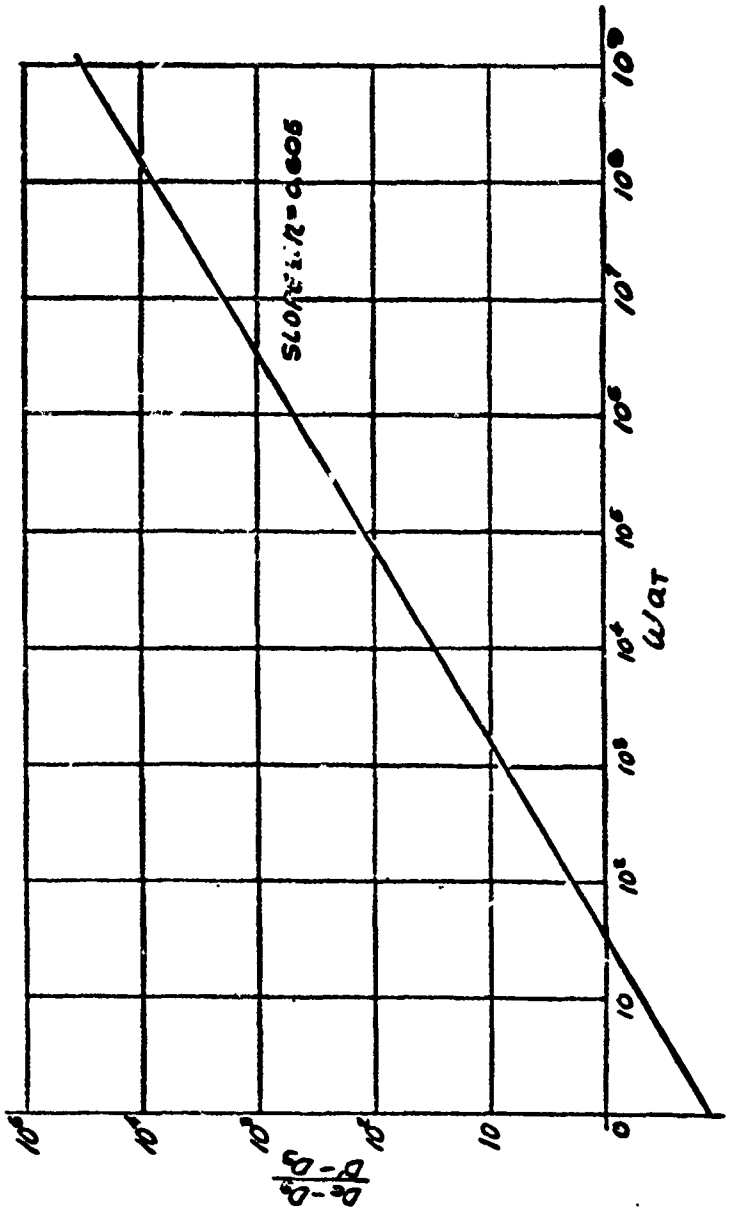

Fig. 2.21. Rectification of Dynamic Compliance Data in terms of the Cole Distribution Function.

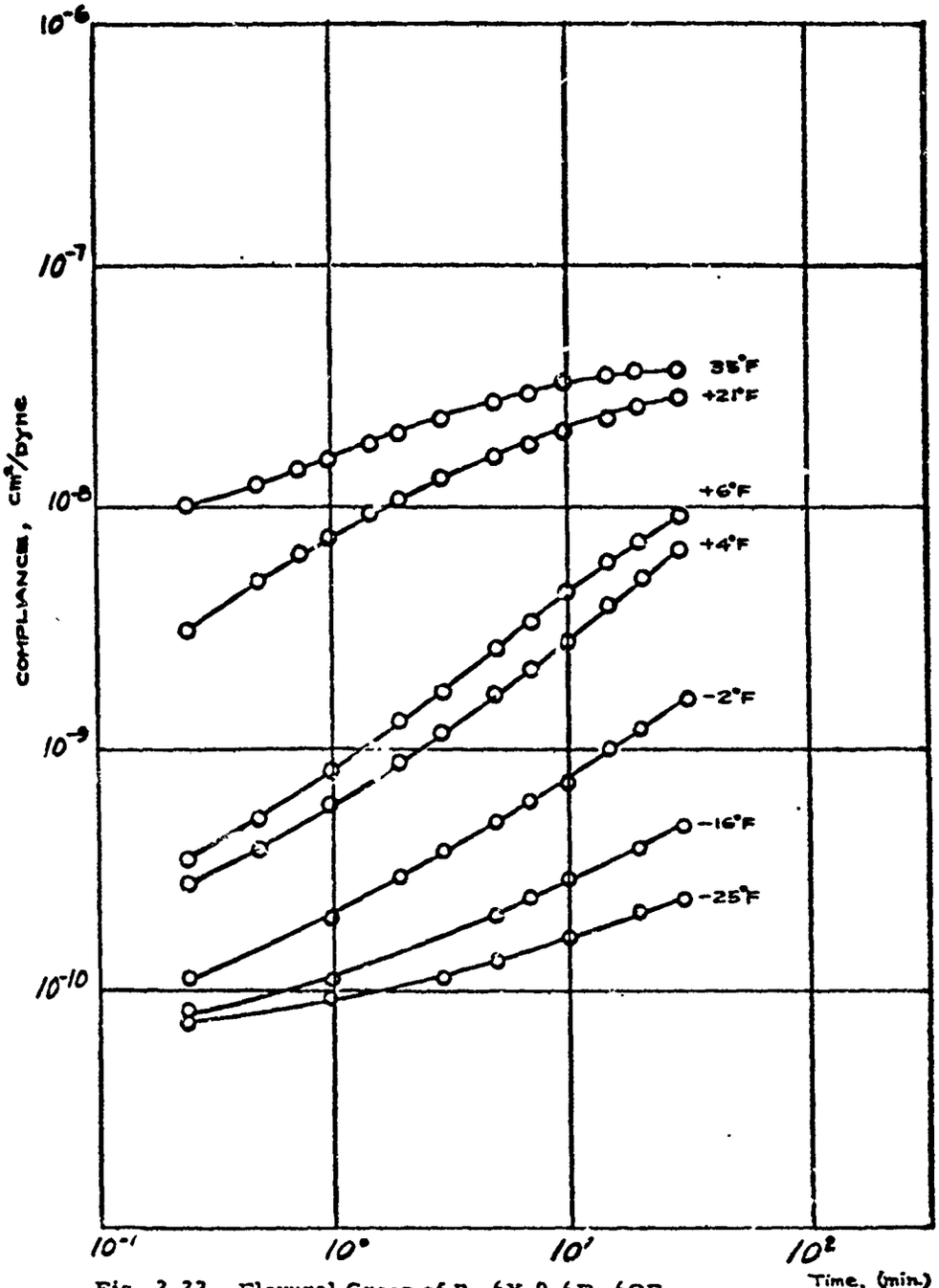

Fig. 2.22. Flexural Creep of R_1-6X-0.6P_1-6OF As a Function of Temperature

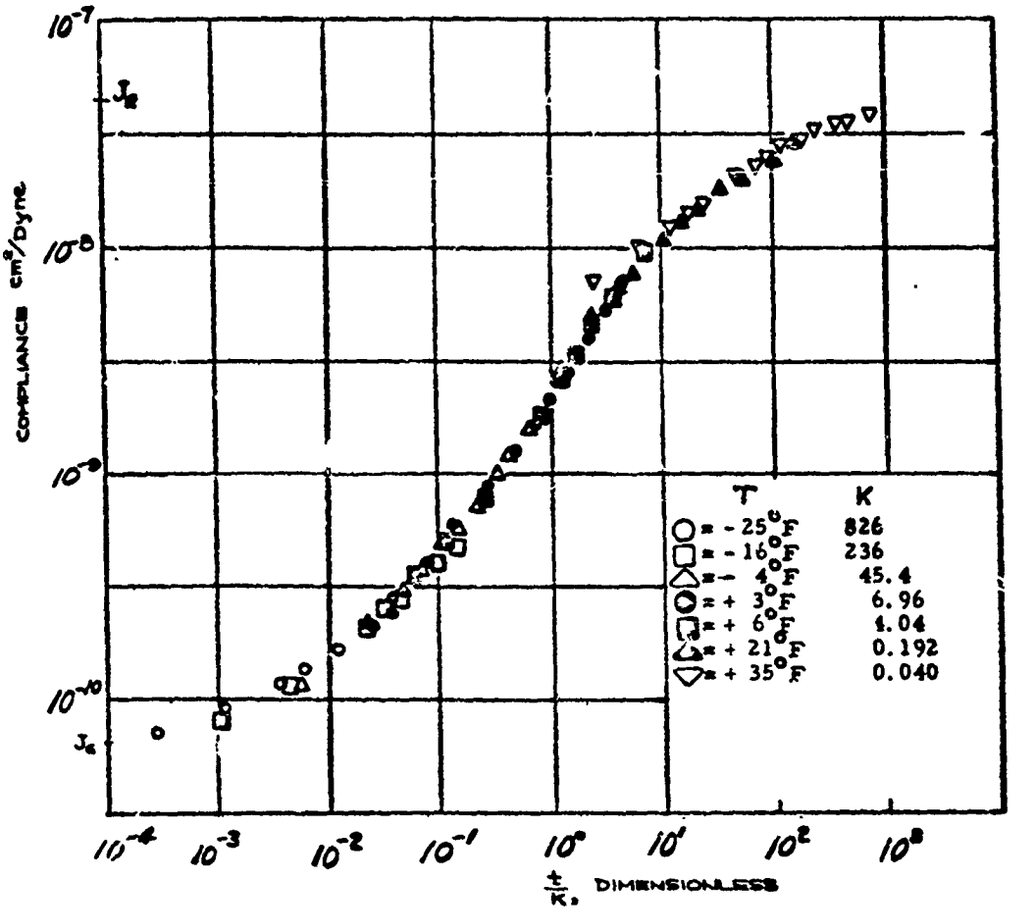

Fig. 2.23. Master Curve for R_1-6X-0.6P_1-60F

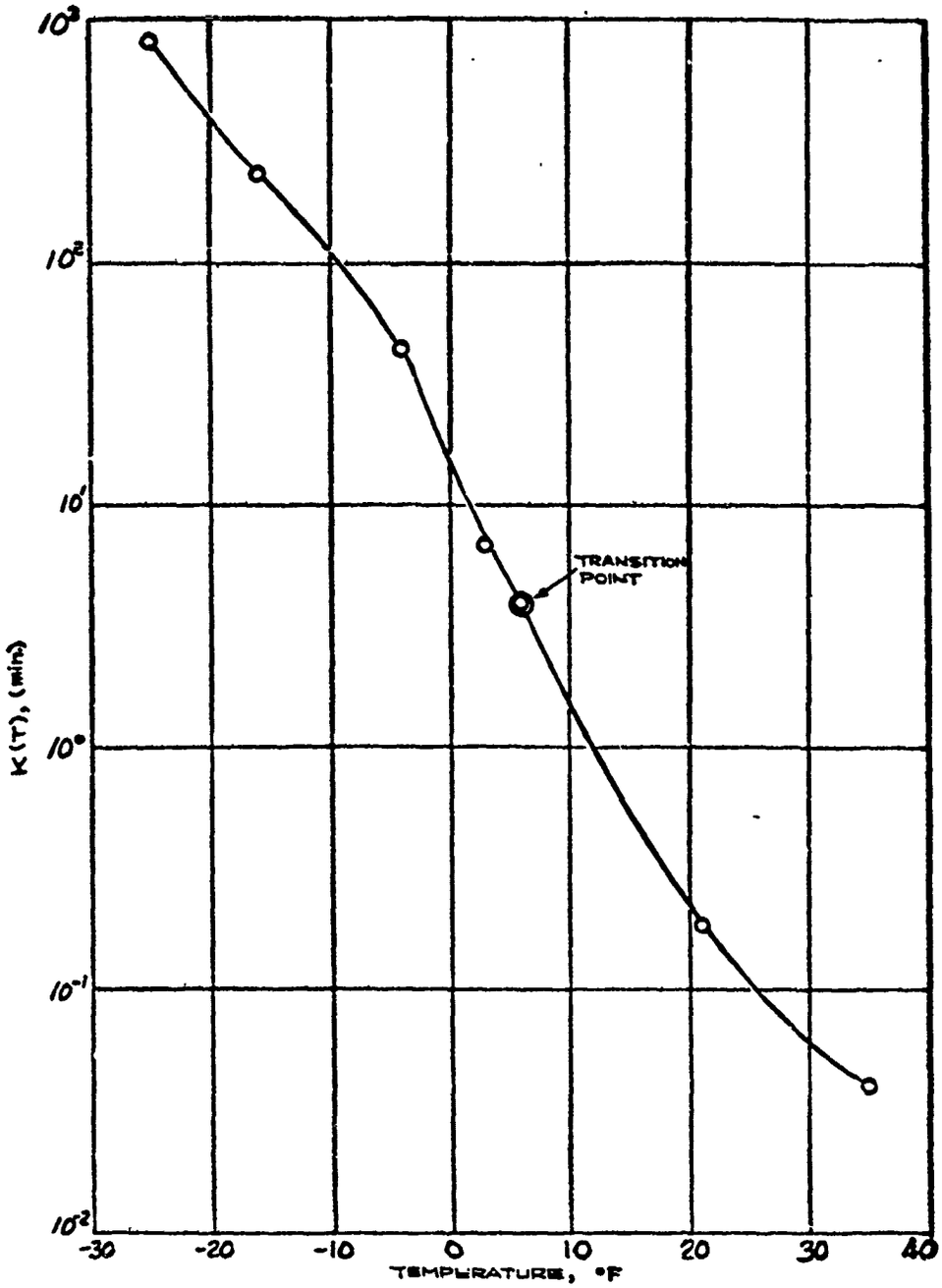

Fig. 2.24. Temperature Dependence of the Shift Factors Associated with R_1-6X-0.6P_1-6OF

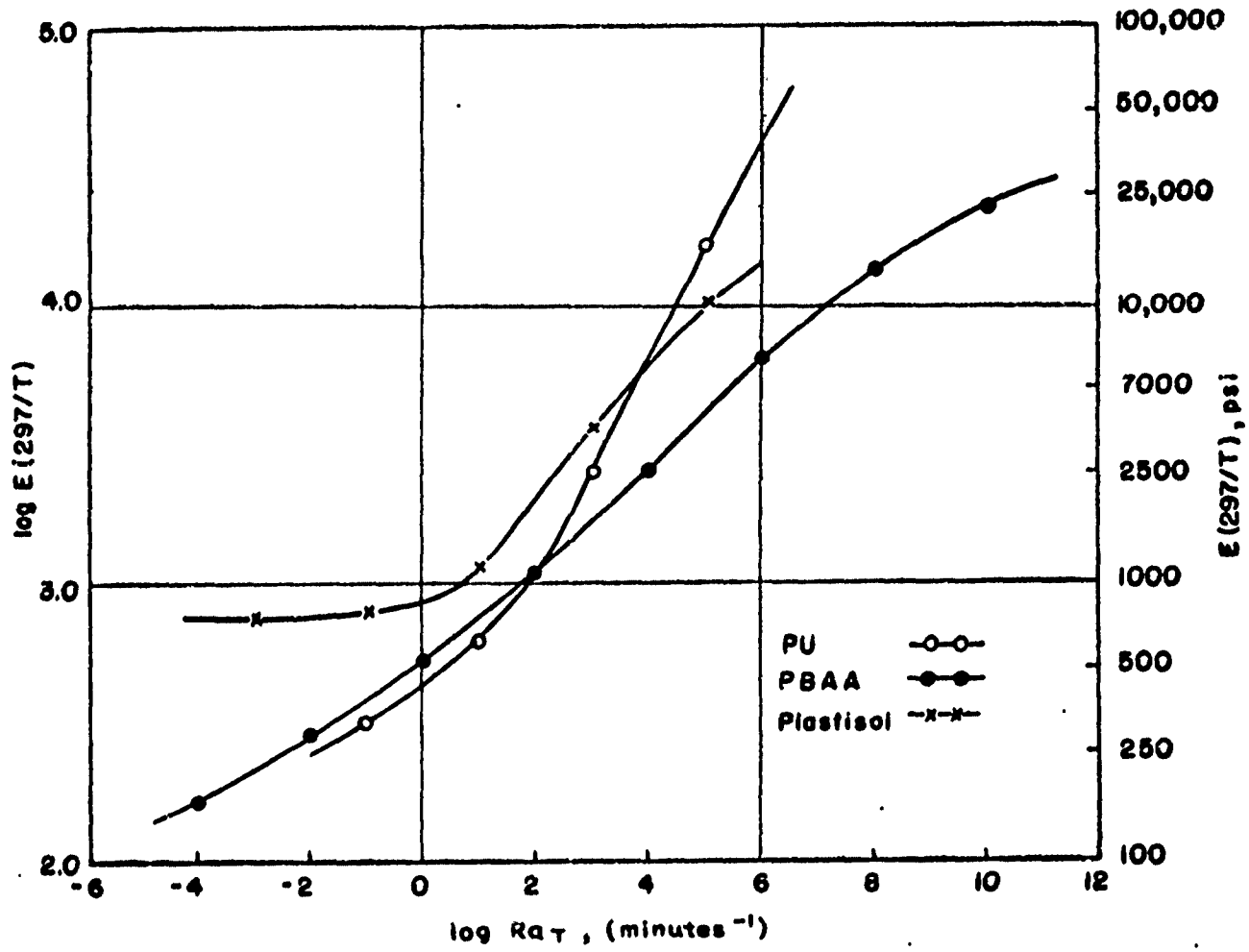

Fig. 2.25. Normalized Modulus Variation with Reduced Strain Rate.

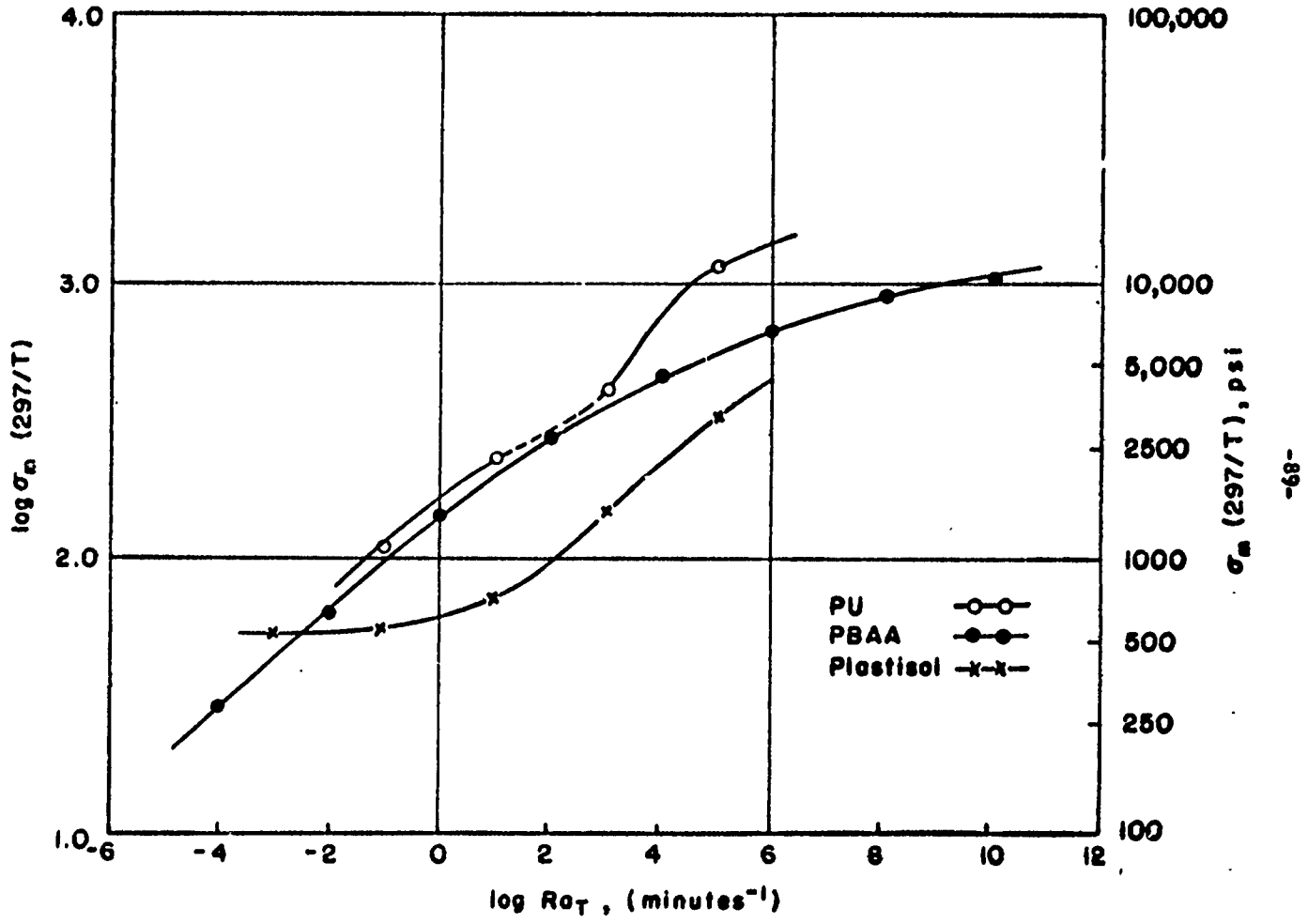

Fig. 2.26. Normalized Maximum Tensile Strength Variation with Reduced Strain Rate.

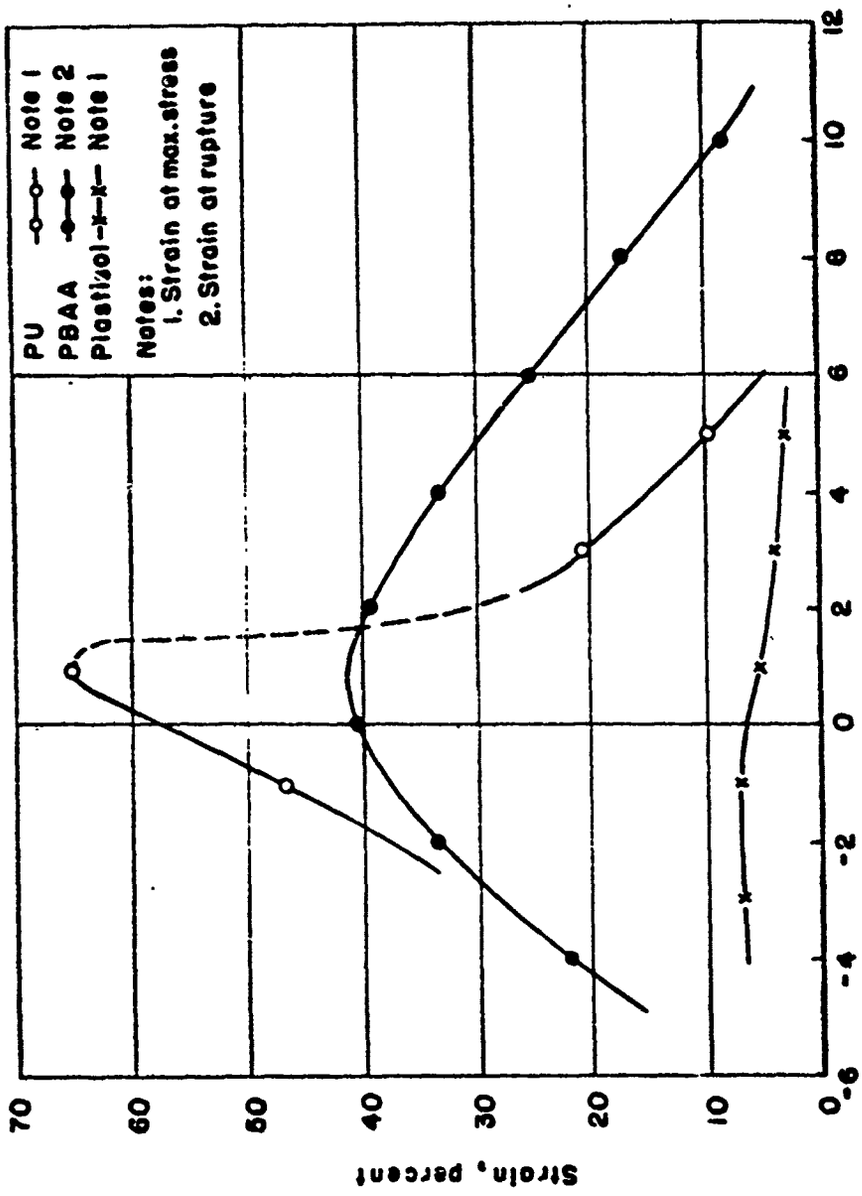

Fig. 2.27. Critical Strain Variation with Reduced Strain Rate.

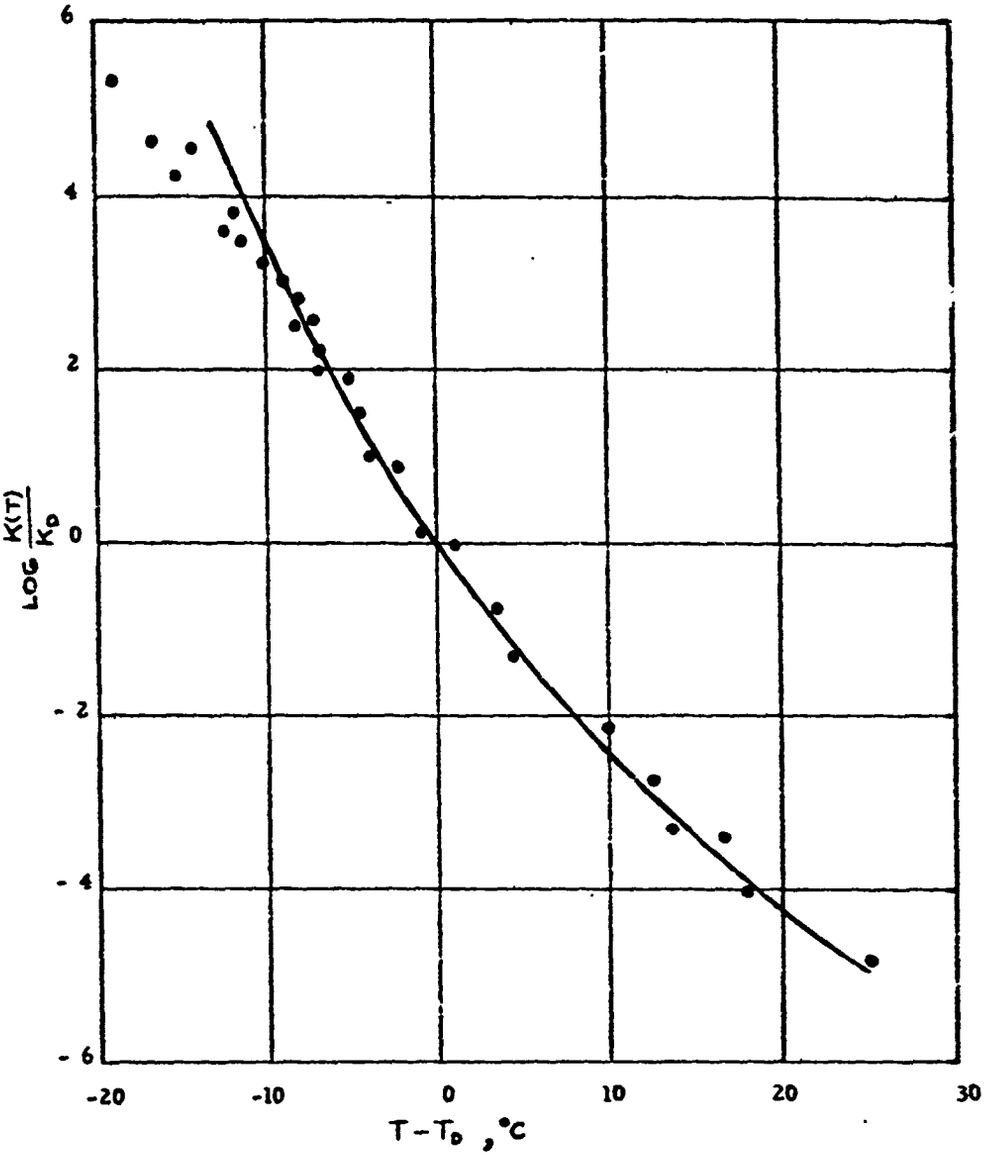

Fig. 2. 28. Tobolsky Curve for Reduced Shift Factors

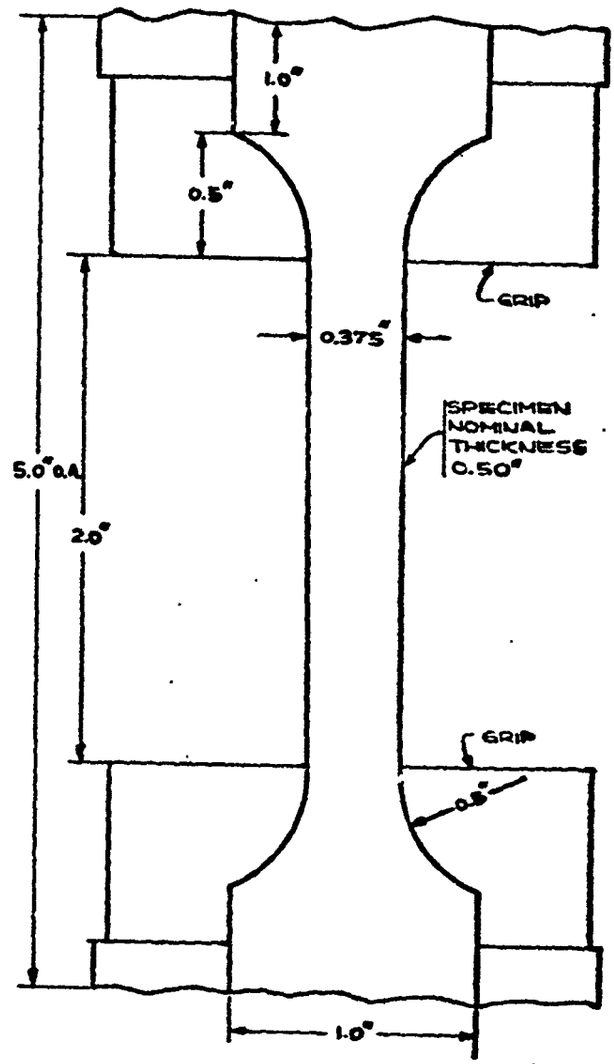

FIG. 2.29. STANDARD JANAF TENSILE SPECIMEN

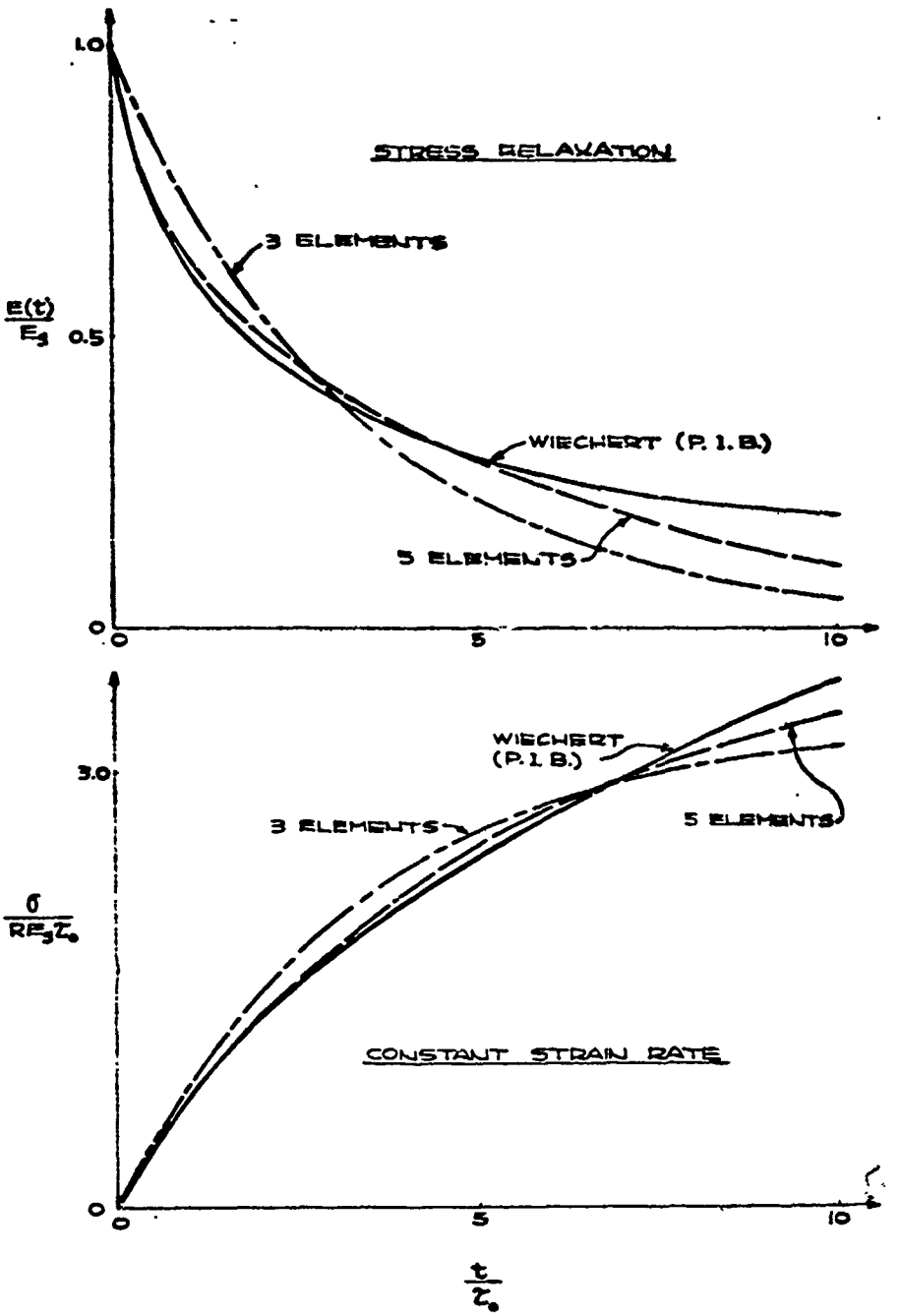

FIG. 2.30 COMPARISION OF MODELS FOR STRESS RELAXATION AND CONSTANT STRAIN RATE TESTS

PERIODIC PRESSURE PULSE:

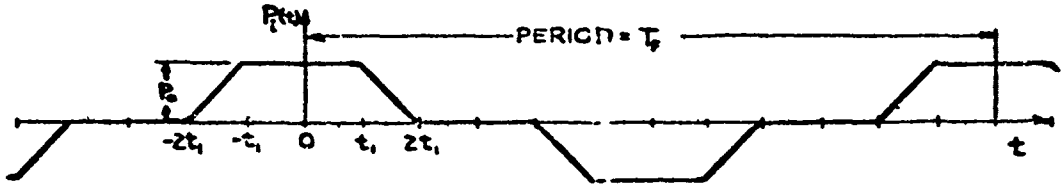

$$\alpha_m \equiv \frac{\left\{ \frac{4}{T_p} \int_0^{\frac{T_p}{4}} \left[P_i(t) - S_m(t) \right]^2 dt \right\}^{\frac{1}{2}}}{\frac{1}{2t_1} \int_0^{2t_1} P_i(t)\, dt} \qquad \text{WHERE:}$$

$$S_m(t) = \frac{4 P_o T_p}{\pi^2 t_1} \sum_{n=1,3,5,\ldots}^{m} \frac{1}{n^2} \sin \frac{n\pi t_1}{T_p} \sin \frac{3n\pi t_1}{T_p} \cos \frac{2n\pi t}{T_p} \; ; \; S_m \to P_i(t) \text{ AS } m \to \infty$$

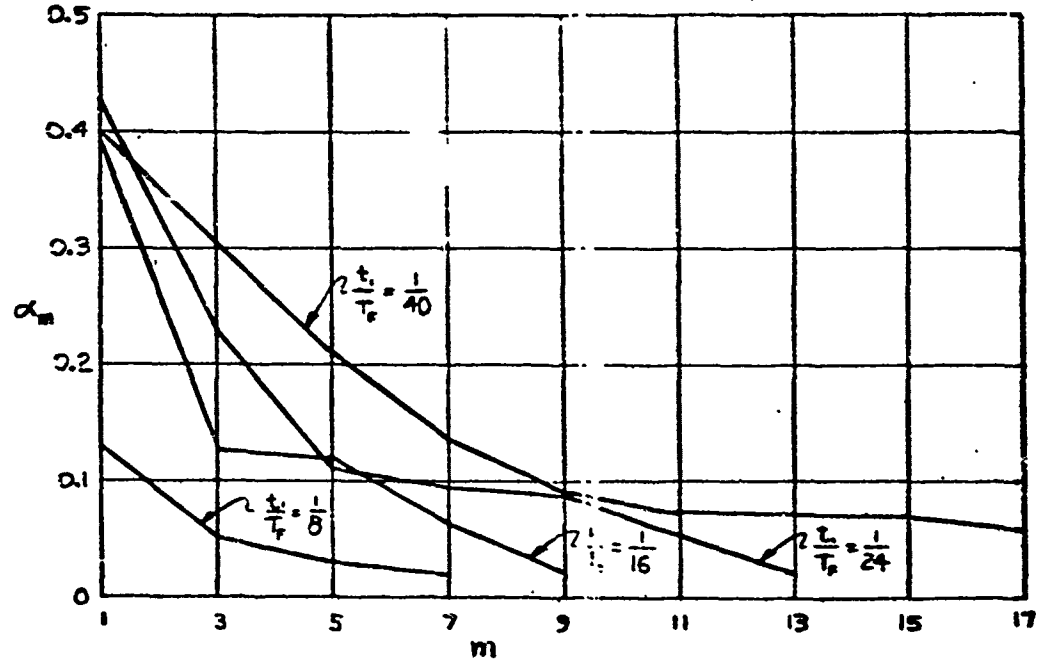

Fig. 2.31. Ratio of Root Mean Square Error to Average Value of Pressure Pulse for Finite Fourier Series Approximation.

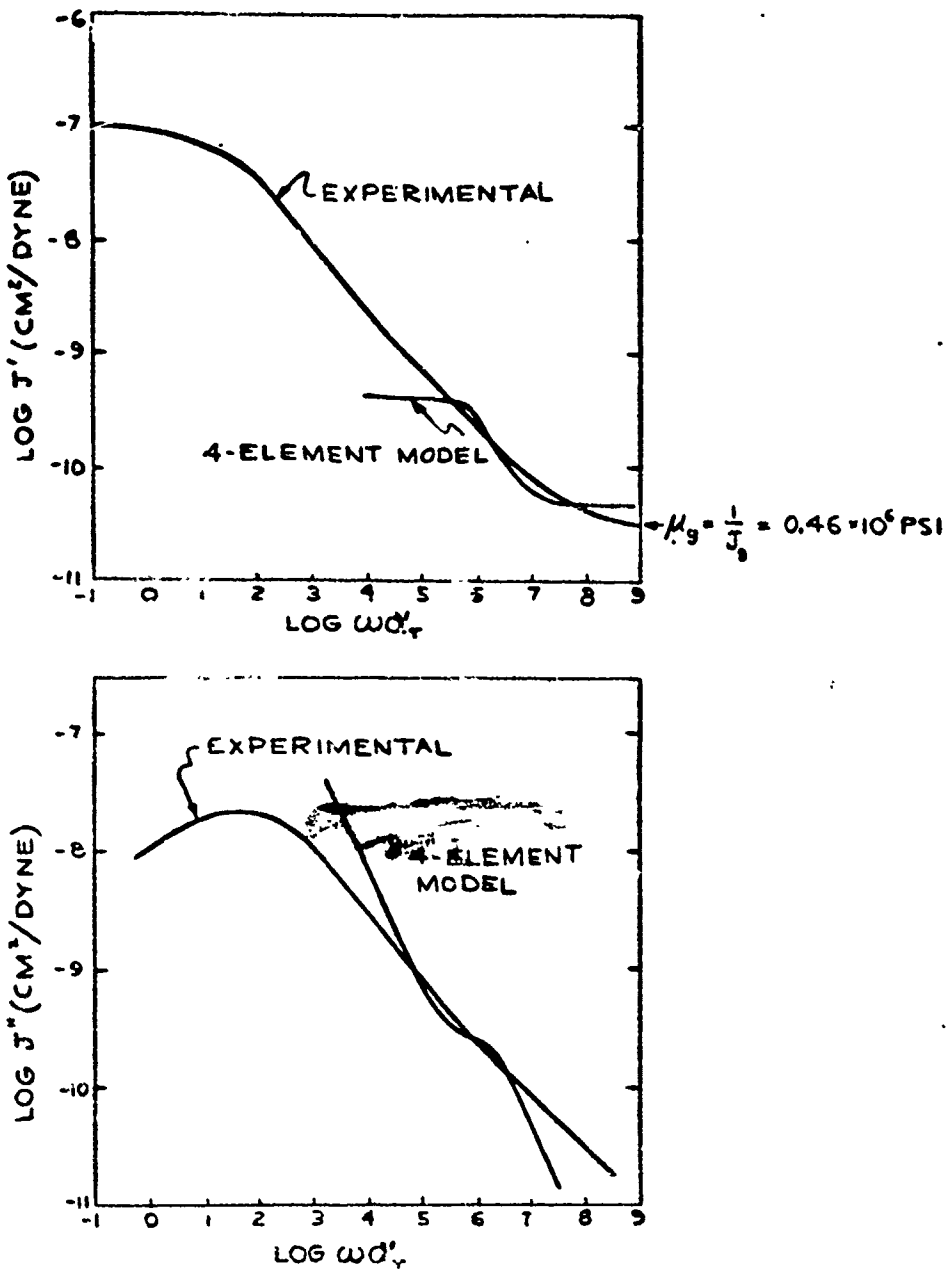

Fig. 2.32. Master Curves for Real and Imaginary Components of Complex Compliance at 54.5°F (12.5°C). (NBS Polyisobutylene).

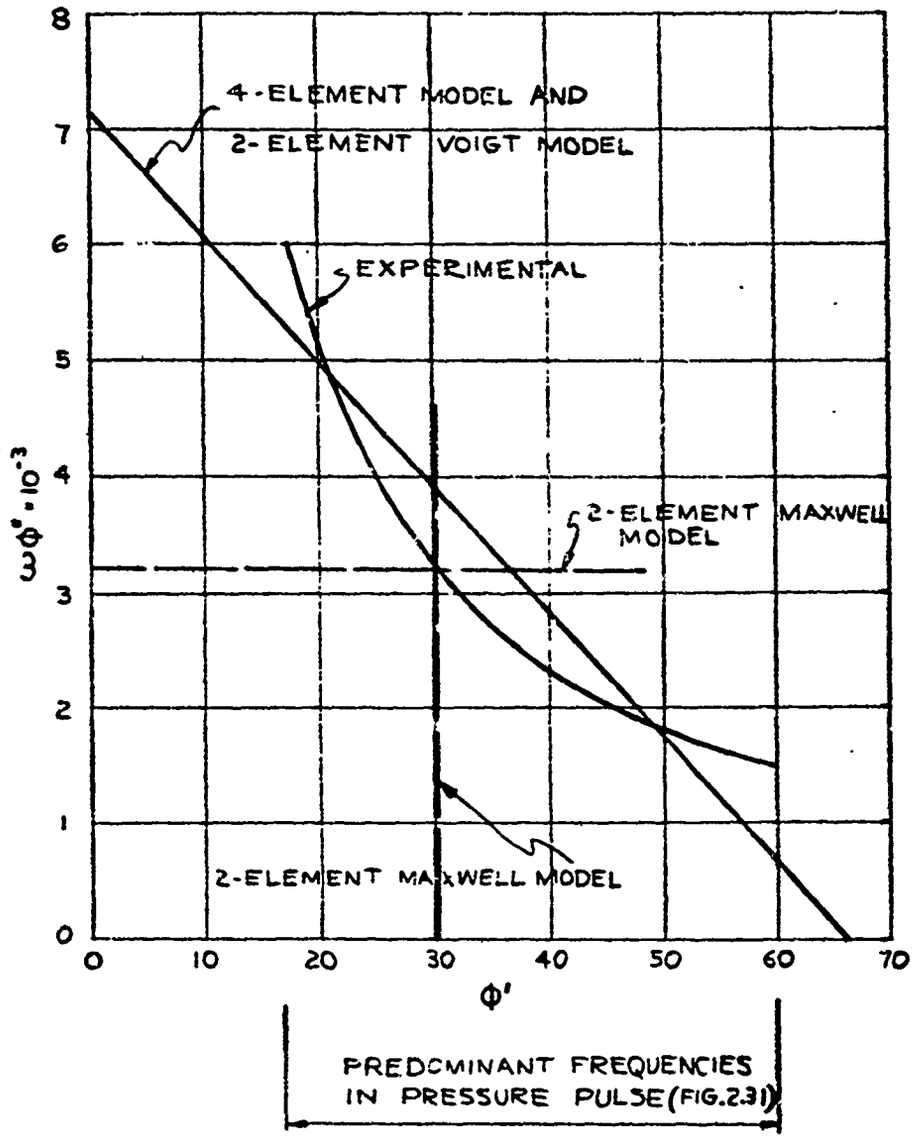

Fig. 2.33. Plot for Determining 2 and 4-Element Model Parameters. (For PIB at -35°F)

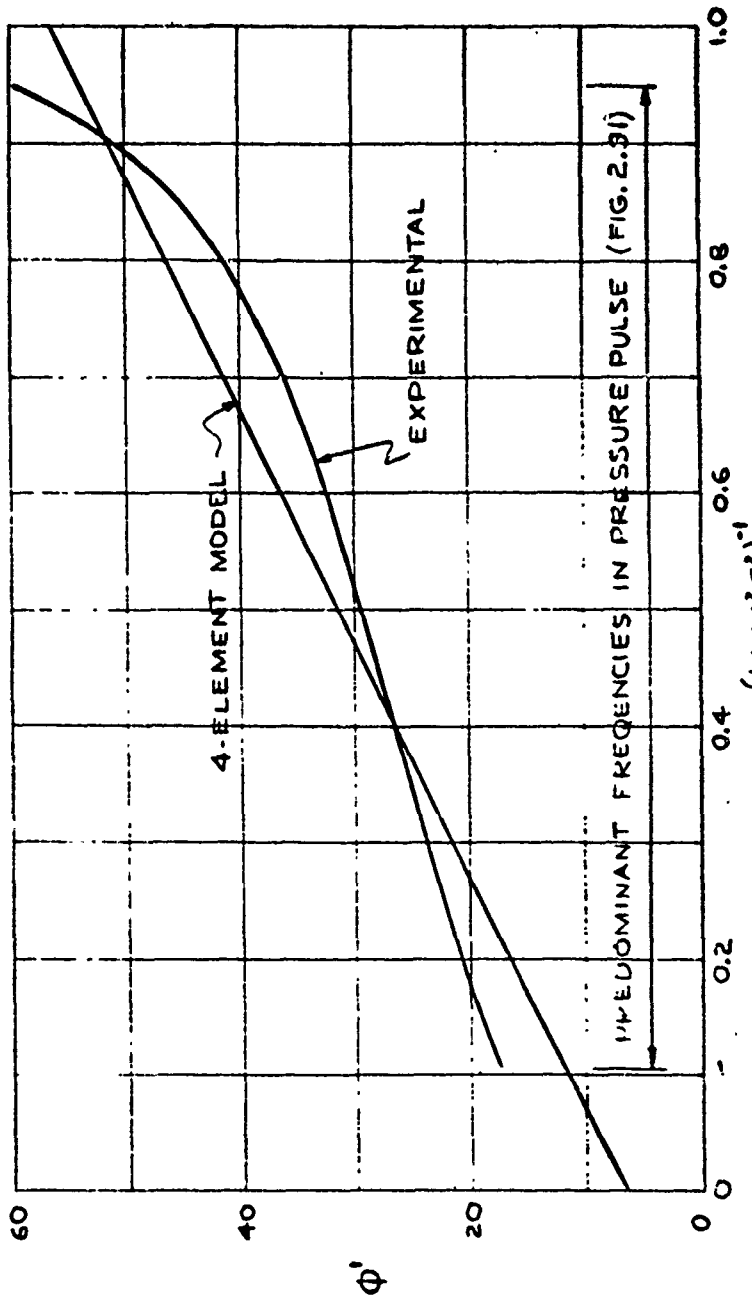

Fig. 2.34. Plot for Determining 4-Element Model Parameters. (For PIB at -35°F)

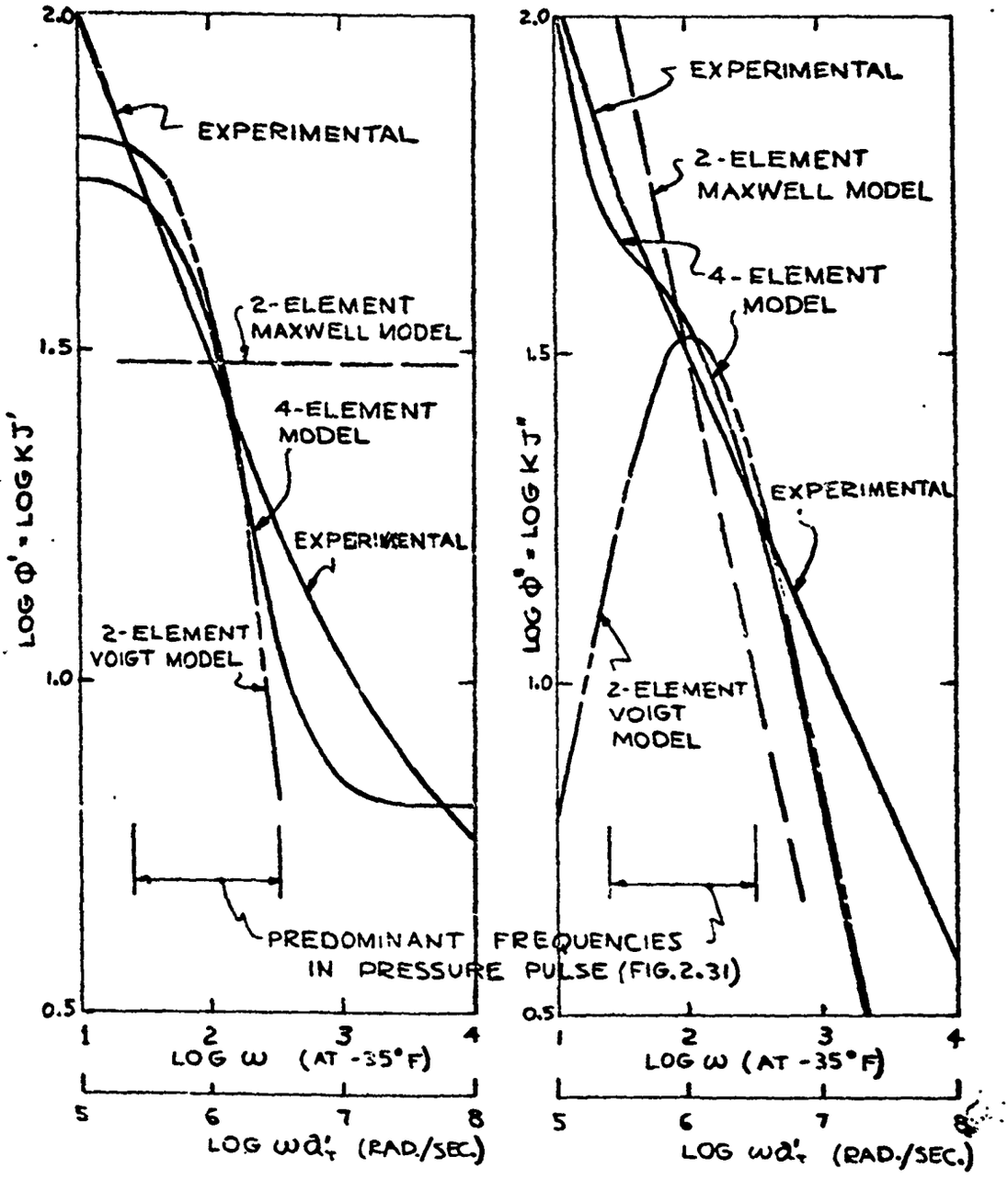

Fig. 2.35. Log-Log Plot of Compliance vs. Reduced Frequency From Experimental Data and 2 and 4-Element Model Response.

3. ENGINEERING ANALYSIS

The first two of the following sections are devoted to the problem of calculating viscoelastic stresses and strains in complex geometries when the material behavior is known through the representations discussed in previous sections. As a matter of background information, viscoelastic stress theory is reviewed for the case of mechanically induced stresses and strains in bodies at a uniform, constant temperature. In particular, it is shown how elastic solutions can be used directly in the viscoelastic analysis. This method of using an "associated" elastic solution is then illustrated with some examples of the estimation of viscoelastic strains in long, hollow, circular cylinders subjected to internal pressurization. Several different property characterizations are used to compare their advantages or disadvantages in obtaining solutions. Following these examples, we show how viscoelastic solutions for cylinders with circular ports may be extended to include the more common star configurations.

A collection of useful elastic solutions are then given which can be extended to viscoelasticity by use of the association analogy, and the final section contains a discussion of several additional grain design problems of current interest.

3.1 Review of Viscoelastic Theory

The equations governing the mechanical behavior of viscoelastic bodies in which the strains are small are the three equilibrium equations (1.2.1); six strain displacement relations (1.2.2); and six stress-strain equations that are similar to the well-known ones of elastic theory (1.2.3), but with differential operators in place of the usual elastic constants. Thus, it is seen that the only difference between the governing system of equations of linear elasticity and linear viscoelasticity lies in the stress-strain relations.

The form of these relations was discussed in Section 2 for the simple cases of tensile, shear, and bulk deformation of isotropic bodies. In addition, it was pointed out that only two of these transfer functions relating the stress and strain are independent. The way in which these two enter in the general three-dimensional stress-strain equations is purely a consequence of geometric symmetry of isotropic bodies; therefore the stress-strain equations of elasticity and viscoelasticity are identical in form, but with any two of the viscoelastic operators E(p), K(p), or μ(p) in place of the elastic constants E, K, or μ. The viscoelastic Poisson's ratio is defined by a ratio of the more basic operators through equation (2.2.10), and generally will have to be replaced by these operators when solving a particular problem.

We turn now to a discussion of a convenient method of solving the governing equations of viscoelasticity for a wide class of problems of practical interest, which was suggested by Lee[3.1]. The equations are all operated on with the Laplace transform so that all dependent variables become functions of the transform parameter, p, rather than time. Assuming zero initial conditions, and denoting transformed variables with a bar, it can be shown that we obtain the transformed equations by simply placing a bar over all variables in equations (1.2.1) and (1.2.2), and interpreting the time derivatives in the transfer functions E(p), K(p), $\mu(p)$ as the transform parameter p. For example, the equilibrium equation in the x-direction becomes

$$\frac{\partial \bar{\sigma}_x}{\partial x} + \frac{\partial \bar{\tau}_{xy}}{\partial y} + \frac{\partial \bar{\tau}_{xz}}{\partial z} + \bar{X} = 0 \qquad (3.1.1)$$

Similarly, the transformed stress-strain equation for ϵ_x (1.2.3) is written

$$\equiv(p)\,\bar{\epsilon}_x = \bar{\sigma}_x - \nu(p)\,(\bar{\sigma}_y + \bar{\sigma}_z) \qquad (3.1.2)$$

The transformed equations (1.2.1) and (1.2.2), along with transformed boundary conditions, represent a complete set for determining the transformed dependent variables stress, strain, and displacement. Once these variables are found as functions of spacial coordinates and p, the Laplace inversion integral (or transform tables) is used to obtain the time dependent solutions.

It is evident that the transformed equations of viscoelasticity have the same spacial character as the elastic equations; thus, if time and space dependence appear as separate factors in the boundary conditions and body forces, then the transformed solutions to a viscoelastic problem will possess the same spacial dependence as an "associated" elastic problem. That is, when body forces can be written as $X = X'(x)\,X''(t)$ (with similar representations for the y and z directions), stress boundary conditions as $F_x = F_x'(x)\,F_x''(t)$ (in which F_x is the x-component of surface force per unit area), and displacement boundary conditions as $u(x) = u'(x)\,u''(t)$, then the transformed viscoelastic stresses and displacements have the same spacewise dependence as those in a geometrically identical elastic body with these body forces and boundary conditions. This correspondence has great practical importance since viscoelastic solutions can be obtained immediately from the associated elastic solutions by:

1. placing bars over dependent variables in the elastic solution;
2. replacing the boundary and body force terms by the corresponding transformed quantities;
3. replacing the elastic constants by the corresponding transformed operators; and
4. inverting the resulting expressions by means of transform tables or the inversion integral to obtain the time dependent solution.

As a final point, it is generally sufficiently accurate to assume that the bulk modulus, instead of being an operator, is a constant, i.e. an elastic response, or in the special case of an assumed incompressible material, $K \to \infty$. For this reason, the final inversion step can often be considerably simplified if the transformed solution is expressed in terms of the (constant) bulk modulus K and one transfer function $\mathcal{M}(p)$ or E(p), or their reciprocals J(p) or D(p).

A simple example. - In order to clarify the procedure of solving a viscoelastic stress problem, we will first consider the simple example of a long, uncased, thick-walled cylinder under internal pressure. The tangential stress in the associated elastic cylinder is given in Section 3.3.2 as

$$\sigma_\theta = \frac{a^2 P_i(t)}{b^2 - a^2}\left(1 + \frac{b^2}{r^2}\right) \qquad (3.1.3)$$

Since there are no material constants in (3.1.3), it follows that the stress in a viscoelastic cylinder is the same. However, this is not true for the radial displacement

$$u = \frac{a^2 P_i(t)(1+\nu)}{(b^2 - a^2)E}\left[(1-2\nu)r + \frac{b^2}{r}\right] \qquad (3.1.4)$$

For simplicity, let us assume that the material deforms much more easily in shear than in bulk so that $\nu \doteq \frac{1}{2}$ and the elastic displacement becomes

$$u = \frac{3}{2}\,\frac{a^2 b^2}{r(b^2 - a^2)}\,\frac{P_i(t)}{E} \qquad (3.1.5)$$

which immediately gives us the transformed viscoelastic displacement as

$$\bar{u}(p) = \frac{3}{2}\,\frac{a^2 b^2}{r(b^2 - a^2)}\,\frac{\bar{P}_i(p)}{E(p)} \qquad (3.1.6)$$

For the first representation, let $E(p) = \tau_v E_v\left[p + 1/\tau_v\right]$ corresponding to the Voigt model, (Figure 2.5). With a step pressure of amplitude p_o ($p_i = 0$, $t < 0$; $p_i = p_o$, $t > 0$) the transformed pressure is $\bar{p}_i = p_o/p$ and therefore

$$\bar{u}(p) = \frac{3}{2}\,\frac{a^2 b^2 p_o}{r(b^2 - a^2)\,p\,(p + 1/\tau_v)\,\tau_v E_v} \qquad (3.1.7)$$

This expression is readily inverted by the tables to give the viscoelastic displacement

$$u(t) = \frac{3}{2} \frac{a^2 b^2 p_o}{r(b^2 - a^2)} \frac{1}{E_v} \left(1 - e^{-\frac{t}{\tau_v}}\right) \qquad (3.1.8)$$

Note that as $t \to \infty$, u approaches the displacement in an elastic cylinder with Young's modulus E_v and Poisson's ratio $\nu = \frac{1}{2}$.

Had we used a four or five element model for the modulus operator, it would have been necessary to solve a quadradic equation to invert the transform. Additional elements would likewise increase the order of the equation which has to be solved to invert $\bar{u}$. However, if the elastic constant is replaced by the compliance operator D(p), this would not be the case since the transformed strain then becomes

$$\bar{u}(p) = \frac{3}{2} \frac{a^2 b^2}{r(b^2 - a^2)} D(p) \bar{p}_i(p) \qquad (3.1.9)$$

With $\bar{p}_i = p_o/p$, the displacement is just proportional to the tensile creep compliance D(t),

$$u(t) = \frac{3}{2} \frac{a^2 b^2}{r(b^2 - a^2)} p_o D(t) \qquad (3.1.10)$$

It is important to observe, in this connection, that it is not necessary to specify a model, but only the experimental values of creep compliance, as determined in the simplest test from a tensile specimen.

The responses (3.1.8) or (3.1.10) can now be used to calculate the displacement for a general pressure-time curve by means of the Duhamel integral. If we denote the response of any linear system to a unit step pressure by $R_s(t)$, then the response R(t) of the system to a general pressure p(t), assumed to vanish for $t < 0$, is given by[3.2]

$$R(t) = \int_0^t R_s(t - \xi) \frac{dp(\xi)}{d\xi} d\xi \qquad (3.1.11)$$

Thus, the radial displacement of the cylinder in terms of the general creep compliance is simply

$$u(t) = \frac{3}{2} \frac{a^2 b^2}{r(b^2 - a^2)} \int_0^t D(t - \xi) \frac{dp(\xi)}{d\xi} d\xi \qquad (3.1.12)$$

To summarize, we can state that this problem has illustrated examples of the general rules:

1. An elastic and viscoelastic stress(displacement) are identical if the elastic variable is independent of material constants.
2. When the elastic solution is a function of only one material constant which enters as a simple factor, the transformed solution can be readily inverted if the viscoelastic operator replacing the constant is chosen such that it appears in the numerator of the transformed expression.
3. The response of a linear system to a step input can be used to calculate the behavior under arbitrary time-dependent loading.

3.2 Application to Grain Ignition.

We will now proceed to discuss, in detail, the calculation of viscoelastic tangential strain at the inner surface of a long, case-bonded grain. The model parameters determined in Section 2.6 will be used in this analysis, and it will be assumed that the bulk modulus is a constant. In addition, erosion of the inner surface will be neglected so that validity of the viscoelastic solution will be limited to times which are short relative to the total burning time.

The associated elastic strain in a long, case-bonded grain, given in Section 3.3.2, can be written as

$$\epsilon_\theta = -\frac{1-\nu^2}{E}\left[-\left(\frac{1-2\nu}{1-\nu}\right) + \frac{2\lambda^2}{\lambda^2-1}\left(1-\frac{p'}{p_i}\right)\right] p_i \qquad (3.2.1)$$

where $\lambda = b/a$, p' = pressure between cylinder and case, and the pressure ratio p'/p_i is

$$\frac{p'}{p_i} = \frac{2(1-\nu^2)}{(1+\nu)\left[1+(1-2\nu)\lambda^2\right] + (\lambda^2-1)(1-\nu_c^2)\frac{bE}{hE_c}} \qquad (3.2.2)$$

Since the viscoelastic properties were given in Section 2.6 in terms of shear compliance ($J = 1/\mu$) and bulk modulus (K), equations (3.2.1) and (3.2.2) will be rewritten in terms of these properties by using the relations (2.2.9) and (2.2.10), which yields

$$\epsilon_\theta = \frac{3p_i}{2K}\frac{\phi}{(3\phi+1)}\left[-1+2\lambda^2(1-\nu_c^2)\,C\,H(\phi)\right] \qquad (3.2.3)$$

where, for convenience, we have defined

$$\phi = KJ \tag{3.2.4a}$$

$$C = \frac{bK}{h E_c} \tag{3.2.4b}$$

$$H(\phi) = \frac{\phi^2\left[1+\frac{1}{2(1-\nu_c^2)C}\right]+\frac{5}{3}\phi\left[1+\frac{2}{(1-\nu_c^2)5C}\right]+\frac{4}{9}}{\phi^2+2\phi\left[1+\frac{1+3\lambda^2}{6(\lambda^2-1)(1-\nu_c^2)C}\right](\lambda^2-1)(1-\nu_c^2)C+\frac{2}{3}(\lambda^2-1)(1-\nu_c^2)C} \tag{3.2.4c}$$

Typical values for the various parameters are $K = 2 \times 10^6$ psi, $E_c = 30 \times 10^6$ psi, $\nu_c = 0.3$, $b/h = 200$, $\lambda = 2$ from which $C = 13.3$. It is observed that the terms containing (C) in the square brackets in $H(\phi)$ are quite small compared to unity if the above numbers are used. In fact, if they are neglected, $H(\phi)$ reduces to

$$H(\phi) = \frac{\phi+\frac{4}{3}}{\phi+2(\lambda^2-1)(1-\nu_c^2)C} = \frac{\phi+1.33}{\phi+72.80} \tag{3.2.5}$$

Actually, if in the numerator 4/3 is neglected compared to ϕ, K will disappear explicitly from (3.2.3) and the incompressible limit case will result. Further analysis, however, will show that for short times, when ϕ may be small, the 4/3 term should be retained. If all terms are retained in $H(\phi)$, we find in the numerical example that

$$H(\phi) = 1.04\frac{(\phi+1.33)(\phi+0.320)}{(\phi+76.82)(\phi+0.316)} \doteq 1.04\frac{\phi+1.33}{\phi+76.82} \tag{3.2.6}$$

so that both the numerator and denominator again become first order in ϕ. This has particular significance in reducing the complexity of the viscoelastic problem in which ϕ is a transfer function. Using the expression for $H(\phi)$ from (3.2.6), the strain is

$$\epsilon_\theta = 0.75\frac{\phi}{(3\phi+1)}\left[-1+101\left\{\frac{\phi+1.33}{\phi+76.82}\right\}\right]p_i \times 10^{-6} \tag{3.2.7}$$

Since ϕ is proportional to the grain's compliance, its limiting values are given by the material's long time (or zero frequency) value and the short time (or infinite frequency) value. From the data for polyisobutylene in Figure 2.32, the largest possible value for ϕ is $\phi(\omega \cong 0) = KJ(\omega \cong 0) = 1.38 \times 10^4$, and the smallest $\phi(\omega = \infty) = KJ(\omega = \infty) = 4.36$. Because the minimum value of ϕ is 4.36, the term -1 will be neglected in (3.2.7), and also we will let $\phi/(3\phi+1) \doteq 1/3$. With these reasonable approximations, the strain is

$$\epsilon_\theta = 25\left[\frac{\phi+1.33}{\phi+76.82}\right]p_i \times 10^{-6} \tag{3.2.8}$$

Without carrying out a viscoelastic analysis, the minimum and maximum values of ϵ_θ can be found for a pressure step p_i applied at $t = 0$ and held constant indefinitely. The initial strain is given by substituting $\phi = 4.36$ into (3.2.8), viz, $\epsilon_\theta (t = 0) = 1.75\, p_i \times 10^{-6}$; and the long time strain is given by using $\phi = 1.38 \times 10^{4}$ in (3.2.8), viz, $\epsilon_\theta (t = \infty) = 25\, p_i \times 10^{-6}$. Although it is tempting to compare these values to the ultimate uniaxial strains, it is important to recognize that these limiting values of strain do not, in general, provide sufficient information to predict whether or not the grain will fail upon ignition; the failure criterion may not only depend upon the strain biaxiality, but also upon the entire strain history and hence the precise way in which ϵ_θ varies with time. (See Section 4)

To illustrate the various procedures, examples will be presented showing the determination of time dependent responses for step and ramp type pressure inputs typical of an ignition loading for a propellant grain. First, discrete-element models will be employed, followed by an exact solution in order to examine the accuracy of the models and to investigate the practicability of by-passing models entirely by using the Fourier inversion integral technique.

3.2.1 Two and four element (bulk elastic)-step and ramp pressure.

The strain will be found first for a unit pressure step and then this solution will be used to find the response for a typical ramp type pulse. With viscoelasticity, we look upon ϕ as being a transfer function of the parameter p. For convenience, we will write (3.2.8) as

$$\bar{\epsilon}_\theta(p) = 25 \times 10^{-6}\, \bar{\xi}(p) \qquad (3.2.9)$$

and define $\bar{\xi}(p)$ as the transformed, normalized strain due to a unit pressure step $s_i(t)$ applied at $t = 0$ ($s_i(t) = 0$, $t < 0$; $s_i(t) = 1$, $t > 0$);

$$\bar{\xi}(p) = \left[\frac{\phi(p) + 1.33}{\phi(p) + 76.82}\right]\bar{s}_i(p) = \left[\frac{\phi(p) + 1.33}{\phi(p) + 76.82}\right]\frac{1}{p} \qquad (3.2.10)$$

$\xi(t)$ will be found first using a four-element model. Recall that by definition $\phi(p) = KJ(p)$, and that $J(p)$ is given by the operational compliance $k(p)$ in Figure 2.13a. Using the same definitions given in Section 2.6.3, $B_g = KJ_g$, $B_1 = KJ_1$, $B_2 = K\tau_1/\eta_2$ we have

$$\phi(p) = B_g + \frac{B_1}{\tau_1 p + 1} + \frac{B_2}{\tau_1 p} \qquad (3.2.11)$$

Substitution of (3.2.11) into (3.2.10) yields

$$\bar{\xi}(p) = \frac{(B_g+1.33)\,p^2+(B_1+B_2+B_g+1.33)\frac{p}{\tau_1}+\frac{B_2}{\tau_1^2}}{(B_g+76.82)\,p^2+(B_1+B_2+B_g+76.82)\frac{p}{\tau_1}+\frac{B_2}{\tau_1^2}}\cdot\frac{1}{p} \qquad (3.2.12)$$

After substituting the model parameters $B_1 = 50$, $B_2 = 9.5$, $B_g = 6.5$, $\tau_1 = 0.925 \times 10^{-2}$ sec. into (3.2.12) and then factoring the denominator, $\bar{\xi}(p)$ becomes

$$\bar{\xi}(p) = 0.094\,\frac{p^2+9.3\times10^2\,p+1.42\times10^4}{(p+7.50)(p+177.5)}\,\frac{1}{p} \qquad (3.2.13)$$

This can be easily inverted to obtain the time dependent normalized strain

$$\xi(t) = 1-0.54\,e^{-7.5t}-0.37\,e^{-177.5t} \qquad (3.2.14)$$

which is plotted in Figure 3.1 for three different time scales. The behavior of ξ for short times, $0 < t < 0.01$, is governed by the second exponential in (3.2.14); while the relatively long time behavior, $t > 0.03$, is determined by the first exponential. It is interesting to see that the time interval in which both exponentials act is in the time scale of the pressure pulse.

The time dependence resulting when the two-element models are used is found in a similar fashion. From Figure 2.11, the operational shear compliance for the Voigt model is

$$\phi(p) = \frac{K J_v}{\tau_v p+1} = \frac{B_v}{\tau_v p+1} \qquad (3.2.15)$$

and for the Maxwell model is

$$\phi(p) = K\left[J_m+\frac{J_m}{\tau_m p}\right] = B_m+\frac{1}{Bp} \qquad (3.2.16)$$

Substituting these expressions into the normalized strain $\xi(t)$, equation (3.2.10), we find for the Voigt model

$$\bar{\xi}(p) = 0.017\left[\frac{p+\frac{B_v+1.33}{1.33\,\tau_v}}{p+\frac{B_v+76.82}{76.82\,\tau_v}}\right]\frac{1}{p} \qquad (3.2.17)$$

and for the Maxwell model

$$\bar{\xi}(p) = \left[\frac{B_m+1.33}{B_m+76.82}\right]\left[\frac{p+\frac{1}{B(B_m+1.33)}}{p+\frac{1}{B(B_m+76.82)}}\right]\frac{1}{p} \qquad (3.2.18)$$

Inversion of (3.2.17) yields for the Voigt model

$$\xi(t) = 0.47 - 0.45 e^{-201 t} \qquad (3.2.19)$$

in which we have used the previously determined parameter values of $\beta_v = 66$, and $\tau_v = 0.925 \times 10^{-2}$ seconds. Similarly, from (3.2.18) we find the response for the Maxwell model

$$\xi(t) = 1 - 0.71 e^{-30t} \qquad (3.2.20)$$

in which we have set $\beta_m = 30$ and $\beta = 0.312 \times 10^{-3}$ seconds.

The response curves shown in Figure 3.1 for both two-element models clearly indicate that a four-element model is needed to obtain sufficient accuracy for times of the order of the pressure rise time, 0.01 seconds. However, it is seen that the four-element response deviates strongly from the exact solution after 0.1 seconds; estimation of strains at times beyond this value will probably require the use of a model with additional elements.

Strain response to the unit pressure step can be used to calculate the response $\psi(t)$ to an arbitrary pressure loading $p_i(t)$ by using the Duhamel integral

$$\psi(t) = \int_0^t \xi(t-u) \frac{dp_i(u)}{du} du \qquad (3.2.21)$$

in which the pressure is assumed to vanish for $t < 0$. The strain follows from equation (3.2.9)

$$\epsilon_0 = 25 \times 10^{-6} \psi(t) \qquad (3.2.22)$$

We will now specialize (3.2.21) to the ramp type pulse illustrated in Figure 3.2 with a derivative defined mathematically as

$$\begin{aligned}
&\frac{dp_i}{dt} = 0 && t < 0 \\
&\frac{dp_i}{dt} = \frac{p_0}{t} && 0 < t < t_1 \\
&\frac{dp_i}{dt} = 0 && t_1 < t < t_2 \\
&\frac{dp_i}{dt} = -\frac{p_0}{t_1} && t_2 < t < t_1 + t_2 \\
&\frac{dp_i}{dt} = 0 && t_1 + t_2 < t
\end{aligned} \qquad (3.2.23)$$

Using the pressure derivative given by (3.2.23), $\psi(t)$ becomes

$$\psi(t) = \frac{p_o}{t_1}\int_0^t \xi(u)\,du \qquad 0<t<t_1$$

$$\psi(t) = \frac{p_o}{t_1}\int_{t-t_1}^t \xi(u)\,du \qquad t_1<t<t_2 \qquad (3.2.24)$$

$$\psi(t) = \frac{p_o}{t_1}\left[\int_{t-t_1}^t \xi(u)\,du - \int_0^{t-t_2} \xi(u)\,du\right] \qquad t_2<t<t_1+t_2$$

$$\psi(t) = \frac{p_o}{t_1}\left[\int_{t-t_1}^t \xi(u)\,du - \int_{t-(t_1+t_2)}^{t-t_2} \xi(u)\,du\right] \qquad t_1+t_2<t$$

The response for the three different models, obtained by substituting (3.2.14), (3.2.19) and (3.2.20) into (3.2.24) is shown in Figure 3.2.

It will be recalled that in the spectral analysis we assumed that most of the strain due to one entire pulse would relax out by the time $t = 12t_1 = 7.12$ seconds. It is seen from the four-element curve that this assumption is valid since only about 10% of the maximum value remains at $t = 12t_1$.

It is important to recognize that the model parameters used in the foregoing analysis are functions of both temperature and time scale of the pressure pulse. More precisely, the parameters depend on where the frequency band of interest lies on the master curve of dynamic data. In order to make a complete design study for various temperatures and pressure rise times, it is necessary to first determine the model parameters as a function of position of this band. Then for each specified pressure rise time and temperature, the appropriate frequency band must be found. However, with each model the grain and case geometry can be varied independently of the model parameters. This assumes, of course, that the strain occuring with the various geometries relaxes out sufficiently rapid in order that the spectral analysis is valid.

3.2.2 Direct incorporation of complex compliance data using Fourier transform-step and ramp pressure.

The transfer function $\phi(p)$ in (3.2.10) generally has to be represented by an infinite element model in order to fit experimental data over the entire time scale.

If the retardation spectrum $L(\tau)$ were known, then

$$\phi(p) \equiv \kappa J(p) = \kappa\left[J_g + \int_0^\infty \frac{L(\tau)d\tau}{\left[p+\frac{1}{\tau}\right]\tau^2}\right] \qquad (3.2.25)$$

could be substituted into equation (3.2.10) and used to invert $\bar{\xi}(p)$. This procedure will usually require contour integration in the complex plane which can be quite laborious. However, application of the Fourier transform and inversion integral enables the strain to be found without using model theory or complex integration, wherein only the assumption of linear viscoelasticity is required.

Therefore, as an alternate method of analysis, an exact solution to the viscoelastic problem will be obtained by using experimental values for dynamic data directly in the Fourier inversion integral. In view of the data existing only in graphical form, it is necessary to use numerical integration. It turns out that it is much easier to perform the numerical inversion if the pressure is a step function rather than a pulse associated with a particular time scale. Thus, as before, we will first determine the strain for a pressure step applied at $t = 0$, and then extend the results to the ramp pressure by using (3.2.24). The Fourier transform of a function $f(t)$ is defined as

$$\bar{f}(\omega) = \int_{-\infty}^{\infty} f(t) e^{-i\omega t} dt \qquad (3.2.26)$$

with the inversion integral

$$f(t) = \frac{1}{2\pi}\int_{-\infty}^{\infty} \bar{f}(\omega)\, e^{i\omega t} d\omega \qquad (3.2.27)$$

Formally operating on linear differential equations with the transform is equivalent, with zero initial conditions, to replacing the time derivative by $i\omega$ and the pressure $s_i(t)$ by $\bar{s}_i(\omega)$; therefore we obtain the Fourier transformed strain from (3.2.10) by simply replacing p by $i\omega$,

$$\bar{\xi}(\omega) = A(\omega)\bar{S}_i(\omega) \qquad (3.2.28)$$

where the complex admittance $A(\omega)$ is defined as

$$A(\omega) = \frac{\phi(i\omega)+1.33}{\phi(i\omega)+76.82} \qquad (3.2.29)$$

However, $\phi(i\omega)$ is actually the nondimensional complex compliance, $\phi^*(\omega)$, defined previously in Section 2.6.3

$$\phi(i\omega) = \phi^*(\omega) = \kappa J^*(\omega) = \phi'(\omega) - i\phi''(\omega)$$

$$\phi'(\omega) = \kappa J'(\omega) \quad ; \qquad \phi''(\omega) = \kappa J''(\omega)$$

Substituting $\phi(i\omega) = \phi'(\omega) - i\phi''(\omega)$ into $A(\omega)$ and rearranging to form the real and imaginary components, we find

$$A(\omega) = A_1(\omega) - i A_2(\omega) \qquad (3.2.30)$$

where

$$A_1(\omega) = \frac{(\phi')^2 + (\phi'')^2 + 78.15\phi' + 102.5}{(\phi')^2 + (\phi'')^2 + 153.6\phi' + 5900}$$

$$A_2(\omega) = \frac{75.5\phi''}{(\phi')^2 + (\phi'')^2 + 153.6\phi' + 5900}$$

It will be convenient to write $A(\omega)$ in an alternative form

$$A(\omega) = |A(\omega)| e^{-i\epsilon(\omega)} \qquad (3.2.31)$$

where

$$|A(\omega)| = \sqrt{A_1^2(\omega) + A_2^2(\omega)}$$

$$\epsilon(\omega) = \tan^{-1} \frac{A_2(\omega)}{A_1(\omega)}$$

Both (3.2.30) and (3.2.31) are plotted in Figure 3.3 by using values for ϕ' and ϕ'' taken directly from the master curves of the real and imaginary components of complex compliance, Figure 2.32.

We have defined $\bar{s}_1(\omega)$ as the transform of a unit step function which vanishes for $t < 0$ and equals unity for $t > 0$. However, the transform cannot be found directly since the transform of the step from (3.2.26) is

$$\int_0^\infty e^{-i\omega t} dt$$

which does not converge to a definite limit. Consequently, we must consider a modified step function

$$S_\gamma(t) = 0 \quad ; \quad t<0$$
$$S_\gamma(t) = e^{-\gamma t} \quad ; \quad t>0 \qquad (3.2.32)$$

and let $\gamma \to 0$ after the final form of the inversion integral is determined. It is shown in the following that γ can be taken identically as zero in the portion of the inversion integral requiring numeral integration, while the portion in which we cannot initially take it as zero can be evaluated analytically. The transform of (3.2.32) is

$$\bar{S}_\gamma(\omega) = \int_0^\infty e^{-t(\gamma+i\omega)} dt = \frac{1}{\gamma + i\omega} \qquad (3.2.33)$$

From (3. 2. 27) and (3. 2. 33), the normalized strain due to a unit pressure step is written formally as

$$\xi(t) = \frac{1}{2\pi} \lim_{\gamma \to 0} \int_{-\infty}^{\infty} A(\omega)\, \bar{S}_\gamma(\omega)\, e^{i\omega t} d\omega$$

$$= \frac{1}{2\pi} \lim_{\gamma \to 0} \int_{-\infty}^{\infty} \frac{A(\omega)}{\gamma + i\omega} e^{i\omega t} d\omega \qquad (3.2.34)$$

In order to numerically integrate (3. 2. 34), it must first be written as a real integral. It is convenient to use form (3. 2. 31) for $A(\omega)$ so that

$$A(\omega) e^{i\omega t} = |A| e^{i(\omega t - \epsilon)} = |A| \left[\cos(\omega t - \epsilon) + i \sin(\omega t - \epsilon)\right] \qquad (3.2.35)$$

Substituting (3. 2. 35) into (3. 2. 34) and writing

$$\frac{1}{\gamma + i\omega} = \frac{\gamma - i\omega}{\gamma^2 + \omega^2}$$

we find

$$\xi(t) = \frac{1}{2\pi} \lim_{\gamma \to 0} \int_{-\infty}^{\infty} \frac{|A|}{\gamma^2 + \omega^2} \left[\gamma - i\omega\right]\left[\cos(\omega t - \epsilon) + i \sin(\omega t - \epsilon)\right] d\omega \qquad (3.2.36)$$

ϵ has been defined as

$$\epsilon = \tan^{-1} \frac{A_2(\omega)}{A_1(\omega)}$$

in which A_2 and A_1 are known only for $\omega > 0$. However, behavior of ϵ for negative ω can be determined from model theory. Reference to the most general models given in Figure 2. 15 show that the real component of complex compliance is even in ω, and the imaginary component is odd in ω. Thus, from (3. 2. 30) it is clear that $|A|$ is an even function while ϵ is odd. Using this fact, we can write (3. 2. 36) as two real integrals with limits from 0 to ∞:

$$\xi(t) = \frac{1}{\pi} \lim_{\gamma \to 0} \int_{0}^{\infty} \frac{|A|\, \omega \sin(\omega t - \epsilon)}{\gamma^2 + \omega^2} d\omega$$

$$+ \frac{1}{\pi} \lim_{\gamma \to 0} \gamma \int_{0}^{\infty} \frac{|A| \cos(\omega t - \epsilon)}{\gamma^2 + \omega^2} d\omega \equiv I_1 + I_2 \qquad (3.2.37)$$

The first integral, defined as I_1, converges uniformly for all γ and hence we can set $\gamma = 0$ under the integral sign. It is seen that if we set $\gamma = 0$ in the second integral I_2, it diverges due to the $1/\omega^2$ term in the integrand and the lower limit being zero. However, a change of variable will allow the limit to be taken. Letting $\omega \to \gamma\Omega$ in I_2, we obtain

$$I_2 = \frac{1}{\pi} \lim_{\gamma \to 0} \int_0^\infty \frac{|A(\gamma\Omega)|}{1+\Omega^2} \cos\left[\gamma\Omega t - \epsilon(\gamma\Omega)\right] d\Omega \qquad (3.2.38)$$

Since I_2 is uniformly convergent in γ, we may set $\gamma = 0$ under the integral sign, thus:

$$I_2 = \frac{1}{\pi} |A(0)| \int_0^\infty \frac{d\Omega}{1+\Omega^2} = \frac{|A(0)|}{2} \qquad (3.2.39)$$

in which we have used the fact that $\epsilon(0) = 0$. Therefore $\xi(t)$ in (3.2.37) is given by

$$\xi(t) = \frac{1}{\pi} \int_0^\infty \frac{|A|}{\omega} \sin(\omega t - \epsilon)\, d\omega + \frac{|A(0)|}{2} \qquad (3.2.40)$$

$\xi(t)$ can now be found by numerical integration. The method employed for the problem in this report was to use Simpson's rule for approximately the first two cycles of $\sin(\omega t - \epsilon)$, and then construct analytical approximations for the remaining range of integration in which the contribution to $\xi(t)$ was relatively small. The result is plotted on log-log paper in Figure 3.4, and for three different time scales in Figure 3.1 indicated as the "exact" response. The strain can be approximated by a few straight lines on log-log paper so that it has a power law form as shown in Figure 3.4.

A very useful approximate relation exists between the real part of the admittance A_1 and the strain $\xi(t)$. Examination shows that $\xi(0.5/\omega) \doteq A_1(\omega)$. Thus, by taking values of $A_1(\omega)$ from Figure 3.3 and plotting these values against $t = 0.5/\omega$, a good approximation to the exact normalized strain is obtained as shown in Figure 3.4. It is expected that thus "rule" will hold as long as the complex admittance has the form shown in Figure 3.3; however, other examples should be examined in order to determine the generality of the rule.

The solution $\xi(t)$ was obtained for a particular geometry in which certain dimensions were assumed. If it is desired to study the responses as a function of dimensional changes, in principle, the complete Fourier inversion must be carried out with each set of dimensions. However, if the rule $\xi(\alpha/\omega) = A_1(\omega)$ is found to hold for one set of dimensions, the strain can be computed directly from this when other sets are used. In the problem just solved $\alpha = 0.5$; however, it may be somewhat different for various materials and may change significantly if radical changes in dimensions are made. In a design study involving dimensional changes, limiting values should be used to check the value for α.

The analytical approximations to $\xi(t)$, given in Figure 3.4, were substituted directly into equations (3.2.24) in order to calculate the normalized strain response for the pressure pulse shown in Figure 3.2. The elastic limit cases for the strain are shown as well as the actual viscoelastic response. The limit cases correspond to the hypothetical situations in which the grain responds with glassy compliance (the smallest possible compliance which is the limiting value at high frequency) and the rubbery or equilibrium compliance (the largest possible compliance which is the limiting value at low frequencies). It is clearly seen that the actual strain history is considerably different from what an elastic limit analysis would indicate.

It is important to recognize that it was not necessary to specify any pressure time scale or temperature in obtaining the fundamental solution $\xi(t)$. This was necessary with the finite-element model analysis and consequently the solutions were valid only for a specified time scale and temperature. Since the solution just obtained is known for all time (the very short time portion is not shown in Figure 3.4, however, it can be found from the inversion integral), it can be used to draw a master response curve which is valid as long as the material's temperature is constant in time. That is, the time-temperature superposition principle discussed in the Section 2.5 can be applied by plotting ξ as a function of (t/a_T). It should be recalled that a small approximation is made in doing this since the linear dependence of compliance on temperature has been neglected. If this dependency is considered, then the admittance plotted against reduced frequency (ωa_T) will change slightly with temperature. However, the present inaccuracy of propellant data does not warrant such a correction.

The master curve for $\xi(t/a_T)$ can be used to make a parametric study of response as a function of temperature and pressure rise time for each set of dimensions assigned to the grain-case geometry. In view of the empirical relation found between the real part of the admittance A_1 and ξ, which becomes $\xi(t/a_T) = \xi(\alpha/\omega a_T) \doteq A_1(\omega a_T)$ in terms of reduced variables, the response $\xi(t/a_T)$ can be found quite readily as a function dimensions if further examination verifies the relation for other examples. Such a set of master curves would allow a complete design study to be made. This conclusion can be contrasted with that made for the solution with finite-element models. It will be recalled that with these simple models each solution could be easily used in a parametric study in which dimensions were changed, and a set of these solutions were needed to study the effect of temperature and pressure pulse variations. Also, if it is desired to take erosion of the inner

boundary into account, the Fourier integral method cannot be used; however, one can use a method such as suggested by Lee and Radok[3.3] in which finite element models are employed. Consequently, we cannot state, in general, that one method is better than the other since the most appropriate one will be determined by the particular problem at hand.

3.2.3 Extension of the solutions to pressurized cylinders with internal star-shaped perforations.

Inasmuch as the stress and displacement solutions presented in this report apply only to circularly perforated cylinders, it is useful to extend these solutions to include the more common star configurations (Figure 3.5). An approximate method based upon elastic concentration factors will be discussed for both elastic and viscoelastic grains. In a paper by Ordahl and Williams[3.4], this method is applied to elastic grains (with and without cases) and several design curves are presented that give preliminary values of stress concentration factors*.

The concentration factor K has been defined as[3.4]

$$K = \frac{\sigma_r^s - \sigma_\theta^s}{\sigma_r - \sigma_\theta} \tag{3.2.41}$$

where σ_r^s, σ_θ^s = radial and tangential (hoop) principal stresses, respectively, in a star perforated grain,

σ_r, σ_θ = radial and tangential principal stresses respectively, in a grain with a circular port.

The stresses σ_r and σ_θ, for either plane stress or the condition of constant strain ϵ_z, are given in Section 3.3.2 as

$$\sigma_r = \left(\frac{b}{r}\right)^2 \frac{p' - p_i}{\left(\frac{b}{a}\right)^2 - 1} + \frac{p_i - \left(\frac{b}{a}\right)^2 p'}{\left(\frac{b}{a}\right)^2 - 1} \tag{3.2.42}$$

$$\sigma_\theta = -\left(\frac{b}{r}\right)^2 \frac{p' - p_i}{\left(\frac{b}{a}\right)^2 - 1} + \frac{p_i - \left(\frac{b}{a}\right)^2 p'}{\left(\frac{b}{a}\right)^2 - 1}$$

* The data was preliminary in the sense that only a limited amount of experimental values was used and that subsequent checks indicate about 20% unconservative results. It is understood that other workers are presently engaged in refining the earlier data.

Also

$$\sigma_r - \sigma_\theta = 2\left(\frac{b}{r}\right)^2 \frac{p' - p_i}{\left(\frac{b}{a}\right)^2 - 1} \qquad (3.2.43)$$

where p_i = internal pressure

p' = external pressure (for a case-bonded grain this is the pressure between the case and grain)

a = inside radius of circular grain, and

b = outside radius of circular grain.

It is seen that ($\sigma_r - \sigma_\theta$) depends only on the pressure difference ($p'-p_i$); so that in order for K to be independent of loading, ($\sigma_r^s - \sigma_\theta^s$) must also be proportional to ($p' - p_i$). This will now be shown. Since linear behavior is assumed, σ_r^s and σ_θ^s are generally written as

$$\sigma_r^s = \beta_1 p_i + \beta_2 p'$$
$$\sigma_\theta^s = \beta_3 p_i + \beta_4 p' \qquad (3.2.44)$$

in which β_1, β_2, β_3, and β_4 are geometrical factors pertaining to a particular configuration and, in general, are space dependent. It should be noted that these factors are independent of material properties since the stresses in (3.2.44) apply to a two dimensional problem with all stress boundary conditions. The stress difference is

$$\sigma_r^s - \sigma_\theta^s = (\beta_1 - \beta_3) p_i + (\beta_2 - \beta_4) p' \qquad (3.2.45)$$

A relationship between the β_i, which must hold for all pressures, can be found by considering the limit case of $p_i = p' = p$. When $p_i = p' = p$, a cylinder of any arbitrary cross-section is in a state of uniform hydrostatic pressure so that $\sigma_r^s = \sigma_\theta^s = -p$, and therefore from (3.2.45) the β_i must satisfy

$$(\beta_1 - \beta_3) = -(\beta_2 - \beta_4) \qquad (3.2.46)$$

Substitution of (3.2.46) into (3.2.45) yields

$$\sigma_r^s - \sigma_\theta^s = (\beta_2 - \beta_4)(p' - p_i) \qquad (3.2.47)$$

which was to be shown.

The maximum stresses and strains occur at the star points, indicated in Figure 3.5, and for this reason the necessary relations will be presented for calculating stresses and strains at this location only. It is clear that because of symmetry there is no shear stress acting along radial lines drawn through the star points which means the stresses at the star points, denoted as σ_r^{sp} and σ_θ^{sp}, are principle stresses.

At the star point (r = a), $K \equiv K_i$ (this corresponds to the notation of reference 3.4 and $\sigma_r^{sp} = -p_i$. Using this notation, σ_θ^{sp} is found from (3.2.41) and (3.2.43) evaluated at r = a:

$$\sigma_\theta^{sp} = K_i \left[\frac{2\left(\frac{b}{a}\right)^2}{\left(\frac{b}{a}\right)^2 - 1} \right] (p_i - p') - p_i \qquad (3.2.48)$$

It is apparent from this result that only when $p_i = 0$ can K_i be interpreted as the ratio of σ_θ^{sp} to σ_θ. It should be emphasized that the above results are independent of material properties if p_i and p' are known; thus, both viscoelastic and elastic stresses can be found using (3.2.48) with the values of K_i given in reference 3.4. However, with a case-bonded grain, p' (assumed uniform) is the pressure between case and grain so that it is related to p_i through geometrical factors and material properties. This necessitates the use of an approximation in which shear stresses at r = b are neglected, and p' is assumed to be the same for both the star and circular configurations if the radius (a) of the circular port is made equal to the radius drawn to the star point. It is evident that this approximation improves as the web fraction b-a/b increases.

Elastic solutions for p' are given in Section 3.3.2 for several pressure problems. With a viscoelastic grain it is necessary to solve a differential equation that arises when elastic constants in the equation for p' are replaced by appropriate differential operators. It may be noted that, in general, p_i and p' have the same time dependence only if the grain is elastic.

The radial, tangential, and axial strains at the star points, denoted as ϵ_r^{sp}, ϵ_θ^{sp}, and ϵ_z^{sp} respectively, are found by substituting $\sigma_r^{sp} = -p_i$ and (3.2.48) into the stress-strain equations

$$\epsilon_r^{sp} = \frac{1}{E}\left[-p_i - \nu(\sigma_\theta^{sp} + \sigma_z^{sp})\right]$$

$$\epsilon_\theta^{sp} = \frac{1}{E}\left[\sigma_\theta^{sp} - \nu(-p_i + \sigma_z^{sp})\right] \qquad (3.2.49)$$

$$\epsilon_z^{sp} = \frac{1}{E}\left[\sigma_z^{sp} - \nu(-p_i + \sigma_\theta^{sp})\right]$$

Two important cases can be distinguished: First, for plane stress ($\sigma_z = 0$)

$$\epsilon_r^{sp} = -\frac{1}{E}\left[(1-\nu)p_i + \nu K_i\left\{\frac{2(\frac{b}{a})^2}{(\frac{b}{a})^2-1}\right\}(p_i - p')\right]$$

$$\epsilon_\theta^{sp} = \frac{1}{E}\left[-(1-\nu)p_i + K_i\left\{\frac{2(\frac{b}{a})^2}{(\frac{b}{a})^2-1}\right\}(p_i - p')\right] \qquad (3.2.50)$$

$$\epsilon_z^{sp} = -\frac{\nu}{E}\left[-2p_i + K_i\left\{\frac{2(\frac{b}{a})^2}{(\frac{b}{a})^2-1}\right\}(p_i - p')\right]$$

For plane strain ($\epsilon_z = 0$):

$$\epsilon_r^{sp} = -\frac{(1-\nu^2)}{E}\left[\left(1-\frac{\nu}{1-\nu}\right)p_i + \frac{\nu}{1-\nu}K_i\left\{\frac{2(\frac{b}{a})^2}{(\frac{b}{a})^2-1}\right\}(p_i - p')\right] \qquad (3.2.51)$$

$$\epsilon_\theta^{sp} = \frac{1-\nu^2}{E}\left[-\left(1-\frac{\nu}{1-\nu}\right)p_i + K_i\left\{\frac{2(\frac{b}{a})^2}{(\frac{b}{a})^2-1}\right\}(p_i - p')\right]$$

An interesting limit case results for incompressible materials ($\nu = \frac{1}{2}$). The first term appearing in the brackets in (3.2.51) will then vanish leaving for plane strain

$$\epsilon_r^{sp} = K_i \epsilon_r(a)$$

$$\epsilon_\theta^{sp} = K_i \epsilon_\theta(a) \qquad (3.2.52)$$

Viscoelastic star point strains are obtained from the applicable set of preceding equations in the usual manner by first replacing E and ν by viscoelastic operators and then inverting to obtain the time dependence.

3.3 A Collection of Useful Formulas.

3.3.1 Range of validity of linear elastic analysis

At the end of Section 2.5, certain conditions were alluded to, under which the propellant could be treated as essentially elastic. The answer to this question was deferred until this section in order to provide directly an application of the viscoelastic theory discussed under Sections 2.4, 2.5, and 2.6. This was done in Sections 3.1 and 3.2, where an ignition type of problem was discussed. This problem is peculiar in the sense that in the first few microseconds after rapidly applied loading at ambient temperature, the propellant changes its mechanical response from glassy to rubbery. In other applications of load at room temperature, we are not

concerned with response in the first few microseconds, but rather with long time behavior, such as slump. Or equivalently, if the load is applied at extremely low temperatures, we are only concerned with short-time behavior. In both these cases, the propellant behaves essentially elastic--rubbery at ambient, or glassy at low temperatures. Thus, it is possible in a large number of cases to assume linear elastic behavior, and thereby use the following collection of elastic solutions directly in an engineering analysis.

Before presenting these formulas, it is important to establish ranges of validity. Thus, at low temperatures it is necessary to know the limit of duration beyond which creep effects enter the picture. Conversely, at ambient temperatures, it is necessary to know the minimum duration within which relaxation effects are still important.

In order to investigate this point, we must first choose a tolerance limit within which the reduced modulus is to be considered elastic. Thus, for the case of short times, if the tolerance limit is denoted by δ_g, and we consider the tensile modulus, for example, then

$$\frac{E_{rel.} - E_e}{E_g - E_e} > 1 - \delta_g \qquad (3.3.1)$$

This criterion guarantees that the propellant acts perfectly elastic, glassy and brittle during the time scale of the experiment at a given temperature. In order to evaluate this time scale, we use the modified power law distribution, Section 2.4.3, and set

$$1 - \delta_g < \left[1 + \frac{t}{K(T)}\right]^{-n} \simeq 1 - n\frac{t}{K(T)} \qquad (3.3.2)$$

so that

$$t_{\substack{max. \\ glassy}} < K(T)\frac{\delta_g}{n} \qquad (3.3.3)$$

Similarly, for long times, with the tolerance limit again denoted by δ_e, we have

$$\frac{E_{rel.} - E_e}{E_g - E_e} < \delta_e \qquad (3.3.4)$$

This criterion guarantees that the propellant acts perfectly elastic and rubbery within the time scale of the experiment at a given temperature. In order to evaluate this time scale, we set

$$\delta > \left[1 + \frac{t}{K(T)}\right]^{-n} \simeq \left[\frac{t}{K(T)}\right]^{-n}, \quad \text{so that} \qquad (3.3.5)$$

$$t_{\substack{\text{min.}\\ \text{rubbery}}} > K(T)\delta^{-\frac{1}{n}} \qquad (3.3.6)$$

By way of comparison, we have the following tabulation for $n = \frac{1}{2}$, $\delta = 10^{-3}$

TABLE 3.1

Material	T_d, °F	$K_{d,\min.}$	$K(-80°F)_{\min.}$	$t_{\substack{\text{min.,}\\ \text{glassy}\\ -80°F}}$	$t_{\substack{\text{min.,}\\ \text{rubbery}\\ -80°F}}$	$K_{\substack{\text{min.}\\ (+80°F)}}$	$t_{\substack{\text{min.,}\\ \text{glassy}\\ +80°F}}$	$t_{\substack{\text{min.,}\\ \text{rubbery}\\ +80°F}}$
unfilled polyurethane binder	−80	2	2	4×10^{-3}	2×10^{6}	2.4×10^{-10}	4.8×10^{-10}	2.4×10^{-4}
one kind of polyurethane propellant	0	2	7.3×10^{64}	15×10^{61}	7.3×10^{70}	14×10^{-8}	28×10^{-11}	14×10^{-2}

It is apparent that, in the case of a propellant with a high brittle or distinctive temperature, relaxation effects are negligible at -80°F, while relaxation is completed with 9 sec. at +80°F. On the other hand, in the case of an unfilled rubber or a propellant with a brittle temperature down around -80°F, relaxation effects are very important down at -80°F, and have completely relaxed out at +80°F.

One can now interpret this extent of relaxation in terms of the mechanical model. For convenience, we use a Wiechert model characterized by a modified power law distribution and ask what the corresponding relaxation times are, below which all dashpots have already relaxed, and above which no dashpots have had time to relax at a given time and temperature. Thus, for the latter case, we set

$$\frac{1-\delta}{\left[1+\frac{t}{K(T)}\right]^n} = \frac{[K(T)]^n}{\Gamma(n)}\int_{\tau_{\min.}}^{\infty} \frac{e^{-\frac{t+K(T)}{\tau}}}{\tau^{n+1}}\,d\tau \qquad (3.3.7)$$

This is equivalent to statement that, at time t and temperature K(T), all dashpots whose relaxation times are less than $\tau_{\min}$ have already relaxed out, in the course of which the modulus has only been reduced by the tolerance factor $(1-\delta)$. We replace $(t + K)/\tau$ by v to obtain

$$\frac{1-\delta}{\left[1+\frac{t}{K(T)}\right]^n} = \frac{[K(T)]^n}{\Gamma(n)}\int_{0}^{\frac{t+K(T)}{\tau_{\min.}}} \frac{e^{-v}v^{n-1}}{[t+K(T)]^n}\,dv \qquad (3.3.8)$$

which yields

$$1-\delta = \frac{\gamma\left[\frac{t+K(T)}{\tau_{\min.}}, n\right]}{\Gamma(n)} \underset{\tau_{\min.} \gg t+K(T)}{\simeq} \frac{\left[\frac{t+K(T)}{\tau_{\min.}}\right]^n}{n} \qquad (3.3.9)$$

so that

$$\frac{t+K(T)}{\tau_{min.}} = [n(1-\delta)]^{\frac{1}{n}} \qquad (3.3.10)$$

or

$$\tau_{min.} = \frac{t+K(T)}{[n(1-\delta)]^{\frac{1}{n}}} \simeq \frac{t+K(T)}{n^{\frac{1}{n}}} \underset{n=\frac{1}{4}}{\doteq} 4\,[t+K(T)] \qquad (3.3.11)$$

Similarly, in order to determine the relaxation time below which all dashpots have already relaxed at given time and temperature, we set

$$\frac{\delta}{\left[1+\frac{t}{K(T)}\right]^n} = \frac{[K(T)]^n}{\Gamma(n)} \int_0^{\tau_{max.}} \frac{e^{-\frac{t+K(T)}{\tau}}}{\tau^{n+1}}\, d\tau \qquad (3.3.12)$$

This is equivalent to the statement that, at time and temperature K(T), all dashpots whose relaxation times are greater than τ_{max} have not yet relaxed out, leaving a tolerance factor δ of the original modulus. We again replace $(t + K)/\tau$ by v to obtain

$$\frac{\delta}{\left[1+\frac{t}{K(T)}\right]^n} = \frac{[K(T)]^n}{\Gamma(n)} \int_{\frac{t+K(T)}{\tau_{max.}}}^{\infty} \frac{e^{-v} v^{n-1}}{[t+K(T)]^n}\, dv \qquad (3.3.13)$$

$$\delta = \frac{\Gamma\left[\frac{t+K(T)}{\tau_{max.}}, n\right]}{\Gamma(n)} \underset{\tau_{max.} \ll t+K(T)}{\simeq} \frac{e^{-\frac{t+K(T)}{\tau_{max.}}}}{\left[\frac{t+K(T)}{\tau_{max.}}\right]^{1-n}}, \text{ so that} \qquad (3.3.14)$$

$$\frac{t+K(T)}{\tau_{max.}} \underset{n=\frac{1}{4}}{\doteq} 5.5 \text{ , or} \qquad (3.3.15)$$

$$\tau_{max.} \doteq [t+K(T)]/5.5 \qquad (3.3.16)$$

Equations (3.3.11) and (3.3.16) show very clearly the cut-off relaxation times follow the time scale of the experiment; the magnification factors 4 and 1/5.5 respectively depend only on the tolerance factor δ, and the log-log slope.

3.3.2 Stress-strain fields in cylinders.

The following pages summarize first the important equations in cylindrical coordinates which define the stress-strain field in both infinite and finite cylinders under various types of loadings. The general cylindrical equations are listed, followed by those restricted to axial symmetry for both three and two-dimensional problems. Following this, simple loadings such as simple tension, internal pressurization and torsion are applied to free and elastically cased hollow tubes. Some relations for solid cylinders are also included. Finally, thermoelastic equations and simple thermal stress fields are presented.

LIST OF STRESS-STRAIN FIELDS IN CYLINDERS

DEFINITIONS OF SYMBOLS AND TERMS

a	- inside radius of cylindrical propellant grain
b	- outside radius of cylindrical propellant grain
c	- outside radius of case, as subscript for case properties
E	- Young's modulus
e	- relative volume change: $\Delta V/V = \epsilon_r + \epsilon_\theta + \epsilon_z$
g	- acceleration due to gravity 32.17 fps
h	- case thickness $\ll$ b
ln	- natural logarithm, base e 2.71
p	- pressure, psi.
r	- radial coordinate
R	- body force in radial direction, as for example, centrifugal force
T	- temperature change from refe[illegible] or initial temperature
u	- radial displacement
v	- tangential displacement
w	- axial displacement
z	- axial coordinate
Z	- body force in axial direction, e.g., gravity
α	- coefficient of thermal expansion
γ	- shear strain
∇	- del operator for differentiation
ϵ_c	- case to propellant modulus ratio $= 2bhE_c / [(b^2-a^2) E]$
ϵ	- normal strain
θ	- tangential coordinate of the cylindrical system
Θ	- body force in tangential direction
μ	- shear modulus of elasticity $= E/ [2(1 + \nu)]$
λ	- Lame constant $= \nu E/ [(1 + \nu)(1 - 2\nu)]$
ν	- Poisson's ratio
ρ	- specific density - lbs/in^3
σ	- normal stress
τ	- shear stress
ϕ	- stress function

Bonded	- adhesion of propellant to case
End effects	- effects due to finite length cylinders: $z = 0$ or $z = \ell$
Necking effect	- shrinking of cross-section due to elongation
Plane stress	- no stress in axial direction: $\sigma_z = 0$
Plane strain	- no strain (displacement) in axial direction: $\epsilon_z = 0$
Second order	- a smaller quantity which is proportional to square of the variable
	- most elastic solutions are first order linear theory
Small strains	- strains of the order of a few percent for linear theory
St. Venant	- (a) localized effects at boundaries die out as boundaries are remote
	- (b) simple first order torsion in which ends rotate as solid disks
Steady flow	- temperature distribution constant with time
Subscript ($^{r}_{\theta}$)	- used to indicate two solutions simultaneously - upper sign option with upper subscript, etc.

CYLINDRICAL EQUATIONS:

EQUILIBRIUM:

$$\frac{\partial \sigma_r}{\partial r} + \frac{1}{r}\frac{\partial \tau_{r\theta}}{\partial \theta} + \frac{\partial \tau_{rz}}{\partial z} + \frac{\sigma_r - \sigma_\theta}{r} + R = 0$$

$$\frac{\partial \tau_{r\theta}}{\partial r} + \frac{1}{r}\frac{\partial \sigma_\theta}{\partial \theta} + \frac{\partial \tau_{\theta z}}{\partial z} + \frac{2\tau_{r\theta}}{r} + \Theta = 0$$

$$\frac{\partial \tau_{rz}}{\partial r} + \frac{1}{r}\frac{\partial \tau_{\theta z}}{\partial \theta} + \frac{\partial \sigma_z}{\partial z} + \frac{\tau_{rz}}{r} + Z = 0$$

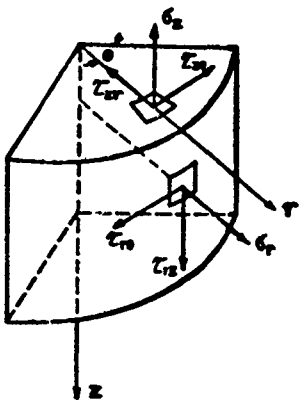

STRESS – STRAIN:

$$\epsilon_r = \frac{1}{E}\left[\sigma_r - \nu(\sigma_\theta + \sigma_z)\right]$$

$$\epsilon_\theta = \frac{1}{E}\left[\sigma_\theta - \nu(\sigma_r + \sigma_z)\right]$$

$$\epsilon_z = \frac{1}{E}\left[\sigma_z - \nu(\sigma_r + \sigma_\theta)\right]$$

$$\gamma_{r\theta} = \frac{\tau_{r\theta}}{\mu}, \quad \gamma_{rz} = \frac{\tau_{rz}}{\mu}, \quad \gamma_{\theta z} = \frac{\tau_{\theta z}}{\mu}, \quad \mu = \frac{E}{2(1+\nu)}$$

DISPLACEMENT:

$$\epsilon_r = \frac{\partial u}{\partial r}, \quad \epsilon_\theta = \frac{u}{r} + \frac{1}{r}\frac{\partial v}{\partial \theta}, \quad \epsilon_z = \frac{\partial w}{\partial z}$$

$$\gamma_{r\theta} = \frac{1}{r}\frac{\partial u}{\partial \theta} + \frac{\partial v}{\partial r} - \frac{v}{r}, \quad \gamma_{rz} = \frac{\partial u}{\partial z} + \frac{\partial w}{\partial r}, \quad \gamma_{\theta z} = \frac{\partial v}{\partial z} + \frac{1}{r}\frac{\partial w}{\partial \theta}$$

COMPATIBILITY:

$$\nabla^4 \phi = 0, \qquad \phi = \text{stress function}$$

$$\nabla^2 = \frac{\partial^2}{\partial r^2} + \frac{1}{r}\frac{\partial}{\partial r} + \frac{1}{r^2}\frac{\partial^2}{\partial \theta^2} + \frac{\partial^2}{\partial z^2}$$

AXIALLY SYMMETRIC EQUATIONS

EQUILIBRIUM:

$$\left.\begin{aligned} &\frac{\partial \sigma_r}{\partial r} + \frac{\partial \tau_{rz}}{\partial z} + \frac{\sigma_r - \sigma_\theta}{r} + R = 0 \\ &\frac{\partial \tau_{rz}}{\partial r} + \frac{\partial \sigma_z}{\partial z} + \frac{\tau_{rz}}{r} + Z = 0 \end{aligned}\right\} \text{ No dependence on } \theta,\ \tau_{r\theta} = \tau_{\theta z} = 0$$

STRAIN - DISPLACEMENT:

$$\epsilon_r = \frac{\partial u}{\partial r}, \quad \epsilon_\theta = \frac{u}{r}, \quad \epsilon_z = \frac{\partial w}{\partial z}, \quad \gamma_{rz} = \frac{\partial u}{\partial z} + \frac{\partial w}{\partial r}$$

(Stress - Strain relation unchanged)

STRESS FUNCTIONAL APPROACH (NO BODY FORCES):

$$\nabla^4 \phi = 0, \quad \nabla^2 \equiv \frac{\partial^2}{\partial r^2} + \frac{1}{r}\frac{\partial}{\partial r} + \frac{\partial^2}{\partial z^2}$$

$$\sigma_r = \frac{\partial}{\partial z}\left[\nu \nabla^2 \phi - \frac{\partial^2 \phi}{\partial r^2}\right]$$

$$\sigma_\theta = \frac{\partial}{\partial z}\left[\nu \nabla^2 \phi - \frac{1}{r}\frac{\partial \phi}{\partial r}\right]$$

$$\sigma_z = \frac{\partial}{\partial z}\left[(2-\nu)\nabla^2 \phi - \frac{\partial^2 \phi}{\partial z^2}\right]$$

$$\tau_{rz} = \frac{\partial}{\partial r}\left[(1-\nu)\nabla^2 \phi - \frac{\partial^2 \phi}{\partial z^2}\right]$$

$$\epsilon_r = -\frac{(1+\nu)}{E}\frac{\partial^3 \phi}{\partial r^2 \partial z}$$

$$\epsilon_\theta = -\frac{(1+\nu)}{E}\frac{1}{r}\frac{\partial^2 \phi}{\partial r \partial z}$$

$$\epsilon_z = \frac{(1+\nu)}{E}\frac{\partial}{\partial z}\left[(1-2\nu)\nabla^2 \phi + \frac{\partial^2 \phi}{\partial r^2} + \frac{1}{r}\frac{\partial \phi}{\partial r}\right]$$

$$u = -\frac{(1+\nu)}{E}\frac{\partial^2 \phi}{\partial r \partial z}$$

$$w = \frac{(1+\nu)}{E}\left[(1-2\nu)\nabla^2 \phi + \frac{\partial^2 \phi}{\partial r^2} + \frac{1}{r}\frac{\partial \phi}{\partial r}\right]$$

AXIALLY SYMMETRIC EQUATIONS - TWO DIMENSIONAL:

EQUILIBRIUM:

$$\frac{\partial \sigma_r}{\partial r} + \frac{\sigma_r - \sigma_\theta}{r} + R = 0$$

STRAIN - DISPLACEMENT:

$$\epsilon_r = \frac{\partial u}{\partial r}, \qquad \epsilon_\theta = \frac{u}{r}, \qquad \epsilon_z = \frac{\partial w}{\partial z}$$

PLANE STRESS:	PLANE STRAIN:
$\sigma_z = 0$	$\epsilon_z = 0$
$\epsilon_r = \frac{1}{E}(\sigma_r - \nu \sigma_\theta)$	$\epsilon_r = \frac{1}{E}\left[\sigma_r - \nu(\sigma_\theta + \sigma_z)\right] = \left(\frac{1-\nu^2}{E}\right)\left[\sigma_r - \left(\frac{\nu}{1-\nu}\right)\sigma_\theta\right]$
$\epsilon_\theta = \frac{1}{E}(\sigma_\theta - \nu \sigma_r)$	$\epsilon_\theta = \frac{1}{E}\left[\sigma_\theta - \nu(\sigma_r + \sigma_z)\right] = \left(\frac{1-\nu^2}{E}\right)\left[\sigma_\theta - \left(\frac{\nu}{1-\nu}\right)\sigma_r\right]$
$\epsilon_z = -\frac{\nu}{E}(\sigma_r + \sigma_\theta)$	

Hence, to change plane stress into plane strain, substitute:

$$\frac{E}{1-\nu^2} \text{ for } E \text{ and } \frac{\nu}{1-\nu} \text{ for } \nu.$$

STRESS FUNCTIONAL APPROACH (NO BODY FORCE):

$$\nabla^4 \phi = 0$$

$$\nabla^2 \equiv \frac{\partial^2}{\partial r^2} + \frac{1}{r}\frac{\partial}{\partial r}$$

$$\sigma_r = \frac{1}{r}\frac{\partial \phi}{\partial r} = \frac{A}{r^2} + 2C$$

$$\sigma_\theta = \frac{\partial^2 \phi}{\partial r^2} = -\frac{A}{r^2} + 2C$$

$$\phi = A \ln r + C r^2$$

PRESSURE – SOLID CYLINDER – NO CASE

TWO DIMENSIONAL PLANE STRESS:

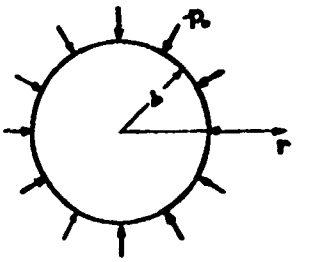

BOUNDARY CONDITIONS:

$\sigma_r = -p_o$: $r = b$

$\sigma_z = 0$: $z = 0, \ell$

STRESSES:

$\sigma_r = \sigma_\theta = -p_o$

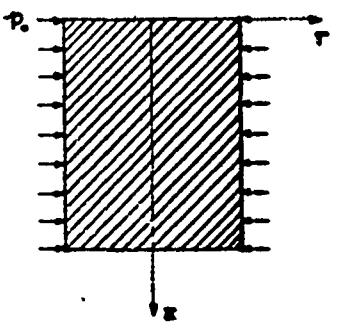

STRAINS & DISPLACEMENTS:

$$\epsilon_r = \epsilon_\theta = -\frac{(1-\nu)}{E} p_o$$

$$u = -\frac{(1-\nu)}{E} p_o r$$

$$\epsilon_z = \frac{2\nu}{E} p_o$$

$$w = \frac{2\nu}{E} p_o z$$

TWO DIMENSIONAL PLANE STRAIN:

Boundary conditions & stresses same except $\epsilon_z = 0$: $z = 0, \ell$ and $\sigma_z = -2\nu p_o$

STRAINS & DISPLACEMENTS:

$$\epsilon_r = \epsilon_\theta = -\frac{(1+\nu)(1-2\nu)}{E} p_o$$

$$u = -\frac{(1+\nu)(1-2\nu)}{E} p_o r$$

ASSUMPTION:

1. No end effects

PRESSURE – SOLID CYLINDER – WITH CASE

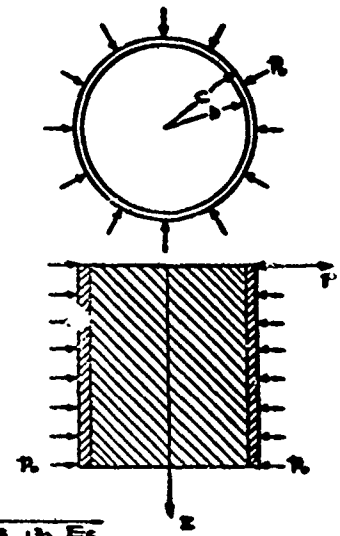

TWO DIMENSIONAL PLANE STRESS:

BOUNDARY CONDITIONS:

$\sigma_r = -p_o$: $r = c$

$u = u_c$, $z = 0$: $r = b$

$\sigma_z = 0$: $z = 0, \ell$

STRESSES IN SOLID CYLINDER:

$$\sigma_r = \sigma_\theta = -p' = \frac{-2c^2 p_o}{(1+\nu_c)c^2 + (1-\nu_c)b^2 + (1-\nu)(c^2-b^2)\frac{E_c}{E}}$$

p' = pressure between cylinder and case

FOR THIN CASE:

$$p' = \frac{p_o}{1+(1-\nu)\frac{h}{b}\frac{E_c}{E}}$$

STRAINS & DISPLACEMENTS IN SOLID CYLINDER:

$$\epsilon_r = \epsilon_\theta = -\frac{(1-\nu)}{E}p'$$

$$u = -\frac{(1-\nu)}{E}p'r$$

$$\epsilon_z = \frac{2\nu}{E}p'$$

$$w = \frac{2\nu}{E}p'z$$

STRESSES IN CASE:

$$\sigma_r = \frac{b^2c^2(p_o-p')}{c^2-b^2}\frac{1}{r^2} + \frac{p'b^2 - p_o c^2}{c^2-b^2}$$

$$\sigma_\theta = -\frac{b^2c^2(p_o-p')}{c^2-b^2}\frac{1}{r^2} + \frac{p'b^2 - p_o c^2}{c^2-b^2}$$

STRAINS & DISPLACEMENTS IN CASE

$$\epsilon_r = \frac{1}{(c^2-b^2)E_c}\left[\frac{b^2c^2(p_o-p')(1+\nu_c)}{r^2} + (p'b^2-p_oc^2)(1-\nu_c)\right]$$

$$\epsilon_\theta = \frac{1}{(c^2-b^2)E_c}\left[-\frac{b^2c^2(p_o-p')(1+\nu_c)}{r^2} + (p'b^2-p_oc^2)(1-\nu_c)\right]$$

$$\epsilon_z = -\frac{2\nu_c(p'b^2-p_oc^2)}{(c^2-b^2)E_c}$$

$$u = \frac{1}{(c^2-b^2)E_c}\left[-\frac{b^2c^2(p_o-p')(1+\nu_c)}{r} + (p'b^2-p_oc^2)(1-\nu_c)r\right]$$

$$w = -\frac{2\nu_c(p'b^2-p_oc^2)}{(c^2-b^2)E_c}z$$

ASSUMPTIONS:

1. No end effects
2. No shear transmitted between cylinder and case.

PRESSURE - SOLID CYLINDER - WITH CASE (CONT.)

TWO DIMENSIONAL PLANE STRAIN:

BOUNDARY CONDITIONS:

$\sigma_r = -p_o$: $r = c$

$u = u_o$: $r = b$

$\epsilon_z = 0$: $z = 0, \ell$

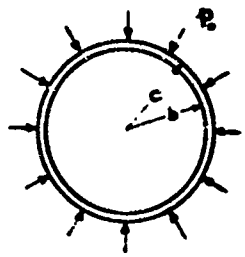

STRESSES IN SOLID CYLINDER:

$$\sigma_r = \sigma_\theta = -p' = \frac{-2(1-\nu_c)c^2 p_o}{c^2 + (1-2\nu_c)b^2 + (1-2\nu)(c^2-b^2)\frac{(1+\nu)E_c}{(1+\nu_c)E}}$$

p' = pressure between cylinder and case

FOR THIN CASE:

$$p' = \frac{p_o}{1 + \frac{(1-2\nu)(1+\nu)}{1-\nu_c^2}\frac{hE_c}{bE}}$$

STRAINS & DISPLACEMENTS IN CYLINDER:

$$\epsilon_r = \epsilon_\theta = -\frac{(1-2\nu)(1+\nu)}{E}p'$$

$$u = -\frac{(1-2\nu)(1+\nu)}{E}p'r$$

STRESSES IN CASE:

$$\sigma_r = \frac{b^2c^2(p_o - p')}{c^2-b^2}\frac{1}{r^2} + \frac{p'b^2 - p_o c^2}{c^2-b^2}$$

$$\sigma_\theta = -\frac{b^2c^2(p_o - p')}{c^2-b^2}\frac{1}{r^2} + \frac{p'b^2 - p_o c^2}{c^2-b^2}$$

$$\sigma_z = \frac{2\nu_c(p'b^2 - p_o c^2)}{c^2-b^2}$$

STRAINS & DISPLACEMENTS IN CASE:

$$\epsilon_r = \frac{1+\nu_c}{(c^2-b^2)E_c}\left[\frac{b^2c^2(p_o-p')}{r^2} + (p'b^2 - p_oc^2)(1-2\nu_c)\right]$$

$$\epsilon_\theta = \frac{1+\nu_c}{(c^2-b^2)E_c}\left[-\frac{b^2c^2(p_o-p')}{r^2} + (p'b^2 - p_oc^2)(1-2\nu_c)\right]$$

$$u = \frac{1+\nu_c}{(c^2-b^2)E_c}\left[-\frac{b^2c^2(p_o-p')}{r} + (p'b^2 - p_oc^2)(1-2\nu_c)r\right]$$

ASSUMPTION:

1. No end effects.

PRESSURE - HOLLOW CYLINDER - EXTERNAL PRESSURE - NO CASE

TWO DIMENSIONAL PLANE STRESS:

BOUNDARY CONDITIONS:

$\sigma_r = 0$: $r = a$

$\sigma_r = -p_o$: $r = b$

$\sigma_z = 0$: $z = 0, l$

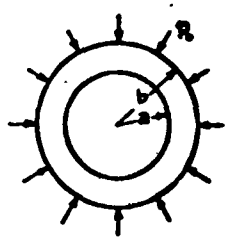

STRESSES:

$$\sigma_r = -\frac{b^2 p_o}{b^2 - a^2}\left(1 - \frac{a^2}{r^2}\right)$$

$$\sigma_\theta = -\frac{b^2 p_o}{b^2 - a^2}\left(1 + \frac{a^2}{r^2}\right)$$

STRAINS & DISPLACEMENTS:

$$\left.\begin{aligned} \epsilon_r &= -\frac{b^2 p_o}{(b^2 - a^2)E}\left[(1-\nu) - (1+\nu)\frac{a^2}{r^2}\right] \\ \epsilon_\theta &= -\frac{b^2 p_o}{(b^2 - a^2)E}\left[(1-\nu) + (1+\nu)\frac{a^2}{r^2}\right] \end{aligned}\right\} u = -\frac{b^2 p_o}{(b^2 - a^2)E}\left[(1-\nu)r + (1+\nu)\frac{a^2}{r}\right]$$

$$\epsilon_z = \frac{2\nu b^2 p_o}{(b^2 - a^2)E}, \qquad w = \frac{2\nu b^2 p_o}{(b^2 - a^2)E} z$$

TWO DIMENSIONAL PLANE STRAIN:

Boundary conditions & stresses same except $\epsilon_z = 0$: $z = 0, l$ and $\sigma_z = -\frac{2\nu b^2 p_o}{b^2 - a^2}$

STRAINS & DISPLACEMENTS:

$$\left.\begin{aligned} \epsilon_r &= -\frac{b^2 p_o (1+\nu)}{(b^2 - a^2)E}\left[(1-2\nu) - \frac{a^2}{r^2}\right] \\ \epsilon_\theta &= -\frac{b^2 p_o (1+\nu)}{(b^2 - a^2)E}\left[(1-2\nu) + \frac{a^2}{r^2}\right] \end{aligned}\right\} u = -\frac{b^2 p_o (1+\nu)}{(b^2 - a^2)E}\left[(1-2\nu)r + \frac{a^2}{r}\right]$$

ASSUMPTION:

1. No end effects

PRESSURE-HOLLOW CYLINDER-INTERNAL PRESSURE-NO CASE

TWO DIMENSIONAL PLANE STRESS:

BOUNDARY CONDITIONS:

$\sigma_r = -p_i$: $r = a$

$\sigma_r = 0$: $r = b$

$\sigma_z = 0$: $z = 0, \ell$

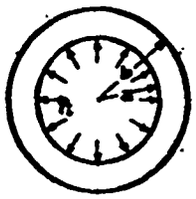

STRESSES:

$$\sigma_r = \frac{a^2 p_i}{b^2 - a^2}\left(1 - \frac{b^2}{r^2}\right)$$

$$\sigma_\theta = \frac{a^2 p_i}{b^2 - a^2}\left(1 + \frac{b^2}{r^2}\right)$$

STRAINS & DISPLACEMENTS:

$$\left.\begin{aligned} \epsilon_r &= \frac{a^2 p_i}{(b^2 - a^2)E}\left[(1-\nu) - (1+\nu)\frac{b^2}{r^2}\right] \\ \epsilon_\theta &= \frac{a^2 p_i}{(b^2 - a^2)E}\left[(1-\nu) + (1+\nu)\frac{b^2}{r^2}\right] \end{aligned}\right\} \quad u = \frac{a^2 p_i}{(b^2 - a^2)E}\left[(1-\nu)r + (1+\nu)\frac{b^2}{r}\right]$$

$$\epsilon_z = -\frac{2\nu}{E}\frac{a^2 p_i}{b^2 - a^2} \quad ,$$

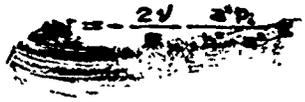

TWO DIMENSIONAL STRAIN:

Boundary conditions & stresses same except $\epsilon_z = 0 : z = 0, \ell$ and $\sigma_z = 2\nu\frac{a^2 p_i}{b^2 - a^2}$

STRAINS & DISPLACEMENTS:

$$\left.\begin{aligned} \epsilon_r &= \frac{a^2 p_i (1+\nu)}{(b^2 - a^2)E}\left[(1-2\nu) - \frac{b^2}{r^2}\right] \\ \epsilon_\theta &= \frac{a^2 p_i (1+\nu)}{(b^2 - a^2)E}\left[(1-2\nu) + \frac{b^2}{r^2}\right] \end{aligned}\right\} \quad u = \frac{a^2 p_i (1+\nu)}{(b^2 - a^2)E}\left[(1-2\nu)r + \frac{b^2}{r}\right]$$

ASSUMPTION :

1. No end effects

PRESSURE-HOLLOW CYLINDER-EXTERNAL PRESSURE-WITH CASE

TWO DIMENSIONAL PLANE STRESS:

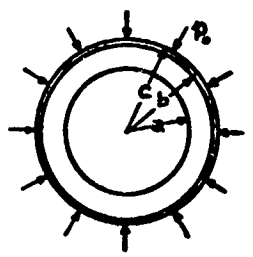

BOUNDARY CONDITIONS:

$\sigma_r = 0$: $r = a$

$u = u_c$, $\tau = 0$: $r = b$

$\sigma_r = -p_o$: $r = c$

$\sigma_z = 0$: $z = 0, \ell$

STRESSES IN HOLLOW CYLINDER:

$$\sigma_r = -\frac{b^2 p'}{b^2 - a^2}\left(1 - \frac{a^2}{r^2}\right)$$

$$p' = \frac{2c^2 p_o}{\frac{(c^2-b^2)E_c}{(b^2-a^2)E}\left[(1+\nu)a^2 + (1-\nu)b^2\right] + \left[(1+\nu_c)c^2 + (1-\nu_c)b^2\right]}$$

$$\sigma_\theta = -\frac{b^2 p'}{b^2 - a^2}\left(1 + \frac{a^2}{r^2}\right)$$

FOR THIN CASE:

$$p' = \frac{p_o}{1 + \left[(1+\nu)a^2 + (1-\nu)b^2\right]\frac{h E_c}{(b^2-a^2) b E}}$$

STRAINS & DISPLACEMENTS IN CYLINDER:

$$\left.\begin{aligned} \epsilon_r &= -\frac{b^2 p'}{(b^2-a^2)E}\left[(1-\nu) - (1+\nu)\frac{a^2}{r^2}\right] \\ \epsilon_\theta &= -\frac{b^2 p'}{(b^2-a^2)E}\left[(1-\nu) + (1+\nu)\frac{a^2}{r^2}\right] \end{aligned}\right\} \quad u = \frac{-b^2 p'}{(b^2-a^2)E}\left[(1-\nu)r + (1+\nu)\frac{a^2}{r^2}\right]$$

$$\epsilon_z = \frac{2\nu b^2 p'}{(b^2-a^2)E}, \qquad w = \frac{2\nu b^2 p'}{(b^2-a^2)E} z$$

STRESSES IN CASE:

$$\sigma_r = \frac{b^2c^2(p_o - p')}{c^2 - b^2}\frac{1}{r^2} + \frac{p'b^2 - p_oc^2}{c^2 - b^2}$$

$$\sigma_\theta = -\frac{b^2c^2(p_o - p')}{c^2 - b^2}\frac{1}{r^2} + \frac{p'b^2 - p_oc^2}{c^2 - b^2}$$

STRAINS & DISPLACEMENTS IN CASE:

$$\left.\begin{aligned} \epsilon_r &= \frac{1}{(c^2 - b^2)E_c}\left[(1+\nu_c)b^2c^2(p_o - p')\frac{1}{r^2} + (1-\nu_c)(p'b^2 - p_oc^2)\right] \\ \epsilon_\theta &= \frac{1}{(c^2 - b^2)E_c}\left[-(1+\nu_c)b^2c^2(p_o - p')\frac{1}{r^2} + (1-\nu_c)(p'b^2 - p_oc^2)\right] \end{aligned}\right\} u = \int \epsilon_r\, dr = r\epsilon_\theta$$

$$\epsilon_z = -\frac{2\nu_c(p'b^2 - p_oc^2)}{(c^2 - b^2)E_c} \quad ,$$

$$w = -\frac{2\nu_c(p'b^2 - p_oc^2)}{(c^2 - b^2)E_c}z$$

ASSUMPTIONS:

1. No end effects
2. No shear between cylinder and case

PRESSURE-HOLLOW CYLINDER-EXTERNAL PRESSURE-WITH CASE-(CONT.)

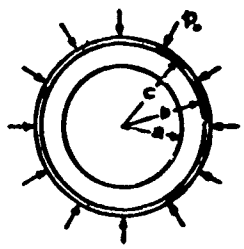

TWO DIMENSIONAL PLANE STRAIN:

BOUNDARY CONDITIONS:

$\sigma_r = 0$: $r = a$

$u = u_c$: $r = b$

$\sigma_r = -p_o$: $r = c$

$\epsilon_z = 0$: $z = 0, l$

STRESSES IN HOLLOW CYLINDER:

$$\sigma_r = -\frac{b^2 p'}{b^2 - a^2}\left(1 - \frac{a^2}{r^2}\right),$$

$$p' = \frac{2(1-\nu_c)c^2 p_o}{\frac{(c^2-b^2)(1+\nu)E_c}{(b^2-a^2)(1+\nu_c)E}\left[a^2+(1-2\nu)b^2\right] + \left[c^2+(1-2\nu_c)b^2\right]}$$

p' = pressure between cylinder and case.

FOR THIN CASE:

$$p' = \frac{p_o}{1 + \left[a^2+(1-2\nu)b^2\right]\frac{(1+\nu)h E_a}{(b^2-a^2)(1-\nu_c^2)bE}}$$

$$\sigma_\theta = -\frac{b^2 p'}{b^2 - a^2}\left(1 + \frac{a^2}{r^2}\right)$$

$$\sigma_z = -\frac{2\nu b^2 p'}{b^2 - a^2}$$

STRAINS & DISPLACEMENTS IN CYLINDER:

$$\epsilon_r = -\frac{(1+\nu)b^2 p'}{(b^2-a^2)E}\left[(1-2\nu) - \frac{a^2}{r^2}\right]$$

$$\epsilon_\theta = -\frac{(1+\nu)b^2 p'}{(b^2-a^2)E}\left[(1-2\nu) + \frac{a^2}{r^2}\right]$$

$$u = -\frac{(1+\nu)b^2 p'}{(b^2-a^2)E}\left[(1-2\nu)r + \frac{a^2}{r}\right]$$

STRESSES IN CASE:

$$\sigma_r = \frac{b^2c^2(p_o - p')}{c^2 - b^2}\frac{1}{r^2} + \frac{p'b^2 - p_oc^2}{c^2 - b^2}$$

$$\sigma_\theta = \frac{-b^2c^2(p_o - p')}{c^2 - b^2}\frac{1}{r^2} + \frac{p'b^2 - p_oc^2}{c^2 - b^2}$$

$$\sigma_z = \frac{2\nu_c(p'b^2 - p_oc^2)}{c^2 - b^2}$$

STRAINS & DISPLACEMENTS IN CASE:

$$\epsilon_r = \frac{1+\nu_c}{(c^2-b^2)E_c}\left[b^2c^2(p_o - p')\frac{1}{r^2} + (1-2\nu_c)(p'b^2 - p_oc^2)\right]$$

$$\epsilon_\theta = \frac{1+\nu_c}{(c^2-b^2)E_c}\left[-b^2c^2(p_o - p')\frac{1}{r^2} + (1-2\nu_c)(p'b^2 - p_oc^2)\right]$$

$$u = \frac{1+\nu_c}{(c^2-b^2)E_c}\left[-b^2c^2(p_o - p)\frac{1}{r} + (1-2\nu_c)(p'b^2 - p_oc^2)r\right]$$

ASSUMPTION:

1. No end effects.

PRESSURE-HOLLOW CYLINDER-INTERNAL PRESSURE-WITH CASE

TWO DIMENSIONAL PLANE STRESS:

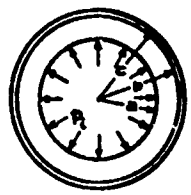

BOUNDARY CONDITIONS:

$\sigma_r = -p_i$: $r = a$

$u = u_c$, $\tau = 0$: $r = b$

$\sigma_r = 0$: $r = c$

$\sigma_z = 0$: $z = 0, \ell$

STRESSES IN HOLLOW CYLINDER:

$$\sigma_r = \frac{a^2 b^2 (p' - p_i)}{b^2 - a^2} \frac{1}{r^2} + \frac{p_i a^2 - p' b^2}{b^2 - a^2}$$

$$\sigma_\theta = -\frac{a^2 b^2 (p' - p_i)}{b^2 - a^2} \frac{1}{r^2} + \frac{p_i a^2 - p' b^2}{b^2 - a^2}$$

$$p' = \frac{2 a^2 p_i}{\left[(1+\nu) a^2 + (1-\nu) b^2\right] + \frac{(b^2 - a^2) E}{(c^2 - b^2) E_c} \left[(1+\nu_c) c^2 + (1-\nu_c) b^2\right]}$$

FOR THIN CASE:

$$p' = \frac{2 a^2 p_i}{\left[(1+\nu) a^2 + (1-\nu) b^2\right] + \frac{(b^2 - a^2) b E}{h E_c}}$$

STRAINS & DISPLACEMENTS IN CYLINDER:

$$\left.\begin{aligned} \epsilon_r &= \frac{1}{(b^2 - a^2) E} \left[(1+\nu) a^2 b^2 (p' - p_i) \frac{1}{r^2} + (1-\nu)(p_i a^2 - p' b^2)\right] \\ \epsilon_\theta &= \frac{1}{(b^2 - a^2) E} \left[-(1+\nu) a^2 b^2 (p' - p_i) \frac{1}{r^2} + (1-\nu)(p_i a^2 - p' b^2)\right] \end{aligned}\right\} u = \int \epsilon_r \, dr = r \epsilon_\theta$$

$$\epsilon_z = -\frac{2\nu (p_i a^2 - p' b^2)}{(b^2 - a^2) E}, \qquad w = -\frac{2\nu (p_i a^2 - p' b^2)}{(b^2 - a^2) E} z$$

STRESSES IN CASE:

$$\sigma_r = \frac{b^2 p'}{c^2 - b^2}\left(1 - \frac{c^2}{r^2}\right)$$

$$\sigma_\theta = \frac{b^2 p'}{c^2 - b^2}\left(1 + \frac{c^2}{r^2}\right)$$

STRAINS & DISPLACEMENTS IN CASE:

$$\left.\begin{aligned} \epsilon_r &= \frac{b^2 p'}{(c^2 - b^2)E_c}\left[(1-\nu_c) - (1+\nu_c)\frac{c^2}{r^2}\right] \\ \epsilon_\theta &= \frac{b^2 p'}{(c^2 - b^2)E_c}\left[(1-\nu_c) + (1+\nu_c)\frac{c^2}{r^2}\right] \end{aligned}\right\} u = \frac{b^2 p'}{(c^2 - b^2)E_c}\left[(1-\nu_c)r + (1+\nu_c)\frac{c^2}{r}\right]$$

$$\epsilon_z = -\frac{2\nu_c b^2 p'}{(c^2 - b^2)E_c}$$

$$w = -\frac{2\nu_c b^2 p'}{(c^2 - b^2)E_c} z$$

ASSUMPTIONS:

1. No end effects.
2. No shear between cylinder and case.

PRESSURE-HOLLOW CYLINDER-INTERNAL PRESSURE-WITH CASE-(CONT.)

TWO DIMENSIONAL PLANE STRAIN:

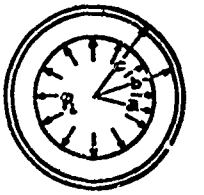

BOUNDARY CONDITIONS:

$\sigma_r = -p_i$: $r = a$

$u = u_c$: $r = b$

$\sigma_r = 0$: $r = c$

$\epsilon_z = 0$: $z = 0, \ell$

STRESSES IN HOLLOW CYLINDER:

$$\sigma_r = \frac{a^2 b^2 (p' - p_i)}{b^2 - a^2} \frac{1}{r^2} + \frac{p_i a^2 - p' b^2}{b^2 - a^2}$$

$$\sigma_\theta = -\frac{a^2 b^2 (p' - p_i)}{b^2 - a^2} \frac{1}{r^2} + \frac{p_i a^2 - p' b^2}{b^2 - a^2}$$

$$\sigma_z = \frac{2\nu (p_i a^2 - p' b^2)}{b^2 - a^2}$$

$$p' = \frac{2(1-\nu) a^2 p_i}{\left[a^2 + (1-2\nu) b^2\right] + \frac{(b^2 - a^2)(1+\nu_c) E}{(c^2 - b^2)(1+\nu) E_c} \left[c^2 + (1-2\nu_c) b^2\right]}$$

p' = pressure between cylinder and case.

FOR THIN CASE:

$$p' = \frac{2(1-\nu) a^2 p_i}{\left[a^2 + (1-2\nu) b^2\right] + \frac{(b^2 - a^2)(1-\nu_c^2) b E}{(1+\nu) h E_c}}$$

STRAINS & DISPLACEMENTS IN CYLINDER:

$$\left.\begin{aligned} \epsilon_r &= \frac{1+\nu}{(b^2 - a^2) E} \left[a^2 b^2 (p' - p_i) \frac{1}{r^2} + (1-2\nu)(p_i a^2 - p' b^2)\right] \\ \epsilon_\theta &= \frac{1+\nu}{(b^2 - a^2) E} \left[-a^2 b^2 (p' - p_i) \frac{1}{r^2} + (1-2\nu)(p_i a^2 - p' b^2)\right] \end{aligned}\right\} u = \int \epsilon_r \, dr = r\epsilon_\theta$$

FORMULAS P-14

STRESSES IN CASE:

$$\sigma_r = \frac{b^2 p'}{c^2 - b^2}\left(1 - \frac{c^2}{r^2}\right)$$

$$\sigma_\theta = \frac{b^2 p'}{c^2 - b^2}\left(1 + \frac{c^2}{r^2}\right)$$

$$\sigma_z = \frac{2\nu_c b^2 p'}{c^2 - b^2}$$

STRAINS & DISPLACEMENTS IN CASE:

$$\left.\begin{aligned} \epsilon_r &= \frac{(1+\nu_c) b^2 p'}{(c^2 - b^2) E_c}\left[(1-2\nu_c) - \frac{c^2}{r^2}\right] \\ \epsilon_\theta &= \frac{(1+\nu_c) b^2 p'}{(c^2 - b^2) E_c}\left[(1-2\nu_c) + \frac{c^2}{r^2}\right] \end{aligned}\right\} u = \frac{(1+\nu_c) b^2 p'}{(c^2 - b^2) E_c}\left[(1-2\nu_c) r + \frac{c^2}{r}\right]$$

ASSUMPTION:

1. No end effects

PRESSURE - HOLLOW CYLINDER - INTERNAL PRESSURE - WITH CASE AND ENDS BONDED

BOUNDARY CONDITIONS:

$\sigma_r = -p_i$: $r = a$

$\sigma_r = 0$: $r = c$

$u = u_c$: $r = b$

$w = w_c$: $z = 0, l$

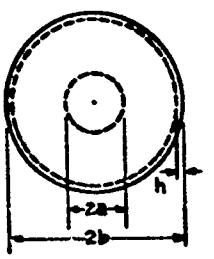

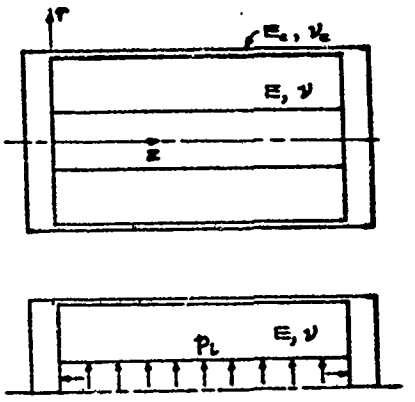

STRESSES IN HOLLOW CYLINDER (PROPELLANT):

$$\sigma_{(r)}^{(\theta)} = \pm \frac{a^2 b^2 (p_o - p_i)}{b^2 - a^2} \frac{1}{r^2} + \frac{p_i a^2 - p_o b^2}{b^2 - a^2},$$

p_o = PRESSURE BETWEEN CASE & PROPELLANT

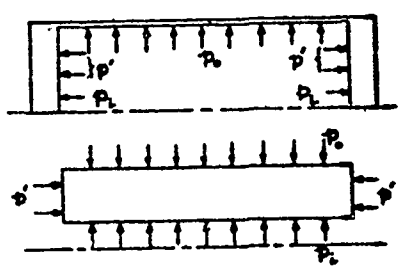

$$\sigma_z = -p',$$

p' = PRESSURE BETWEEN ENDS & PROPELLANT

$$\frac{2(1-\nu^2)\varepsilon_c^2 + \left\{2 - \nu + \nu_c(1-2\nu)\right\}\varepsilon_c}{(1+\nu)\left\{(1-2\nu)\frac{b^2}{a^2}+1\right\}\varepsilon_c^2 + \left\{\left[3-\nu(1+4\nu_c)\right]\frac{b^2}{a^2} + (1+\nu)\right\}\varepsilon_c + 2(1-\nu_c^2)\frac{b^2}{a^2}} p_i$$

$$p' = \frac{2\nu\left\{(1+\nu)\left(\frac{b^2}{a^2}-1\right)\right\}\varepsilon_c^2 + \left\{\left[-(1+3\nu)+2\nu_c(2+\nu)\right]\frac{b^2}{a^2} - (1+\nu)\right\}\varepsilon_c - 2(1-\nu_c^2)\frac{b^2}{a^2}}{\left[\frac{b^2}{a^2}-1\right]\left[(1+\nu)\left\{(1-2\nu)\frac{b^2}{a^2}+1\right\}\varepsilon_c^2 + \left\{\left[3-\nu(1+4\nu_c)\right]\frac{b^2}{a^2} + (1+\nu)\right\}\varepsilon_c + 2(1-\nu_c^2)\frac{b^2}{a^2}\right]} p_i$$

WHERE

$$\varepsilon_c = \frac{2bh\,E_c}{(b^2-a^2)E} \quad \text{(THIN CASE)}$$

STRAINS & DISPLACEMENTS IN PROPELLANT:

$$\epsilon_{(r\theta)} = \frac{1}{E}\left[\pm(1+\nu)\frac{a^2b^2(p_o-p_i)}{b^2-a^2}\frac{1}{r^2} + (1-\nu)\frac{p_i a^2 - p_o b^2}{b^2-a^2} + \nu p'\right]$$

$$\epsilon_z = -\frac{1}{E}\left[p' + 2\nu\left(\frac{p_i a^2 - p_o b^2}{b^2-a^2}\right)\right]$$

$$u = \frac{1}{E}\left[-(1+\nu)\frac{a^2b^2(p_o-p_i)}{b^2-a^2}\frac{1}{r} + (1-\nu)\frac{p_i a^2 - p_o b^2}{b^2-a^2}r + \nu p' r\right]$$

$$w = -\frac{1}{E}\left[p' + 2\nu\left(\frac{p_i a^2 - p_o b^2}{b^2-a^2}\right)\right]z$$

STRESSES IN CASE:

$$\sigma_{(r\theta)} = \frac{b p_o}{2h}\left(1 \mp \frac{b^2}{r^2}\right) \qquad \text{(THIN CASE)}$$

$$\sigma_z = p'' = \frac{(b^2-a^2)p' + a^2 p_i}{2bh}$$

STRAINS & DISPLACEMENTS IN CASE:

$$\epsilon_{(r\theta)} = \frac{1}{E_c}\left[\mp(1+\nu_c)\frac{b^2 p_o}{2h}\frac{1}{r^2} + (1-\nu_c)\frac{b p_o}{2h} - \nu_c p''\right]$$

$$\epsilon_z = \frac{1}{E_c}\left[p'' - \nu_c\frac{b p_o}{h}\right]$$

$$u_c = \frac{1}{E_c}\left[(1+\nu_c)\frac{b^2 p_o}{2h}\frac{1}{r} + (1-\nu_c)\frac{b p_o}{2h}r - \nu_c p'' r\right]$$

$$w_c = \frac{1}{E_c}\left[p'' - \nu_c\frac{b p_o}{h}\right]z$$

ASSUMPTIONS:

1. ENDS & CASE BONDED TO PROPELLANT.
2. UNIFORM END EFFECTS WITH END PLATES TRANSMITTING FORCES FROM p_i & p' INTO THIN CYLINDRICAL CASE IN TENSION.
3. NO BENDING EFFECTS INCLUDED FROM ENDS; ASSUMING ONLY HOOP (σ_θ) & AXIAL (σ_z) STRESSES UNIFORM IN CASE UP TO ENDS.

STRESS ON INNER RADIUS OF PROPELLANT:

$$\sigma_\theta\Big|_{r=a} = \frac{1}{\frac{b^2}{a^2}-1}\left[\frac{(1+\nu)\left\{(1-2\nu)\frac{b^2}{a^2}-2(1-\nu)\frac{b^2}{a^2}+1\right\}\varepsilon_c^2+\left\{[3-\nu(1+4\nu_c)]\frac{b^2}{a^2}+2(\nu-\nu_c)\frac{b^2}{a^2}+(1+\nu)\right\}\varepsilon_c+2(1-\nu_c^2)(1+\frac{b^2}{a^2})\frac{b^2}{a^2}}{(1+\nu)\left\{(1-2\nu)\frac{b^2}{a^2}+1\right\}\varepsilon_c^2+\left\{[3-\nu(1+4\nu_c)]\frac{b^2}{a^2}+(1+\nu)\right\}\varepsilon_c+2(1-\nu_c^2)\frac{b^2}{a^2}}\right]p_i$$

STRAIN & DISPLACEMENT ON INNER RADIUS:

$$\epsilon_\theta\Big|_{r=a} = \frac{u}{a}\Big|_{r=a}$$

$$= \frac{1}{E\left(\frac{b^2}{a^2}-1\right)}\left[\frac{(1+\nu)^2(1-2\nu)\left(\frac{b^2}{a^2}-1\right)^2\varepsilon_c^2+(1+\nu)\left\{[3-\nu(1+4\nu_c)]\frac{b^2}{a^2}-[\nu+2\nu_c(1-3\nu)]\frac{b^2}{a^2}+(1-2\nu)\right\}\varepsilon_c+2(1-\nu_c^2)\left\{(1+\nu)\frac{b^2}{a^2}+(1-2\nu)\right\}\frac{b^2}{a^2}}{(1+\nu)\left\{(1-2\nu)\frac{b^2}{a^2}+1\right\}\varepsilon_c^2+\left\{[3-\nu(1+4\nu_c)]\frac{b^2}{a^2}+(1+\nu)\right\}\varepsilon_c+2(1-\nu_c^2)\frac{b^2}{a^2}}\right]p_i$$

STRAIN & DISPLACEMENT ON OUTER RADIUS:

$$\epsilon_\theta\Big|_{r=b} = \frac{u}{b}\Big|_{r=b}$$

$$= \frac{1}{E\left(\frac{b^2}{a^2}-1\right)}\left[\frac{\{(1+\nu)[4(1-\nu)-\nu_c]\frac{b^2}{a^2}-\nu_c(1-2\nu)\}\varepsilon_c+2(2-\nu)(1-\nu_c^2)\frac{b^2}{a^2}}{(1+\nu)\left\{(1-2\nu)\frac{b^2}{a^2}+1\right\}\varepsilon_c^2+\left\{[3-\nu(1+4\nu_c)]\frac{b^2}{a^2}+(1+\nu)\right\}\varepsilon_c+2(1-\nu_c^2)\frac{b^2}{a^2}}\right]p_i$$

AXIAL STRAIN & DISPLACEMENT:

$$\varepsilon_z\Big|_{z=L} = \frac{w}{L}\Big|_{z=L}$$

$$= \frac{1}{E\left(\frac{b^2}{a^2}-1\right)}\left[\frac{(1+\nu)\left\{[1-4\nu_c(1-\nu)]\frac{b^2}{a^2}+(1-2\nu)\right\}\varepsilon_c+2(1-2\nu)(1-\nu_c^2)\frac{b^2}{a^2}}{(1+\nu)\left\{(1-2\nu)\frac{b^2}{a^2}+1\right\}\varepsilon_c^2+\left\{[3-\nu(1+4\nu_c)]\frac{b^2}{a^2}+(1+\nu)\right\}\varepsilon_c+2(1-\nu_c^2)\frac{b^2}{a^2}}\right]p_i$$

TENSION – SOLID OR HOLLOW CYLINDER – NO CASE

BOUNDARY CONDITIONS:

$$\sigma_z = \sigma_o = \frac{P}{A} = \frac{P}{\pi(b^2-a^2)} \quad : \quad z = 0,\ \ell$$

$$\sigma_r = 0 \quad : \quad r = a,\ b$$

} for solid cylinder let $a \to 0$

STRAINS:

$$\epsilon_r = \epsilon_\theta = -\frac{\nu \sigma_o}{E}$$

$$\epsilon_z = \frac{\sigma_o}{E}$$

DISPLACEMENTS:

$$u = -\frac{\nu \sigma_o}{E} r$$

$$w = \frac{\sigma_o}{E} z$$

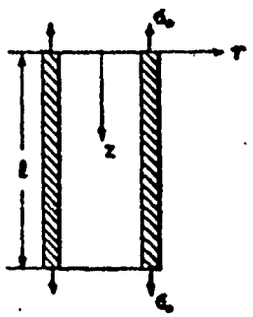

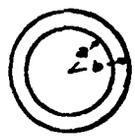

ASSUMPTIONS:

1. No end effects – either ends contract as given by u or we consider only regions $> 0(b-a)$ from ends (St. Venant).

2. σ_o distributed uniformly over ends, or equivalent with same total pressure & consider only regions $> 0(b-a)$ from ends.

3. Small strains where A can be considered constant (no necking effect).

TENSION - SOLID OR HOLLOW CYLINDER - WITH CASE - BONDED - CYLINDER AND CASE IN TENSION - UNIFORM STRESS

BOUNDARY CONDITIONS:

$\sigma_z = \sigma_o = \frac{P}{\pi(c^2-a^2)}$; $z = 0, \ell$

$\sigma_r = 0$: $r = a, c$

$u = u_c$: $r = b$

} For solid cylinder: let $a \to 0$ throughout

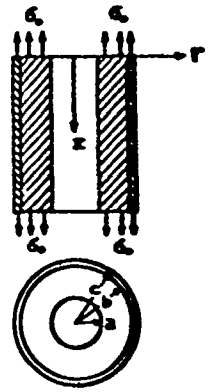

c-b=h

STRESS ON CYLINDER:

$\sigma_z = \sigma_o$

$\sigma_r = -p'$: $r = b$,

$$p' = -\frac{\nu\left(1-\frac{\nu_c E}{\nu E_c}\right)\sigma_o}{\frac{b^2}{b^2-a^2}\left[(1-\nu)+(1+\nu)\frac{a^2}{b^2}\right]+\frac{b^2}{c^2-b^2}\left(\frac{E}{E_c}\right)\left[(1-\nu_c)+(1+\nu_c)\frac{c^2}{b^2}\right]}$$

FOR THIN CASE:

$$p' = -\frac{\nu\left(1-\frac{\nu_c E}{\nu E_c}\right)\sigma_o}{\frac{b^2}{b^2-a^2}\left[(1-\nu)\quad\cdot\frac{a^2}{b^2}\right]+\frac{bE}{hE_c}}$$

STRAINS & DISPLACEMENTS OF CYLINDER:

$$\epsilon_{(r)} = -\frac{1}{E}\left\{\nu\sigma_o + \frac{b^2 p'}{b^2-a^2}\left[(1-\nu) \mp (1+\nu)\frac{a^2}{r^2}\right]\right\}$$

$$\epsilon_z = \frac{\sigma_z}{E}$$

$$u = -\frac{1}{E}\left\{\nu\sigma_o r + \frac{b^2 p'}{b^2-a^2}\left[(1-\nu)r + (1+\nu)\frac{a^2}{r}\right]\right\},$$

$$w = +\frac{\sigma_o}{E} z$$

STRESSES ON CASE:

$\sigma_z = \sigma_o$

$$\sigma_r = \frac{b^2 p'}{c^2-b^2}\left(1-\frac{c^2}{r^2}\right)$$

STRAINS & DISPLACEMENTS OF CASE 1:

$$\epsilon_r = -\frac{1}{E_c}\left\{\nu_c \sigma_0 - \frac{b^2 p'}{c^2-b^2}\left[(1-\nu_c) - (1+\nu_c)\frac{c^2}{r^2}\right]\right\}$$

$$\epsilon_\theta = -\frac{1}{E_c}\left\{\nu_c \sigma_0 - \frac{b^2 p'}{c^2-b^2}\left[(1-\nu_c) + (1+\nu_c)\frac{c^2}{r^2}\right]\right\}$$

$$\epsilon_z = \frac{2\nu_c}{E_c}\left[\nu_c \sigma_0 - \frac{b^2 p'}{c^2-b^2}(1-\nu_c)\right]$$

$$u_c = -\frac{1}{E_c}\left\{\nu_c \sigma_0 r - \frac{b^2 p'}{c^2-b^2}\left[(1-\nu_c)r + (1+\nu_c)\frac{c^2}{r}\right]\right\}$$

$$w_c = \frac{2\nu_c}{E_c}\left[\nu_c \sigma_0 - \frac{b^2 p'}{c^2-b^2}(1-\nu_c)\right]z$$

ASSUMPTIONS:

1. No end effects
2. Small strains
3. Shear due to $w - w_c$ of lesser importance than matching $u = u_a$

For $[w_c = w]_{z=0}$:

$$p'\Big|_{z=0} = \frac{-\frac{1}{E}(1-2\nu_c^2\frac{E}{E_c})\sigma_0}{\frac{b^2}{c^2-b^2}(1-\nu_c)} \approx -\frac{\frac{1}{E}(1-2\nu_c^2\frac{E}{E_c})\sigma_0}{\frac{b}{2h}(1-\nu_c)}$$

$$\approx O\left(\frac{h}{bE}\sigma_0\right) \ll \sigma_0$$

TENSION - SOLID OR HOLLOW CYLINDER - WITH CASE - BONDED CYLINDER & CASE IN TENSION - UNIFORM STRAIN

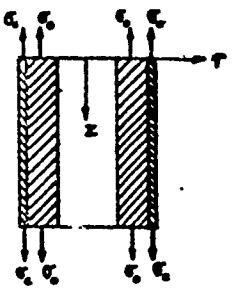

BOUNDARY CONDITIONS:

$\sigma_r = 0$: $r = a, c$

$u = u_c$: $r = b$

$w = w_c$: $z = 0, \ell$

$$\bar{\sigma} = \frac{P}{A} = \frac{\pi\left[(b^2-a^2)\sigma_o + (c^2-b^2)\sigma_c\right]}{\pi(c^2-a^2)}$$

$$\approx \frac{(b^2-a^2)\sigma_o + 2bh\sigma_c}{b^2-a^2} \qquad \text{[Thin case]}$$

STRESSES ON CYLINDER:

$\sigma_z = \sigma_o$

$\sigma_r = -p'$: $r = b$

$$p' = -\frac{\nu\sigma_o - \nu_c\frac{E}{E_c}\sigma_c}{\frac{b^2}{b^2-a^2}\left[(1-\nu)+(1+\nu)\frac{a^2}{b^2}\right] + \frac{b^2}{c^2-a^2}\left(\frac{E}{E_c}\right)\left[(1-\nu_c)+(1+\nu_c)\frac{c^2}{b^2}\right]}$$

FOR THIN CASE:

$$p' = -\frac{\nu\sigma_o - \nu_c\frac{E}{E_c}\sigma_c}{\frac{b^2}{b^2-a^2}\left[(1-\nu)+(1+\nu)\frac{a^2}{b^2}\right] + \frac{bE}{hE_c}}$$

STRAINS & DISPLACEMENTS OF CYLINDER:

$$\epsilon_{(r,\theta)} = -\frac{1}{E}\left\{\nu\sigma_o + \frac{b^2p'}{b^2-a^2}\left[(1-\nu) \mp (1+\nu)\frac{a^2}{r^2}\right]\right\}$$

$$\epsilon_z = \frac{\sigma_o}{E}$$

$$u = -\frac{1}{E}\left\{\nu\sigma_o r + \frac{b^2p'}{b^2-a^2}\left[(1-\nu)r + (1+\nu)\frac{a^2}{r}\right]\right\}$$

$$w = \frac{\sigma_o}{E}z$$

STRESSES ON CASE:

$$\sigma_z = \sigma_c$$

$$\sigma_r = \frac{b^2 p'}{c^2 - b^2}\left(1 - \frac{c^2}{r^2}\right)$$

STRAINS & DISPLACEMENTS OF CASE:

$$\epsilon_{(r)} = -\frac{1}{E_c}\left\{\nu_c \sigma_c - \frac{b^2 p'}{c^2 - b^2}\left[(1-\nu_c) \mp (1+\nu_c)\frac{c^2}{r^2}\right]\right\}$$

$$\epsilon_z = \frac{2\nu_c}{E_c}\left[\nu_c \sigma_c - \frac{b^2 p'}{c^2 - b^2}(1-\nu_c)\right]$$

$$u_c = -\frac{1}{E_c}\left\{\nu_c \sigma_c r - \frac{b^2 p'}{c^2 - b^2}\left[(1-\nu_c)r + (1+\nu_c)\frac{c^2}{r}\right]\right\}$$

$$w_c = \frac{2\nu_c}{E_c}\left[\nu_c \sigma_c - \frac{b^2 p'}{c^2 - b^2}(1-\nu_c)\right]z$$

ASSUMPTIONS:

1. No end effects
2. Small strains
3. $w = w_c$: $\quad \sigma_c = \frac{2\nu_c E}{E_c}\left[\nu_c \sigma_c - \frac{b^2 p'}{c^2 - b^2}r(1-\nu_c)\right]$

TENSION - SOLID OR HOLLOW CYLINDER - WITH CASE - BONDED CASE IN TENSION OR CYLINDER IN TENSION

See previous pages for cylinder & case both in tension and uniform strain:

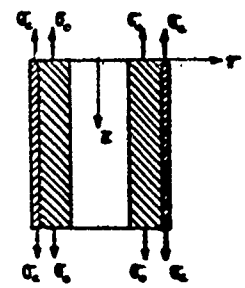

FOR CASE ONLY IN TENSION:

Let: $\sigma_o = 0$ & $w \neq w_c$

FOR CYLINDER ONLY IN TENSION:

Let: $\sigma_c = 0$ & $w \neq w_o$

ASSUMPTIONS:

1. No end effects.
2. Small strains.
3. Shear due to $w - w_c$ of lesser importance than matching $u = u_c$.

TORSION EQUATIONS--ST. VENANT

ASSUMPTIONS:

1. No dependence on θ coordinate (not same as twist: $\theta=\frac{\alpha}{b}$)
2. $\sigma_r=\sigma_z=\tau_{r\theta}=\tau_{rz}=0$, no body forces
3. $\epsilon_z=0$ (or $\theta=\frac{\alpha}{b}\ll 1$)

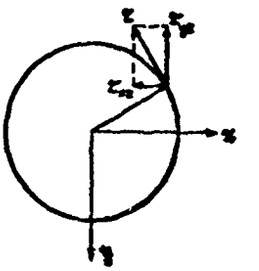

EQUILIBRIUM:

$$\frac{\partial \tau_{\theta z}}{\partial z}=0$$

STRESS-STRAIN:

$$\gamma_{\theta z}=\frac{\tau_{\theta z}}{\mu}$$

STRAIN-DISPLACEMENT:

$$\gamma_{r\theta}=\frac{\partial v}{\partial r}-\frac{v}{r}=0,$$

$$\gamma_{\theta z}=\frac{\partial v}{\partial z}$$

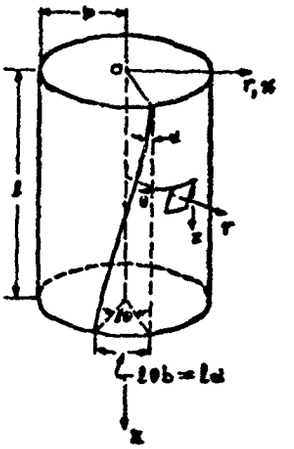

BOUNDARY CONDITIONS:

1. Ends ($z=0,\ l$) rotate as solid disks $\Rightarrow v$ linear in r:
2. Cylindrical surface ($r=b$) uniformly twisted $\Rightarrow \tau_{\theta z}$ const., for $r=b$.

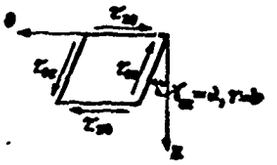

CARTESIAN COORDINATE FORM:

$$\tau_{yz}=\mu\theta x,\quad \tau_{xz}=-\mu\theta y,\quad \sigma_x=\sigma_y=\sigma_z=\tau_{xy}=0$$

$$u=-\theta xy,\quad v=\theta zx,\quad w=0$$

TORSION EQUATIONS – SECOND ORDER

ASSUMPTIONS:

1. No dependence on θ coordinate
2. $\sigma_r = \sigma_z = \tau_{r\theta} = \tau_{rz} = 0$
3. No body forces

FROM RIVLIN'S NOTES,* PAGE 81 & 83:

$$\epsilon_z = -\frac{\theta^2}{4A\,a_1(a_1+3a_2)}\left\{B\left[a_2(a_1+2a_2)-a_1(2a_2-a_3)\right]\right\}$$

where the a_i are coefficients of the energy expression:

$$W = a_1 J_2 + a_2 J_1^2 + a_3 J_1 J_2 + a_4 J_1^3 + a_5 J_3$$

where the J_i are invariants of increasingly higher orders.

CIRCULAR HOLLOW CYLINDER:

$$A = \pi(b^2 - a^2)$$

$$B = I = \pi\frac{(b^4 - a^4)}{2}$$

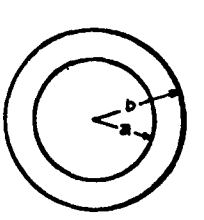

ELASTIC SOLUTIONS:

$$a_1 = -\frac{E}{4(1+\nu)}$$

$$a_2 = \frac{E}{8}\,\frac{1-\nu}{(1+\nu)(1-2\nu)}$$

$$a_3 = a_4 = a_5 = 0$$

$$\epsilon_z = -\frac{\theta^2}{4}\left(\frac{1-\nu}{1+\nu}\right)(b^2+a^2)$$

FORMULAS t-2

* R. S. RIVLIN, "FINITE ELASTIC DEFORMATIONS" delivered to The Engineering Division, California Institute of Technology, 1953.

TORSION – SOLID OR HOLLOW CYLINDER – NO CASE

BOUNDARY CONDITIONS:

$$\tau = \tau_{z\theta} = \mu\theta r = \frac{\mu a r}{b},$$

$$\sigma_z = \tau_{zr} = 0: \quad z = 0, \ell$$

$$\sigma_r = \tau_{r\delta} = \tau_{r\theta} = 0: \quad r = b \ (\Rightarrow \sigma_\theta = 0)$$

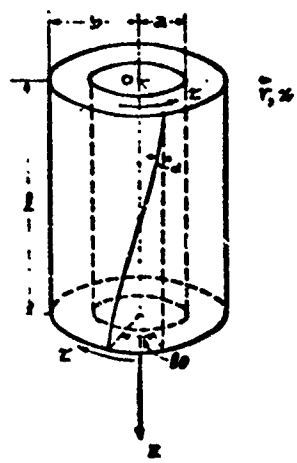

STRAINS & DISPLACEMENTS:

$$\gamma = \gamma_{z\theta} = \frac{\tau}{\mu} = \theta r$$

$$\epsilon_r = \epsilon_\theta = \epsilon_z = \gamma_{rz} = \gamma_{r\theta} = 0$$

$$v = \int \gamma_{z\theta}\, dz = \theta r z$$

$$u = w = 0$$

TORQUE:

$$M_t = -\frac{\pi\mu\theta}{2}(b^4 - a^4)$$

ASSUMPTIONS:

1. End surfaces ($z = 0, \ell$) rotate as solid disks
2. Surfaces $z = \text{const.}$ remain plane
3. $\epsilon_z = 0 \Rightarrow \beta \ll 1$

SECOND ORDER DISPLACEMENT:

$$\epsilon_z = -\left(\frac{1-\nu}{1+\nu}\right)\frac{b^2}{4}\theta^2$$

TORSION – SOLID OR HOLLOW CYLINDER – WITH CASE

CYLINDER AND CASE UNDER TORSION

BOUNDARY CONDITIONS:

$\tau = \tau_{z\theta} = \bar{\mu}\theta r$, $\sigma_z = \tau_{zr} = 0$: $z = 0, \ell$

$r = \tau_{rz} = \tau_{r\theta} = 0$: $r = c$ ($\Rightarrow \sigma_\theta = 0$)

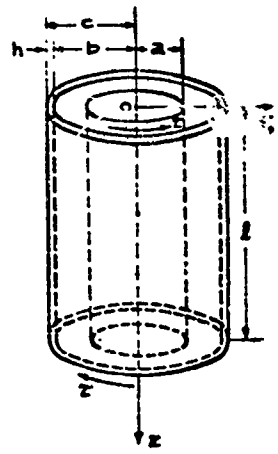

STRAINS & DISPLACEMENTS:

$\gamma = \theta r$, $\quad v = \theta r z$

$\epsilon_r = \epsilon_\theta = \epsilon_z = \gamma_{rz} = \gamma_{r\theta} = u = w = 0$

TORQUE:

$$M = M_t + M_c$$

$$= \frac{\pi\mu\theta}{2}(b^4 - a^4) + \frac{\pi\mu_c\theta}{2}(c^4 - b^4)$$

$$\simeq \frac{\pi\mu\theta}{2}(b^4 - a^4) + 2\pi\mu_c\theta h b^3, \quad \text{for thin case}, \quad (h \equiv c - b)$$

EQUIVALENT SHEAR MODULUS:

$$\bar{\mu} \equiv \frac{b^4 - a^4}{c^4 - a^4}\mu + \frac{c^4 - b^4}{c^4 - a^4}\mu_c$$

$$\simeq \mu + \frac{4b^3 h}{b^4 - a^4}\mu_c, \quad \text{for thin case}.$$

$$\simeq \mu + \frac{4h}{b}\mu_c, \quad \text{for solid cylinder \& thin case}$$

ASSUMPTIONS:

1. End surfaces ($z = 0, \ell$) rotate as solid disks.
2. Surfaces $z = \text{const.}$ remain plane.
3. $\epsilon_z = 0 \Rightarrow \theta \ll 1$
4. No normal (σ_r) interaction between cylinder and case.

TORSION - SOLID OR HOLLOW CYLINDER - WITH CASE. CASE UNDER TORSION - CYLINDER UNBONDED

BOUNDARY CONDITIONS:

$\tau = \tau_{z\theta} = \mu_c \theta r, \quad \sigma_z = \tau_{zr} = 0:$

$z = 0, \ell \quad b \leq r \leq c$ (case only)

$\sigma_r = \tau_{rz} = \tau_{r\theta} = 0: \quad r = c$

All stresses zero on cylinder in linear theory.

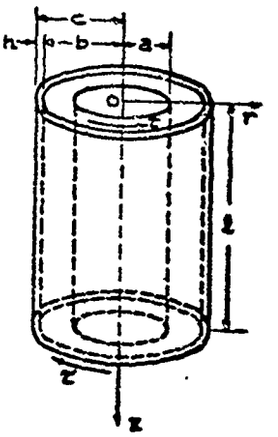

STRAINS & DISPLACEMENTS OF CASE:

$\gamma_{z\theta} = \theta r, \qquad v = \theta r z,$

$\epsilon_r = \epsilon_\theta = \epsilon_z = \gamma_{rz} = \gamma_{r\theta} = u = w = 0$

TORQUE:

$$M = M_c = \frac{\pi \mu_c \theta}{2}(c^4 - b^4)$$

$$\simeq 2\pi \mu_c \theta h b^3, \text{ for thin case}$$

ASSUMPTIONS:

1. Torque applied only to case.
2. Cylinder in no way receives shear from case or end plates.
3. $\epsilon_z = 0$, hence $\theta \ll 1$

SECOND ORDER THEORY:

$\epsilon_z \simeq -\left(\frac{1-\nu}{1+\nu}\right)\frac{b^2}{2}\theta^2$, and if endplates are flat they impose a stress on the cylinder:

$\sigma_z = \epsilon_z E$, assuming $E \ll E_c$ and no shear transmitted.

FORMULAS 1-5

TORSION - SOLID OR HOLLOW CYLINDER - WITH CASE
CASE UNDER TORSION - CYLINDER BONDED TO CASE

BOUNDARY CONDITIONS:

$\tau_{z\theta} = \bar{\mu}\theta r$, $\sigma_z = \tau_{zr} = 0$:

$z = 0, l$ & $b \le r \le c$ (only to case)

$\sigma_r = \tau_{rz} = \tau_{r\theta} = 0$: $r = c$

$v_c = v = \theta b z$: $r = b$

NOTE: This is identical to torsion applied to both case and cylinder at $z = 0, l$.

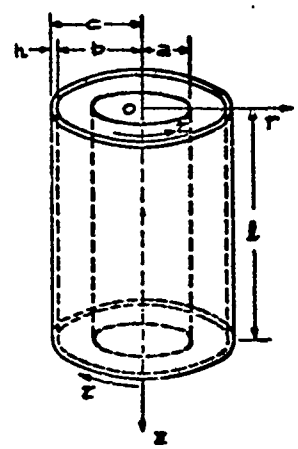

STRAIN & DISPLACEMENT:

$\gamma_{\theta z} = \theta r$,

$v = \theta r z$

TORQUE:

$M \propto \frac{\pi\mu\theta}{2}(b^4 - a^4) + 2\pi\mu_c\theta h b^3$, thin case

EQUIVALENT SHEAR MODULUS:

$\bar{\mu} \propto \mu + \frac{4b^3h}{b^4 - a^4}\mu_c$, thin case

$\propto \mu + \frac{4h}{b}\mu_c$ for solid cylinder & thin case

TORSION - SOLID OR HOLLOW CYLINDER - WITH CASE
CYLINDER UNDER TORSION - UNBONDED

BOUNDARY CONDITIONS:

$\tau = \tau_{z\theta} = \mu\theta r, \quad \sigma_z = \tau_{zr} = 0$:

$z = 0, l \quad \& \quad 0 \leq r \leq b$ (cylinder only)

$\sigma_r = \tau_{rz} = \tau_{r\theta} = 0$: $\quad r = c$

All stresses zero on case in linear theory.

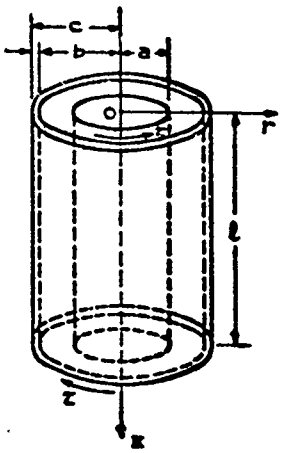

STRAINS & DISPLACEMENTS of cylinder:

$\gamma_{z\theta} = \theta r, \quad v = \theta r z,$

$\epsilon_r = \epsilon_\theta = \epsilon_z = \gamma_{rz} = \gamma_{r\theta} = u = w = 0$

TORQUE:

$$M = \frac{\pi\mu\theta}{2}(b^4 - a^4)$$

ASSUMPTIONS:

1. Torque applied only to cylinder.
2. Case in no way receives shear from cylinder or endplates.
3. $\epsilon_z = 0$, hence $\theta \ll 1$

SECOND ORDER THEORY:

$$\epsilon_z = -\left(\frac{1-\nu}{1+\nu}\right)\left(\frac{b^4-a^4}{b^2-a^2}\right)\frac{\theta^2}{4}$$

NOTE: If cylinder is nonelastic, this strain is different. In fact, Rivlin has found this to be positive for rubber.

GRAVITY-SOLID OR HOLLOW CYLINDER-WITH CASE-PURE SHEAR

EQUILIBRIUM:

$$\frac{\partial \tau_{rz}}{\partial r} + \frac{\tau_{rz}}{r} + \rho g = 0$$

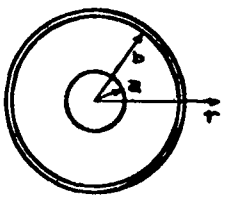

BOUNDARY CONDITIONS:

$$\tau_{rz} = 0 : \quad r = a$$

$$w = 0 : \quad r = b$$

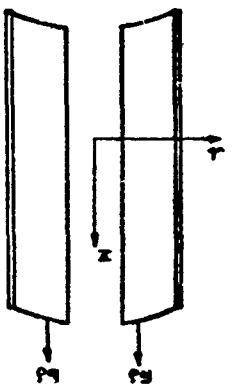

STRESSES:

$$\tau_{rz} = \frac{\rho g}{2}\left(\frac{a^2}{r} - r\right)$$

STRAIN & DISPLACEMENT:

$$\gamma_{rz} = \frac{\rho g}{2\mu}\left(\frac{a^2}{r} - r\right)$$

$$w = \frac{\rho g}{2\mu}\left(\frac{b^2 - r^2}{2} - a^2 \ln \frac{b}{r}\right)$$

ASSUMPTIONS:

1. RIGID CASE.
2. NO END EFFECTS OR EQUIVALENTLY AN INFINITELY LONG CYLINDER.

THERMOELASTIC EQUATIONS

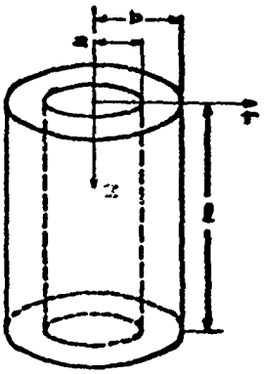

EQUILIBRIUM:

$$\frac{\partial \sigma_r}{\partial r} + \frac{\sigma_r - \sigma_\theta}{r} = 0$$

STRESS FUNCTION:

$$\sigma_r = \frac{\phi}{r}, \quad \sigma_\theta = \frac{\partial \phi}{\partial r}$$

STRESS-STRAIN:

$$\epsilon_r = \frac{1}{E}\left[\sigma_r - \nu(\sigma_\theta + \sigma_z)\right] + \alpha T$$

$$\epsilon_\theta = \frac{1}{E}\left[\sigma_\theta - \nu(\sigma_r + \sigma_z)\right] + \alpha T$$

$$\epsilon_z = \frac{1}{E}\left[\sigma_z - \nu(\sigma_r + \sigma_\theta)\right] + \alpha T$$

$$\left.\begin{aligned} \sigma_r &= \lambda e + 2\mu\epsilon_r - \frac{\alpha E T}{1-2\nu} \\ \sigma_\theta &= \lambda e + 2\mu\epsilon_\theta - \frac{\alpha E T}{1-2\nu} \\ \sigma_z &= \lambda e + 2\mu\epsilon_z - \frac{\alpha E T}{1-2\nu} \end{aligned}\right\} \quad e = \epsilon_r + \epsilon_\theta + \epsilon_z$$

$$\lambda = \frac{\nu E}{(1+\nu)(1-2\nu)}, \quad \mu = \frac{E}{2(1+\nu)}$$

COMPATIBILITY:

$$r\frac{d\epsilon_\theta}{dr} + \epsilon_\theta - \epsilon_r = 0$$

PLANE STRESS:

$$\frac{d^2\phi}{dr^2} + \frac{1}{r}\frac{\partial \phi}{\partial r} - \frac{\phi}{r^2} = -\alpha E \frac{\partial T}{\partial r} \qquad \phi = -\frac{\alpha E}{r}\int_a^r T r\,dr + \frac{C_1 r}{2} + \frac{C_2}{r}$$

PLANE STRAIN:

$$\frac{\partial^2\phi}{\partial r^2} + \frac{1}{r}\frac{\partial \phi}{\partial r} - \frac{\phi}{r^2} = -\frac{\alpha E}{1-\nu}\frac{\partial T}{\partial r} \qquad \phi = -\frac{\alpha E}{1-\nu}\frac{1}{r}\int_a^r T r\,dr + \frac{C_1 r}{2} + \frac{C_2}{r}$$

C_1 & C_2 ARE DETERMINED FROM BOUNDARY CONDITIONS.

TEMPERATURE - SOLID OR HOLLOW CYLINDER - NO CASE

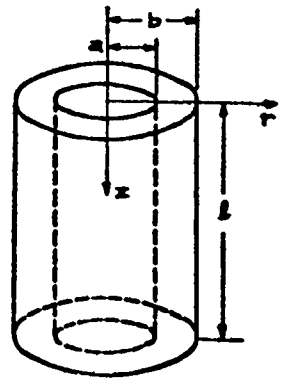

PLANE STRESS:

BOUNDARY CONDITIONS:

$\sigma_r = 0 : \quad r = a, b$

$\sigma_z = 0$

STRESSES:

$$\sigma_r = \frac{\alpha E}{(b^2-a^2)}\left(1-\frac{a^2}{r^2}\right)\int_a^b Tr\,dr - \frac{\alpha E}{r^2}\int_a^r Tr\,dr$$

$$\sigma_\theta = \frac{\alpha E}{b^2-a^2}\left(1+\frac{a^2}{r^2}\right)\int_a^b Tr\,dr + \frac{\alpha E}{r^2}\int_a^r Tr\,dr - \alpha E T$$

STRAINS & DISPLACEMENTS:

$$\epsilon_r = \frac{\alpha}{b^2-a^2}\left[(1-\nu)-(1+\nu)\frac{a^2}{r^2}\right]\int_a^b Tr\,dr - \frac{(1+\nu)\alpha}{r^2}\int_a^r Tr\,dr + (1+\nu)\alpha T$$

$$\epsilon_\theta = \frac{\alpha}{b^2-a^2}\left[(1-\nu)+(1+\nu)\frac{a^2}{r^2}\right]\int_a^b Tr\,dr + \frac{(1+\nu)\alpha}{r^2}\int_a^r Tr\,dr$$

$$\epsilon_z = -\frac{2\nu\alpha}{b^2-a^2}\int_a^b Tr\,dr + (1+\nu)\alpha T$$

$$u = \frac{\alpha}{b^2-a^2}\left[(1-\nu)r+(1+\nu)\frac{a^2}{r}\right]\int_a^b Tr\,dr + \frac{(1+\nu)\alpha}{r}\int_a^r Tr\,dr$$

$$w = \left[-\frac{2\nu\alpha}{b^2-a^2}\int_a^b Tr\,dr + (1+\nu)\alpha T\right]z$$

TEMPERATURE CONSTANT:

$\sigma_r = \sigma_\theta = 0$

$\epsilon_r = \epsilon_\theta = \epsilon_z = \alpha T$

$u = \alpha T r$

$w = \alpha T z$

ASSUMPTION:

1. NO END EFFECTS.

TEMPERATURE - SOLID OR HOLLOW CYLINDER - NO CASE

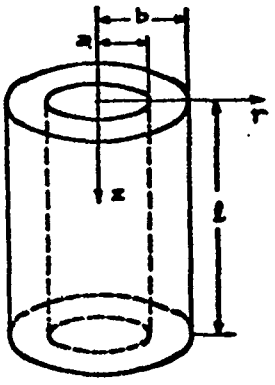

PLANE STRAIN:

BOUNDARY CONDITIONS:

$\sigma_r = 0 : \quad r = a, b$

$w = 0$

STRESSES:

$$\sigma_r = \frac{\alpha E}{(1-\nu)(b^2-a^2)}\left(1-\frac{a^2}{r}\right)\int_a^b T r dr - \frac{\alpha E}{(1-\nu)r^2}\int_a^r T r dr$$

$$\sigma_\theta = \frac{\alpha E}{(1-\nu)(b^2-a^2)}\left(1+\frac{a^2}{r}\right)\int_a^b T r dr + \frac{\alpha E}{(1-\nu)r^2}\int_a^r T r dr - \frac{\alpha E T}{1-\nu}$$

$$\sigma_z = \frac{2\nu\alpha E}{(1-\nu)(b^2-a^2)}\int_a^b T r dr - \frac{\alpha E T}{1-\nu}$$

STRAINS & DISPLACEMENTS:

$$\epsilon_r = \frac{(1+\nu)\alpha}{(1-\nu)(b^2-a^2)}\left[(1-2\nu)-\frac{a^2}{r^2}\right]\int_a^b T r dr - \frac{(1+\nu)\alpha}{(1-\nu)r^2}\int_a^r T r dr + \frac{1+\nu}{1-\nu}\alpha T$$

$$\epsilon_\theta = \frac{(1+\nu)\alpha}{(1-\nu)(b^2-a^2)}\left[(1-2\nu)+\frac{a^2}{r^2}\right]\int_a^b T r dr + \frac{(1+\nu)\alpha}{(1-\nu)r^2}\int_a^r T r dr$$

$$u = \frac{(1+\nu)\alpha}{(1-\nu)(b^2-a^2)}\left[(1-2\nu)r+\frac{a^2}{r}\right]\int_a^b T r dr + \frac{(1+\nu)\alpha}{(1-\nu)r}\int_a^r T r dr$$

TEMPERATURE CONSTANT:

$\sigma_r = \sigma_\theta = 0$

$\sigma_z = -\alpha E T$

$\epsilon_r = \epsilon_\theta = (1+\nu)\alpha T$

$u = (1+\nu)\alpha T r$

ASSUMPTION:

1. NO END EFFECTS.

TEMPERATURE - SOLID OR HOLLOW CYLINDER - WITH CASE

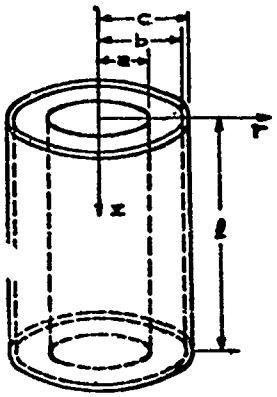

PLANE STRESS:

BOUNDARY CONDITIONS:

$\sigma_r = 0 : \quad r = a, c$

$\sigma_z = 0$

$u|_{r=b} = u_c|_{r=b}$ (ASSUME $w \approx w_c$)

STRESSES IN PROPELLANT:

$$\sigma_r = -\frac{b^2 p'}{b^2-a^2}\left(1-\frac{a^2}{r^2}\right) + \frac{\alpha E}{b^2-a^2}\left(1-\frac{a^2}{r^2}\right)\int_a^b T r\,dr - \frac{\alpha E}{r^2}\int_a^r T r\,dr$$

$$\sigma_\theta = -\frac{b^2 p'}{b^2-a^2}\left(1+\frac{a^2}{r^2}\right) + \frac{\alpha E}{b^2-a^2}\left(1+\frac{a^2}{r^2}\right)\int_a^b T r\,dr + \frac{\alpha E}{r^2}\int_a^r T r\,dr - \alpha E T$$

STRAINS & DISPLACEMENTS IN PROPELLANTS:

$$\epsilon_r = -\frac{b^2 p'}{E(b^2-a^2)}\left[(1-\nu)-(1+\nu)\frac{a^2}{r^2}\right] + \frac{\alpha}{b^2-a^2}\left[(1-\nu)-(1+\nu)\frac{a^2}{r^2}\right]\int_a^b T r\,dr - \frac{(1+\nu)\alpha}{r^2}\int_a^r T r\,dr + (1+\nu)\alpha T$$

$$\epsilon_\theta = -\frac{b^2 p'}{E(b^2-a^2)}\left[(1-\nu)+(1+\nu)\frac{a^2}{r^2}\right] + \frac{\alpha}{b^2-a^2}\left[(1-\nu)+(1+\nu)\frac{a^2}{r^2}\right]\int_a^b T r\,dr + \frac{(1+\nu)\alpha}{r^2}\int_a^r T r\,dr$$

$$\epsilon_z = \frac{2b^2\nu p'}{E(b^2-a^2)} - \frac{2\nu\alpha}{b^2-a^2}\int_a^b T r\,dr + (1+\nu)\alpha T$$

$$u = -\frac{b^2 p'}{E(b^2-a^2)}\left[(1-\nu)r+(1+\nu)\frac{a^2}{r}\right] + \frac{\alpha}{b^2-a^2}\left[(1-\nu)r+(1+\nu)\frac{a^2}{r}\right]\int_a^b T r\,dr + \frac{(1+\nu)\alpha}{r}\int_a^r T r\,dr$$

$$w = \left[\frac{2b^2\nu p'}{E(b^2-a^2)} - \frac{2\nu\alpha}{b^2-a^2}\int_a^b T r\,dr + (1+\nu)\alpha T\right]z$$

$$p' = \frac{\dfrac{2\alpha}{(b^2-a^2)}\displaystyle\int_a^b T r\,dr - \alpha_c T}{\dfrac{\left[(1-\nu)b^2+(1+\nu)a^2\right]}{(b^2-a^2)E} + \dfrac{b}{hE_c}}$$

TEMPERATURE - SOLID OR HOLLOW CYLINDER - WITH CASE

PLANE STRESS CONT'D.:

STRESSES IN CASE:

$$\sigma_r = \frac{b^2 p'}{c^2-b^2}\left(1-\frac{c^2}{r^2}\right)+\frac{\alpha_c E_c}{c^2-b^2}\left(1-\frac{b^2}{r^2}\right)\int_b^c T r\,dr - \frac{\alpha_c E_c}{r^2}\int_b^r T r\,dr$$

$$\sigma_\theta = \frac{b^2 p'}{c^2-b^2}\left(1+\frac{c^2}{r^2}\right)+\frac{\alpha_c E_c}{c^2-b^2}\left(1+\frac{b^2}{r^2}\right)\int_b^c T r\,dr + \frac{\alpha_c E_c}{r^2}\int_b^r T r\,dr - \alpha_c E_c T$$

STRAINS & DISPLACEMENTS IN CASE:

$$\epsilon_r = \frac{b^2 p'}{E_c(c^2-b^2)}\left[(1-\nu_c)-(1+\nu_c)\frac{c^2}{r^2}\right]+\frac{\alpha_c}{c^2-b^2}\left[(1-\nu_c)-(1+\nu_c)\frac{b^2}{r^2}\right]\int_b^c T r\,dr + \\ -\frac{(1+\nu_c)\alpha_c}{r^2}\int_b^r T r\,dr + (1+\nu_c)\alpha_c T$$

$$\epsilon_\theta = \frac{b^2 p'}{E_c(c^2-b^2)}\left[(1-\nu_c)+(1+\nu_c)\frac{c^2}{r^2}\right]+\frac{\alpha}{c^2-b^2}\left[(1-\nu_c)+(1+\nu_c)\frac{b^2}{r^2}\right]\int_b^c T r\,dr \\ +\frac{(1+\nu_c)\alpha_c}{r^2}\int_b^r T r\,dr$$

$$\epsilon_z = -\frac{2\nu_c b^2 p'}{E_c(c^2-b^2)} - \frac{2\nu_c \alpha_c}{c^2-b^2}\int_b^c T r\,dr + (1+\nu_c)\alpha_c T$$

$$u_c = \frac{b^2 p'}{E_c(c^2-b^2)}\left[(1-\nu_c)r+(1+\nu_c)\frac{c^2}{r}\right]+\frac{\alpha_c}{c^2-b^2}\left[(1-\nu_c)r+(1+\nu_c)\frac{b^2}{r}\right]\int_b^c T r\,dr \\ +\frac{(1+\nu_c)\alpha_c}{r}\int_b^r T r\,dr$$

$$w_c = \left[-\frac{2\nu_c b^2 p'}{E_c(c^2-b^2)} - \frac{2\nu_c \alpha_c}{c^2-b^2}\int_b^c T r\,dr + (1+\nu_c)\alpha_c T\right] z$$

(FOR THIN CASE)

$$u_c = \frac{b^2 p'}{h E_c} + \alpha_c b T$$

$$w_c = \left[-\frac{\nu_c b p'}{h E_c} + \alpha_c T\right] z$$

TEMPERATURE – SOLID OR HOLLOW CYLINDER – WITH CASE

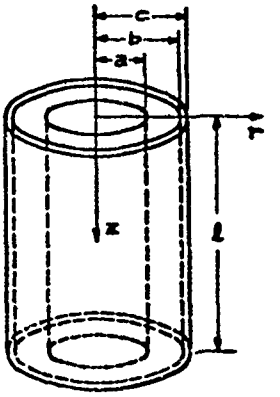

PLANE STRAIN:

BOUNDARY CONDITIONS:

$\sigma_r = 0 : \quad r = a, c$

$w = 0$

STRESSES IN PROPELLANT:

$$\sigma_r = -\frac{b^2 p'}{(b^2-a^2)}\left(1-\frac{a^2}{r^2}\right)+\frac{\alpha E}{(1-\nu)(b^2-a^2)}\left(1-\frac{a^2}{r^2}\right)\int_a^b Tr\,dr - \frac{\alpha E}{(1-\nu)r^2}\int_a^r Tr\,dr$$

$$\sigma_\theta = -\frac{b^2 p'}{(b^2-a^2)}\left(1+\frac{a^2}{r^2}\right)+\frac{\alpha E}{(1-\nu)(b^2-a^2)}\left(1+\frac{a^2}{r^2}\right)\int_a^b Tr\,dr+\frac{\alpha E}{(1-\nu)r^2}\int_a^r Tr\,dr - \frac{\alpha E T}{(1-\nu)}$$

$$\sigma_z = \frac{2\nu b^2 p'}{(b^2-a^2)}+\frac{2\nu\alpha E}{(1-\nu)(b^2-a^2)}\int_a^b Tr\,dr-\frac{\alpha\nu E T}{(1-\nu)}$$

STRAINS & DISPLACEMENTS IN PROPELLANT:

$$\epsilon_r = -\frac{(1+\nu)b^2 p'}{E(b^2-a^2)}\left[(1-2\nu)-\frac{a^2}{r^2}\right]+\frac{(1+\nu)\alpha}{(1-\nu)(b^2-a^2)}\left[(1-2\nu)-\frac{a^2}{r^2}\right]\int_a^b Tr\,dr - \frac{\alpha(1+\nu)}{(1-\nu)r^2}\int_a^r Tr\,dr+\frac{(1+\nu)}{(1-\nu)}\alpha T$$

$$\epsilon_\theta = -\frac{(1+\nu)b^2 p'}{E(b^2-a^2)}\left[(1-2\nu)+\frac{a^2}{r^2}\right]+\frac{(1+\nu)\alpha}{(1-\nu)(b^2-a^2)}\left[(1-2\nu)+\frac{a^2}{r^2}\right]\int_a^b Tr\,dr + \frac{(1+\nu)\alpha}{(1-\nu)r^2}\int_a^r Tr\,dr$$

$$u = -\frac{(1+\nu)b^2 p'}{E(b^2-a^2)}\left[(1-2\nu)r+\frac{a^2}{r}\right]+\frac{(1+\nu)\alpha}{(1-\nu)(b^2-a^2)}\left[(1-2\nu)r+\frac{a^2}{r}\right]\int_a^b Tr\,dr + \frac{(1+\nu)\alpha}{(1-\nu)r}\int_a^r Tr\,dr$$

TEMPERATURE – SOLID OR HOLLOW CYLINDER – WITH CASE

$$p' = \frac{E\frac{2\alpha(1+\nu)}{(b^2-a^2)}\int_a^b Tr\,dr - \alpha_c T(b)(1+\nu_c)E}{\frac{(1+\nu)[(1-2\nu)b^2+a^2]}{(b^2-a^2)} + \frac{(1-\nu_c^2)bE}{hE_c}} \qquad \text{(FOR THIN CASE)}$$

PLANE STRAIN CONT'D.:

STRESSES IN CASE:

$$\sigma_r = \frac{b^2p'}{(c^2-b^2)}\left(1-\frac{c^2}{r^2}\right) + \frac{\alpha_c E_c}{(1-\nu_c)(c^2-b^2)}\left(1-\frac{b^2}{r^2}\right)\int_b^c Tr\,dr - \frac{\alpha_c E_c}{(1-\nu_c)r^2}\int_b^r Tr\,dr$$

$$\sigma_\theta = \frac{b^2p'}{(c^2-b^2)}\left(1+\frac{c^2}{r^2}\right) + \frac{\alpha_c E_c}{(1-\nu_c)(c^2-b^2)}\left(1+\frac{b^2}{r^2}\right)\int_b^c Tr\,dr + \frac{\alpha_c E_c}{(1-\nu_c)r^2}\int_b^r Tr\,dr - \frac{\alpha_c E_c T}{(1-\nu_c)}$$

$$\sigma_z = \frac{2\nu b^2p'}{(c^2-b^2)} + \frac{2\nu_c\alpha_c E_c}{(1-\nu_c)(c^2-b^2)}\int_b^c Tr\,dr - \frac{\alpha_c\nu_c E_c T}{(1-\nu_c)}$$

STRAINS & DISPLACEMENTS IN CASE:

$$\epsilon_r = \frac{(1+\nu_c)b^2p'}{E_c(c^2-b^2)}\left[(1-2\nu_c)-\frac{c^2}{r^2}\right] + \frac{(1+\nu_c)\alpha_c}{(1-\nu_c)(c^2-b^2)}\left[(1-2\nu_c)-\frac{c^2}{r^2}\right]\int_b^c Tr\,dr$$
$$- \frac{(1+\nu_c)\alpha_c}{(1-\nu_c)r^2}\int_b^r Tr\,dr + \frac{(1+\nu_c^2)}{(1-\nu_c)}\alpha_c T$$

$$\epsilon_\theta = \frac{(1+\nu_c)b^2p'}{E_c(c^2-b^2)}\left[(1-2\nu_c)+\frac{c^2}{r^2}\right] + \frac{\alpha_c(1+\nu_c)}{(c^2-b^2)(1-\nu_c)}\left[(1-2\nu_c)+\frac{c^2}{r^2}\right]\int_b^c Tr\,dr$$
$$+ \frac{(1+\nu_c)\alpha_c}{(1-\nu_c)r^2}\int_b^r Tr\,dr$$

$$u_c = \frac{(1+\nu_c)b^2p'}{E_c(c^2-b^2)}\left[(1-2\nu_c)r+\frac{c^2}{r}\right] + \frac{\alpha_c(1+\nu_c)}{(c^2-b^2)(1-\nu_c)}\left[(1-2\nu_c)r+\frac{c^2}{r}\right]\int_b^c Tr\,dr$$
$$+ \frac{(1+\nu_c)\alpha_c}{(1-\nu_c)r}\int_b^r Tr\,dr$$

$$u_c = \frac{(1-\nu_c^2)b^2p'}{hE_c} + \alpha_c bT \qquad \text{(FOR THIN CASE)}$$

FORMULAS AT-7

TEMPERATURE-UNIFORM-HOLLOW CYLINDER-WITH CASE & ENDS BONDED

BOUNDARY CONDITIONS:

$\sigma_r = 0$: $r = a$

$\sigma_r = 0$: $r = b+h$

$u = u_c$: $r = b$

$w = w_c$: $z = 0, \ell$

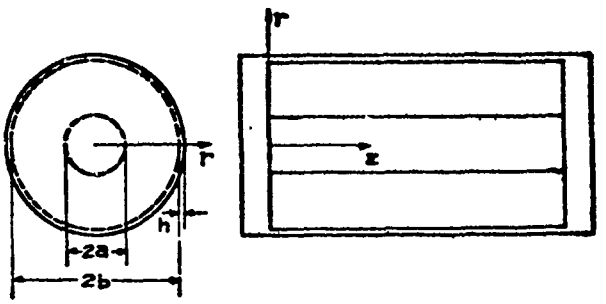

STRESSES IN HOLLOW CYLINDER (PROPELLANT):

$$\sigma_{(r_\theta)} = \pm \frac{a^2 b^2 p_o}{b^2 - a^2} \frac{1}{r^2} - \frac{p_o b^2}{b^2 - a^2},$$

p_o: PRESSURE BETWEEN CASE & PROPELLANT

$$\sigma_z = -p',$$

p': PRESSURE BETWEEN ENDS & PROPELLANT

$$p_o = \frac{\left[(1+\nu)\varepsilon_c^2 + (1+\nu_c)\varepsilon_c\right]\left(\frac{b^2}{a^2}-1\right)(\alpha-\alpha_c)ET}{(1+\nu)\left\{(1-2\nu)\frac{b^2}{a^2}+1\right\}\varepsilon_c^2 + \left\{\left[3-\nu(1+4\nu_c)\right]\frac{b^2}{a^2}+(1+\nu)\right\}\varepsilon_c + 2(1-\nu_c^2)\frac{b^2}{a^2}}$$

$$p' = \frac{\left[(1+\nu)\left(\frac{b^2}{a^2}-1\right)\left(\frac{b^2}{a^2}+1\right)\varepsilon_c^2 + 2(1+\nu_c)\frac{b^2}{a^2}\left(\frac{b^2}{a^2}-1\right)\varepsilon_c\right](\alpha-\alpha_c)ET}{\left[\frac{b^2}{a^2}-1\right]\left[(1+\nu)\left\{(1-2\nu)\frac{b^2}{a^2}+1\right\}\varepsilon_c^2 + \left\{\left[3-\nu(1+4\nu_c)\right]\frac{b^2}{a^2}+(1+\nu)\right\}\varepsilon_c + 2(1-\nu_c^2)\frac{b^2}{a^2}\right]}$$

WHERE

$$\varepsilon_c = \frac{2bh\,E_c}{(b^2-a^2)E} \quad \text{(THIN CASE)}$$

STRAINS & DISPLACEMENTS IN PROPELLANT:

$$\epsilon_{(\theta)} = \frac{1}{E}\left[\pm(1+\nu)\frac{a^2b^2p_o}{b^2-a^2}\frac{1}{r^2} - (1-\nu)\frac{p_ob^2}{b^2-a^2} + \nu p'\right] + \alpha T$$

$$\epsilon_z = -\frac{1}{E}\left[p' - 2\nu\frac{p_ob^2}{b^2-a^2}\right] + \alpha T$$

$$u = \frac{1}{E}\left[-(1+\nu)\frac{a^2b^2p_o}{b^2-a^2}\frac{1}{r} - (1-\nu)\frac{p_ob^2}{b^2-a^2}r + \nu p'r\right] + \alpha Tr$$

$$w = -\frac{1}{E}\left[p' - 2\nu\frac{p_ob^2}{b^2-a^2}\right]z + \alpha Tz$$

STRESSES IN CASE:

$$\sigma_{(\theta)} = \frac{bp_o}{2h}\left(1 \mp \frac{b^2}{r^2}\right) \qquad \text{(THIN CASE)}$$

$$\sigma_z = p'' = \frac{(b^2-a^2)p' + a^2p_i}{2bh}$$

STRAINS & DISPLACEMENTS IN CASE:

$$\epsilon_{(\theta)} = \frac{1}{E_c}\left[\mp(1+\nu_c)\frac{b^2p_o}{2h}\frac{1}{r^2} + (1-\nu_c)\frac{bp_o}{2h} - \nu_c p''\right] + \alpha_c T$$

$$\epsilon_z = \frac{1}{E_c}\left[p'' - \nu_c\frac{bp_o}{h}\right] + \alpha_c T$$

$$u_c = \frac{1}{E_c}\left[(1+\nu_c)\frac{b^2p_o}{2h}\frac{1}{r} + (1-\nu_c)\frac{bp_o}{2h}r - \nu_c p''r\right] + \alpha_c Tr$$

$$w_c = \frac{1}{E_c}\left[p'' - \nu_c\frac{bp_o}{h}\right]z + \alpha_c Tz$$

ASSUMPTIONS:

1. ENDS & CASE BONDED TO PROPELLANT.
2. UNIFORM END EFFECTS WITH END PLATES TRANSMITTING FORCES FROM p_i & p' INTO THIN CYLINDRICAL CASE IN TENSION.
3. NO BENDING EFFECTS INCLUDED FROM ENDS; ASSUMING ONLY HOOP (σ_θ) & AXIAL (σ_z) STRESSES UNIFORM IN CASE UP TO ENDS.
4. UNIFORM TEMPERATURE CHANGE SAME IN PROPELLANT & CASE.

FORMULAS AT-2

TEMPERATURE – STEADY FLOW – PLANE STRESS – NO CASE

TEMPERATURE DISTRIBUTION:

$$T = T_o + \frac{T_i - T_o}{\ln\left(\frac{b}{a}\right)} \ln\left(\frac{b}{r}\right), \quad a \le r \le b$$

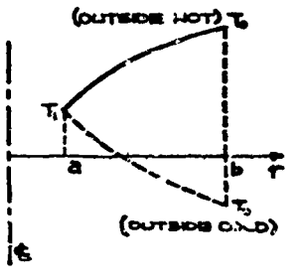

STRESSES:

$$\sigma_r = \frac{\alpha E (T_i - T_o)}{2 \ln\frac{b}{a}} \left\{ - \ln\frac{b}{r} - \frac{a^2}{b^2 - a^2}\left(1 - \frac{b^2}{r^2}\right) \ln\frac{b}{a} \right\}$$

$$\sigma_\theta = \frac{\alpha E (T_i - T_o)}{2 \ln\frac{b}{a}} \left\{ 1 - \ln\frac{b}{r} - \frac{a^2}{b^2 - a^2}\left(1 + \frac{b^2}{r^2}\right) \ln\frac{b}{a} \right\}$$

STRAINS & DISPLACEMENTS:

$$\epsilon_r = \frac{\alpha (T_i - T_o)}{2 \ln\frac{b}{a}} \left\{ -\nu + (1+\nu) \ln\frac{b}{r} - \frac{a^2}{b^2 - a^2}\left[(1-\nu) - (1+\nu)\frac{b^2}{r^2}\right] \ln\frac{b}{a} + \frac{2T_o}{T_i - T_o} \ln\frac{b}{a} \right\}$$

$$\epsilon_\theta = \frac{\alpha (T_i - T_o)}{2 \ln\frac{b}{a}} \left\{ 1 + (1+\nu) \ln\frac{b}{a} - \frac{a^2}{b^2 - a^2}\left[(1-\nu) + (1+\nu)\frac{b^2}{r^2}\right] \ln\frac{b}{a} + \frac{2T_o}{T_i - T_o} \ln\frac{b}{a} \right\}$$

$$\epsilon_z = \frac{\alpha (T_i - T_o)}{2 \ln\frac{b}{a}} \left\{ -\nu + 2(1+\nu) \ln\frac{b}{r} + \frac{2\nu a^2}{b^2 - a^2} \ln\frac{b}{a} + \frac{2T_o}{T_i - T_o} \ln\frac{b}{a} \right\}$$

$$u = \frac{\alpha (T_i - T_o)}{2 \ln\frac{b}{a}} \left\{ r + (1+\nu) r \ln\frac{b}{r} - \frac{a^2}{b^2 - a^2}\left[(1-\nu) r + (1+\nu)\frac{b^2}{r}\right] \ln\frac{b}{a} + \frac{2T_o r}{T_i - T_o} \ln\frac{b}{a} \right\}$$

$$w = \frac{\alpha (T_i - T_o)}{2 \ln\frac{b}{a}} \left\{ -\nu + 2(1+\nu) \ln\frac{b}{r} + \frac{2\nu a^2}{b^2 - a^2} \ln\frac{b}{a} + \frac{2T_o}{T_i - T_o} \ln\frac{b}{a} \right\} z$$

TEMPERATURE - STEADY FLOW - PLANE STRAIN - NO CASE

TEMPERATURE DISTRIBUTION:

$$T = T_o + \frac{T_i - T_o}{\ln \frac{b}{a}} \ln \frac{b}{r}, \quad a \le r \le b$$

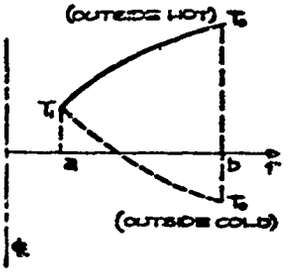

STRESSES:

$$\sigma_r = \frac{\alpha E (T_i - T_o)}{2(1-\nu) \ln \frac{b}{a}} \left[- \ln \frac{b}{r} - \frac{a^2}{b^2 - a^2} \left(1 - \frac{b^2}{r^2}\right) \ln \frac{b}{a} \right]$$

$$\sigma_\theta = \frac{\alpha E (T_i - T_o)}{2(1-\nu) \ln \frac{b}{a}} \left[1 - \ln \frac{b}{r} - \frac{a^2}{b^2 - a^2} \left(1 + \frac{b^2}{r^2}\right) \ln \frac{b}{a} \right]$$

$$\sigma_z = \frac{\alpha E (T_i - T_o)}{2(1-\nu) \ln \frac{b}{a}} \left[\nu - 2 \ln \frac{b}{r} - \frac{2\nu a^2}{b^2 - a^2} \ln \frac{b}{a} - \frac{2(1-\nu) T_o}{T_i - T_o} \ln \frac{b}{a} \right]$$

STRAINS & DISPLACEMENTS:

$$\epsilon_r = \frac{\alpha (1+\nu)(T_i - T_o)}{2(1-\nu) \ln \frac{b}{a}} \left\{ -\nu + \ln \frac{b}{r} - \frac{a^2}{b^2 - a^2} \left[(1-2\nu) + \frac{b^2}{r^2} \right] \ln \frac{b}{r} + \frac{2(1-\nu) T_o}{T_i - T_o} \ln \frac{b}{a} \right\}$$

$$\epsilon_\theta = \frac{\alpha (1+\nu)(T_i - T_o)}{2(1-\nu) \ln \frac{b}{a}} \left\{ (1-\nu) + \ln \frac{b}{r} - \frac{a^2}{b^2 - a^2} \left[(1-2\nu) - \frac{b^2}{r^2} \right] \ln \frac{b}{a} + \frac{2(1-\nu) T_o}{T_i - T_o} \ln \frac{b}{a} \right\}$$

$$u = \frac{\alpha (1+\nu)(T_i - T_o)}{2(1-\nu) \ln \frac{b}{a}} \left\{ (1-\nu) r + r \ln \frac{b}{r} - \frac{a^2}{b^2 - a^2} \left[(1-2\nu) r + \frac{b^2}{r} \right] \ln \frac{b}{a} + \frac{2(1-\nu) T_o}{T_i - T_o} r \ln \frac{b}{a} \right\}$$

3.3.3 Composite, hollow cylinder of K layers under internal pressure.

Inasmuch as it is often of interest to analyze a multi-layered concentric geometry and hence be able to study the inclusion of a liner between the grain and case, or a radial incrementally cast grain, some elastic analyses pertaining to this case are summarized[1.3] by Pister.

Consider the nth layer of a long right circular cylinder where we let r_n denote inner radius, p_n pressure at r_n, $r_n + 1$ denote outer radius, $p_n + 1$ pressure at $r_n + 1$.

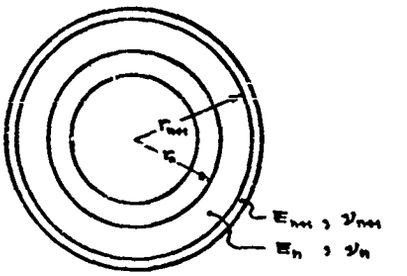

For plane stress the general solution of the displacement equilibrium equation is

$$u_n(r) = A_n r + \frac{B_n}{r} \tag{3.3.17}$$

where

$$A_n = \frac{1-\nu_n}{E_n} \frac{p_n r_n^2 - p_{n+1} r_{n+1}^2}{r_{n+1}^2 - r_n^2}$$

$$B_n = \frac{1+\nu_n}{E_n} \frac{r_n^2 r_{n+1}^2 (p_n - p_{n+1})}{r_{n+1}^2 - r_n^2} \tag{3.3.18}$$

The k-1 continuity conditions at the internal boundaries together with the stress boundary conditions at the external boundaries are sufficient to determine the constants A_n, B_n for each cylinder in a given case (or alternatively, the internal boundary pressures). The continuity conditions are of the type

$$u_n = u_{n+1} \quad \text{at} \quad r = r_{n+1}, \qquad n = 1, 2, \cdots, k-1 \tag{3.3.19}$$

Combining equations (3.3.17), (3.3.18) and substituting in (3.3.19) leads to the result:

$$L_n p_n + M_n p_{n+1} + N_n p_{n+2} = 0 \quad , \qquad n = 1, 2, \cdots, k-1 \tag{3.3.20}$$

where

$$L_n = \frac{2r_n^2}{E_n}\left(r_{n+2}^2 - r_{n+1}^2\right)$$

$$-M_n = \left[\left(\frac{1-\nu_n}{E_n} r_{n+1}^2 + \frac{1+\nu_n}{E_n} r_n^2\right)\left(r_{n+2}^2 - r_{n+1}^2\right) + \left(\frac{1-\nu_{n+1}}{E_{n+1}} r_{n+1}^2 + \frac{1+\nu_{n+1}}{E_{n+1}} r_{n+2}^2\right)\left(r_{n+1}^2 - r_n^2\right)\right] \quad (3.3.21)$$

$$N_n = \frac{2r_{n+2}^2}{E_{n+1}}\left(r_{n+1}^2 - r_n^2\right)$$

To determine stresses and/or displacements in the nth layer, obtain p_n, $p_n + 1$ from the solution of equation (3.3.20) and use in conventional cylinder equations, setting $p_i = p_n$ and $p_o = p_{n+1}$. For plane strain replace E_n by $E_n/(1-\nu_n^2)$ and ν_n by $\nu_n/(1-\nu_n)$.

Example: Internal pressure in three-layer cylinder

$$\left.\begin{aligned} p_1 &= p_i \\ p_3 &= 0 \end{aligned}\right\} \text{ External body conditions}$$

Setting n = 1, 2 in equations (3.3.20) gives (using above conditions)

$$L_1 p_2 + M_1 p_3 = 0$$
$$L_2 p_2 + M_2 p_3 = 0$$

whose solution is

$$p_2 = \frac{-L_1 M_2 p_i}{M_1 M_2 - L_2 N_1} \quad , \qquad p_3 = \frac{L_1 L_2 p_i}{M_1 M_2 - L_2 N_1}$$

L, M, N can be evaluated from equation (3.3.21)

Pressures p_1, p_2, p_3 can be used in equations given in Section 3.3.2 for the determination of stresses and displacements in the layers of the cylinder. In view of the cumbersome algebra involved, results will be given explicitly only for the instance in which the outer two layers are thin.

Thin Liner and Thin Case

$$\frac{h_2}{b} \ll 1, \quad \frac{h_1}{b} \ll 1, \quad \lambda = \frac{b}{a}$$

p' = interface pressure at $r = b$

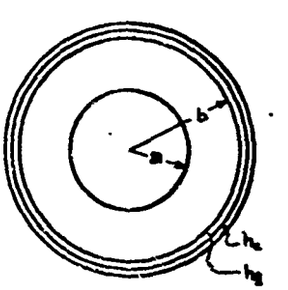

Plane Strain

$$p' = \frac{2P_i(1-\nu)}{\left[1+(1-2\nu)\lambda^2 + \frac{\lambda^2-1}{\frac{h_c E_c}{bE}\left(\frac{1+\nu}{1-\nu_c^2}\right) + \frac{h_l E_l}{bE}\left(\frac{1+\nu}{1-\nu_l^2}\right)}\right]}$$

$\left\{\begin{matrix}\text{Stresses}\\ \text{Strains}\end{matrix}\right\}$ in cylinder, same as formulas P-12, P-14 in Section 3.3.2, using above value of p'.

Stress in case:

$$\sigma_\theta = \frac{p'}{\frac{h_c}{b} + \frac{h_l}{b}\frac{E_l}{E}}$$

Stress in liner:

$$\sigma_\theta = \frac{p'}{\frac{h_l}{b} + \frac{h_c}{b}\frac{E_c}{E_l}}$$

Discussion of Results:- As can be seen from the expression for p on the previous page, the presence of the liner does not affect the stress distribution in the grain, since the dominating term $h_c E_c/bE$ causes the fraction $(\lambda^2 - 1)/[\sim\sim]$ to vanish for typical geometry and materials. Accordingly, the liner is of no significance pressurewise, as long as the ratio $h_c E_c/bE$ remains large, as it will for metal cases. In the event that non-metal cases with significantly lower moduli are used, or if grain stiffness were increased, the liner could become important in determining stress distribution due to pressure.

3.3.4 Temperature distributions in cylinders.

The thermal stress solutions given in the previous Section 3.3.2 require knowledge of the temperature distributions. Temperature changes in propellants are due almost exclusively to heat conduction and the (exothermic or endothermic) reactions during curing. Temperature change due only to straining is inconsequential, whereas radiation during long space flights may be more detrimental to the chemical composition of the propellant than in heating. At any rate, we shall first consider temperature distributions from the heat conduction equations reviewed in this section.

While temperature distributions are generally transient in nature, the stresses and strains can often be calculated assuming elastic response. This is the case when the mean relaxation time of the material is appreciably larger or smaller than the characteristic time for thermal diffusion, $(\kappa\alpha^2)^{-1}$, (see Section 3.4.5).

Particular mention should also be made of the Rohm and Haas articles[3.5] and those of Nichols et al [3.6, 3.7], dealing with thermal conditions during casting and curing.

TEMPERATURE DISTRIBUTIONS

HEAT TRANSFER EQUATION:

$$K\left(\frac{\partial^2 T}{\partial r^2}+\frac{1}{r}\frac{\partial T}{\partial r}+\frac{1}{r^2}\frac{\partial^2 T}{\partial \theta^2}+\frac{\partial^2 T}{\partial z^2}\right)+Q_1=c\rho\frac{\partial T}{\partial t}$$ (INFINITELY LONG CYLINDER)

RADIAL HEAT FLOW WITHOUT INTERNAL HEAT SOURCES:

$$K\left(\frac{\partial^2 T}{\partial r^2}+\frac{1}{r}\frac{\partial T}{\partial r}\right)=\frac{\partial T}{\partial t}, \qquad K\equiv\frac{K}{\rho c}$$

TYPES OF BOUNDARY CONDITIONS:

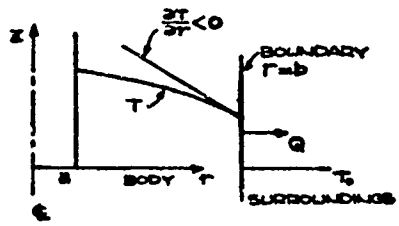

1.) $T=T_0$, CONSTANT TEMPERATURE

2) $\frac{\partial T}{\partial r}=0$, NO HEAT FLOW (INSULATED)

3) $\frac{\partial T}{\partial r}=$ CONST., PRESCRIBED FLOW RATE

4.) $K\frac{\partial T}{\partial r}+H(T-T_0)$ OR $\frac{\partial T}{\partial r}=h(T-T_0)$, RADIATION CONDITION,

T_0 = TEMP. OF SURROUNDINGS,

$Q=-2\pi bK\frac{\partial T}{\partial r}$ = HEAT FLUX/UNIT LENGTH

5) $Q=2\pi b\sigma E(T^4-T_0^4)$, BLACK BODY RADIATION, T_0 ABSOLUTE

STEADY STATE RADIAL FLOW:

$$T=T_0+\frac{T_1-T_0}{\ln\left(\frac{b}{a}\right)}\ln\left(\frac{b}{r}\right),$$

$T=T_1$: $r=a$

$T=T_0$: $r=b$

$$Q=-2\pi rK\frac{\partial T}{\partial r}=\frac{2\pi K(T_1-T_0)}{\ln\left(\frac{b}{a}\right)}$$

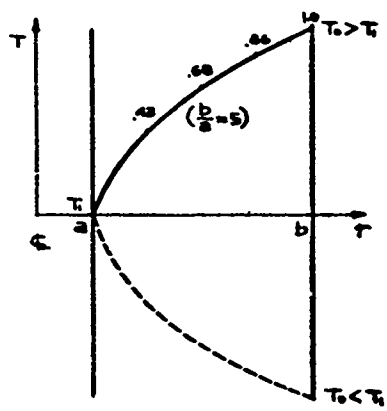

TRANSIENT RADIAL FLOW:

$$K\left(\frac{\partial^2 T}{\partial r^2}+\frac{1}{r}\frac{\partial T}{\partial r}\right)=\frac{\partial T}{\partial t}$$

SEPARATING VARIABLES:

$$T(r,t)=R(r)e^{-K\alpha^2 t}$$

$$\frac{d^2R}{dr^2}+\frac{1}{r}\frac{dR}{dr}+\alpha^2 R=0\,, \qquad \text{BESSEL'S EQUATION}$$

REFERENCE: 3.8.

TEMPERATURE INITIALLY ZERO, OUTSIDE TEMPERATURE SUDDENLY RAISED TO T_0:

$$T=T_0\frac{\ln\left(\frac{r}{a}\right)}{\ln\left(\frac{b}{a}\right)}$$

$$-\pi T_0\sum_{n=1}^{\infty}\frac{e^{-K\alpha_n^2 t}J_0(a\alpha_n)J_0(b\alpha_n)}{J_0^2(a\alpha_n)-J_0^2(b\alpha_n)}\left[J_0(r\alpha_n)Y_0(a\alpha_n)-Y_0(r\alpha_n)J_0(a\alpha_n)\right]$$

WHERE α_n ARE ROOTS OF:

$$J_0(a\alpha)Y_0(b\alpha)-Y_0(a\alpha)J_0(b\alpha)=0$$

REFERENCE: 3.9.

WHERE $N\equiv Y$, $R=\frac{b}{a}$

TRANSIENT RADIAL FLOW (CONT.):

TEMPERATURE INITIALLY ZERO, INNER SURFACE INSULATED, OUTER SURFACE – CONVECTION TO SURROUNDING GASEOUS MEDIUM OF TEMPERATURE T_g; DIMENSIONS OF CYLINDER; $R_i < r < R_e$

$$\frac{T_g - T}{T_g} = \sum_1^\infty f_1(m, B, \delta_i)\, f_2(p\delta_i, m\delta_i)\, e^{-\mathcal{F}\delta_i^2}$$

$$\mathcal{F} = \frac{\alpha t}{R_e^2} \qquad B = \frac{hR_e}{\lambda},$$

h = CONVECTION COEFFICIENT

λ = THERMAL CONDUCTIVITY

$$m = \frac{R_i}{R_e}$$

$$p = \frac{r}{R_e}$$

δ_i = ROOTS OF $\quad J_1(m\delta)\left[\delta Y_1(\delta) - B Y_0(\delta)\right] = Y_1(m\delta)\left[\delta J_1(\delta) - B J_0(\delta)\right]$

$$f_1(m, B, \delta_i) = \frac{\pi B J_1(m\delta_i)\left[\delta_i J_1(\delta_i) - B J_0(\delta_i)\right]}{\left[\delta_i J_1(\delta_i) - B J_0(\delta_i)\right]^2 - (B^2 + \delta_i^2) J_1^2(m\delta_i)}$$

$$f_2(p\delta_i, m\delta_i) = J_0(p\delta_i)\, Y_1(m\delta_i) - Y_0(p\delta_i)\, J_1(m\delta_i)$$

REFERENCE : 3.20.

3.4 Discussion of Other Design Applications

While it is obviously impossible to discuss analysis techniques for all the various design configurations which might be proposed for solid rocket grains, it is pertinent, nevertheless, to discuss some of the factors which will be encountered in design applications. As intimated earlier the pressure or simulated ignition loading of a thick walled hollow cylinder, even as extended to star grains through the use of concentration factors is at best only an approximation to the actual problem, whether treated viscoelastically or elastically. It does, however, serve the very useful purpose of conditioning the analyst's intuition which then permits him to make judicious extrapolations. In order to further develop this background, it is therefore advisable to investigate other cases of an idealized nature.

3.4.1 Spherical grains

The simplest geometric extension of the hollow cylinder is the hollow sphere. Here again it is possible to obtain some fairly useful results, although the basic formulas are developed for the complete shell, i.e. no port is considered for the exhaust to escape. Such discontinuity effects would have to be superimposed upon the basic stress distribution later. If the inside and outside radii and pressure of the hollow sphere are a and b, and p_i and p_o respectively, the following relations have been deduced[3.10].

Pressure loading. - For an uncased elastic sphere, one has

$$\sigma_r = \frac{\left(\frac{r}{a}\right)^3 (p_i - \lambda^3 p_o) - \lambda^3 (p_i - p_o)}{\left(\frac{r}{a}\right)^3 (\lambda^3 - 1)} \quad ; \quad \lambda \equiv \frac{b}{a} \tag{3.4.1}$$

$$\sigma_\theta = \frac{\left[\lambda^3 + 2\left(\frac{r}{a}\right)^3\right] p_i - \lambda^3 \left[2\left(\frac{r}{a}\right)^3 + 1\right] p_o}{2\left(\frac{r}{a}\right)^3 (\lambda^3 - 1)} \tag{3.4.2}$$

$$\frac{u_r}{r} = \frac{p_i}{E(\lambda^3-1)\left(\frac{r}{a}\right)^3}\left[(1-2\nu)\left(\frac{r}{a}\right)^3 + \frac{(1+\nu)}{2}\lambda^3\right] - \frac{\lambda^3 p_o}{E(\lambda^3-1)\left(\frac{r}{a}\right)^3}\left[(1-2\nu)\left(\frac{r}{a}\right)^3 + \frac{1+\nu}{2}\right] \tag{3.4.3}$$

If there is a thin reinforcing case of wall thickness h and modulus E_c and Poisson's ratio ν_c, and the sphere is subjected to uniform internal pressure, the pressure at the propellant case interface, $\bar{p}$, is

$$\frac{\bar{p}}{p_i} = \frac{3(1-\nu)}{2(1-2\nu)\lambda^3 + (1+\nu) + (1-\nu_c)(\lambda^3-1)\frac{E b}{E_c h}} \tag{3.4.4}$$

which for a rigid case, $Eb/E_c h \ll 1$, reduces for an incompressible material to

$$\frac{\bar{p}}{p_i} = \left.\frac{3(1-\nu)}{1+\nu}\right|_{\nu=\frac{1}{2}} = 1 \qquad (3.4.5)$$

as it should. These formulas can be compared with the similar ones for the hollow cylinder and certain associations can be drawn, particularly the occurrence of the λ^3 factor instead of λ^2.

Thermal loading. - Consider the situation of uniform temperature rise, ΔT, of the entire case bonded assembly. The equivalent interface pressure on the grain, allowing for a thin liner with properties denoted by primes, is

$$\frac{\bar{p}}{2E\alpha\Delta T} = \frac{\left(1-\frac{\alpha'}{\alpha}\right) + \frac{(\alpha'/\alpha)-(\alpha_c/\alpha)}{1+\frac{1-\nu_c}{1-\nu'}\frac{E'h'}{E_c h}}}{\frac{2(1-2\nu)\lambda^3+(1+\nu)}{\lambda^3-1} + \frac{(1-\nu_c)\,Eb/(E_c h)}{1+\frac{1-\nu_c}{1-\nu'}\frac{E'h'}{E_c h}}} \qquad (3.4.6)$$

For a mechanically rigid case ($E_2 \to \infty$),

$$\frac{\bar{p}}{2E\alpha\Delta T} = \frac{(\lambda^2-1)\left[1-(\alpha_c/\alpha)\right]}{2(1-2\nu)\lambda^3+(1+\nu)} \qquad (3.4.7)$$

with an associated strain at the inside radius

$$\epsilon_\theta(a) = -\frac{3\lambda^3(1-\nu)\left[1-(\alpha_2/\alpha)\right]\alpha E\Delta T}{2(1-2\nu)\lambda^3+(1+\nu)} \qquad (3.4.8)$$

If one has the case of steady heat flow through the grain, such that the case is at a temperature T_o and the inside at a temperature T_i, such that the temperature distribution is

$$T = (T_i - T_o)\frac{\frac{\lambda a}{r}-1}{\lambda-1} + T_o \qquad (3.4.9)$$

there results, at the interface, a pressure of

$$\frac{\bar{p}}{E\alpha(T_i-T_o)} = \frac{(3\nu-1)\lambda^2+\nu\lambda-1}{(1-\nu)\left[2(1-2\nu)\lambda^3+1+\nu\right]} \qquad (3.4.10)$$

3.4.2 Spherical-cylindrical junctions.

One problem which has continually caused difficulty is the stress field where the cylinder and head end joins. The actual problem is tremendously complicated by the star intersections; consequently at the present time one can only hope to estimate the order of magnitude of the stresses by a knowledge of the cylinder and

spherical solutions independently, and the gross moment across the wall estimated from thin shell theory. (The pressure stress concentration factors for the cylindrical grain[3.4] are expected to be conservative if applied to spherical sections.) Durelli[3.11], however, has recently obtained some photoelastic data for this combined geometry with web fractions of the order of fifty percent which should provide at least one check point for engineering estimates.

Outside of photoelastic tests, it does not seem possible, at this time, to obtain very accurate estimates of stresses in this geometry when it is further complicated by star cut outs and igniter ports. The analyst will have to continue relying upon indirect inferences of the stress field, including the proper use of concentration factors for related geometries as developed by Neuber[3.12] and Peterson[3.13].

3.4.3 Environmental and handling loads.

The usual engineering consideration must be given to handling and shipping loads, whose assessment is frequently complicated by potential thin shell instability of the assembly. Another problem of concern is the effect of vibration upon the grain and the grain-liner bond during shipping. Some exploratory work along these lines has been reported by Baltrukonis[3.14].

In the sense that gravity force is environmental loading, one could consider the problem of slump during storage within this category. Two basic problems of interest arise when the gravity vector is vertical and horizontal. The first of these has been treated by Knauss[3.15], which will be discussed subsequently in connection with failure criteria, and the second has recently been analyzed by Lianis[3.16]. It is felt that sufficient initial information is now available to demonstrate the methods of analysis which should be employed, as well as providing some preliminary design data. It should also be mentioned that the slump problem during storage is closely related, from the analysis standpoint, to the acceleration inertia problem. This aspect of the problem has also been included by Knauss, whose solution permits estimates of grain deformation when the base of the grain is bonded or free from the base support. His work also comments upon the use of gelatin models for visualizing the state of deformation.

3.4.4 Buckling stability of motors

One other problem associated with grain slumping, which might be mentioned, is that due to the stabilization of the shell by the low modulus propellant. It may be noted that the bonding restraint at the case wall may lead to a different mechanism of buckling than for simple internal pressure in the thin shell due to the interface shear. As might be expected, the buckling strength of the shell is increased. In one investigation, Goree and Nash[3.17] found the buckling stress in axial compression to be increased from 5 to 65 percent with increase of R/t ratio (R = shell radius, t = thickness) from .333 to .667. The modulus ratio was of the order of 10^5. In certain design applications therefore, the designer may be in a position to take advantage of the increased rigidity.

3.4.5 Thermal loadings

The problem of thermal cycling is one of the most difficult of those facing the analyst. It is important to review the kinds of problems which can be solved in a relatively straightforward manner, and then discuss those which are nearly intractable. There are two problems for which present theory is adequate and useful information can be deduced.

Steady-state approximation. - The first of these pertains to a grain assembly whose temperature is very slowly changed. In this case the temperature distribution is known, namely ΔT = constant, and any mechanical stresses arise solely from the differences in the coefficients of thermal expansion of the component materials. In the special case of a long tubular grain, this loading is equivalent to a uniformly distributed interface pressure (Section 3.3.2, formula ΔT-7)

$$p' = \frac{E\left[(1+\nu)\alpha - (1+\nu_c)\alpha_c\right]\Delta T}{\dfrac{(1+\nu)\left[(1-2\nu)b^2 + a^2\right]}{(b^2-a^2)} + \dfrac{(1-\nu_c^2)bE}{h E_c}} \qquad (3.4.11)$$

and is thus reducible to a pressure loading for which analyses and concentration factors are available.[3.4]

The second problem is that of a steady-state temperature distribution such as imposed by constant temperatures, T_o and T_i on the outside and inside respectively. Thus, whereas the former temperature distribution was constant in both the time and space dimensions, this latter one corresponds to one which is constant only in time. The interaction of temperature and mechanical properties is thus confined to allowing, for example, $E = E\left[T(r,\theta)\right]$ which requires

essentially that the governing differential equations now include coefficients which become space dependent, but nevertheless are still linear. Such analyses have been conducted in the past, particularly in connection with gun barrel design; contributions have, for example, been made by Hilton[3.18]. Furthermore, the time independent feature implies an elastic stress-strain law. Hence this problem also can be solved in a reasonably accurate and practical manner, and previously obtained concentration factors[3.19] may be used.

A rough idea of the magnitudes of strain and case bonding stress can be obtained through use of the steady state elastic solution for a tubular grain with temperature independent properties. For a case bonded grain in plane strain subjected to a temperature T_o on the outside and T_i on the inside, the temperature distribution is

$$T = \frac{T_o \ln(\frac{r}{a}) + T_i \ln(\frac{b}{r})}{\ln(\frac{b}{a})} \qquad (3.4.12)$$

The interface pressure at the case bonding, assuming an incompressible propellant is (Section 3.3.2, formula ΔT-7)*

$$p' = \frac{\alpha E}{3 + \frac{E}{m_c}}\left[(T_o - T_i)\left(1 - \frac{\lambda^2-1}{2\ln\lambda}\right) + (T_o - T_R)(\lambda^2-1)\left\{1 - \frac{2\alpha_c}{3\alpha}(1+\nu_c)\right\}\right] \qquad (3.4.13)$$

where α_c and α are the linear thermal expansion coefficients of the case and propellant respectively, m_c the effective case rigidity $E_c h / [2(1-\nu_c^2)(\lambda^2-1)\, b]$, $\lambda = b/a$, and T_R the temperature for zero strain, say the cure temperature. Similarly the strain at the internal surface, useful in determining low temperature operating limits is *

$$\epsilon_\theta(a) = \frac{3}{2}\frac{\alpha(T_o - T_R)}{1 + \frac{3m_c}{E}}\left[\left\{\frac{T_o - T_i}{T_o - T_R}\right\}\left\{1 - \frac{3(\lambda^2-1)m_c}{E}\right\}\left\{\frac{1}{\lambda^2-1} - \frac{1}{2\ln\lambda}\right\}\right. \qquad (3.4.14)$$
$$\left. + \left\{1 + 2\lambda^2\frac{m_c}{E}\frac{\alpha_c}{\alpha}(1+\nu_c) - \frac{3(\lambda^2-1)m_c}{E}\right\}\right]$$

which may be multiplied by the concentration factor $K_t K_g$ for an internally slotted grain[3.19].

* The expressions for interface pressure and strain at the internal surface which are given on page 87 of reference 4.2 are in error; the above equations (3.4.13) and (3.4.14), should be used instead.

If the inside and outside temperatures of a 50 percent web fraction grain are the same, but $\Delta T^{\circ}F$ below T_R, one finds a tensile stress at the bond of the order of $\sigma_r(b) \sim 10 \alpha E/\Delta^{\circ}$ or approximately 50 psi per $100^{\circ}F$ temperature drop. Without allowing for a concentration factor, the internal tensile strain may be of the order of 10 percent per $100^{\circ}F$ temperature drop. Thus, conditions at either the bond or the internal surface may be significant upon cooling. Geckler[3.20] has also observed that transient considerations upon heating from the lower temperatures lead to thermal stresses of sizeable magnitude near the star points which may also contribute to grain cracking. Also, Zwick[3.21] has shown that when the temperature of the shell is suddenly changed, elastic stresses are monotonic functions of time, and hence the maximum stresses occur either initially or finally. However, if and when this is true for a viscoelastic material requires further study.

General transient problem. - The general problem of thermal strain analysis involves first the knowledge or determination of the transient temperature distribution. As mentioned, Geckler[3.20] has charted certain transient data for hollow cylinders, Nichols and Presson[3.7] have determined the transient temperatures during curing cycles including the heat sources due to the chemical energy of polymerization. In this more general case, therefore, the temperature depends upon both space and time; specifically, the dashpot viscosities and ice the stress-strain law changes with time. It is this temperature dependence of the material properties which causes the increased complexity since the governing differential equations then have coefficients which are both space and time dependent. In addition, time dependent strains may result from either of two diffusion type processes: transient temperature variations or viscoelastic material behavior. Unfortunately, it is not clear a priori that one effect will always dominate to the extent that analytical simplicity may be achieved by always neglecting one with respect to the other; although some limits, based upon the validity of elastic approximations, have been discussed in Section 3.3.1. The only complication which does not enter is that the characteristic burning rate of propellants usually exceeds the thermal diffusion rate, so that when a pressurized grain is burning out, the temperature distribution in the unburned propellant remains essentially unchanged and only the viscoelastic pressure stresses need be calculated.

Returning to the sensitivity of mechanical properties to temperature, it is found that even if an assumption of linear viscoelastic behavior is valid, there is in general no associated or equivalent elastic problem such as exists in the temperature independent problem. Morland and Lee[3.22] have recently analyzed this

situation, incorporating a time-temperature shift function. It provides the relation between physical time and a dimensionless reduced time, t'; namely

$$t' = \int_0^t \frac{du}{K[T(u)]} \qquad (3.4.15a)$$

Note that when temperature is constant in time,

$$t' = \frac{t}{K(T)} \qquad (3.4.15b)$$

which corresponds to the notation in Section 2.5. Hence for materials following this shift law, one would deduce that the characteristic stress-strain, time-temperature dependent, law for linearly viscoelastic media could be written in the same form as discussed in earlier sections except that the reduced time t' would be used instead of t.

However, while the coefficients in the stress-strain law are constant using the reduced time, the equilibrium and compatibility relations, in their usual linear form, are a function of the physical time t. It is when the stress-strain law is written in physical time, or alternately, the equilibrium law is written in reduced time, preparatory to solving a particular analytical problem, that complications arise. To illustrate the difficulties, consider a special case following from Morland and Lee's formulation; an infinitely long hollow thick-walled cylinder, symmetrically loaded. Furthermore assume that the propellant material is viscoelastic in shear only, remaining elastic in bulk or dilatation response. The following equations then apply.

Equilibrium: $$\frac{\partial \sigma_r}{\partial r} + \frac{\sigma_r - \sigma_\theta}{r} = 0 \qquad \sigma_{r,\theta} = f(r;t) \qquad (3.4.16)$$

Compatibility: $$\frac{\partial \epsilon_\theta}{\partial r} - \frac{\epsilon_r - \epsilon_\theta}{r} = 0 \qquad \epsilon_{r,\theta} = f(r;t) \qquad (3.4.17)$$

Stress-strain:

Dilatation- $$\sigma_r + \sigma_\theta + \sigma_z = 3K\left[\epsilon_r + \epsilon_\theta + \epsilon_z - 3\alpha(T - T_R)\right] \qquad (3.4.18)$$

K = bulk modulus, constant

Shear- $$\left[a_n \frac{d^n}{dt'^n} + \cdots + a_0\right](\sigma_r - \sigma_\theta) = \left[b_m \frac{d^m}{dt'^m} + \cdots + b_0\right](\epsilon_r - \epsilon_\theta) \qquad (3.4.19)$$

a_n, b_m = experimental material constants

Upon assuming for example a plane strain configuration which prescribes ϵ_z, and using the stress-strain law to express σ_z in terms of the remaining four unknowns σ_r, σ_θ, ϵ_r and ϵ_θ, the above four equations are sufficient to

determine the solution, using of course $t' = \int_0^t du/K[T(u)]$ where the time dependent temperature distribution is presumed known from a previous solution of the heat-conduction problem.

For analytical simplicity, Morland and Lee investigated the steady state situation $T = T(r)$ with an assumption of individual mechanical and thermal incompressibility, i.e. $\epsilon_r + \epsilon_\theta + \epsilon_z = 0$ and $\alpha = 0$ respectively. In this case and for plane strain ($\epsilon_z = 0$), one had $\epsilon_r = -\epsilon_\theta$ and both strains were easily determined in physical time using the compatibility equation, e.g. $\epsilon_r = F(t)/r^2$. The stresses were then investigated using

$$\frac{\partial \sigma_r(r;t)}{\partial r} + \frac{\sigma_r(r;t) - \sigma_\theta(r;t)}{r} = 0 \qquad (3.4.20a)$$

$$\left[\frac{a_n}{\{T(r)\}^n}\frac{\partial^n}{\partial t^n} + \cdots + a_0\right][\sigma_r(r;t) - \sigma_\theta(r;t)] = \left[\frac{b_m}{\{T(r)\}^m} + \cdots + b_0\right]\frac{2F(t)}{r^2} \qquad (3.4.20b)$$

for Kelvin and Maxwell models. The essential feature here is that the Laplace transform technique could still be employed, if desired, to solve a set of partial differential equations with variable, spacewise but not time-wise, coefficients.

With perhaps a more appropriate assumption for propellant materials, which are to the first approximation mechanically incompressible but with a finite coefficient of thermal expansion, one might assume a Poisson's ratio of one half. If further, a plane strain assumption $\epsilon_z = \alpha(T - T_R)$ is employed, approximate equations for this situation, including non-steady state temperature, can be deduced*

$$\frac{\partial \sigma_r}{\partial r} + \frac{\sigma_r - \sigma_\theta}{r} = 0 \qquad (3.4.21a)$$

$$\frac{\partial \epsilon_\theta}{\partial r} - \frac{\epsilon_r - \epsilon_\theta}{r} = 0 \qquad (3.4.21b)$$

$$\sigma_r + \sigma_\theta = 2K[\epsilon_r + \epsilon_\theta - 2\alpha(T - T_R)] \qquad (3.4.21c)$$

---

* Actually the coefficient in the dilitation stress-strain law becomes $3K/(1+\nu)$ where ν, in the Laplace transform representation, stands for a time dependent operator ratio. On the other hand, $\nu = \frac{1}{2}$ for propellants so this approximation is introduced for simplicity in the equations to yield $2K$, a constant by hypothesis ignoring the fact that a consistent use of $\nu = \frac{1}{2}$ would require K, elastically equal to $E/3(1-2\nu)$, to be infinite.

$$\left[a_n \frac{d^n}{dt'^n} + \cdots + a_0\right](\sigma_r - \sigma_0) = \left[b_m \frac{d^m}{dt'^m} + \cdots + b_0\right](\varepsilon_r - \varepsilon_0) \qquad (3.4.22)$$

where it is now observed that the strain analysis cannot be conveniently separated from the stress analysis. As previously noted the last equation has constant coefficients only in the associated time, t', and if written in terms of the physical time becomes a partial differential equation with both spacewise and timewise complicated coefficients. Aside from the curing problem, these are the type equations which must be solved to study the thermal cycling problem.

While a numerical solution of these equations may be called for, it is in order to inquire as to possible limit cases of practical interest. As mentioned earlier, two diffusion type processes are involved, first the thermal diffusion characterized by terms such as $T \approx e^{-\kappa \alpha_n^2 t}$, and second the viscoelastic deformation responding to $u \approx e^{-\frac{t'}{\tau}} = e^{-\frac{t}{\kappa(T)\tau}}$ so that a consideration of the typical time constants $\tau\kappa(T)$ and $(\kappa\alpha_n^2)^{-1}$ or their ratio - relaxation time to heating time - becomes pertinent.

$$\frac{t_R}{t_H} = \kappa(T)\tau\kappa\alpha_n^2 \equiv \frac{\kappa\alpha_n'^2 \tau \kappa(T)}{a^2} \qquad (3.4.23)$$

If a hollow tubular grain is at zero initial temperature, i.e. reference value, and the case at r = b is raised to a temperature T_0 while the internal temperature at r = a remains at zero, the transient thermal distribution is (see Section 3.3.4)

$$\frac{T}{T_0} = \frac{\ln\left(\frac{r}{a}\right)}{\ln\left(\frac{b}{a}\right)} - \pi \sum \frac{J_0^2(a\alpha_n)\, e^{-\kappa\alpha_n^2 t}}{J_0^2(a\alpha_n) - J_0^2(b\alpha_n)} \left[J_0(r\alpha_n) Y_0(b\alpha_n) - Y_0(r\alpha_n) J_0(b\alpha_n)\right] \qquad (3.4.24)$$

where κ is the diffusivity and α_n are the roots of

$$J_0(a\alpha_n) Y_0(b\alpha_n) - Y_0(a\alpha_n) J_0(b\alpha_n) = 0 \qquad (3.4.25)$$

Carslaw and Jaeger tabulate these roots. For a 50 percent web fraction, b/a = 2, and $\alpha_n' = a\,\alpha_n = 3.12,\ 6.27,\ 9.42$ respectively for $n = 1, 2, 3$.

For example, if (T) is of order one, then choosing the lowest eigenvalue of the temperature distribution, $\alpha_1' = 3.12$, a characteristic propellant diffusivity of 10^{-6} ft^2/sec, and assuming medium sized grains, say, two foot diameter or larger, one has approximately $t_R/t_H \approx 10^{-5}\tau$. Considering that characteristic relaxation times range in the order of seconds or less, one concludes that most of th viscoelastic deformation relaxes much faster than the temperature is changing, unless the particular propellant relaxation spectrum is heavily weighted in the longer times.

It may be justifiable then to proceed upon the assumption that the temperature distribution is quasi-steady, $T = T(r, t_o)$. With this assumption, a Laplace transform of the shear stress strain equation with respect to physical time may be taken, and an associated elastic problem--with space varying temperature dependent properties--can be formulated, and in principle be inverted to give the desired result. This type of analysis is similar to that proposed by Hilton[3.23], except a Fourier transform was suggested in order to make use of the complex modulus representation.

By way of concluding this section, it may be said that if the characteristic loading or diffusion times t_H are large or small compared to the relaxation time t_R then thermoelastic analysis with or without space varying temperature dependence may be applied with a reasonable expectation of success. If, however, these times are of the same order, then one would attempt to introduce first a quasi-steady temperature distribution and proceed with the viscoelastic analysis. On the other hand, in the vicinity of the transition region when $t_R \approx t_H$, a combined transient viscoelastic analysis is necessary[3.24]. At the present time only approximations to this situation can be attempted pending further study and improvements in appropriate analysis techniques.

REFERENCES

3.1 Lee, E.H.: Stress Analysis in Viscoelastic Bodies. Technical Report No. 8 NOrd 11496, Brown University, June 1954.

3.2 von Karman, T.; Biot, M.A.: Mathematical Methods in Engineering. McGraw-Hill Book Company, Inc., New York, p. 403, 1940.

3.3 Lee, E.H.; Radok, J.R.M.: Stresses in Elastically Reinforced, Visco-Elastic Tubes with Internal Pressure. Brown University, PA-TR/15, NOrd 16471, April 1956.

3.4 Ordahl, D.D.; Williams, M.L.: Preliminary Photoelastic Design Data for Stresses in Rocket Grains. Jet Propulsion, June 1957.

3.5 Clem, J.D.; Groetzinger, W.H.; Johnson, J.E.; Parr, C.H.: Quarterly Progress Report on Weapons Research, Rohm and Haas Co., Report No. P-47-5, April 10, 1957.

3.6 Nichols, P.L.: Control of Chemical and Physical Factors in the Application of Casting Resins. Society of Plastics Engineer's Journal, November 1956.

3.7 Nichols, P.L.; Presson, A.G.: Heat-Transfer Calculations Related to Solid Propellant Curing. California Institute of Technology, Jet Propulsion Laboratory, Report No. 20-68, September 17, 1953.

3.8 Carslaw, H.S.; Jaeger, J.C.: Conduction of Heat in Solids. Oxford, Clarendon Press, Sections 79, 126, 137, (1947).

3.9 Jahnke, E.; Emde, F.: Tables of Functions. 4th Ed. Dover Publications, pp. 205-206, 1945.

3.10 Williams, M.L.; Stimpson, L.D.: Some Basic Structural Analysis Equations for a Spherical Motor. Internal report to U.S. Naval Ordnance Test Station, China Lake, California, November 1959.

3.11 Riley, W.F.; Durelli, A.J.: Boundary Stresses at the Ends of Pressurized Cylindrical Holes Axially Located in a Large Cylinder. Society of Experimental Stress Analysis, Vol. 17, no. 1, p. 115, 1959.

3.12 Neuber, H.: Theory of Notch Stresses. Edwards Bros., Ann Arbor, 1946.

3.13 Peterson, R.E.: Stress Concentration Design Factors. Wiley, New York, 1953

3.14 Baltrukonis, J.; Gottenberg, W.G.; Schreiner, R.N.: The Dynamic Response of a Finite Rigid Mass Concentrically Carried by a Viscoelastic Disk. Engineering Mechanics Report EM 10-21, Space Technology Laboratories, 1960.

3.15 Knauss, W.G.: Displacements in a Finite Hollow Cylinder Under Axial Acceleration. GALCIT SM 60-17, California Institute of Technology, September 1960 (rev. January 1961).

3.16 Lianis, G.: Stresses and Strains in Solid Propellants During Storage. American Rocket Society, Paper No. 1592-61, February 1961.

3.17 Goree, W.S.; Nash, W.A.: Elastic Stability of Circular Cylindrical Shells Stabilized by a Soft Elastic Core. Interim Technical Report No. 4, Dept. of Engineering Mechanics, University of Florida, May 1960.

3.18 Hilton, H.H.: Thermal Stresses in Bodies Exhibiting Temperature Dependent Elastic Properties. Journal of Applied Mechanics, Vol. 19, pp. 350-354, 1952.

3.19 Williams, M.L.: Some Thermal Stress Design Data for Rocket Grains. American Rocket Society Journal, April 1959.

3.20 Geckler, R.D.: Thermal Stresses in Solid Propellant Grains, Jet Propulsion, February 1956.

3.21 Zwick, S.A.: Thermal stresses in an Infinite, Hollow Case-Bonded Cylinder. Jet Propulsion, Vol. 27, no. 8, pp 872-876, August 1957.

3.22 Morland, L.W.; Lee, E.H.: Stress Analysis for Linear Viscoelastic Materials with Temperature Variation. Brown University, Division of Applied Mathematics, Technical Report No. 1, (NOrd 18594/1), Sept. 1959.

3.23 Hilton, H.H.; Hassan, H.A.; Russell, H.G.: Analytical Studies of Thermal Stresses in Media Possessing Temperature Dependent Viscoelastic Properties. WADC TR 53-322, September 1953.

3.24 Muki, R.; Sternberg, E.: On Transient Thermal Stresses in Viscoelastic Materials with Temperature-Dependent Properties. ASME Applied Mechanics Division. Paper No. 60-WA-124, December 1960.

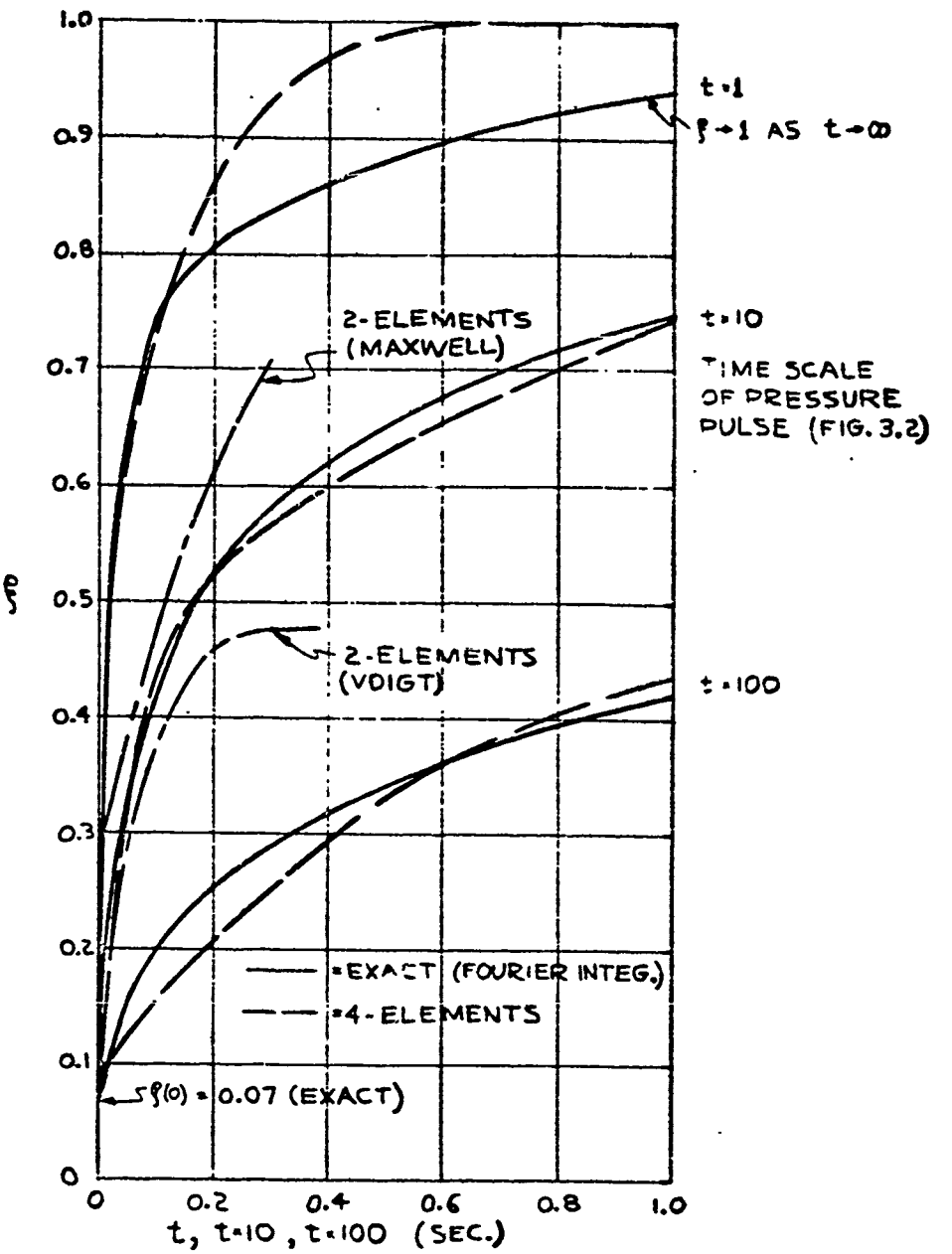

Fig. 3.1. Time Dependence of Normalized Strain Due to Unit Pressure Step Applied at t = 0 (For PIB at -35°F)

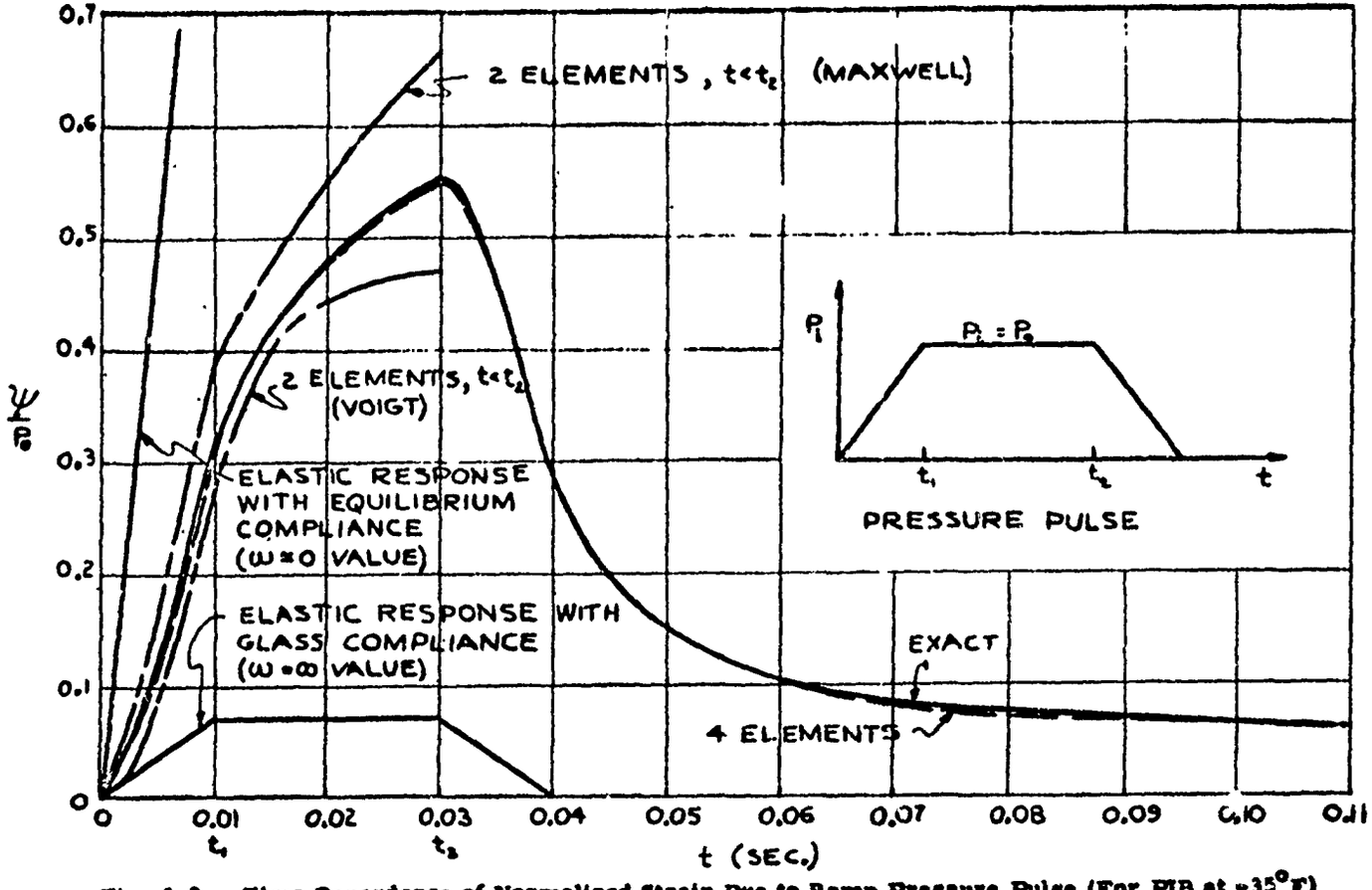

Fig. 3.2. Time Dependence of Normalised Strain Due to Ramp Pressure Pulse (For PIB at -35°F)

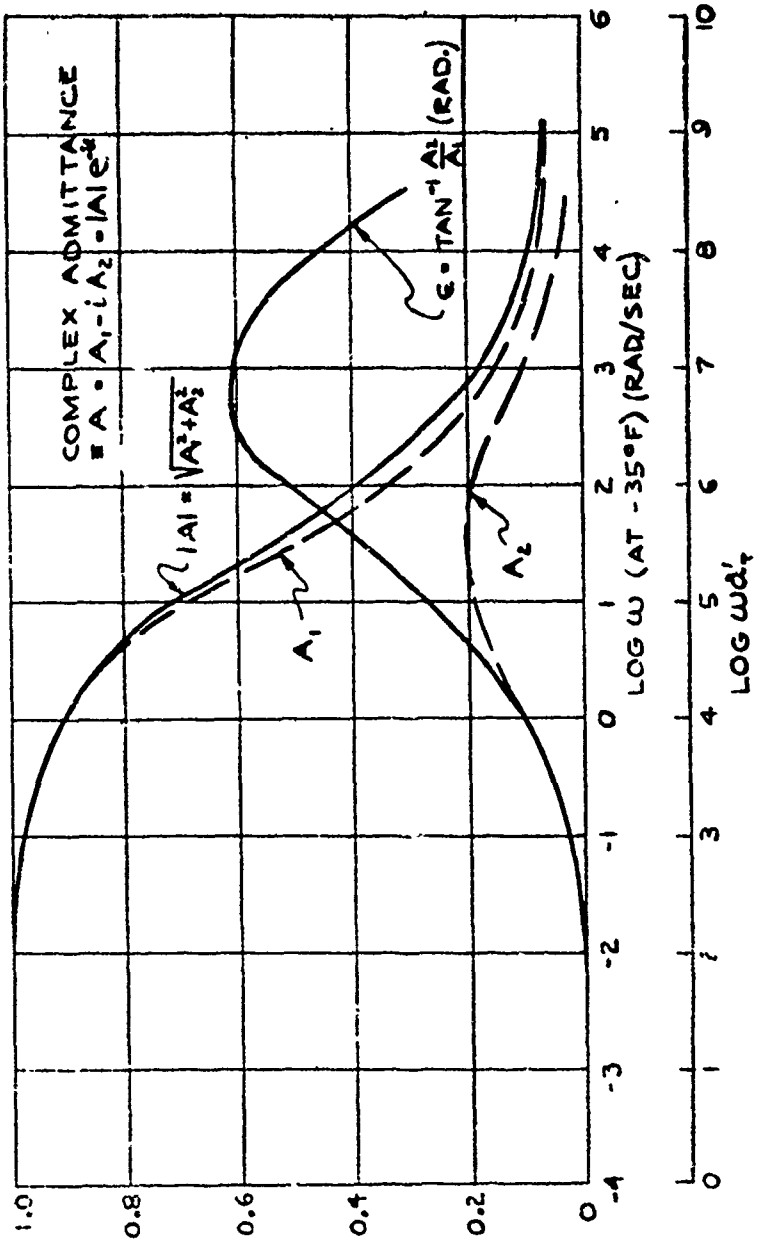

Fig. 3.3. Complex Admittance of Normalised Strain

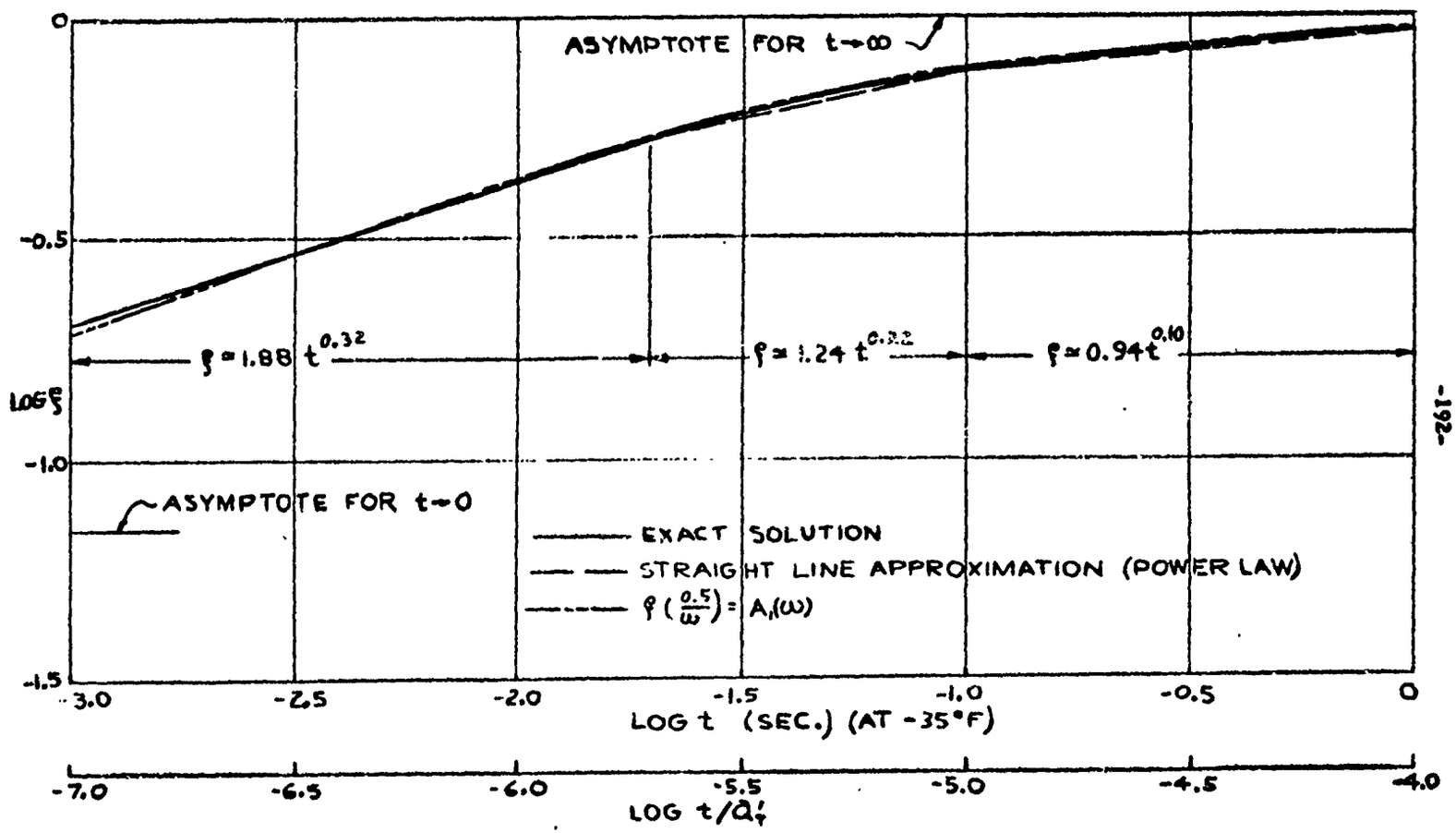

Fig. 3.4. Log-Log Plot of Normalized Strain Due to Unit Pressure Step Applied at t = 0.

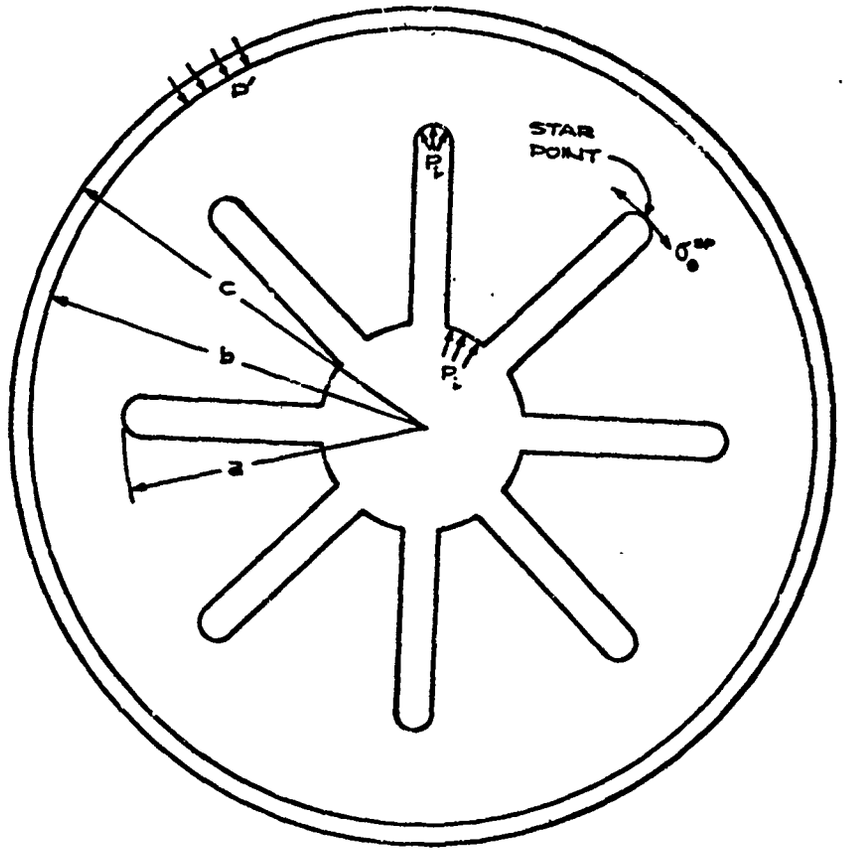

FIG. 3.5. CASE-BONDED GRAIN WITH INTERNAL STAR-SHAPED PERFORATIONS

4. FAILURE ANALYSIS

4.1 Common Types of Failure Criteria

It has been repeatedly emphasized in the previous sections that a complete analysis of the structural behavior of a solid propellant rocket motor includes not only a stress or strain analysis, but also a failure analysis. Whereas we have previously aimed primarily at investigating methods of estimating the stresses or strains in a viscoelastic propellant material due to prescribed applied loads, we now propose to treat the companion problem of predicting the maximum imposed loading at which either excessive deformation or fracture threshold is reached.

In facing this problem, there are several difficulties to be overcome, some of which are beyond present capabilities. Basically, most present failure data has been obtained using uniaxial specimens tested to failure at a constant strain rate. It remains to be seen whether such data may be used in situations where the strain varies signi cantly with time, as during firing of the rocket. Aside from the correlation of multiaxial and uniaxial stress fields, some sort of strain rate weighting factor will probably have to be incorporated in order to associate failure at an arbitrarily varying strain rate with that at constant strain rate. One such hypothesis will be proposed. Another important aspect, particularly as it pertains to fracture, is the implication of the analytical simplicity introduced by the infinitesimal deformation assumption. Most fracture analysis, even for rubbery viscoelastic media, is conducted neglecting squares of the strain compared to the strain itself. It is expected that significant trends will be revealed satisfactorily, but more sophisticated analysis will be required before a definite quantitative measure of this assumption can be obtained. Finally, it should be recognized that,practically speaking, rubbery materials are essentially elastic all the way to fracture, and hence an elastic or visco-elastic analysis, including large strain effects if necessary, is appropriate without having to consider plastic or visco-plastic effects.

4.1.1 Deformation criteria

Turning now to failure considerations, there are two basic structural engineering criteria, deformation and fracture. By the way of example in solid propellant applications, they are exemplified by slump and grain cracking, respectively. Generally, the first of these is tied in rather closely with ballistic perform-

ance and storage procedures, that is to say, a maximum permissible deformation without fracture is more or less arbitrarily prescribed. If this is the case, it becomes a simple matter to complete the analysis by finding the loading or time corresponding to that state when this deformation is reached by applying the viscoelastic analysis techniques previously developed.

One illustration is the situation wherein a second-stage rocket grain may be fired vertically and subjected to inertial loading for short periods, say, of the order of minutes. On the other hand, the grain, perhaps for logistic reasons, may be stored vertically for extended periods, and in this condition also subjected to vertical gravity forces but over a considerably longer time. Both of these situations require the prediction of time dependent deformations -- the first under $\underline{n}$ g gravity loading for short time, the second for one g loads over long time.

An elastic approximation for such a condition has been given by Knauss[4.1] wherein it is shown that the inward radial constriction of a thick-walled case-bonded cylindrical grain at the base depends upon the support conditions. If the base is completely unsupported, the throat area does not choke at all, but takes up the general deformation pattern shown in the sketch. On the other hand, if the base is rigidly supported, there will be a choking tendency as shown. Its magnitude, in the particular case where the web fraction was fifty percent, was found to

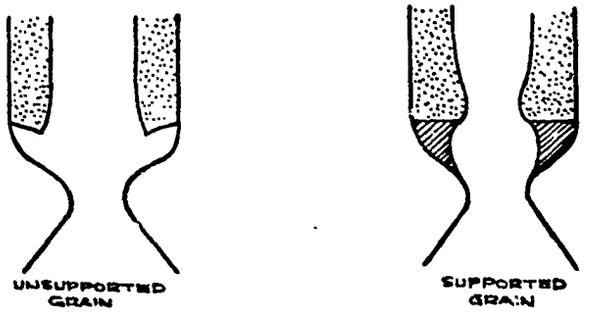

be of the order

$$\frac{\Delta a}{a} \approx 20 \frac{\rho b n}{E} \qquad (4.1.1)$$

where $\Delta a/a$ is the relative change in port radius, ρ the density (pci) of the propellant, and $\underline{n}$ the number of times gravity load. To examine the effect upon ballistic performance, one could compute the relative change in port area $\Delta Ap/Ap$

to be twice the above figure. The previous calculation is based upon an elastic analysis, when E is the elastic modulus. One approximation to the time dependent deformation for incompressible materials can be obtained[4.2] by replacing E by its viscoelastic equivalent, which for a three element model gives

$$\frac{\Delta A_p}{A_p} \approx \frac{40\,\rho b n}{E_e}\left[1-\left(1-\frac{E_e}{E_g}\right)e^{-\frac{E_g}{E_g}\frac{t}{\tau}}\right] \qquad (4.1.2)$$

where it may be easily checked that for long times $E \to E_e$, the rubbery modulus, and for short times $E \to E_g$, the glassy modulus. Alternately one may approximate the tensile creep compliance $D_{crp}(t) \approx \epsilon(t)/\sigma_o$, using a form similar to that derived for the relaxation modulus from a modified power law distribution function (2.4.85), which is

$$D_{crp}(t) = D_g + (D_e - D_g)\left[1+\frac{(D_e/D_g)^{\frac{1}{2n}}K(T)}{t}\right]^{-n} \qquad (4.1.3)$$

which for long and short times checks the elastic and glassy compliances D_e and D_g respectively, and in the transition region, $t \to K$, gives

$$D_{crp}(t) = D_g + (D_e - D_g)\left[1+\left(\frac{D_e}{D_g}\right)^{\frac{1}{2n}}\right]^{-n} \doteq \sqrt{D_e D_g} \qquad (4.1.4)$$

consistent with the relaxation modulus value (2.5.4). In this case, one may use (4.1.3) and write

$$\frac{\Delta A_p}{A_p} \approx 40\,\rho b n\, D_{crp}(t) \qquad (4.1.5)$$

From the experimental standpoint, it would also be approximately correct to use uniaxial tensile strain creep data at constant stress as $D_{crp}(t)$ in (4.1.5)

In any event, the relative amount of choking is seen to depend upon the mechanical properties, including the characteristic relaxation time. If therefore the maximum permissible blockage were specified as the design criterion, one could compute the time at which it would be exceeded for a given gravity load. A reasonably large grain, for example, might have an upper bound of approximately ten percent per g at room temperature.

Slump may also occur during environmental storage of a grain in the horizontal position. This situation has recently been considered by Lianis[4.3] and the results may be used in a similar fashion as those above to predict deformation configurations.

The analysis given is approximate, but is presented to make the point that if a deformation criterion is imposed, it is merely necessary to refine the appropriate deformation analysis to the accuracy desired for the prediction. As the procedure is straightforward, although not necessarily simple in a given problem because the strain analysis itself is complicated, no additional remarks upon the deformation criterion will be included at this time.

4.1.2 Fracture criteria

In contrast to deformation, the mechanics of fracture requires a fundamentally different type of investigation. Fracture first occurs on the microscopic scale where the medium, particularly for filled propellants, is non-continuous. Hence the analysis techniques, based as they are upon the assumption of a macroscopic continuum, are not valid at the point of fracture. For this reason the problem of fracture analysis is markedly more complicated inasmuch as it requires a knowledge of molecular behavior not smoothed out by the macroscopic averaging process. On the other hand, it has proved possible to determine certain extremely useful gross fracture characteristics, for example uniaxial tensile strength as a function of strain rate and temperature. From the engineering standpoint, it is desirable to extend, empirically if necessary, such limited information on special test samples to more complex geometries such as a star grain.

The general requirement for such a correlation is by no means new, although a precise statement for viscoelastic materials has not been particularly emphasized. Nadai[4.4] enumerates, for example, several different fracture criteria, primarily as used in the study of metals, and it is worth restating them here. Each criterion defines some particular functional of the stress field or strain field, the value of which is to be determined empirically, because molecular theories of strength are not advanced to the point of calculating such limits theoretically. When the appropriate functional is exceeded, the associated yield, rupture, or fracture takes place. Seven such criteria are listed below:

a) the maximum principal stress
b) the maximum principal strain
c) the maximum principal stress difference (or shear stress)
d) the maximum principal strain difference (or shear strain)
e) the maximum total strain energy
f) the maximum distortional strain energy
g) the maximum conserved distortional strain energy

Criteria (a) and (b) utilize the fact that the maximum stress (strain) at any point in the material is the largest of the three principal stresses (strains), σ_1, σ_2, σ_3 (e_1, e_2, e_3) at this point. In simple and biaxial tensile fields, these functionals are identical with the yield or ultimate stresses and strains for these fields respectively.

Criteria (c) and (d) stem from the observation that many materials, particularly those which evince ductile fracture (sometimes known as shear fracture) do so along a pair of planes or a cone lying in the direction of greatest shear. The maximum shear stress has the value $\frac{1}{2}(\sigma_1 - \sigma_3)$ and is obtained on a plane inclined 45° to the direction of the principal normal stresses. This criterion is not suitable for mathematical formulation since it is necessary to determine first the maximum or minimum stresses (or strains).

An alternate criterion based on a mean value of the principal stress differences was proposed by von Mises[4.5]. This takes the form

$$\sqrt{2}\,\sigma_0 = \sqrt{(\sigma_1-\sigma_2)^2+(\sigma_2-\sigma_3)^2+(\sigma_3-\sigma_1)^2} \qquad (4.1.6)$$

and σ_0 is termed the mean deviatoric stress. For both simple uniaxial tension and biaxial tension, σ_0 is identical with the yield or fracture stress. For pure shear on the other hand, the yield stress turns out to be $\sigma_0/\sqrt{3}$.

The mean deviatoric stress (or strain) has not been listed as a separate criterion proposed by Huber and Hencky[4.6]. They observe that

$$W_d = \frac{\sigma_0^2}{6\mu} = \frac{(\sigma_1-\sigma_2)^2+(\sigma_2-\sigma_3)^2+(\sigma_3-\sigma_1)^2}{12\mu} \qquad (4.1.7)$$

This mean deviatoric stress is also $3/\sqrt{2}$ times a quantity known as the octahedral shear stress. The total strain energy listed under (e) was proposed by Baltrami and Haigh[4.7]. It does not prove satisfactory since there is no correlation between behavior in pure shear and in pure hydrostatic compression. The conserved distortional strain energy refers to the energy stored in a viscoelastic or plastic material, i.e. over and above what has been dissipated. The theory of application of this criterion is still not in a satisfactory state.

The important point to note is that no universal fracture criterion has been established, and that the success of a given fracture hypothesis depends in large measure upon the material with which it is associated.

In the case of elastomers, in contrast to metals, it is necessary to extend

the usual concept of brittle and ductile failure. Ductile fracture in metals is characterized by irrecoverable distortion and permanent set, analogous to the behavior of an uncrosslinked polymer which also evinces unlimited, unrecoverable flow. On the other hand crosslinked polymers, the type ordinarily employed as propellant components, recover completely from straining almost all the way to fracture even though the strain at failure may reach several hundred percent compared to elastic brittle failure in metals of only a few percent. In the remainder of this section therefore, we shall restrict the discussion to crosslinked polymers, and shall use the term elastic fracture as the large strain analog of small strain fracture customarily referred to as brittle. In either case, however, the stress-strain relation is elastic, or potentially viscoelastic, with the distinguishing feature being the strain magnitude at failure. With this understanding therefore a propellant material might have a brittle fracture below the glass temperature but an elastic fracture above it. It still remains however to deduce which of the various criteria is appropriate for predicting the fracture. Inasmuch as no exhaustive investigation of fracture criteria for elastomers has been reported to the authors' knowledge, although Rivlin and Thomas [4.8] have proposed an important extension of the Griffith fracture criterion which will be discussed later, it would appear that the proper approach is to examine test data in conjunction with certain of the aforementioned criteria, and inquire if any of them give reasonable correlation.

The following paragraphs therefore will present a summary and discussion of some current and proposed tests and their correlation, after a restatement of some of the germane characteristics of elastomers. Before continuing, it is appropriate to define the terms elastomer and polymer as used in this text.

A polymer is a network of long molecular chains which may or may not be tied together chemically. An important characteristic of all long chain structures is the glass transition temperature T_g above which polymers behave rubberlike, and below which, glasslike. If the polymer chains are not tied together chemically, the structure is termed a plastic--a brittle plastic below T_g and a rubbery plastic above T_g. The extent of the elastic deformation evinced prior to flow to rupture in the rubbery plastic is markedly a function of interchain entanglement and therefore of chain stiffness or structure.

If on the other hand the polymer chains are tied together chemically, the structure is termed an elastomer or rubber--a brittle rubber below T_g and a rubbery rubber above T_g. The extent of the elastic deformation evinced prior

to rupture in a rubbery rubber is markedly a function of chain length between crosslinks, and is not markedly sensitive to chain structure.

Both rubbers and plastics become increasingly viscoelastic as the temperature is lowered. In general, rubbers have lower glass transition temperatures than plastics, and so become viscoelastic and then brittle in lower temperature ranges than plastics.

4.2 Material Characteristics of Amorphous Elastomers

A composite solid propellant is a highly filled rubber. Ballistic missile logistics demand that the filler be oxidatively energetic in order to deliver high specific impulse during the combustion processes. The current science of propellant chemistry has narrowed the inventory of such useful oxidizers to combinations of ammonium perchlorate and aluminum. In this combination, the aluminum serves to prevent over-oxidation of the rubber fuel and at the same time, by virtue of its high exothermic heat of combustion, overcomes the disadvantages imparted to the exhaust gas by its high molecular weight.

Rheological studies have shown that it is expedient to incorporate the filler as a trimodally distributed agglomerate of particles, ranging from one to 250 microns in diameter with the mean size occurring at about 30 microns. Single crystal studies have shown that the aluminum-rubber bond in tension is approximately 90 psi, and that of the oxidizer rubber about 30 psi. Since the tensile strength of a filled rubber lies in the range 20 to 200 psi at room temperature, it is seen that the filler-binder interaction contributes an important feature to the mechanical behavior of such composites. Because of its relatively high bulk and shear moduli, the filler may be assumed to be absolutely rigid.

The binder, according to current standards, is a synthetic rubber, negligibly crystalline, with a molecular weight between juncture points anywhere from 10 to 100,000. These juncture points may be branch-points at which a tri- or tetra-functional monomer has been incorporated into a condensation polymerization system; or they may be crosslinks effected, not by vulcanization, but by mixed condensation-addition polymerization. The mechanical properties of the binder, without its filler, are not the same as those of the pure rubber. The polymerization process is markedly affected by the presence of the filler.

Needless to say, the mechanical properties of such a composite are a quite complicated function of the properties of the binder, of the volume fraction, particle size distribution, and adhesion of the filler. In order to understand the

fracture mechanics of such a system, it is appropriate to study first the fracture mechanics of unfilled rubbers, and then study the modifications produced by various degrees of filler. In carrying out this comparison, it is extremely important to remember that the filler not only modifies the mechanical properties, but also the molecular structure of the binder, so that it is necessary to understand how the mechanical properties of a rubber depend upon molecular structure.

Finally, before proceeding with this study, it is appropriate to ask: what are the important modifications introduced by the filler? Experimental studies on propellants have shown three differences from unfilled rubbers. First, the tensile properties of filled rubbers are very different from their compression properties. Secondly, yield occurs in a series of steps; it may be necessary to distirguish among several types of yield. For example, it may be important, from the ballistic viewpoint, to define yield as the point at which the propellant has become porous enough, by virtue of mechanical strain, to increase its burning rate beyond a safe value. This critical porous strain may be less than the strain at which mechanical failure will occur. Thirdly, relaxation of stress progresses long after the rubber component has relaxed to its rubbery modulus; this indicates that a reshuffling of the adhesion bonds and positions of filler particles is a continuing process.

The next sections discuss the elastic fracture of rubbers and unfilled binders.

4.2.1 Unfilled non-viscous elastomers

As the title of this section indicates, the materials with which we are dealing store energy reversibly until fracture. This behavior is associated with very low or very high rate straining of elastomers. During fracture, energy is released which can, in principle, be accounted for by the kinetic energy and surface energy imparted to the new crack. The crack acts as a point of stress concentration but the local stress far away from the crack will remain below the yield stress of the material and thus continue to store energy elastically until the crack propagates through the material, at which time all the remaining strain energy will be converted into kinetic energy. Cracks per se will not be considered at this point but some insight into the failure of unfilled elastomers can be gained by considering the ultimate behavior of uniaxial tensile specimens.

Examples of unfilled elastomers are natural rubber, butyl rubber, styrene-butadiene rubber (SBR, formerly GRS), and polyurethane rubber. All such

rubbers evince large shear deformations prior to yield or cracking, and should therefore be characterized by a theory which allows for large deformations. The simplifications of small strain theory not withstanding, some progress assuming large strains is possible for the usual uniaxial tensile specimen failures. Rivlin [4.9] has shown that the strain energy of a unit volume of undeformed rubber may be appropriately expressed as a function of three strain invariants, which, for an incompressible material, assume the form:

$$I_1 = \lambda_1^2 + \lambda_2^2 + \lambda_3^2 \qquad (4.2.1a)$$

$$I_2 = \frac{1}{\lambda_1^2} + \frac{1}{\lambda_2^2} + \frac{1}{\lambda_3^2} \qquad (4.2.1b)$$

$$I_3 = \lambda_1^2 \lambda_2^2 \lambda_3^2 \qquad (4.2.1c)$$

where λ_i is the extension ratio of the coordinate acted on by the normal stress σ_i. Application of the principle of virtual work leads to the stress-strain relation* in terms of the true stress $\bar{\sigma}_i$:

$$\bar{\sigma}_i = \sigma_i \lambda_i = 2\left[\lambda_i^2 \frac{\partial W}{\partial I_1} - \frac{1}{\lambda_i^2}\frac{\partial W}{\partial I_2}\right] + \bar{K} \qquad (4.2.2)$$

where $\bar{K}$ is, in general, a function of the coordinates, but not of the strain invariants.

In order to use (4.2.2), it is necessary to understand the nature of the strain energy density function W, and in particular, to procure an analytical representation which holds as close to rupture as possible. We shall take as our type material, for this study, unfilled natural gum rubber vulcanizate, the simple stress-strain curve for which is reproduced [4.10] in Figure 4.1. It is characteristic of natural rubbers that they possess a sharp increase in stress beyond 500% elongation. Most synthetic rubbers break near this elongation.

An empirical method for rectifying simple tensile data [4.11] obtained on incompressible elastomers is based on the following observations. The initial portion of the stress-strain curve is fairly well represented by

$$\sigma = E\left(1 - \frac{1}{\lambda}\right) = E\,\frac{\lambda - 1}{\lambda} \qquad (4.2.3)$$

*When shear forces as well as normal forces are acting, the λ_i's are replaced by a set of appropriate strain tensors. In what follows, (4.2.2) will suffice.

which is equivalent to plotting the data versus the true stress $\bar{\sigma}$, i.e.

$$\bar{\sigma} = E(\lambda - 1) \tag{4.2.4}$$

Note that for large extension ratios (4.2.3) approaches the limiting value $\sigma = E$. In order to provide for the rapid increase in stress with later portions of the curve at large strain, (4.2.3) may be modified more or less arbitrarily to

$$\sigma = E\frac{\lambda - 1}{\lambda^2}\lambda \rightarrow \frac{E(\lambda-1)}{\lambda^2} e^{\beta(\lambda - \frac{1}{\lambda})} \tag{4.2.5}$$

which reduces to (4.2.4) for $\beta = \frac{1}{2}$ at small strains,

$$e^{\frac{1}{2}(\lambda - \frac{1}{\lambda})} \rightarrow \lambda \tag{4.2.6}$$

One can use (4.2.5) in plotting the data (Figure 4.2) as

$$\ln \frac{\sigma\lambda^2}{\lambda - 1} = \ln E + \beta\left(\lambda - \frac{1}{\lambda}\right) \tag{4.2.7}$$

where it is observed that the stress in kg/cm^2 is given by

$$\sigma = 7.39 \frac{\lambda - 1}{\lambda^2} e^{0.416(\lambda - \frac{1}{\lambda})} \quad ; \quad 1 < \lambda < 6 \tag{4.2.8a}$$

$$\sigma = 0.705 \frac{\lambda - 1}{\lambda^2} e^{0.80(\lambda - \frac{1}{\lambda})} \quad ; \quad \lambda > 6 \tag{4.2.8b}$$

We proceed to define $\lambda = 6$ as a yield point and observe that the modulus after yield is reduced by slightly more than a factor of 10, indicating that the network resistance has been drastically lowered. Since modulus is proportional to cross links per unit volume, we infer that the loss in cross-link concentration arises from the slippage or tearing of entanglements, and that only the true chemical crosslinks remain to offer resistance. Support for this inference is deduced from the observation that the exponential factor now behaves more like λ^2 than λ, since β has doubled. This means that the load rather than the true stress is proportional to strain, the proportionality constant now behaving like a spring constant; lateral effects have suddenly become unimportant; the network loops now offer little or no resistance.

The exponential factor $\exp \beta(\lambda - \lambda^{-1})$ is not amenable to quadrature and so the area under the curve in Figure 4.1 was evaluated stepwise by Simpson's Rule and the resulting strain energy plotted in Figure 4.3. This smooth monotonically increasing function of λ is nicely rectified by plotting W vs $(I_1 - 3)$ as network

theory [4.12] demands, (Figure 4.4). Again note the yield at $\lambda = 6$. Below yield, the strain energy function is closely approximated by

$$W = \frac{\mu}{2}(I_1 - 3) \doteq 0.883(I_1 - 3) \qquad (4.2.9)$$

so that the shear and Young's moduli are approximately 1.76 kg/cm^2 and 5.28 kg/cm^2, respectively; this is a somewhat lower value than that obtained from Figure 4.2, but this is so because in (4.2.8) a higher value of E is needed to compensate for $\beta = \frac{1}{2}$; in other words, only the initial portion of the tensile curve can be represented in the form (4.2.8) with $\beta = \frac{1}{2}$ and $E = 5.28$.

4.2.2 Filled non-viscous elastomers

The most striking difference between filled and unfilled elastomers is the so-called blanching phenomenon or pullaway of the binder from the filler. As indicated in the introduction, this makes for three observations. First, the pullaway occurs in steps, undoubtedly depending upon the distribution of adhesion bond strengths between oxidizer and binder. Second, it does not occur in compression. Third, after pullaway, relaxation not of the network, but of the strain energy located at the surface of the void spaces, occurs. This is demonstrated by the fact that a typical filled rubber, after three months at constant strain (30%), might relax its modulus from 500 psi to 5 psi. And then, upon complete recovery of the applied strain at the end of a second three months, will resume its initial modulus minus the contribution that arose from the adhesion to the filler. If this cycle is repeated a second time, the modulus will relax and return to nearly the same value.

Because of this reversible shuffling back and forth of the filler particles, it follows that the time rate of change of the local stress distribution in a filled rubber must be quite complicated and that the rupture criterion may be significantly more complex than that which is proposed above for an unfilled rubber. One can start by neglecting relaxation, i.e., working with short time data. On this basis then, the curvature of a tensile stress curve is to be ascribed entirely to pullaway effects without reshuffling. The modulus decreases because adhesion bonds are broken and because the propellant dilates. This dilation effect is shown in Figure 4.5 where Poisson's ratio is plotted versus axial strain, the local strains having been carefully measured photographically. Figure 4.6 shows how the modulus is increased in the region of negative strain or compression. The

question arises: what sort of elastic behavior is evinced by such a material when it is subjected to combined tension and compression?

Effect of orthotropic moduli. A relatively simple case arises in the pressurization of an infinitely long hollow unbonded tube of propellant, internally pressurized, the analysis of which will be pursued here. Since the algebra is quite involved, only the essential features will be sketched. It is thought that this type of analysis will become increasingly important as the nature of the pull-away effect becomes more completely understood.

As a result of internal pressurization, all radial and axial elements of the propellant tube are in compression. The hoop elements, however, are in tension so that an orthotropic response may occur. Jaeger [4.13] shows that for such a case, where the orthotropic material properties are with respectto cylindrical coordinates, the stress-strain relations are

$$\sigma_\theta = C_{33}\epsilon_\theta + C_{13}\epsilon_r + C_{13}\epsilon_z \quad , \quad \tau_{r\theta} = C_{44}\gamma_{r\theta} \qquad (4.2.10)$$

$$\sigma_r = C_{13}\epsilon_\theta + C_{11}\epsilon_r + (C_{11}-2C_{66})\epsilon_z \quad , \quad \tau_{\theta z} = C_{44}\gamma_{\theta z}$$

$$\sigma_z = C_{13}\epsilon_\theta + (C_{11}-2C_{66})\epsilon_r + C_{11}\epsilon_z \quad , \quad \tau_{rz} = C_{66}\gamma_{rz}$$

By analogy with isotropic theory, we have

$$C_{66} = \mu \qquad (4.2.11)$$

$$C_{33} = \lambda_{TT} + 2\mu$$

$$C_{13} = \lambda_{TC}$$

$$C_{11} = \lambda_{CC} + 2\mu$$

Since the hoop direction is the only one in tension, C_{33} is the coefficient that one would measure in triaxial tension so that $(C_{33}-2\mu)$ is indicated by the Lame constant with a double subscript T. Likewise, $(C_{11}-2\mu)$ is the Lame constant one gets from triaxial compression, and is designated by the double subscript C. The coefficient C_{13} is an interaction coefficient which could be measured in mixed triaxial compression tension. i.e., pulling in one direction and squeezing on the two sides. In the isotropic case, the constants reduce to

$$C_{33}-2\mu = C_{13} = C_{11}-2\mu = \lambda = K - \frac{2}{3}\mu \qquad (4.2.12)$$

where K is now the hydrostatic bulk modulus in compression. In the problem at hand, we have

$$\sigma_\theta = C_{13}\frac{u}{r} + C_{12}\frac{du}{dr} \tag{4.2.13}$$

$$\sigma_r = C_{13}\frac{u}{r} + C_{11}\frac{du}{dr} \tag{4.2.14}$$

$$\sigma_z = C_{13}\frac{u}{r} + (C_{11}-2\mu)\frac{du}{dr} \tag{4.2.15}$$

where u is the radial displacement. Substitution of the above relations into the equation of stress equilibrium

$$\frac{d\sigma_r}{dr} + \frac{\sigma_r-\sigma_\theta}{r} = 0 \tag{4.2.16}$$

yields

$$\frac{d^2u}{dr^2} + \frac{1}{r}\frac{du}{dr} - \frac{C_{33}}{C_{11}}\frac{u}{r^2} = 0 \tag{4.2.17}$$

Note that, by direct observation, $\lambda_{rr} \ll \lambda_{cc}$ (because of the pullaway effect) and therefore $C_{33}/C_{11} < 1$. The solution of (4.2.17) is given by

$$u = Ar^k + Br^{-k} \tag{4.2.18}$$

$$\sigma_r = \frac{A}{r^{1-k}}\left(C_{12}+\sqrt{C_{11}C_{33}}\right) + \frac{B}{r^{1+k}}\left(C_{12}-\sqrt{C_{11}C_{33}}\right) \tag{4.2.19}$$

where $k = (C_{33}/C_{11})^{\frac{1}{2}}$. The constants A and B can now be evaluated at $r = a$, and $r = b$, where $\sigma_r = -P$ and 0 respectively. The result is

$$\frac{\sigma_r}{p} = -\frac{a^{1+k}\left(b^{2k}-r^{2k}\right)}{r^{1+k}\left(b^{2k}-a^{2k}\right)} \tag{4.2.20}$$

$$\frac{\sigma_\theta}{p} = \frac{\beta\, a^{1+k}\left(b^{2k}+r^{2k}\right)}{r^{1+k}\left(b^{2k}-a^{2k}\right)} \tag{4.2.21}$$

$$\frac{C_{11}u}{pr} = \frac{k\left[\left(\frac{b}{r}\right)^{1+k}+\left(\frac{b}{r}\right)^{1-k}\right] + \frac{C_{12}}{C_{11}}\left[\left(\frac{b}{r}\right)^{1+k}-\left(\frac{b}{r}\right)^{1-k}\right]}{\left[k^2-\left(\frac{C_{12}}{C_{11}}\right)^2\right]\left[\left(\frac{b}{a}\right)^{1+k}-\left(\frac{b}{a}\right)^{1-k}\right]} \tag{4.2.22}$$

$$= \frac{a^{1+k}\left[\left(k-\frac{C_{12}}{C_{11}}\right)r^{2k}+\left(k+\frac{C_{12}}{C_{11}}\right)b^{2k}\right]}{r^{1+k}\left(k^2-\frac{C_{12}^2}{C_{11}^2}\right)\left(b^{2k}-a^{2k}\right)}$$

Note that if $C_{13}/C_{11} > k$, the radial displacement is negative. However this is not physically possible since the work done by the internal pressure must always be positive; hence one should find experimentally that $C_{13}/C_{11} < k$. The most significant difference from the isotropic case arises in the occurrence of fractional rather than integral exponent powers of the radial coordinate. The

strain concentration factor is defined by the ratio of $\frac{u}{r}\Big|_a$ to $\frac{u}{r}\Big|_b$, which leads to

$$K_\epsilon = \frac{\left(k - \frac{C_{12}}{C_{11}}\right)\left(\frac{a}{b}\right)^{2k} + \left(k + \frac{C_{12}}{C_{11}}\right)}{2k\left(\frac{a}{b}\right)^{1+k}} \simeq \left[\frac{k + \frac{C_{12}}{C_{11}}}{2k}\right]\left(\frac{b}{a}\right)^{1+k} \qquad (4.2.23)$$

for a thick-webbed shell. In the isotropic case, where k = 1, (4.2.23) reduces to the correct expression $\sim\left(\frac{b}{a}\right)^2$.

The same treatment can be applied to the case-bonded propellant. It will be necessary in this and many other situations to solve for the point at which the hoop stress changes sign. By following this procedure, one can avoid trial and error techniques. In general, problems of this nature will best be solved with the aid of digital computational aids. Before programming, however, it will be necessary to determine the strain energy function for the propellant in both compression and tension. The theory of finite elastic deformation of anisotropic materials has been presented by Green and Zerna[4.14] so that, in principle, the pullaway effect can be handled all the way to rupture if the strain energy density function is known.

4.3 Uniaxial Test Data

Considering the implied necessity for obtaining material property data for fracture investigations, such as the strain energy density function just mentioned, it is appropriate to review some of the current tests commonly being conducted, and their applicability to the problem at hand.

4.3.1 Standard variable-strain rate testing

By far the largest accumulation of data relates to fracture under simple uniaxial tension. For solid propellant materials these tests have normally been conducted on standard JANAF specimens (Figure 2.29)at variable strain rates and temperatures. One common testing machine is the Instron tester which will impose constant crosshead motion through a range of speeds from 0.02 to 20 inches per minute, over a temperature range between-100°F and 160°F. The output of the machine is an automatically recorded force-time trace to fracture (Figure 4.7) which provides the basic experimental information. Depending upon the magnitude of strain to fracture, the data is converted into plots of nominal or true stress, i.e. force divided by original or actual cross sectional area, versus strain. The accuracy of the latter quantity is frequently open to question

because the elongation, or crossbead separation, is not distributed evenly over the specimen length and some "effective length" must be selected. It is common practice to use an effective length of 2.7 inches for the JANAF specimen. It has been noted in an earlier section however that Baldwin[2.17] has had some success in using a square flat end, bonded specimen which reduces the amount of flow near the grips and hence removes part of the gage length indeterminacy.

The uncertainty in the basic data emphasizes the desirability, and near necessity, of developing local strain indicating devices for low modulus materials. Several improvements along these lines have been attempted, such as using gage marks near the center of longer specimens, or circle patterns distributed over the length. While some increase in accuracy has been reported, the data serve also to indicate in many cases a basic nonhomogeneity in strain distribution due to the filler particles in the propellant.

Neglecting nevertheless these important experimental refinements and working only with the reduced experimental stress-strain data, one turns next to the problem of organizing the extensive test information for many temperatures and strain rates in useful form. Presuming for the most part that maximum stress, σ_m, and strain at maximum stress, ε_m, are the more significant quantities Smith has shown for a wide variety of polymers that a very reasonable correlation of ultimate tensile properties can be obtained if the data are plotted against the logarithm of a reduced time parameter (see Section 2.5) $a_T R$, where R is the constant strain rate at which the test was conducted and a_T is the Williams, Landel, Ferry (WLF)[4.15] temperature shift factor, (2.5.6)

$$\text{Log } a_T = \text{Log } \frac{t}{t_u} = \frac{C_1 (T - T_s)}{C_2 + T - T_s} \qquad (4.3.1)$$

a_T can also be interpreted as the ratio of the time to measure some phenomena at temperature T to the time to measure the same phenomena at the reference temperature T_s. This relation can also be cast in the Tobolsky form (2.5.5).

A set of his typical strain data is shown in Figure 4.8, and similar stress data in Figure 4.9. Note in the latter case the stress has been normalized by a temperature ratio because polymer theory predicts a linear increase of retractive forces with absolute temperature. Both sets of data were normalized as described in section 2.5 by using the temperature shift factor, experimentally deduced from separately shifting (i) strain at ultimate stress data, (ii) maximum stress data, and (iii) modulus data, and finding all three agreed if $C_1 = -8.86$, $C_2 = 101.6$

and $T_s = 269^{\circ}K$ (2.5.6). That such a convenient and near universal correlation exists for ultimate properties is extremely useful, and among other things, permits one to predict with fair precision the uniaxial tensile fracture behavior over wide ranges of strain rate and temperature from a limited set of test data.

Figures 2.25-2.27 show some typical data for the tensile modulus, ultimate stress, and ultimate strain of various propellant compositions in order to indicate the range of properties to be anticipated at different strain rates and temperatures. It should be emphasized however that marked deviations from these data may be expected for particular compositions of ingredients within the class prescribed.

Before passing on to a consideration of fracture under multi-axial load conditions, it should be observed that the temperature shift correlation is reasonably well founded experimentally but that the limited strain rate capability of the Instron tester is not particularly well suited for verifying the correlation over wide extremes. This may be noted in Figure 4.8 where the test data at various temperatures barely overlap. One would feel much more confident if, for example, the open circle ($160^{\circ}F$) data obtained over the $1/Ra_T$ range 5 to 8 could be extended to lower values by increasing the strain rate, hence lower $1/Ra_T$, at the same $160^{\circ}F$ temperature. Bearing in mind however the limitation of the tester, approximately 20 inches per minute cross head motion maximum, it is impossible to fulfill this desire without changing the specimen, which would not be particularly acceptable.

4.3.2 High strain rate testing

The obvious answer is to inquire if higher rate testers would be available. Several have been developed. One of these is the Allegheny Instrument Company device[4.17] which is generally well known. Another is one developed by E. I. Du Pont de Nemours and described in a recent paper by Jones [4.18]. Basically this latter machine, which achieves high loading rates by means of a controlled explosion of smokeless powder in the head, can strain JANAF specimens up to approximately 200,000 inches per minute. While it is premature to generalize, indications from this and other high speed tester work are that the theoretical WLF shift factor for ultimate fracture of tensile JANAF specimens is sufficiently valid for engineering purposes.

4.4 Multiaxial Testing

Inasmuch as the uniaxial testing procedures for simple JANAF tension specimens are well known and data reduction techniques widely disseminated, the subject has been rather shortly dismissed. On the other hand, from a structural standpoint as distinguished from the quality control objective, the important subject of the fracture behavior of viscoelastic materials subjected to biaxial and triaxial loadings needs considerable amplification, but suffers from lack of experimental data. At the present time, it is proposed to discuss some possible experiments in this area with particular emphasis upon their suitability for solid propellant materials and due regard for testing equipment convenience.

4.4.1 Pressurized tensile tests

Perhaps one of the simplest extensions of the present uniaxial tensile test using the Instron tester is to enclose the specimen in a leak proof container filled with air or liquid maintained at an arbitrary compressive pressure. Within the same criticisms of the basic test with no external pressure, a triaxial tension-compression stress field can be imposed. Suppose that the geometry is as shown on the sketch. Then the stress and strain analysis for the central portion of the specimen subjected to the uniaxial tensile stress gives

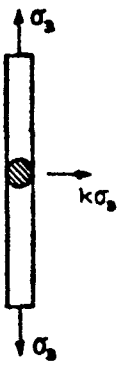

$$\sigma_3 = \sigma \quad ; \quad \varepsilon_3 = \frac{\sigma_3}{E}\left[1 - 2\nu k\right] \tag{4.4.1}$$

$$\sigma_1 = \sigma_2 = k\sigma \; ; \quad \varepsilon_1 = \varepsilon_2 = \frac{\sigma_3}{E}\left[-\nu + (1-\nu)k\right] \tag{4.4.2}$$

One would expect therefore an apparent uniaxial modulus for this triaxial field of

$$E_a = \frac{E}{1 - 2\nu k} \tag{4.4.3}$$

where, because in the tests as described k is negative corresponding to a compressive stress, the apparent modulus would be smaller than the uniaxial modulus.

For small strains it would in principle be possible to deduce the (elastic) value of Poisson's ratio.

As in the former case, these tests could be conducted at various strain rates and temperatures.

4.4.2 Poker chip tests

Another test that may be conducted with relative ease consists of cementing a thin circular disk of propellant between two parallel end faces of two circular steel plates being subjected to tension. The softer disk sandwiched between the harder bars will be restrained, because of its thinness, from its usual contraction perpendicular to the load and hence generate a triaxial tension stress field.

The elementary analysis for this case may be made by assuming the disk infinitely thin such that the external radius is sufficiently far from the center to assume the only non-zero displacement, w, is in the axial direction. Under these conditions, one is led to deduce for small deformations

$$\sigma_3 = \sigma \quad ; \quad \varepsilon_3 = \frac{\sigma(1-2\nu)(1+\nu)}{E(1-\nu)} \qquad (4.4.4a)$$

$$\sigma_1 = \sigma_2 = \frac{\nu}{1-\nu}\sigma \quad ; \quad \varepsilon_1 = \varepsilon_2 = 0 \qquad (4.4.4b)$$

so that the apparent axial modulus becomes

$$E_a = E\left[\frac{1-\nu}{(1-2\nu)(1+\nu)}\right] \qquad (4.4.4c)$$

where it may be noted that for propellants, which are characteristically nearly incompressible, i.e., $\nu = \frac{1}{2}$, the triaxial tension approaches hydrostatic with a consequent infinite apparent axial stiffness.

A fairly extensive and revealing investigation into the use of this test for an incompressible rubber has been reported in two papers by Gent and Lindley[4.19-4.20]. When one attempts to improve the analysis outlined above, the major difficulty arises in determining the stresses and strains throughout the disk. Whereas the previous analysis assumes the edges are infinitely far from the center, in the actual test piece there will be a local necking of the propellant, however slight, as the assembly is subjected to tension. When this effect is accounted for the analysis becomes considerably more complicated. For an incompressible material, Gent and Lindley have given an approximation to the apparent axial modulus which depends on the thickness, h, of the disk or radius a,

$$E_a = E\left[1+\frac{1}{2}\left(\frac{a}{h}\right)^2\right] \qquad (4.4.5)$$

where it may be observed that the apparent modulus, as before, becomes infinite as the thickness approaches zero.

Furthermore their fracture data, reproduced in Figure 4.10, shows for the various compositions indicated by the different curves that the axial stress to cause fracture increases as the disk thickness decreases. They have suggested that the limit for zero thickness is twice the value for large thickness. While it is tempting to thus extrapolate the data, it is not unreasonable to expect the curve near zero h/a to change slope. Realizing that the breaking stress used by Gent and Lindley is in reality an averaged stress over the face of disk, it would be appropriate to obtain an improved approximation. This can actually be obtained using the principle of minimum complementary energy. The outline of such a solution, given in Appendix I and not restricted to incompressible materials, predicts a stress distribution that is a power law in the radius and hyperbolic in the thickness, and for the limiting situation of zero thickness (infinite radius) gives the proper limiting value $\sigma_r/\sigma_z = \nu'/(1-\nu)$. Further calculations to investigate the utility of this solution in interpreting the experimental failure data would be desirable.

By conducting such tests as reported above, using an Instron tester, the usual ranges of interest in strain rate and temperature can be covered and the possibility of strain rate-temperature shift further explored.

4.4.3 Diametral compression of a disk

Fitzgerald[4.21] has suggested that the disk type specimen may also be used in an alternate manner to examine a mixed tension-compression biaxial stress field. If a circular disk of uniform thickness, h, is loaded in diametral compression by a load, P, the stresses at the center are of opposite sign and equal to[4.22]

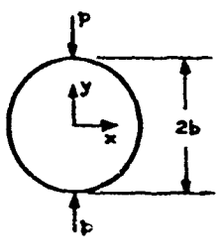

$$\sigma_x(0,0) = \frac{P}{\pi b h} \qquad (4.4.6)$$

$$\sigma_y(0,0) = -\frac{3P}{\pi b h} \qquad (4.4.7)$$

Furthermore the diametral extension, $2u(b,0)$ along the horizontal ($y = 0$) plane is

$$2u(b,0) = \frac{P}{Eh}\left[\frac{4}{\pi} - 1 + \nu\right] \qquad (4.4.8)$$

Providing there is not local failure at the point of load application, this specimen has the advantage that the critical stresses occur at the center and may be easily observed. Furthermore, measurements of the horizontal extension permit an indirect check on the accuracy of the foregoing formulas. Presumably as long as the extension stays linear with the applied load, even though the deformations near the point of application may be large, one would feel justified in using these stress formulas based upon infinitesimal deformation theory. From the standpoint of fracture, Fitzgerald has found[4.21] that the character of failure at the center changes from tensile to shear depending upon the temperature of the test. This latter point, of course, emphasizes its potential significance as a sensitive test for determining a fracture criteria.

Incidentally, it may be observed in passing that the range of central stresses which can be imposed, i.e. $\sigma_y/\sigma_x = -3$ from (4.4.6) and (4.4.7) above, could be extended by the use of elliptical instead of circular specimens, although at some expense in experimental simplicity.

4.4.4 Torsion of rod specimens

Among the various types of mechanical testing, torsion stands as particularly important. There are several reasons for this. First of all, a cylindrical specimen subjected to a small angle of twist undergoes pure shear; the applied torque is directly proportional to the measured twist angle per unit length, the proportionality constant being the shear modulus. Thus the torsion properties for small strain should be independent of Poisson's ratio.

As the shear strain is increased, however, new effects enter the picture. Finite elastic theory predicts a lengthening of the specimen known as the Poynting effect.

It may be deduced that

$$\lambda^3 = 1 + \frac{k^2}{4}(b^2 - a^2) \qquad (4.4.9)$$

where $\lambda = \frac{l}{l_0}$ is the axial extension ratio

a, b are the inner, outer radius of the cylinder respectively

k is the angle of twist per unit length

One obtains the preceding relation by application of finite elastic theory to the strain transformation defined by

$$\bar{r} = \frac{r}{\sqrt{\lambda}}$$

$$\bar{\theta} = \theta + kz$$

$$\bar{z} = \lambda z$$

where the bars refer to the deformed coordinates of material points. The undetermined constant which enters into the theory because of the incompressibility condition is determined by setting the integral of the axial stress over the end face equal to zero. Figure 4.11 shows a plot of λ^3-1 vs k^2, taken from recent data[4.23] on polyurethane propellant. Note the excellent straight line correlation in agreement with theory. The theoretical value of the slope is 1/8 in^2/rad^2, whereas the measured value turns out to be 1/7 in^2/rad^2. Considering the assumptions made in deriving (4.4.9) the agreement is excellent. The most important observation that can be deduced from this is that the elastic properties of the binder predominate at least up to three percent shear strain. A similar type of verification is provided by the recent data of Bergen, Messersmith and Rivlin on filled rubbers[4.24].

On the other hand, indications are the elongation will decrease as the twist is increased further. This is to be expected since the pullaway of the binder from the filler will tend to convert the local shear into local simple tension around the filler particles. What effect this will have upon fracture in torsion is not known. It is suspected that the fracture criterion will not be as simple for a filled elastomer as an unfilled one, therefore torsion should provide an excellent way to check out the applicability of the distortion strain energy criterion. Furthermore, torsion under superimposed hydrostatic pressure can then be used to check out the importance of anisotropy.

4.4.5 Hollow tube tests

Providing a satisfactory strain measurement is available, the behavior of an internally pressurized thin or thick walled cylinder up to and including burst would yield fracture information under biaxial tension, for zero axial stress, or with the added triaxiality depending upon the nature of a finite longitudinal stress. This type of specimen has been used with mixed success at the U. S. Naval Ordnance Test Station[4.25] employing an oil for the pressurization. The major

difficulties aside from such obvious ones as preventing leakage, are to obtain an accurate strain history and to measure the applied time varying pressure. These tests can be used upon either thin or thick walled cylinders, and with or without being enclosed in a case. In some cases it will be more convenient to check out a thin case-bonded design using externally mounted wire strain gages and inferring the tube, or even star point, strains by working backward using the theoretical solution. For most purposes however, the resultant case to grain stiffness is so high that accuracy is poor.

The main advantage of such a test is its reasonably close similarity to an actual operational configuration. If the pressure-time rise is appropriately regulated, the test could be useful in predicting fracture under a varying and typical strain rate history.

It should also be mentioned that it is possible to extend the rod torsion tests mentioned in the preceding section to hollow cylinders, preferably thin walled because of the relative accuracy with which the theoretical solution is known. Another test variation using the hollow tube is the possibility of using this geometry to examine the effect of orthotropy of multi-layered cylinders. Some preliminary analysis along these lines was presented by Pister in Section 3.3.3. The results of his continuing program, including some planned experiments, should furnish evidence for or against the desirability of this test geometry for orthotropic propellant media studies.

4.4.6 Specimens with initial cracks

Multiaxial testing can also be extended to include the biaxial stress field which exists near the point of a crack in a medium which has already begun to fracture. We shall consider the state of stress in several initially cracked configurations and their associated stress fields, and criteria for crack propagation.

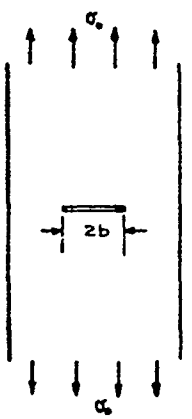

Thin sheets subjected to stretching: A common configuration for metal sheet specimens not used

extensively for propellants is the tensile strip containing a crack perpendicular to the load. This test in conjunction with Griffith fracture theory[4.26] is used to determine critical crack length, i.e., to find what size crack or flaw a given material of specified thickness will sustain under a specified external stress before it becomes unstable and propagates catastrophically. For catastrophic propagation of a brittle fracture Griffith deduced that, for a crack of length 2b, the applied stress σ_0 must exceed

$$\sigma_{cr.} = \sqrt{\frac{4ET}{\pi(2b)}} \qquad (4.4.10)$$

where T is the characteristic surface tension of the material, pounds per inch. For glass $T \sim 10^{-3}$ pounds per inch.

Propellant materials are however not usually thought of as brittle materials except in the glassy regions where (4.4.10) might of course be expected to apply. In 1953, Rivlin and Thomas[4.8] proposed an extension of the Griffith hypothesis for the rupture of rubber and found it was possible to correlate the tearing, providing T was interpreted merely as a "characteristic energy" and not necessarily the surface tension. For the gum rubbers examined $T \sim 100$ inch pounds per square inch. In the process of establishing this correlation, Rivlin and Thomas, and their subsequent collaborators, were able to get by with rather gross approximations of the stress fields. It is appropriate at this point, particularly as fracture criteria will be discussed in a later section, to state some of the characteristic features of the biaxial stress state near the point of a crack.

The classic problem in this field was solved in 1913 by Inglis[4.27] who calculated the stresses in the vicinity of an elliptical hole in an infinite sheet. Since then many investigators have worked upon related problems. Rather recently a somewhat general analysis for the geometry shown in the preceding figure has been given by Ang and Williams[4.28] for an orthotropic sheet subjected to combined stretching and bending, wherein the sheet is assumed infinitely wide with respect to the initial crack length 2b. These results show that the elastic stress distribution along the line of crack prolongation and assuming small deformations is

$$\sigma_x(x,0) = \sigma_y(x,0) - \sigma = \frac{\sigma_0 b^2}{\sqrt{x^2-b^2}\,[x+\sqrt{x^2-b^2}]} \qquad (4.4.11)$$

and near the crack point, $x = b + \epsilon$,

$$\sigma_x(\epsilon,0) = \sigma_y(\epsilon,0) = \frac{\sigma_\infty}{\sqrt{2\epsilon/b}} + \cdots \qquad (4.4.12)$$

so that (i) the normal stresses at the crack point are equal leading to a two-dimensional hydrostatic tension and (ii) infinite stress magnitudes exist at the crack point. Further analysis[4.29] shows that the circumferential variation of stress around the crack is such that the maximum stress occurs not along the direction of propagation but ± 60 degrees off to either side. The octahedral stress variation also peaks off to the side ± 70 degrees. Such deductions show the complexity of the stress distribution near a crack and suggest that a more refined stress analysis be incorporated when assessing the fracture of viscoelastic materials.

There are, however, three factors which should be emphasized. First, is the elastic analysis valid for viscoelastic materials? It will be recalled that if all the boundary conditions on a linearly viscoelastic material are prescribed in terms of stress, as in this particular case, then the viscoelastic stress distribution is identical with the elastic one. Second, the mathematically infinite stress at the crack point is physically inadmissible. On the other hand, one can in the average sense hypothesize the existence of a small region of constant finite stress with a characteristic radial extent δ which would give a stress distribution such as shown in the sketch. In a metal specimen, such a region may be associated with the area of plastic flow; the equivalent association for viscoelastic materials might be in terms of an agglomeration or bundle of polymer chains, and from the data of Greensmith[4.30-4.31] at low strain rates seems to be of order 10^{-2} inch. Third, if the strains are so large, will not the assumptions of infinitesimal theory be violated? The answer is yes, but the mathematical solution of the finite deformation problem is nearly intractable. Some exploratory work of Blatz[4.32] however indicates that the stress singularity

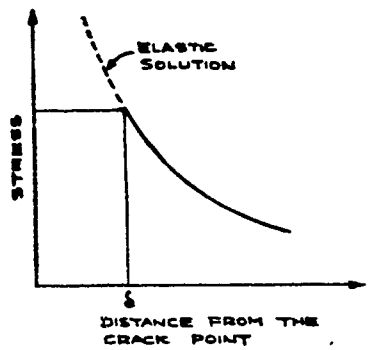

will probably not be removed, and hence one would expect errors in magnitude but not in the principle.

Finally, the centrally cracked geometry is not the only one which can be investigated experimentally. One obvious alternative is the externally cracked specimen and another is a one-sided crack geometry. Some analysis for the former is possible[4.33] while the latter is complicated by a lack of geometrical symmetry. No experimental data for viscoelastic materials is known for the

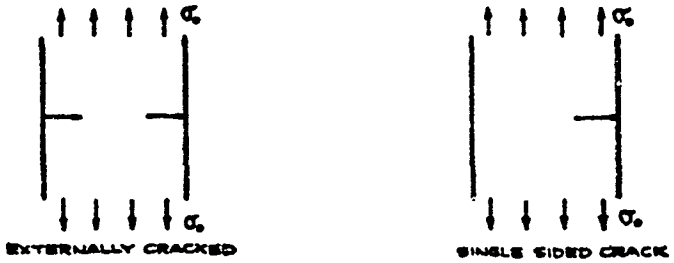

former, although Rivlin and Thomas[4.8] have used the latter extensively in their experiments.

Thin sheets subjected to bending. Another loading of considerable interest is in an initially cracked specimen subjected to bending. While the same centrally cracked geometry as before could be used, and analyzed using the Ang-Williams solution[4.28] taking into account some important amplifications by Knowles and Wang[4.34], it is more customary and experimentally more convenient to use a slit specimen (see insert) or trouser-leg specimen. From the analysis standpoint, the experimental specimen should be reasonably thick so that the applied loading produces only bending stresses near the crack point. When the specimen becomes thin, and particularly when stretched to large deformations as done by Rivlin and Thomas[4.8] (see insert) a complicated bending-stretching interaction problem results which is beyond classical treatments[4.28]. On the other hand, the strain energy of deformation is mainly confined to stretching of the trouser legs with a high but localized strain energy at

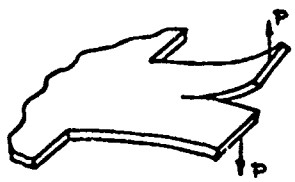

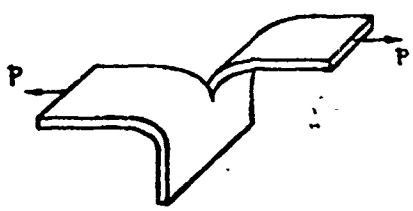

the crack point. It is this feature, as incorporated by Rivlin and Thomas, which accounts for the reasonably good correlation of tearing threshhold and characteristic energy.

On the other hand, it will no doubt be necessary to conduct certain bending and extensional tests designed to permit the maximum use of available analytical solutions to investigate the general applicability of a "characteristic energy" criterion, T. Specifically, as will be discussed later, there may be an important general connection which can be established between T and, say, the distortion strain energy.

Threshold criteria. As indicated earlier the first criterion for the elastic fracture of rubbery materials resulted from an extension of the Griffith brittle fracture theory[4.26] by Rivlin and Thomas[4.8]. The Griffith theory for thin flat sheets of thickness h, results from considering the change in strain energy in a specimen when a crack of initial length 2b, which is presumed small compared to any planar length in the extends a small amount $\Delta(2b)$ exposing a small increment of newly formed surface with surface tension, T. Assuming that this specimen is initially stretched by a stress σ_0, and then clamped at its ends in this position, the strain energy in the sheet will be reduced as the crack grows as the energy in the new crack surfaces increases. In the limit when the specimen parts, all the strain energy will have been transferred into surface energy. Analytically this change in potential energy V' becomes *

$$V' = \frac{\pi (2b)^2 \sigma_0^2 h}{4E} - 2(2b)Th \qquad (4.4.13)$$

where the first term is the strain energy and the second is the work overcome by the surface forces on both sides of the newly formed crack. At the equilibrium position of the crack just before catastrophic crack propagation, these two contributions balance, or the change in V', $\partial V/\partial(2b)$, is zero.

$$\frac{\partial V'}{\partial(2b)} = \frac{\pi \sigma_0^2 (2b)h}{2E} - 2Th = 0 \qquad (4.4.14)$$

which implies that the critical stress at equilibrium for a crack of length 2b is

$$\sigma_0 = \sigma_{cr} = \sqrt{\frac{4ET}{\pi(2b)}} \qquad (4.4.15)$$

*See Timoshenko and Goodier (4.22), for a brief description of the essential features of the theory.

which relation was stated earlier (4.4.10). The energy in the specimen at this stress, by substituting into (4.4.13) is

$$-V'_{cr.} = 2bhT \qquad (4.4.16)$$

from which denoting the cross section area of the specimen by A = 2bh the surface tension can be found as

$$T = -\left.\frac{\partial V'_{cr.}}{\partial A}\right|_{l} \qquad (4.4.17)$$

if the energy changes are evaluated or measured at a fixed length, i.e. clamped ends.

Rivlin and Thomas[4.8] followed by various collaborations of Greensmith and Thomas[4.30-31, 4.35-38] have proceeded to examine the application of a similar criterion for rubber. They find that one does seem to exist as measured upon various geometries and loading conditions but T should be viewed as a characteristic energy loss not necessarily restricted to surface tension. The fact that T is relatively constant, at a fixed strain rate, for various geometries is encouraging. If one approximates their data analytically, it is found that[4.31]

$$T \doteq 6\times10^5\left(\frac{3.6}{t_{sec}}\right)^{\frac{1}{6}} \qquad \text{at} \quad 90°c \qquad (4.4.18)$$

and

$$T \doteq 40\times10^5\left(\frac{0.48}{t_{sec}}\right)^{\frac{1}{6}} \qquad \text{at} \quad 25°c \qquad (4.4.19)$$

where t is the time to failure which reflects the strain rate sensitivity, and T is in ergs per cm^2. (10^7 ergs/cm^2 ≐ 60 in-lbs/in^2).

They further observe that T can be approximated by the relation[4.31]

$$T \simeq W_d\, \underline{d} \qquad (4.4.20)$$

where W_d is approximately the critical strain energy density for failure as determined in an initially uncracked tensile specimen, $W_d^* \cong \sigma_0^2/(2E)$, and $\underline{d}$ is the apparent size of the flaw or the diameter of the crack or razor blade cut at the crack point in the unloaded position. And finally, Greensmith[4.31] presents some data which suggests that W_d^* may be approximated at 25°C by

$$W_d^* = 500 \times 10^8 \left(\frac{100}{t_{sec}}\right)^{\frac{1}{2}} \qquad (4.4.21)$$

so that dividing (4.4.19) by (4.4.21), there results that

$$d \approx 0.03 \text{ cm} \approx 0.01 \text{ in.} \qquad (4.4.22)$$

which is of the order of the measurements also observed by Braden and Gent[4.39-40]. In principle then one may obtain the characteristic tearing energy by measuring the energy density required to fail a tensile specimen and reduce it by the diameter of the flaw.

It is possible to arrive at their results for a flat sheet by an alternate interpretation in terms of the characteristic average stress distance, δ, introduced earlier. If the σ_x and σ_y stress (4.4.12) are averaged locally in the vicinity of the crack point, one can deduce

$$\bar{\sigma} = \sigma_\infty \sqrt{\frac{2b}{\delta}} \qquad (4.4.23)$$

so that the factor $(2b/\delta)^{\frac{1}{2}}$ is essentially a stress concentration factor. Compute the distortion strain energy taking account of the stress field at the crack $\sigma_x = \sigma_y$ and $\sigma_z = 0$ to find

$$W_d = \sigma_x^2(0,0)/(6\mu) \cong \bar{\sigma}^2/(6\mu) \qquad (4.4.24)$$

so that using (4.4.23) and assuming incompressibility, the critical strain energy density at failure in this specimen becomes

$$W_d = \frac{\sigma_\infty^2}{2E} \frac{2b}{\delta} \qquad (4.4.25)$$

But using the classic Griffith interpretation (4.4.15) in the form

$$T = \left(\frac{\sigma_\infty^2}{2E}\right) \pi b$$

one finds

$$T = \frac{\pi}{2} W_d \delta \qquad (4.4.26)$$

which of course is the same form as (4.4.20) but associates a characteristic distance within the material with failure.

It is also possible to show the connection with local radius of curvature (4.41) by working with the general solution for the crack field. By integrating

the elastic stress field to find the displacements, one can compute in particular the displacements of the crack boundary for the deformed, i.e. loaded, specimen. For the internally cracked specimen the shape of the crack or hole is elliptical [4.28] and the radius of curvature at the sharp point of the crack, R, can be associated with the applied stress as

$$R = 4b\left(\frac{\sigma_o}{E}\right)^2 \qquad (4.4.27)$$

and hence using (4.4.23)

$$2R = d = \delta\left(\frac{2\bar{\sigma}}{E}\right)^2 \qquad (4.4.28)$$

so that in comparison with (4.4.26)

$$T = \frac{\pi}{2} W_d\, d\left(\frac{E}{2\bar{\sigma}}\right)^2 \qquad (4.4.29)$$

which would also agree with (4.4.20) if the local value of averaged stress at the crack approached values of twice the tensile modulus*.

It should be emphasized that these latter associations have been made after utilizing the assumptions of infinitesimal elastic deformations for sheet specimens whereas the work of Rivlin et al. includes large strain measurements on various geometries. Nevertheless it is encouraging to see that the effects predicted by more sophisticated stress analysis are not inconsistent with these other experiments and analysis.

Crack propagation. It is possible to make some headway in estimating the velocity of crack propagation in a viscoelastic material after the fracture threshhold has been exceeded. The primary new effect is the delay time in the fracture introduced by the rate sensitivity of the material. A simple model was proposed in one of the previous progress reports[1.6], and is included in Appendix I. A simple Voigt model and a limiting strain criterion for failure was assumed, and any rate effect on the ultimate strain at failure was supressed. By using the important fact that the elastic and viscoelastic stress distributions are identical, and the assumption of Voigt behavior, the viscoelastic deformations could be computed. When the local average strain at the crack over the length δ

*This type of assumption has been invoked by H. Neuber, Theory of Notch Stresses, in estimating the maximum stress at a crack point in metals.

was exceeded the crack would elongate by an amount δ, the stress field would also translate by an amount δ, but the new strain increments would add to those stored while the first element δ was breaking. The velocity of propagation was then estimated as $v_i = \delta/t_{R_i}$ where t_{R_i} is the time for the i-th element to rupture. The result estimates the initial velocity as

$$v_1 = \frac{1}{2(\sqrt{2}-1)} \cdot \frac{\sigma_s/E_v}{\varepsilon^*} \frac{\sqrt{t\,\delta}}{\tau} \qquad (4.4.30)$$

where ε^* is the ultimate strain and E_v the tensile modulus and τ the relaxation time of the Voigt model. From McCullough's preliminary test data[4.42], it was possible to deduce a value for δ which turned out to be 10^{-3} inch, not in unreasonable agreement with the 10^{-2} inch static value deduced from the Greensmith experiments.

Subsequent growth of the crack in terms of the distance s from the crack point, was found to be

$$\frac{s}{b} \approx \left[\frac{\pi}{4\sqrt{2}} \frac{\sigma_s/E_v}{\varepsilon^*} \frac{t}{\tau}\right]^2 \qquad \frac{4\delta}{b} \leq \frac{s}{b} \ll 1 \qquad (4.4.31)$$

and

$$\frac{s}{b} \approx \frac{1}{4} e^{\left[\frac{\pi}{2\sqrt{2}} \frac{\sigma_s/E_v}{\varepsilon^*} \frac{t}{\tau}\right]} \qquad \frac{s}{b} \gg 1 \qquad (4.4.32)$$

which latter value becomes suspect for large times because the velocity of propagation is unbounded in contrast to reality, probably because the inertia terms have been omitted from the equations of motion for this viscoelastic material. Braden and Gent[4.39-40] have measured crack growth in sheet specimens in an ozone atmosphere and find velocities of one-tenth inch per minute at low applied stresses, consistent with McCullough's measurements, but also find the velocity is nearly independent of stress level at low stresses, whereas (4.4.31) predicts a reasonably strong stress dependence.

As a final word it is possible to improve the above results using essentially a general viscoelastic model based upon an approximation to the creep compliance (4.1.3). It will be found that the strains along the crack in an incompressible material are

*

$$\varepsilon_y(x,0;t)=\frac{1}{E}\left[\sigma_y-\nu\sigma_x\right]\doteq\frac{1}{E}\left[\sigma_y-\tfrac{1}{2}\sigma_x\right]$$

$$=\sigma_0\left[1+\frac{\frac{b^2}{2}}{\sqrt{x^2-b^2}\left\{x+\sqrt{x^2-b^2}\right\}}\right]\left[D_g+(D_e-D_g)\left\{1+\frac{\left(\frac{D_e}{D_g}\right)^{\frac{1}{m}}K(T)}{t}\right\}^{-m}\right]$$

(4.4.33)

and a similar expression for $\varepsilon_x(x,0;t)$ using the Appendix. The procedure outlined can be repeated. The time when ε_y reaches a critical value ε^* can be computed from the above; the stress and strain analysis in δ steps can be repeated, although it is immediately evident that the computations become somewhat more involved, even if account is taken of the primary glassy response at the crack point. Nevertheless (4.4.33) has the important advantage of approximately the entire spectrum of relaxation times of the material, and furthermore, as rate sensitivity on failure criteria will be discussed in the final section, one can compute the strain rate at any time. This can be carried out for the biaxial strain field if desired. One can now use this knowledge of stress, stress rate, strain and strain rate distribution in time and space in conjunction with failure criteria, including rate effects, to investigate the mechanics of viscoelastic crack propagation with reasonable precision--if not simplicity!

4.5 Selection of the Failure Criterion

In accordance with the remarks introducing this chapter, it will be assumed that the elastic type of fracture is characteristic of cross-linked propellants, and therefore, that yield and fracture occur almost simultaneously. It should be recalled that in contrast to brittle fracture of many metals, propellants may sustain considerable strain before failure, and therefore in terms of strain at break rubbers may be characterized by several hundred percent, metals by a few tenths of a per cent.

A brittle material must be able to fail in at least two ways--either by dilatation or by distortion. For example, a sample subjected to hydrostatic compression will suddenly collapse its volume when the critical pressure is reached; or in hydrostatic tension which is not an easy stress field to generate, it will suddenly

tear. Gent and Lindley[4.20] have measured this triaxial yield stress for vulcanized rubbers and shown it to be around 80 psi. Presumably, the failure stress in compression will be much higher. Bridgman[4.43] shows that one should expect a minimum of several hundred thousand psi yield stress. These facts show quite clearly that the distortion strain energy alone or, indeed, any failure criterion which involves shear forces, is not adequate to explain hydrostatic failure, since hydrostatic forces generate no shear strains. Similarly, a sample may be caused to fail in pure shear, applied in torsion. No measurements of the torsile yield stress appear to have been reported for polymeric materials, but the existence of a torsile yield stress means that any failure criterion based on dilatation alone is inadequate.

It follows therefore, in the most general case, that each material must be characterized by at least two failure criteria, and that there must exist conditions under which both types of failure may occur simultaneously. Also it should not be expected, in general, that the two criteria are independent. For example, the critical shear stress in torsion may be a function of the amount of superimposed hydrostatic pressure or hydrostatic tension. In the following section, a geometric description of these concepts will be presented.

4.5.1 Geometry of normal yield stress or yield strain space

Because of the many criteria for fracture, it is convenient to have a method which permits the analyst to visualize their region of possible application. Inasmuch as the three principal stresses are orthogonal and participate in all stress theories of failure, one way of presenting the criteria is in terms of principal stress space where the magnitudes of σ_1, σ_2, and σ_3 are measured along the orthogonal axes to form octants. A similar approach could be adopted for strains. The rupture of an uniaxial tensile specimen at the stress σ_3^* would therefore correspond to a point on the σ_3 axis at the particular value σ_3^*. Other combined loadings would in a similar manner correspond to other points on a rupture surface $F(\sigma_1, \sigma_2, \sigma_3) = \text{constant}$, where the object of failure testing would be to perform experiments under all different combinations of combined stresses in order to trace out the failure surface in all octants. Presumably there would be many surfaces, each corresponding to a given strain rate for which the surface was obtained. Then, having obtained such surfaces experi-

mentally, the analyst would proceed to check out various criteria in the different octants and the one lying closest to the test surface would be the desired failure criterion.

Strain energy criteria. Inasmuch as critical values of strain energy, either in terms of stress or strain, are among the most prominent hypotheses, we shall proceed to develop the geometrical interpretation, assuming for necessary simplicity at this time that the material is linearly elastic and that infinitesimal deformation theory applies. Furthermore it is always possible to choose coordinates in which no shears act along three orthogonal axes and so only principle (normal) stresses and strains will be treated. In practice, most mechanical testing is applied to specimens whose geometry guarantees that the applied normal stresses are indeed principal stresses. In this sense, the stress-strain law may be written:

$$\sigma_i = (\kappa - \tfrac{2}{3}\mu)\vartheta + 2\mu\epsilon_i \quad ; \quad i = 1, 2, 3 \quad ; \quad \vartheta = \epsilon_1 + \epsilon_2 + \epsilon_3 \qquad (4.5.1)$$

The mean hydrostatic stress is given by:

$$\sigma = \frac{\sigma_1 + \sigma_2 + \sigma_3}{3} = \kappa\vartheta \qquad (4.5.2)$$

The total strain energy is given by:

$$W = \frac{1}{2}\sigma_i\epsilon_i = \frac{\kappa}{2}\vartheta^2 + \frac{2}{3}\mu(\vartheta^2 - 3\vartheta_2) \qquad (4.5.3)$$

where $\vartheta_2 = \epsilon_1\epsilon_2 + \epsilon_2\epsilon_3 + \epsilon_3\epsilon_1$ and where the double subscript indicates summation. The dilatational strain energy is computed from the volume change by:

$$W_{dil.} = \frac{1}{2}\sigma\vartheta = \frac{\kappa}{2}\vartheta^2 \qquad (4.5.4)$$

and thus the distortional strain energy is given by:

$$W_{dist.} = \frac{2}{3}\mu(\vartheta^2 - 3\vartheta_2) \qquad (4.5.5)$$

If the strains are replaced by stresses, Equations (4.5.2) and (4.5.3) may be rewritten as:

$$W_{dil.} = \frac{\sigma^2}{2\kappa} \qquad (4.5.6)$$

$$W_{dist.} = \frac{3\sigma^2 - \Theta_2}{2\mu} \qquad (4.5.7)$$

where $\Theta_2 = \sigma_1\sigma_2 + \sigma_2\sigma_3 + \sigma_3\sigma_1$

Reasonable critical values (denoted by asterisks) may be anticipated at this time for both forms of the strain energy function. For example, in simple tension, Equation (4.5.7) reduces to:

$$W^*_{dist.} = \frac{\sigma_T^2}{6\mu} \qquad (4.5.8)$$

where σ_T is the simple tensile strength at yield. Inspection of the various simple tensile data on propellants immediately reveals that the distortion strain energy will probably not exceed 10 psi. For many propellants, this is a generous figure, as is well realized by anyone who has flexed dogbone tensile specimens to fracture in his fingers. Continuum rubbers, on the other hand, may well reach 1000 psi at failure. Thus, the effects of the filler particles are markedly evident in this drastic reduction of the distortion strain energy.

Recent unpublished triaxial test data obtained on tablet-shaped specimens present some evidence as to the magnitude of the dilatational strain energy for propellants. In the case of polyurethane propellant, the triaxial stress rises to 100 psi before rupture at 0.7 percent strain. These figures correspond to a bulk modulus of 14000 psi, much lower than that observed in hydrostatic compression; the associated dilatational strain energy is only 35 psi. For continuum rubbers, the data of Gent and Lindley[4.20] indicate a dilatational strain energy of 30 psi. Thus, the filler particles do seem to reduce markedly this latter quantity.

Imagine now a rubbery linear elastic material characterized by the following four parameters:

K = 250000 psi

μ = 150 psi

$W^*_{dil.}$ = 25 psi in tension, infinite in compression

$W^*_{dist.}$ = 5 psi, independent of the value of hydrostatic stress.

The question arises: what ranges of triaxial stress or triaxial strain will such a material sustain without yield. Let us first look at the geometry in the stress space defined by the three orthogonal directions of normal stress. The dilatational criterion may be expressed as:

$$3\sqrt{2K W^{*}_{dil.}} \equiv 3\sigma^{*} \geq \sigma_1 + \sigma_2 + \sigma_3 \qquad (4.5.9)$$

where σ^* is the value of the hydrostatic tensile stress at which yield or failure will occur. Equation (4.5.9) represents a plane surface in normal stress space, located at a distance $\sqrt{3}\,\sigma^*$ from the origin, and whose normal is oriented at an angle of 54° 44' to each of the principal axes ($\cos\beta = \frac{1}{\sqrt{3}}$). Equation (4.5.9) thus expresses the sine qua non for application of the distortion criterion. For the given material, $\sigma^* \doteq 3500$ psi.

The distortion criterion may be expressed as:

$$2\mu W^{*}_{dist} \geq \frac{\sigma_1^2+\sigma_2^2+\sigma_3^2-\sigma_1\sigma_2-\sigma_2\sigma_3-\sigma_3\sigma_1}{3} \qquad (4.5.10)$$

$$\geq \frac{(\sigma_1-\sigma_2)^2+(\sigma_2-\sigma_3)^2+(\sigma_3-\sigma_1)^2}{6} \leq \frac{\sigma_T^2}{3} \qquad (4.5.11)$$

The form (4.5.11) is convenient because it allows one to introduce the values of the maximum shear stresses which are given by:

$$\tau_i = \frac{\sigma_j - \sigma_k}{2} \quad , \qquad i,j,k \qquad (4.5.12)$$

It follows that:

$$2\mu W^{*}_{dist.} \equiv \frac{3}{2}\tau_n^2 \geq \frac{2}{3}(\tau_1^2+\tau_2^2+\tau_3^2) \qquad (4.5.13)$$

where τ_n is the octahedral shear stress which operates in the particular planes whose normal is directed at 54° 44' to the principal axis. The name arises because that part of the plane which lies completely in the octant of pure tension forms one face of an octahedron. Comparison of (4.5.11) and (4.5.13) shows that

$$\tau_n = \frac{\sqrt{2}}{3}\sigma_T \doteq 31.6 \text{ psi.} \quad \text{, for the given material.} \qquad (4.5.14)$$

Since simple tensile strength is a more familiar quantity than octahedral shear strength, the geometry of the yield surface will be described by the former parameter ($\doteq$ 67 psi) coupled with the hydrostatic tensile strength. The surface represented by (4.5.11) is best visualized after making the following transformation:

$$p = \sqrt{3}\,\sigma \qquad (4.5.15a)$$

$$r^2 + p^2 = \sigma_1^2 + \sigma_2^2 + \sigma_3^2 \qquad (4.5.15b)$$

$$r \sin\theta = \frac{\sigma_2 - \sigma_3}{\sqrt{2}} \qquad (4.5.15c)$$

Substitution yields:

$$r \leq \sqrt{\frac{2}{3}}\,\sigma_T = \sqrt{3}\,\tau_o \doteq 54.8 \text{ psi.} \qquad (4.5.16)$$

These equations state that the distortion yield surface is a right circular cylinder whose radius is 81.6 percent of the simple tensile strength, and whose axis (the hydrostatic vector) is normal to dilatational yield surface. The length of this cylinder is determined by Equation (4.5.15a) with $\sigma = \sigma^* \doteq 3500$ psi, and at this point, the cylinder is capped by the dilatational yield plane. The intersection of the cylinder with this plane defines a circle on which failure occurs simultaneously by dilatation and distortion. Any stress field which lies inside the cylinder but outside the dilatational yield plane will produce failure by dilatation. Any stress field which lies outside the cylinder but inside the dilatational yield plane will produce failure by distortion. Finally, any stress field which lies both inside the cylinder and the dilatational plane will be sustained by an elastic body. All these statements are depicted in Figure (4.12), which shows a two-dimensional carpet of the yield surface. Because of the form of Equations (4.5.4) and (4.5.5.), the geometry of the yield surface is exactly the same in normal strain space.

If, in addition to the critical value of the hydrostatic tension, it were possible to assign a similar value for hydrostatic compression, then the cylinder would be capped by two dilatational yield surfaces, one in octant I, in which all stresses are positive or tensile, the other in octant VIII, in which all stresses are negative or compressive. The failure mode and stress quality in all octants may be denoted as follows:

Octant	σ_1	σ_2	σ_3	possible failure modes	number of positive stresses
I	+	+	+	distortion and/or tensile dilatation	3
II	+	+	-	distortion	2
III	+	-	+	distortion	2
IV	+	-	-	distortion	1
V	-	+	+	distortion	2
VI	-	+	-	distortion	1
VII	-	-	+	distortion	1
VIII	-	-	-	dilatation and/or compressive dilatation	0

By virtue of equivalence of the three principal axes, it is noted that there are four categories of octants characterized by the number of stresses of the same sign. Thus octants II, III and V are similar, and octants IV, VI, and VII are similar. This means that, for an isotropic material, only four octants need to be tested. If in addition, it is known that the compressive properties are the same as the tensile properties, then only 2 octants need be tested. On the other hand if the material is anisotropic, or if anisotropy is induced by virtue of straining, then it will be necessary to check six octants for an orthtropic material, and eight for a completely aeolotropic material.

It must be noted here, in passing, that stress-induced anisotropy presents a real problem in the case of filled rubbers. Consider, for example, an internally pressurized hollow cylinder with the radial axis in compression and the tangential axis in tension. Because of the dewetting of the binder in tension its modulus and Poisson's ratio in the tangential direction will differ from those in the radial direction. Thus, orthotropic behavior is indicated and at least six octants must be checked.

Other failure criteria. Suppose now that the given material fails by the Tresca condition, which is assumed when the maximum principal stress difference reaches a critical value. Note that this reduces the dependence of the failure criterion from three stresses in the energy case to two, namely, the largest and the smallest. A logical check on such a theory is to determine whether the failure criterion depends on the value of the intermediate stress.

Taking $\sigma_i > \sigma_j > \sigma_k$, the maximum stress difference or maximum shear stress is given by $\tau = \frac{\sigma_i - \sigma_k}{2}$ (4.5.12), A logical extension of this theory was proposed by Mohr, who suggested that

$$\frac{\sigma_i - \sigma_k}{2} = f\left(\frac{\sigma_i + \sigma_k}{2}\right) \qquad (4.5.17)$$

Proceeding as before, it is easily shown that the condition (4.5.12) defines six planes which intersect to form a hexagonal prism, which is precisely inscribed in the strain energy cylinder. In the case of Mohr's condition, the six planes become six curved surfaces, the elements of which are generators of non-circular cylinders. It is readily observed that the mathematical analysis connected with such conditions leads to insurmountable difficulties. Suffice it to say that the Hencky condition is usually an adequate approximation, even when physics dictates that the Tresca or Mohr condition represents reality. Similar surfaces develop

in normal strain space, only the values of the parameters are different.

Finally, let us suppose that the given material fails when the maximum principal stress or maximum principal strain reaches a critical value. In this case, the failure criterion in stress space is expressed as:

$$\sigma_k < \sigma_j < \sigma_i \leq \sigma_T \quad (i, j, k, \text{ permuted randomly}) \qquad (4.5.18)$$

This condition defines the position of three orthogonal planes which intersect the principal stress axes at σ_T and intersect each other to form a cube. If there is no critical condition for compression, the faces of the cube will extend to infinity in the octants II through VII. A critical value of the simple compressive stress will serve to define three other planes which will intersect in octant VIII to render the cube finite. In this case the center of the cube will have coordinates

$\sigma_i = \sigma_j = \sigma_k = \frac{\sigma_T + \sigma_c}{2}$, where σ_c is negative and larger in magnitude than σ_T. Again, the same geometry but different values of the parameters will obtain in the normal strain space.

It is clear that if the hydrostatic yield surface intersects the hydrostatic vector at a distance greater than $\sqrt{3}\,\sigma_T$, there is no possibility of dilatational failure, whereas, if $\sigma < \sigma_T$, then the intersection of the hydrostatic yield surface with the cube defines the line element on which both types of failure may occur simultaneously.

Coupled criteria. An interesting situation occurs when the two failure criteria are coupled. Suppose, for example, that the critical value of the distortion strain energy is some function of the mean hydrostatic pressure. Since the point in normal stress space corresponding to the mean hydrostatic pressure lies on the hydrostatic vector, the coupled criterion suggests that the radius of the circle which intersects the cylindrical distortion energy surface is a function of the position of this point. Thus the general failure surface based on coupled criteria will no longer be a cylinder but will still be a figure of revolution with varying circular section and with figure axis still on the hydrostatic vector. This may be stated analytically as:

$$\sqrt{\mu W_{dist.}} = f(\sigma) \qquad (4.5.19)$$

It is readily observed that by allowing the radius of the figure to increase as the position on the figure axis approaches the origin, the figure can be made

to approach a cuboid. Thus, by the simple expedient of coupling the failure criteria, the condition of failure by maximum principal stress can be approximated.

The situation may be summarized as follows. The Huber-Hencky octahedral shear stress criterion defines one limiting case of failure which is a right circular cylinder capped by the dilatational plane. The maximum principal stress criterion defines another limiting surface which is a cube, possibly intersected by the dilatational plane. The actual surface for any given material probably lies somewhere between these extremes. The problem is to define the extent of coupling.

For pure elastic materials, it makes no difference whether the failure surface is cast in normal stress or normal strain space, as long as the elastic laws are known right out to failure, even if non-linear. Obviously, the values of the yield parameters in strain space will differ from those in stress space. And since one should be interested in introconverting one set of data to the other, Poisson's ratio looms as a very important parameter. Thus the need exists for accurate experimental determination of this quantity under all conditions.

This may be seen as follows. First invert (4.5.1) as:

$$\sigma_i - \left(1 - \frac{2}{3}\frac{\mu}{K}\right)\sigma = 2\mu\epsilon_i \quad , \quad \text{or} \qquad (4.5.20a)$$

$$\sigma_i - \frac{3\nu}{1+\nu}\sigma = 2\mu\epsilon_i \quad , \quad \text{or} \qquad (4.5.20b)$$

$$\sigma_i - \nu(\sigma_j + \sigma_k) = E\epsilon_i \qquad (4.5.20c)$$

For the case $\epsilon_i > \epsilon_j > \epsilon_k$, (4.5.20b) shows that $\sigma_i > \sigma_j > \sigma_k$. Therefore the maximum principal strain failure criterion ($\epsilon_i < \epsilon_T$) is associated with, in stress space, the criterion:

$$\sigma_i - \nu(\sigma_j + \sigma_k) \leq E\epsilon_T \qquad (4.5.20d)$$

This is the equation of a plane, which intersects the principal axes at $\sigma_i, \sigma_j, \sigma_k = \frac{E\epsilon_T}{1-2\nu}$, $\frac{-E\epsilon_T}{\nu}$, $\frac{-E\epsilon_T}{\nu}$ in octant IV. Because of the equivalence of the principal stresses, there are two other congruent planes which intersect in octants VI and VII. The three planes intersect at a point which lies on the hydrostatic vector at a distance $\frac{\sqrt{3}}{1-2\nu}$ from the origin. Thus the yield surface in normal stress space associated with the maximum principal strain criterion is a trigonal pyramid (Figure 4.13), whose faces extend out to negative infinity. The slopes and intercepts of these faces depend strongly on the value of ν .

4.5.2 Mechanical procurement of failure data.

Aside from the obvious point of experimentally verifying that a given propellant under consideration is linearly viscoelastic in the first place, failure analysis indicates that testing need be carried out in sufficient octants to enable one to decide whether the material is anisotropic or not. In addition, testing must also be carried out at various points within an octant in order to pin down the position of the failure surface within the given octant. Since, in general, this can involve a prohibitively large number of tests, it is expedient to reduce this number by a symmetry argument. Assuming that the propellant material is isotropic, it follows that a given deformation field is insensitive to any ordering of the principal axes which border on the given octant. This means, for example, that interchange of the x and y axes, in any test in which these axes are the principal axes of the specimen, produces no effect upon the mechanical parameters that characterize the stress-strain field. The same argument holds even if anisotropy is induced as a result of applied strain. It only fails when the material is anisotropic to start with. It follows that only one-eighth of any octant bounded by two of the three coordinate axes and a third axis collinear with the hydrostatic vector need define the region within which testing can be carried out. This can be seen very nicely by referring to Figures 4.14 - 4.23. The set of four tests--biaxial tension, hydrostatic tension, parallel-plate tension, and simple tension (Figures 4.14 - 4.17)--form a sequence which defines the trace of the yield surface in the plane defined by one of the coordinate axes and the hydrostatic vector. In order to complete the definition of the position of the yield surface, it is merely necessary to determine the trace in the plane bounded by any two of the coordinate axes, for example, the same plane in which the biaxial test is depicted in Figure 4.14. And finally, an additional check may be provided by tests at some intermediate points. It is believed that the sequence of tests outlined in Figures 4.14 - 4.17 is sufficient to pin down the yield surface within the extent of variation that ordinarily accompanies failure testing in any one octant.

The remainder of the sequence of Figures 4.18 - 4.23 shows the mapping of stress vectors produced by tests in other octants. The sequence was chosen (cf below) from the total possible number of combinations of positive/negative/and zero stress components; but was numbered in a fashion better suited to the discussion of mapping within octant I.

\+ + + triaxial-hydrostatic tension - octant I

\+ + + triaxial-parallel plate tension-octant I

+	+	0	biaxial-planes I II, I IV, I III
+	+	-	torsion-pure shear- octants II, VII, III, VI
+	0	0	uniaxial-tension-along each positive axis
+	0	-	torsion stretch - planes II III, II VI, III VI, II VII, III VII, VI VII
+	-	-	torsion compression - octants IV, V, VI
0	0	0	identify-coordinate origin
0	0	-	uniaxial-compression-along each negative axis
0	-	-	biaxial-compression-planes V VIII, VI VIII, VII VIII
-	-	-	triaxial-hydrostatic compression - octant VIII
-	-	-	triaxial-parallel plate compression - octant VIII

The tests chosen to generate the various mappings of the stress vector are those in common use today. The introduction of other types is primarily a question of experimental ingenuity.

4.5.3 Unfilled non-viscous elastomers-large strain effects.

In Section 4.2.1, the character of the stress-strain curve in simple tension was discussed for natural rubber vulcanizate. Apart from pointing out that the strain at rupture is large, nothing was said about the failure criterion. On the other hand, nothing was said about the effect of large strains upon the nature of the failure criterion in 4.5.2. It is important to tie these two sections together in order to evaluate realistically the failure of unfilled elastomers, and then filled elastomers, or propellants.

Let us recall that many unfilled elastomers or continuum rubbers are generally well characterized by incompressibility, and a strain energy function of the form (4.2.9). Associated with this function is a stress-strain law of the form (4.2.2). Let us now calculate the various failure criteria with the aid of these expressions. Denote alternate values by an asterisk and order the subscripts in the fashion $\lambda_i > \lambda_j > \lambda_k$, or $\sigma_i > \sigma_j > \sigma_k$.

From (4.2.2) it follows that the ultimate true stress is given by:

$$\bar{\sigma}_i^* = \mu (\lambda_i^{*2} + \bar{k}) \tag{4.5.21}$$

where $\bar{k}$ is determined from the condition

$$\lambda_i^* \lambda_j^* \lambda_k^* = 1 \tag{4.5.22}$$

The maximum of the three values among $\bar{\sigma}^*_i$, $\bar{\sigma}^*_j$, $\bar{\sigma}^*_k$ is appropriate for a criterion based on maximum principal stress. If maximum principal stress difference is chosen, one must write:

$$2\bar{\sigma}^*_{max.} = \bar{\sigma}^*_i - \bar{\sigma}^*_k = \mu(\lambda^{*2}_i - \lambda^{*2}_k) \qquad (4.5.23)$$

Note that this may be numerically greater or lesser than the maximum principal stress depending whether $\bar{\sigma}^*_k$ is positive or negative.

The maximum principal strain difference derives from (4.5.23) after division by twice the shear modulus, using the fact that the Murnaghan (or finite) strain is given by

$$\epsilon_i = \frac{\lambda^*_i - 1}{2} \qquad (4.5.24)$$

$$\frac{\bar{\sigma}^*_{max.}}{\mu} = \frac{\bar{\sigma}^*_i - \bar{\sigma}^*_k}{2\mu} = \frac{\lambda^{*2}_i - \lambda^{*2}_k}{2} \qquad (4.5.25)$$

This latter quantity is greater than the maximum principal strain for

$$\lambda^*_i > 1 + \sqrt{1 + \lambda^{*2}_k}$$

The expression for the mean deviatoric stress may be simplified by introducing (4.2.1a,b,c) to yield:

$$\bar{\sigma}_d = \frac{1}{2}\sqrt{(\bar{\sigma}^*_i - \bar{\sigma}^*_j)^2 + (\bar{\sigma}^*_j - \bar{\sigma}^*_k)^2 + (\bar{\sigma}^*_k - \bar{\sigma}^*_i)^2} = \mu\sqrt{I_1^2 - 3I_2} \qquad (4.5.26)$$

Note that this quantity is greater than $W_{dist} = \frac{\mu}{2}(I_1 - 3)$ for $I_1 > 2\sqrt{1 + I_2} = 1$
The mean deviatoric strain derives from (4.5.26) after division by twice the shear modulus. All these results are summarized in Table 4.1. In particular, the formulas for uniaxial and homogeneous biaxial stress fields are also tabulated.

Some comments regarding Table 4.1 are in order. First of all, note that for the uniaxial stress field all the yield criteria, with the exception of the maximum principal strain and distortion strain energy, are proportional to the same factor $(\lambda^2 - \lambda^{-1})$. A similar situation holds for the equal biaxial tension case, except that the factor is $(\lambda^2 - \lambda^{-4})$. In both stress fields the ultimate stresses are simply equal to the ultimate strain times twice the shear modulus. Second, if the strains are large, all of the criteria are proportional to λ^2. One might suspect therefore that the problem of defining an ultimate criteria for an incompressible elastomer is straightforward: measure λ at yield (or fracture)

in any kind of stress field, and as long as $\lambda \geq 3$ the error made in failing to distinguish among them is of the order of 5 - 10%. If, however, the fracture strain is small, of the order of 20 to 30 percent as it may be in actual rocket motors, the criteria will depend upon the stress state. The similarity of the strain proportionality factor for many of the criteria implies, however, that it may be sufficient when designing experiments to contemplate testing the hypothesis in only three of the original seven of Table 4.1, namely (i) mean deviatoric stress (stress distortion), (ii) distortion strain energy (strain distortion), and (iii) maximum principal (normal) strain, as suggested earlier in this section.

TABLE 4.1

	Yield Criterion	Uniaxial Stress Field	Equal Stress Field	General Stress Field
1	maximum principal strain	$\lambda - 1$	$\lambda - 1$	$\lambda - 1$
2	maximum strain difference	$\frac{1}{2}(\lambda^2 - \frac{1}{\lambda})$	$\frac{1}{2}(\lambda^2 - \frac{1}{\lambda^4})$	$\frac{1}{2}(\lambda_i^2 - \lambda_j^2)$
3	mean deviatoric strain	$\frac{1}{2}(\lambda^2 - \frac{1}{\lambda})$	$\frac{1}{2}(\lambda^2 - \frac{1}{\lambda^4})$	$\frac{1}{2}\sqrt{I_1^2 - 3I_2}$
4	maximum principal stress	$\mu(\lambda^2 - \frac{1}{\lambda})$	$\mu(\lambda^2 - \frac{1}{\lambda^4})$	$\mu\lambda_i^2 + \bar{k}$
5	maximum stress difference	$\mu(\lambda^2 - \frac{1}{\lambda})$	$\mu(\lambda^2 - \frac{1}{\lambda^4})$	$\mu(\lambda_i^2 - \lambda_j^2)$
6	mean deviatoric stress	$\mu(\lambda^2 - \frac{1}{\lambda})$	$\mu(\lambda^2 - \frac{1}{\lambda^4})$	$\mu\sqrt{I_1^2 - 3I_2}$
7	distortion strain energy	$\frac{\mu}{2}(\lambda^2 + \frac{2}{\lambda} - 3)$	$\frac{\mu}{2}(2\lambda^2 + \frac{1}{\lambda^4} - 3)$	$\frac{\mu}{2}(I_1 - 3)$

As an illustration of how one might predict the ultimate values of the yield stresses and strains in equal biaxial tension and pure shear from uniaxial ultimate strain data represented by λ^*, consider the following calculation based upon a maximum distortion strain energy criterion.

From equations (4.2.1a), (4.2.2) and (4.2.9), we have

$$I_{1_{uni.}} = \lambda^{*2} + \frac{2}{\lambda^*} \qquad (4.2.1a)$$

$$\bar{\sigma}_{uni.} = \mu(\lambda^{*2} - \frac{1}{\lambda^*}) \qquad (4.2.2)$$

$$W_{max.} = \frac{\mu}{2}(I_1 - 3) \qquad (4.2.9)$$

where λ^* is known from experiment. Now for an equal biaxial stress field, using a subscript b, the first invariant is

$$I_{1_b} = 2\lambda_b^2 + \frac{1}{\lambda_b^4} \tag{4.5.27}$$

whereupon equating the strain energies using (4.2.9) and the respective values of I_1, find

$$2\lambda_b^2 + \frac{1}{\lambda_b^4} = \lambda^{*2} + \frac{2}{\lambda^*}$$

One root is obviously

$$\lambda_b = \frac{1}{\sqrt{\lambda^*}}$$

which corresponds to biaxial compression and is extraneous. The other root is

$$\lambda_b = \frac{1}{\sqrt{-\frac{\lambda^*}{2} + \sqrt{(\lambda^*/2)^2 + 2/\lambda^*}}} \tag{4.5.28}$$

For large λ^*, we have: $\lambda_b \to \lambda^*/\sqrt{2}$. which is a useful rule of thumb for predicting biaxial failure (large strain) in a rubber when the ultimate uniaxial strain is known. Similarly, the associated stress ratio can be calculated as $\bar{\sigma}_b/\bar{\sigma}_{uni} = \frac{1}{2}$. On the other hand, for small strains such that the maximum value of the strain energy is small enough so that λ may be approximated by $1+\epsilon$, then it follows that $\epsilon_b \approx \epsilon^*/2$, and $\bar{\sigma}_b \approx \bar{\sigma}_{uniaxial}$ at fracture.

For the second case, pure shear generated in a material by applying the extension field

$$\lambda_x = \lambda_s \quad ; \qquad \lambda_y = 1 \quad ; \qquad \lambda_z = \lambda_s^{-1} \tag{4.5.29}$$

leads to

$$W = \frac{\mu}{2}(\lambda_s^2 - 2 + \bar{\lambda}_s^2) = \frac{\mu}{2}\frac{(\lambda_s^2-1)^2}{\lambda_s^2} = \frac{\mu}{2}(\lambda^{*2} + \frac{2}{\lambda^*} - 3) \tag{4.5.30}$$

For large λ

$$\lambda_s \approx \lambda^* - \frac{1}{2\lambda^*} \tag{4.5.31}$$

$$\frac{\sigma_s}{\bar{\sigma}_{uni}} \approx \frac{\lambda^* - \frac{1}{2\lambda^{*2}}}{\lambda^* - \frac{1}{\lambda^{*2}}} \tag{4.5.32}$$

whereas if the strains are small

$$\frac{\epsilon_s}{\epsilon_{uni}} \approx \frac{\sqrt{3}}{2} \tag{4.5.33}$$

$$\frac{\sigma_s}{\sigma_{uni}} \approx \frac{4}{3} \qquad (4.5.34)$$

Returning to specific consideration of a particular unfilled elastomer, consider the fracture characteristics of gum rubber. The properties of the simple tensile curve at yield and at rupture are summarized in Table 4.2 along with some predicted and measured values obtained for other stress distributions. In connection with these properties, a few comments can be made.

The extension ratio at yield is taken to be 6 on the basis of the discontinuity in slope in the curve of Figure 4.[illegible]. The associated σ, W and σ_d are tabulated. For large strains, it is necessary to adapt a definition of the mean deviatoric strain based on finite elastic theory. It is convenient to work with Murnaghan's definition of strain:

$$\frac{1}{2}(\lambda_i^2 - 1) = \epsilon_i \qquad (4.5.35)$$

so that

$$\frac{1}{2}(I_1 - 3) = \vartheta \qquad (4.5.36)$$

TABLE 4.2

Fracture Properties of an Unfilled Gum Rubber Vulcanizate
(μ = 1.76 kg/cm^2, E = 5.28 kg/cm^2, 1 kg/cm^2 = 14.22 psi)

Property	Table 1 Ref. Line	Failure Mode	Simple Tension	Homogeneous Biaxial Tension		Heterogeneous Triaxial Tension
λ	1	yield	6.00	*4.30	†6.82	6.00
$-\sigma$	4	↓	12.0	7.58	12.0	4.85
W_d	7	↓	29.9	29.9	69.2	29.9
σ_d	6	↓	12.0	7.58	12.0	4.85
e_d	3	↓	17.9	17.9	44.9	17.9
λ	1	fracture	7.65	-	-	-
σ	4	↓	32.0	-	32.0	5.81
W_d	7	↓	62.4	62.4	-	-
σ_d	6	↓	32.0	-	32 0	-
e_d	3	↓	29.2	-	-	-

* energy criterion
† deviatoric stress criterion

Now define the strain deviators and mean deviatoric strain by:

$$e_i = \epsilon_i - \frac{\theta}{3} \tag{4.5.37}$$

$$e_d = \sqrt{3/2\,(e_1^2 + e_2^2 + e_3^2)} = \frac{1}{2}\sqrt{(I_1^2 - 3I_2)} \tag{4.5.38}$$

after some algebraic manipulation. This is the last yield parameter tabulated.

Of the five chosen, most likely candidates for the yield criterion are W, σ_d and λ, as mentioned earlier. To date, the data necessary to place these quantities on a firm experimental basis have not been procured. In the meanwhile, some predictions will be made for biaxial and triaxial tension. Comparison is established with the only available multiaxial data [4.20]

In the first column, under the heading of biaxial tension, it is assumed that rupture occurs always at a given value of the strain energy, approximately 30 psi. Notice that it takes less biaxial stress, and of course, less biaxial strain to effect yield and presumably rupture under this assumption. If, on the other hand, the mean deviatoric stress is chosen for the yield criterion (second column), then the sample in biaxial tension fails at the same stress level as in simple tension, but at a much higher strain energy level. The calculations are carried out with the aid of (4.2.2).

The case of triaxial tension introduces some new features into the picture. In the first place, a truly incompressible material cannot deform under triaxial tension unless at least one lateral dimension is allowed to strain. This can be accomplished for example by bonding a cylindrical sample between two rigid steel plates. In this case, incompressibility of the specimen is preserved by necking of the sample. Gent and Lindley[4.20] subjected such poker-chip specimens to tension and found that the stress-strain curve is linear up to a point at which the sample suddenly develops an internal void; they term this the triaxial yield point. They show, to a good approximation, that the average applied stress level S' (kg/cm^2) at which the void occurs is given by (4.4.5)

$$S' = E e' \left[1 + \frac{a^2}{2h^2}\right] = P'_m \left[\frac{1}{2} + \frac{h^2}{a^2}\right] \tag{4.5.39}$$

where e' is the strain level at yield

a is the radius of the tablet (cm)

h is the thickness of the tablet (cm)

p'_m is the maximum hydrostatic pressure acting on the yield surface just prior to yield (kg/cm^2)

For samples characterized by h/a = 0.3, they measured the yield stress for a number of rubbers and found experimentally

$$S' = 0.50 + 0.55\,E = 0.59\,P'_m \qquad (4.5.40)$$

by (4.5.39), so that

$$P'_m = 0.85 + 0.94\,E \qquad (4.5.41)$$

Insertion of the tensile modulus of 5.28 into (4.5.41) yields the tabulated value of 5.81 kg/cm^2 for the indirectly measured triaxial stress on the yield surface just prior to yield.

It is possible to calculate how the high triaxial stress originates. Gent and Lindley assume that a tiny microscopic void is present to start with at the center of the disk. They assume further that the void is stretched radially like a spherical cavity, and they compute the stress P'_m as the point at which the cavity becomes infinitely large. This treatment can be modified for two reasons. First, when the cavity has grown large, the radially symmetric stress distribution will become distorted. Moreover, from the start the cavity is not being elongated equally in all three directions. Actually, it may be more like extension in the direction normal to the flat specimen with zero displacement in the two transverse directions. Since such a displacement field is impossible for a cavity in an incompressible medium, however, it may be assumed that the cavity is a small cylinder, lying with its axis perpendicular to the pull direction, and being stretched radially with its axial length held fixed. This will be closer to reality than the case of the spherical cavity. The solution of this problem is a classical case in finite elastic theory[4.14] the details of which need not concern us here. Suffice it to point out that the radial stress in the medium around the cavity is given by

$$\frac{\bar{\sigma}_r}{\mu} = \ln\left(\frac{\lambda_a}{\lambda}\right) + \frac{1}{\lambda^2} - \frac{1}{\lambda_a^2} \qquad (4.5.42)$$

where the bar over the stress symbol indicates true stress and

λ is the radial extension ratio $= \frac{1}{r}\sqrt{a^2 - a^2 + r^2}$

a is the radius of the undeformed cavity.

Far away from the cavity, $\lambda \to 1$ and the stress approaches P'_m.

$$\frac{P_m'}{\mu} = \ln \lambda_a + 1 - \frac{1}{\lambda_a^2} \qquad (4.5.43)$$

Likewise, the tangential stress at the surface of the cavity is given by

$$\left(\frac{\bar{\sigma}_\theta}{\mu}\right)_a = \lambda_a^2 - \frac{3}{2\lambda_a^4} \qquad (4.5.44)$$

which, for $\lambda \geq 3$, behaves exactly like simple tension; this checks the facts because the surface of the cylinder is assumed to stretch tangentially, but not axially. On this basis, we choose the yield value for λ_a to be that in simple tension, namely 6.00. Substitution into (4.5.43) yields for P_m' a value of 4.85 kg/cm^2 (tabulated under the heading σ at yield), in excellent agreement with the measured value. Furthermore, it is to be expected that the measured value will be higher since it is a measured break rather than yield.

The first strain invariant under the radial stretching of the cylinder is given by

$$I_1 = \lambda_a^2 + 1 + \frac{1}{\lambda_a^2} \qquad (4.5.45)$$

so that using (4.2.9)

$$W_d = \frac{\mu}{2}\left(\lambda_a^2 + 1 + \frac{1}{\lambda_a^2} - 3\right) = 0.883(34.0) = 29.9 \qquad (4.5.46)$$

Thus the strain energy remains constant as in simple tension. With admittedly only fragmentary evidence it appears that it may not be a poor assumption to take W_d as the yield criterion. In this particular case, the criterion states that this particular gum rubber vulcanizate cannot sustain more than 30 kg/cm^2 or 425 in-lbs/in^3 of strain energy density without yielding. It is suggested, however, that similar experiments to those of Gent and Lindley in both tension and compression be expedited to provide the data needed to define the yield criterion.

Illustrative example: On the basis of the suggestion made in the previous section, the strain energy criterion will be tentatively adopted in order to demonstrate the use of a failure criterion. In the strict sense of the word, finite elastic theory should be used, but since not many design engineers have familiarized themselves with the intricacies of this treatment, an analysis based on infinitesimal theory will first be presented. We consider the classical case of pressurization of an infinitely long hollow bonded cylinder in an elastic case. Since the nomenclature from here on is familiar, interjections will be sparse. Superscript

bar refers to properties of the metal case. Using (4.2.9) in the form

$$W_d = \frac{2}{3}\mu\left[\left(\frac{du}{dr}\right)^2 - \frac{u}{r}\frac{du}{dr} + \left(\frac{u}{r}\right)^2\right] \tag{4.5.47}$$

with p as the internal pressure, one finds upon the appropriate substitution that at the inner surface

$$W_d = \frac{p^2}{6\mu}\frac{(1-2\nu)^2(a/b)^2(1-\phi)^2 + 3(1+\phi-2\nu)^2}{[1+\phi-2\nu+(a/b)^2(1-\phi)]^2} \tag{4.5.48}$$

where $\phi = \frac{\mu}{\bar{\mu}}\left[1-(3-2\bar{\nu})/5\right]$ is the effective case rigidity.

For an infinitely stiff case, for example, and typical large web fractions,

$$p_{max.} \approx 30\sqrt{W_d} \tag{4.5.49}$$

which upon using $W_d = (\mu/2)(I_1-3)$ from Table 4.2, gives a maximum internal allowable pressure of 170 psi. Figure (4.24) shows how W_d varies with Poisson's ratio for the particular case when $\phi = 0.004$, $a/b = 0.25$ and $p = 1000$ psi. Note that W_d increases very rapidly as ν falls below $\frac{1}{2}$. The need for such a large strain energy will in part be eased by relaxation effects in the propellant. But a very important reason that results in these high values lies in the error made by assuming small strain theory out to rupture. The error made is akin to assuming that the initial slope of the tensile curve remains constant to rupture. Thus the value of 900 psi is not to be treated as universal, particularly when large strains are involved. On the other hand, calculations of this sort based on small strain theory do become more meaningful at low temperatures. There the stress-strain curve does become linear, while the ratio of μ to $\bar{\mu}$ increases, as does the relative case rigidity effect.

Because it is extremely important to be able to apply the strain energy criterion to practical cases, the finite elastic analysis of the infinitely long internally pressurized cylinder is carried out in Appendix 4.3 in order to show the type of error which may occur when using small strain theory. The analysis is an extension of the results that were presented for the cavity, and in order to keep it fairly simple, it is necessary to assume incompressibility. The analysis can be carried out for a compressible material with a bit more difficulty, but for present propellant materials, a representative strain energy density function is not available.

The result given for the assumed incompressible material is

$$W_d = \frac{p^2\phi}{2\left[(a/b)\,p\phi + \mu\,(a/b)^2\right]} \qquad (4.5.50)$$

$$\frac{p}{\mu} = \frac{(a/b)^2(\lambda_a^2 - 1)}{\phi} \qquad (4.5.51)$$

which is the large strain analog to (4.5.48). For small case rigidities,

$$p_{max.} \approx 2\left(\frac{a}{b}\right)^2 \frac{W_d}{\phi} \qquad (4.5.52)$$

and it is easily seen by comparing (4.5.49) and (4.5.52) that the energy increases quadratically with pressure in small strain theory, but for large strains approaches a linear asymptote in pressure.

Thus this illustrative calculation demonstrates that if the grain design is such to permit large strains in the propellant, much lower demands will be placed upon the allowable strain energy than were indicated by, for example, the 900 psi figure obtained by extrapolating the small strain theory.

4.5.4 Filled non-viscous elastomers

In returning now to the practical problem of rocket grain analysis, it is unfortunate that so little can be said as to how far the conjectures of the previous section can be ex·d. It is clear that fracture prediction will not be nearly as simple for high·· ..led elastomers or propellants, since the materials are compressible and may yield at strains as low as 20 percent ($\lambda = 1.20$) where as can be seen from Table 4.1 the criteria depend upon the stress state. Until more experimental data becomes available, it will be necessary to rely upon a mixture of continuum analysis and engineering judgment.

Possible fracture criteria: It has been suggested that in the case of unfilled elastomers, the distortion strain energy adequately represents the onset of fracture or yield. In the case of filled elastomers, two factors complicate the situation; one deals with the cutting of the polymer chains on the sharp edges of the filler engendered by the high local stresses around the particles, the other is the generation of voids as the binder is pulled away from the filler. Simple modifications to the strain energy function to account for these factors can be proposed as a point of departure for future work.

The first modification deals with the cutting of polymer chains. This inference is borne out by constant strain test data (i) as strain is increased, time

to rupture decreases, (ii) at a given strain, the modulus decreases with time. Thus, from stress relaxation studies at various strain levels, it is possible to correlate the modulus with some function of time and strain level and also temperature. The strain energy criterion now becomes:

$$W = \frac{1}{2}\mu(t, \lambda, T)[I_1 - 3] \tag{4.5.53}$$

Secondly, the void volume must be accounted for since the strain energy is defined per unit volume of unstrained material. If β is the void fraction engendered by pullaway at a given λ, then (4.5.53) becomes

$$W_d = \frac{1}{2}\mu(t, \lambda, T)[I_1 - 3][1 - \beta(\lambda)] \tag{4.5.54}$$

where W_d is now measured on the sample including voids. Measurements of void volumes can be done microscopically on thin films.

Until more definitive experimental data becomes available no attempt will be made to present an example of typical calculations using actual propellant material properties. It will be necessary to assume that the behavior of filled elastomers is sufficiently interpretable by unfilled elastomer analysis to permit stress and strength analysis calculations in propellant grains, and to rely upon engineering judgment in assessing the results and their pertinence to the design problem.

4.6 Cumulative Damage Theory

In any discussion of failure theory for viscoelastic materials, it is necessary to show the correlation between experimental data accumulated at constant strain rates, and actual test and environmental conditions wherein the strain rate may change slowly, rapidly or variably during the time under consideration. In other words one may pass from one failure surface to another as the strain rate changes. Pending the determination of more precise procedures, it has been proposed that one may use a cumulative damage concept similar to that used in metal fatigue analysis, in order to account for the amount or percentage of resistance to failure used up as the strain rate takes on various values during the loading history.

4.6.1 Review of the Miner Law

By way of review, it may be recalled that Miner [4.44] investigated the

use of a cumulative damage criterion in aluminum, where the basic concept was simply to add together the relative percentages of damage at each stress level (based on total number of cycles to damage at each stress level) until a hundred percent damage was attained. Others[4.45] have extended this concept to other metals and loading conditions in a more general (non-linear) way.

Consider for example, a specific illustration where the usual fatigue criteria for metals of N cycles to failure at a constant stress σ^* (Figure 4.25) is inappropriate. Such a situation often occurs when the loading spectrum is not a constant stress. Hence while one may expect one million cycles before failure at say 50,000 psi stress, suppose the applied stress is halved to 25,000 psi after only a half million cycles. The natural question then arises - how many more cycles will the specimen withstand before failure? The usual approach has been to consider the problem from the standpoint of a cumulative damage. In the foregoing example one would say half the "life", say $\frac{1}{2} N_{50,000}$, had been used up when the stress was reduced. The specimen would then be expected to withstand half the life, i.e. $\frac{1}{2} N_{25,000}$, at the reduced stress. The total life for this particular assumed spectrum would therefore be $\frac{1}{2} (N_{50,000} + N_{25,000})$. The general formulation for a spectrum of M loadings σ_i, $(i = 1, 2, 3 \ldots M)$, is

$$\sum_{i=1}^{M} \left(\frac{N_i}{N_{R_i}} \right)^n = 1 \qquad (4.6.1)$$

where the life $L = \sum_{i=1}^{M} N_i$. N_i is the number of cycles at the stress σ_i, and N_{R_i} is the number of cycles to rupture at the stress σ_i. In the simple example chosen, a linear cumulative damage law was assumed; hence $n = 1$.

4.6.2 Cumulative damage concept for rate-sensitive media.

Based upon the preceding concept, it is proposed to inquire whether or not some similar law might be postulated for polymers, whose time dependence analogously to cycles is associated with strain rate. Smith has found a correlation between ultimate strain and strain rate, with temperature as a parameter (Figure 4.26), for specimens tested in uniaxial tension at a constant strain rate. For most practical applications the strain rate varies during a test, particularly if the applied load or pressure is changing. It would therefore be desirable to be able to associate the failure of specimens subjected to a varying strain rate to that at constant rate for which data, e.g. a Smith curve, has been obtained.

Suppose now that constant temperature conditions are assumed for simplicity, and write

$$\sum_{i=1}^{M}\left(\frac{t_i}{t_{R_i}}\right)^n = 1 \qquad \text{with} \qquad T = \sum_{i=1}^{M} t_i \tag{4.6.2}$$

where t_i and t_{R_i} are the time the specimen is held at the strain rate $\dot{\epsilon}_i$ and the time to failure at $\dot{\epsilon}_i$ respectively. T is the total time to rupture for the spectrum of strain rates $\dot{\epsilon}_i (i = 1, 2, 3 \ldots M)$. Passing now to an integral form of the linear cumulative failure law,

$$\int_0^T \frac{dt(\dot{\epsilon})}{t_R(\dot{\epsilon})} = 1 \tag{4.6.3}$$

from which T is to be determined for a specified spectrum $t(\dot{\epsilon})$ and Smith curve $t_R(\dot{\epsilon})$.

As a practical matter, it is often inconvenient to work with the times themselves. Actually, given

$$\epsilon = \epsilon(x_i, t) \tag{4.6.4}$$

from an analytical viscoelastic strain analysis, then by differentiation

$$\dot{\epsilon} = \dot{\epsilon}(x_i, t) \tag{4.6.5}$$

or inverting

$$t = t(x_i, \dot{\epsilon}) \tag{4.6.6}$$

alternate forms are possible. For the constant strain rate failure data (Figure 4.26), $\epsilon_R = \dot{\epsilon} t_R$, so that

$$t_R = \frac{\epsilon_R(\dot{\epsilon})}{\dot{\epsilon}} \tag{4.6.7}$$

where an analytical representation of Figure 4.29, $t_R = t_R(\dot{\epsilon})$, is required if numerical integration is to be avoided. The alternate scheme in (4.6.3) is to replace dt by $(\partial t/\partial \dot{\epsilon})\partial \dot{\epsilon}$ and work completely in the rate space.

As an example to illustrate the mechanics of applying the postulate, assume, to simplify the calculations, that the actual strain response of the particular geon. ^ry under study is simple creep (Figure 4.27), viz.

$$\epsilon = \epsilon_0 (1 - e^{-\frac{t}{\tau}}) \tag{4.6.8}$$

where ϵ_o is the initial strain. From (4.6.8) however the strain rate, by differentiation following (4.6.5), is

$$\dot{\epsilon} = \frac{\epsilon_o}{\tau} e^{-\frac{t}{\tau}} = \dot{\epsilon}_o e^{-\frac{t}{\tau}} \tag{4.6.9}$$

where $\dot{\epsilon}_o$ is the initial strain rate. Now by (4.6.6) one has

$$t = \tau \ln\left(\frac{\dot{\epsilon}_o}{\dot{\epsilon}}\right) \tag{4.6.10}$$

and

$$\frac{\partial t}{\partial \dot{\epsilon}} = -\frac{\tau}{\dot{\epsilon}} \tag{4.6.11}$$

Turning now to the Smith curve, but replotting the data (Figure 4.28) in the form $t_R = t_R(\dot{\epsilon})$ where the ultimate strains ϵ_R are indicated by hashmarks on the curve, one proceeds to curve fit the data. For illustrative purposes it is sufficient to approximate the actual Smith curve by the dashed line

$$t_R = \frac{0.2}{\dot{\epsilon}} \tag{4.6.12}$$

This form incidentally may be recognized as approximating the actual failure data by a constant rather than rate dependent ultimate strain -- in this case $\epsilon_R^* = 0.2$.

With the assumed viscoelastic analysis yielding (4.6.10) and (4.6.11), and with an approximate failure threshhold given by (4.6.12), the cumulative damage postulation gives simply

$$1 = \int_{\dot{\epsilon}_o}^{\dot{\epsilon}(\tau)} \frac{1}{\tau_R(\dot{\epsilon})} \frac{\partial t}{\partial \dot{\epsilon}} d\dot{\epsilon} = \int_{\dot{\epsilon}}^{\dot{\epsilon}(\tau)} \frac{\dot{\epsilon}}{\epsilon_R^*}\left(-\frac{\tau}{\dot{\epsilon}}\right) d\dot{\epsilon} = -\frac{\tau}{\epsilon_R^*}\dot{\epsilon}\Big|_{\dot{\epsilon}_o}^{\dot{\epsilon}(\tau)} \tag{4.6.13}$$

and hence

$$\frac{\epsilon_R^*}{\tau} = \dot{\epsilon}_o - \dot{\epsilon}(\tau) = \dot{\epsilon}_o\left(1 - e^{-\frac{\tau}{\tau}}\right) \tag{4.6.14}$$

so that failure would be anticipated when the initial strain rate $\dot{\epsilon}_o = \epsilon_o/\tau$ duced by the amount ϵ_R^*/τ. For a τ, the characteristic relaxation . . say 1 second and $\epsilon_R^* = 0.2$, failure should occur when the initial strain rate is reduced by 0.2 in/in/sec.

The life is then found to be proportional to the characteristic relaxation time, viz.

$$T = \tau \ln\left[\frac{1}{1-(\epsilon_* \tau)/\dot{\epsilon}_*}\right] \qquad (4.6.15)$$

While certain liberties have been taken in approximating the failure data in order to demonstrate the means of carrying through the estimate of failure time, the steps are believed to affect the results in degree, not in principle. Indeed, given an actual viscoelastic strain analysis, the failure hypothesis could be tested by numerically integrating (4.6.3) using the actual Smith type data for the particular material involved.

There are, however, fundamental points still to be resolved; first, the form of the cumulative damage criterion, and second, its pertinence to combined, rather than solely uniaxial tensile, strain fields. With regard to the first, one might postulate an average value of $t(\dot{\epsilon})/t_R(\dot{\epsilon})$ over the strain rate range $\dot{\epsilon}_*$ to $\hat{\dot{\epsilon}}$ equaling unity. Also S. R. Valluri has suggested as an alternative, a cumulative energy correlation based upon integrations of $\partial\ \partial t(\frac{1}{2}\epsilon^2)$, inasmuch as he observes the Smith data straightens out well on log-log paper when $\epsilon\dot{\epsilon}$ is plotted versus t_R.

While it is too early to make definitive statements regarding the application of cumulative damage concepts to elastomers, certain initial experiments have not disproved its applicability. L. D. Stimpson has performed one set of preliminary unpublished tests using polyurethane tensile specimens at the Jet Propulsion Laboratory in the following way. Suppose two different samples are strained to failure at constant strain rate, one at a higher rate than the other (see inserts).

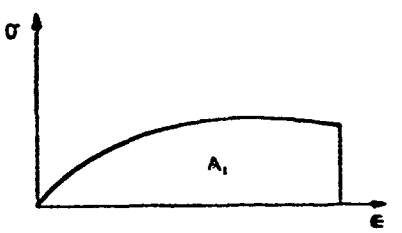

LOWER RATE = R_1

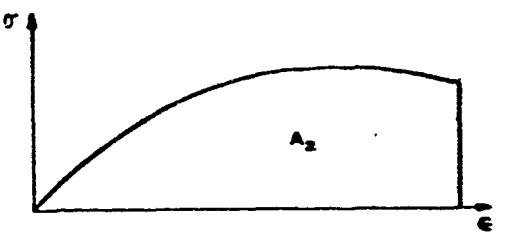

HIGHER RATE = R_2

Now suppose instead that the first sample had been strained on the Instron testing machine at its rate, R_1, only part way and then strained the remainder of the way at the higher rate, R_2, as follows.

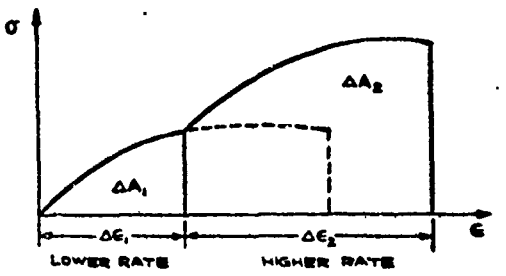

Linear accumulation based on strains then would be

$$\frac{\Delta\epsilon_1}{\epsilon_1} + \frac{\Delta\epsilon_2}{\epsilon_2} = 1 \qquad (4.6.16)$$

whereas based on energy $= \int \sigma d\epsilon$ = areas under curves would give

$$\frac{\Delta A_1}{A_1} + \frac{\Delta A_2}{A_2} = \frac{\int_0^{\Delta\epsilon_1} \sigma d\epsilon}{\int_0^{\epsilon_1} \sigma d\epsilon} + \frac{\int_{\Delta\epsilon_1}^{\Delta\epsilon_1+\Delta\epsilon_2} \sigma d\epsilon}{\int_{\epsilon_1}^{\epsilon_1+\epsilon_2} \sigma d\epsilon} = 1 \qquad (4.6.17)$$

In order to examine the extent of correlation on either of these two bases, several samples have been run at various strain-rates and some have been run with mid-path changes in strain-rate. Figure 4.29 is a typical run in which three different strain-rates were used.

In spite of the few tests made with noticeable scatter in the results and certain shortcomings in the technique of changing rate, the results show that accumulation based on either strain or energy appears feasible. It is felt that there will be more means for determining the best basis of accumulation at strain-rates higher than feasible on Instron equipment. Runs at lower temperatures and moderate rates on an Instron may also produce a similar result. Certainly many more runs need to be made in order to account for the statistical variation in propellant specimens.

Table 4.3 presents the results from some of the preliminary tests showing the values obtained upon accumulation based on strain and energy. A value of unity represents an accurate cumulative result, whereas spreads of values

are due, in part, to sample variation. A slight bias above unity seems to exist and has been found to be even larger in the latest runs which suggests non-linear accumulation may be more accurate. Roughly speaking, the initial sample variations are at most about ± 10% whereas the cumulative spreads are about ±20%. The actual standard deviations are shown and about double in the cumulative process. This increase in spread is expected and corresponds with that found in metal fatigue tests.

In order to make Table 4.3 more understandable, consider the first accumulation run, no. 1878. Preliminary tests made separately at 74% strain/min and at 7.4% strain/min all the way to failure resulted in mean values for strain to break of 64% and 41%, respectively. In run no. 1878 a specimen was strained at the first rate until it had reached 32% elongation or half its potential strain. Then it was continued at the second (lower) rate until break which was an additional 24.5% elongation (based on original length). Performing the accumulation based on strain,

$$\frac{32\%}{64\%} + \frac{24.5\%}{41\%} = 1.10 \qquad (4.6.18)$$

which appears under the total accumulation column. The energy accumulation was performed in a similar way with 53% of the potential energy occurring during the first strain-rate and 49% during the second (based on total energies at the respective constant rates from previous tests taken all the way to break). These energy percentages are tabulated immediately below the strain-rates in the table.

In another separate series of unpublished tests, McCullough of The Thiokol Chemical Corp. has essentially repeated the experiment using a polyisobutylene-acrylic acid propellant. His degree of correlation has also been encouraging although not conclusive. He obtained 15 to 20 percent deviation when predicting mixed rate results from constant rate data, with the standard deviation being somewhat smaller for a strain rather than energy correlation.

Should subsequent experiments establish that some sort of cumulative damage hypothesis has quantitative merit in simple examples, it would then be appropriate to attempt requirements in the form of non-linear accumulation, variable temperature situations, and combined stress or strain fields.

TABLE 4.3. CUMULATIVE DAMAGE

Run No.	Strain Rates (in/in/min) % Accumulated at each S. R. (Energy Basis) 1st	2nd	3rd	4th	Total Accumulation Strain Basis	Energy Basis	Standard Deviations Energy Basis	Initial Data
1878	.74	.074						
	53	49			1.10	1.02		
1879	.074	.74						
	46	51			.97	.97		
1880	.74	.074						
	51	36			.88	.87		
1881	.074	.74						
	43	85			1.38	1.28	0.14	0.07
1882	.74	.074						
	20	66			.84	.86		
1883	.074	.74						
	14	83			.99	.97		
1884	.74	.074						
	19	77			.97	.96		
1955	.037	.37						
	41	64			1.11	1.05		
1956	.037	.37						
	42	68			1.14	1.10		
1957	.37	3.7						
	53	30			.79	.83		
1958	.37	3.7						
	41	72			1.41	1.24	0.18	0.08
1959	.037	3.7						
	19	105			1.21	1.13		
1960	.037	3.7						
	13	64			.78	.77		

TABLE 4.3 CUMULATIVE DAMAGE (continued)

Run No.	Strain Rate (in/in/min) % Accumulated at each S.R. (Energy Basis) 1st	2nd	3rd	4th	Total Accumulation Strain Basis	Energy Basis	Standard Deviations Energy Basis	Initial Data
1961	.037	.37	3.7					
	14	30	70		1.20	1.14		
1962	.037	.37	3.7					
	13	31	54		1.02	.98		
1963	.037	.37	3.7				0.11	0.08
	28	50	34		1.09	1.12		
1964	.037	.37	3.7					
	44	32	27		.97	1.03		
2093	.0074	.074	.74					
	19	27	54			12		
2094	.0074	.074	.74					
	11	30	67			1.08		
2095	.0074	.074	.74					
	23	48	59			1.22		
2096	.0074	.074	.74					
	17	48	63			1.18		
2097	.0074	.074	.74	7.4			0.17	0.07
	5	8	19	87		1.19		
2098	.0074	.074	.74	7.4				
	3	7	18	101		1.29		
2099	.0074	.074	.74	7.4				
	1	6	21	81		1.09		
2100	.0074	.074	.74	7.4				
	8	9	19	77		1.13		

REFERENCES

4.1 Knauss, W.G.: Displacements in a Finite Hollow Cylinder Under Axial Acceleration. GALCIT SM 60-17, California Institute of Technology. September 1960 (rev. January 1961).

4.2 Williams, M.L.: Mechanical Properties and the Design of Solid Propellant Motors. Progress in Astronautics and Rocketry, Vol. 1, Academic Press, Inc., New York, September 1960, p. 67.

4.3 Lianis, G.: Stresses and Strains in Solid Propellants During Storage. American Rocket Society, Paper No. 1592-61, February 1961.

4.4 Nadai, A.: Theory of Flow and Fracture of Solids. p. 175, McGraw-Hill Book Company, Inc. 1950.

4.5 Mises, R.V.: Die Differential und Integral-Gleichungen der Mechanik and Physik, Vol. 2, p. 605, 1927.

4.6 Hencky, H.; Angew, Z.: Math. Mechanick, Vol. 4, p. 323, 1924.

4.7 Haigh, B.P.: Engineering, Vol. 190, p. 158, 1920.

4.8 Rivlin, R.S.; Thomas, A.G.: Rupture of Rubber. I. Characteristic Energy for Tearing. Journal of Polymer Science, Vol. 10, no. 3, p. 291, 1953.

4.9 Rivlin, R.S.: Philosophical Transactions, A 240, pp. 459, 491, 509, (1948)

4.10 Treloar, L.R.: Physics of Rubber Elasticity. 2, Oxford, 1953.

4.11 Martin, G.M.; Roth, F.L.; Stiehler, R.D.: Journal of Research of the National Bureau of Standards, December 1958.

4.12 Treloar, L.R.: Physics of Rubber Elasticity. Chapter IV, 1953.

4.13 Jaeger, J.C.: Elasticity Fracture and Flow, p. 65, Methuen, 1956.

4.14 Green, A.E.; Zerna, W.: Theoretical Elasticity. Chapter V, Oxford, 1956.

4.15 Williams, M.L.; Landel, R.F.; Ferry, J.D.: The Temperature Dependence of Relaxation Mechanisms in Amorphous Polymers and Other Glass-Forming Liquids. Journal of American Chemical Society, Vol. 77, pp 3701-3707, 1955.

4.16 Williams, M.L.: Structural Problems in Solid Propellant Motor Design. GALCIT SM 60-24, California Institute of Technology. AGARD meeting, Paris, France, February 1961.

4.17 Brettschneider, H.; Dale, W.: Experience with the Alinco High Rate Tensile Tester. Bulletin of 17th Meeting of JANAF Physical Properties Panel, p. 43, May 1958.

4.18 Jones, J.: Tensile Testing of Elastomers at Ultra High Strain Rates. Presented at High Rate Symposium, Boston, Massachusetts, January 1960.

4.19 Gent, A.N.; Lindley, P.B.: Compression of Bonded Rubber Blocks. Publication No. 324, Journal of British Rubber Producer's Association, Vol. 173, p. 111, 1959.

4.20 Gent, A.N.; Lindley, P.B.: Internal Rupture of Bonded Rubber Cylinder in Tension. Proceedings of Royal Society, A. Vol. 249, p. 195, 1959.

4.21 Fitzgerald, J.E.: A Biaxial Test for Solid Propellants. Bulletin of 19th Meeting of JANAF Physical Properties Panel, September 1960.

4.22 Timoshenko, S.; Goodier, J.N.: Theory of Elasticity. McGraw-Hill Book Company, Inc., New York, 1951.

4.23 Dowler, W.; Lewis, C.; Stimpson, L.D.: Torsion Testing of Solid Propellants. Bulletin of 18th Meeting of JANAF Physical Properties Panel, p. 27, June 1959.

4.24 Bergen, N.; Messersmith, W.; Rivlin, R.S.: The Stress Relation for Biaxial Deformation of Filled High-Polymers. ASME Meeting, New York City, December 1959.

4.25 Ordahl, D.D.: Burst Tests on Solid Propellants. (NOTS Burst Test) Bulletin of 8th Meeting of JANAF Physical Properties Panel, p. 7, July 1953.

4.26 Griffith, A.A.: The Phenomena of Rupture and Flow in Solids. Philosophical Transactions of the Royal Society (London), Series A, Vol. 221, pp 163-198, 1921. See also: The Theory of Rupture. Proceedings of the First International Congress for Applied Mechanics, pp. 55-63, 1924.

4.27 Inglis, C.E.: Stresses in a Plate Due to the Presence of Cracks and Sharp Corners. Transactions of the Institute of Naval Architects (London), Vol. LV, pp. 219-230, 1913.

4.28 Ang, D.D.; Williams, M.L.: Combined Stresses in an Orthotropic Plate Having a Finite Crack. GALCIT SM 60-1, California Institute of Technology, January 1960. (To be published in Journal of Applied Mechanics)

4.29 Williams, M.L.: On the Stress Distribution at the Base of a Stationary Crack. Journal of Applied Mechanics, March 1957.

4.30 Greensmith, H.W.: Rupture of Rubber. VII. Effect of Rate of Extension in Tensile Tests. Journal of Applied Polymer Science, Vol. 3, no. 8, p. 175, 1960.

4.31 Greensmith, H.W.: Rupture of Rubber. VIII. Comparison of Tear and Tensile Rupture Measurements. Journal of Applied Polymer Science, Vol. 3, no. 8, p. 183, 1960.

4.32 Blatz, P.J.: Finite Elastic Analysis of the Deformation of a Wedge-Shaped Crack. GALCIT SM 60-9, California Institute of Technology, June 1960.

4.33 Williams, M.L.: Stress Distribution for an Externally Cracked Plate in Tension. GALCIT SM 60-23, California Institute of Technology, Nov. 1960.

4.34 Knowles, J.K.; Wang, N.M.: On the Bending of an Elastic Plate Containing a Crack. GALCIT SM 60-11, California Institute of Technology, July 1960. (Journal of Mathematics and Physics, January 1961)

4.35 Thomas, A.G.: Rupture of Rubber. II. The Strain Concentration at an Incision. Journal of Polymer Science, Vol. 18, p. 177, 1955.

4.36 Greensmith, H. W.; Thomas, A.G.: Rupture of Rubber. III. Determination of Tear Properties. Journal of Polymer Science, Vol. 18, p. 189, 1955.

4.37 Greensmith, H. W.: Rupture of Rubber. IV. Tear Properties of Vulcanizates Containing Carbon Black. Journal of Polymer Science, Vol. 21, p. 175, 1956.

4.38 Thomas, A.G.: Rupture of Rubber. VI. Further Experiments on the Tear Criterion. Journal of Polymer Science, Vol. 3, no. 8, p. 168, 1960.

4.39 Braden, M.; Gent, A.N.: The Attack of Ozone on Stretched Rubber Vulcanizates. I. The Rate of Cut Growth. Journal of Applied Polymer Science, Vol. 3, no. 7, p. 90, 1960.

4.40 Braden, M.; Gent, A.N.: The Attack of Ozone on Stretched Rubber Vulcanizates. II. Conditions for Cut Growth. Journal of Applied Polymer Science, Vol. 3, no. 7, p. 100, 1960.

4.41 Williams, M.L.: Discussion of: "Analysis of Stresses and Strains Near the End of a Crack Traversing a Plate (Journal of Applied Mechanics, Sept. 1957, by G.R. Irwin)". Journal of Applied Mechanics, Vol. 25, no. 2, p. 299, June 1958.

4.42 McCullough, J.: Studies on Velocity of Crack Propagation. Internal Report to Chemistry Department, Thiokol Chemical Corporation, Redstone Division, Huntsville, Alabama, September 1959.

4.43 Bridgeman, P.W.: Physics of High Pressure. Bell and Sons Ltd., London, 1958.

4.44 Miner, M.A.: Cumulative Damage in Fatigue. Journal of Applied Mechanics, pp. A-159-164, September 1945.

4.45 Freudenthal, A.M.; Heller, R.A.: Cumulative Fatigue Damage of Aircraft Structural Materials. Part 2: 2024 and 7075 Aluminum Alloy Additional Data and Evaluation. Columbia University WADC TN 55-273, October 1956.

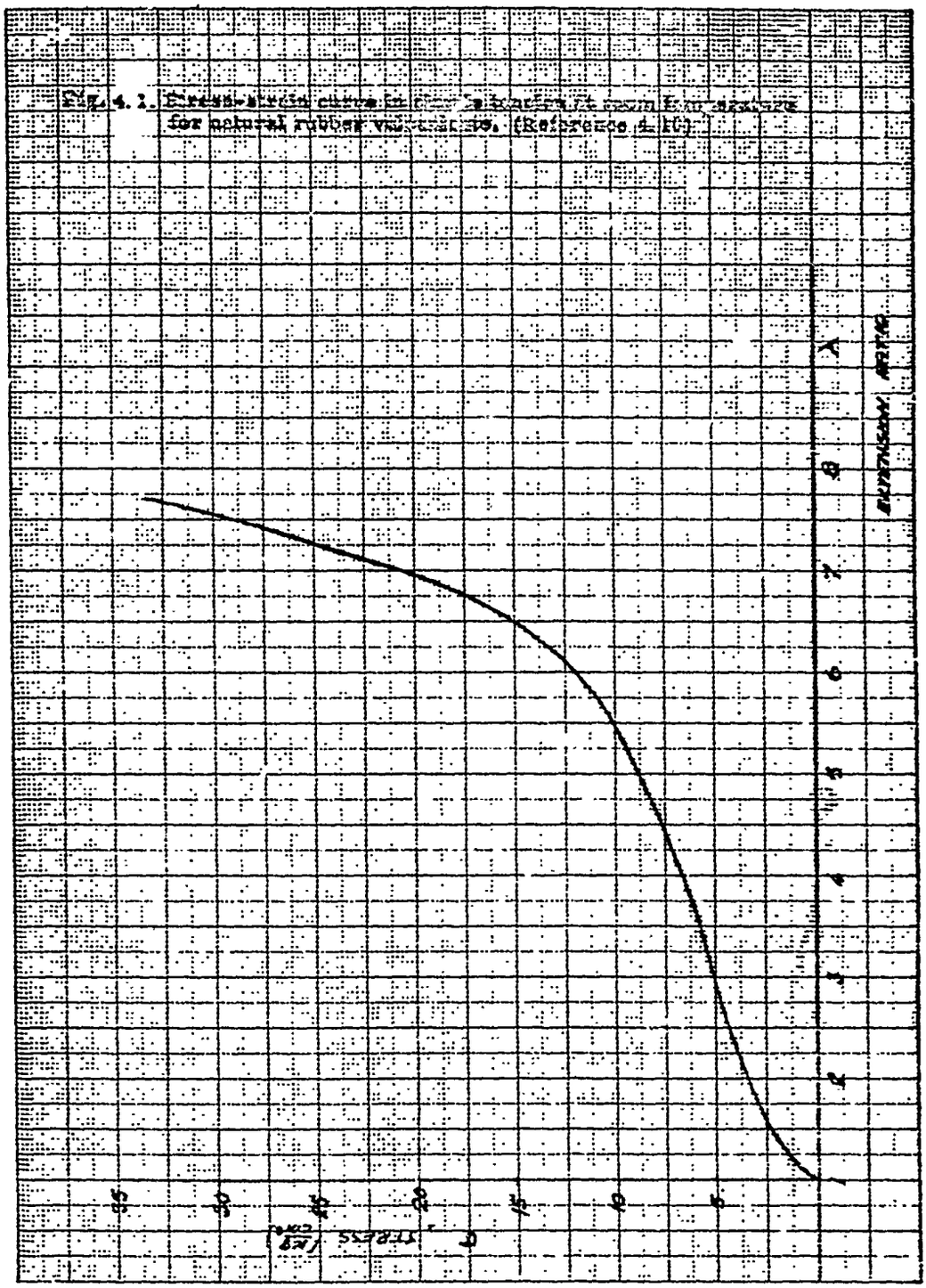

Fig. 4.1. Stress-strain curve for [illegible] for natural rubber vulcanizate. (Reference 4.10)

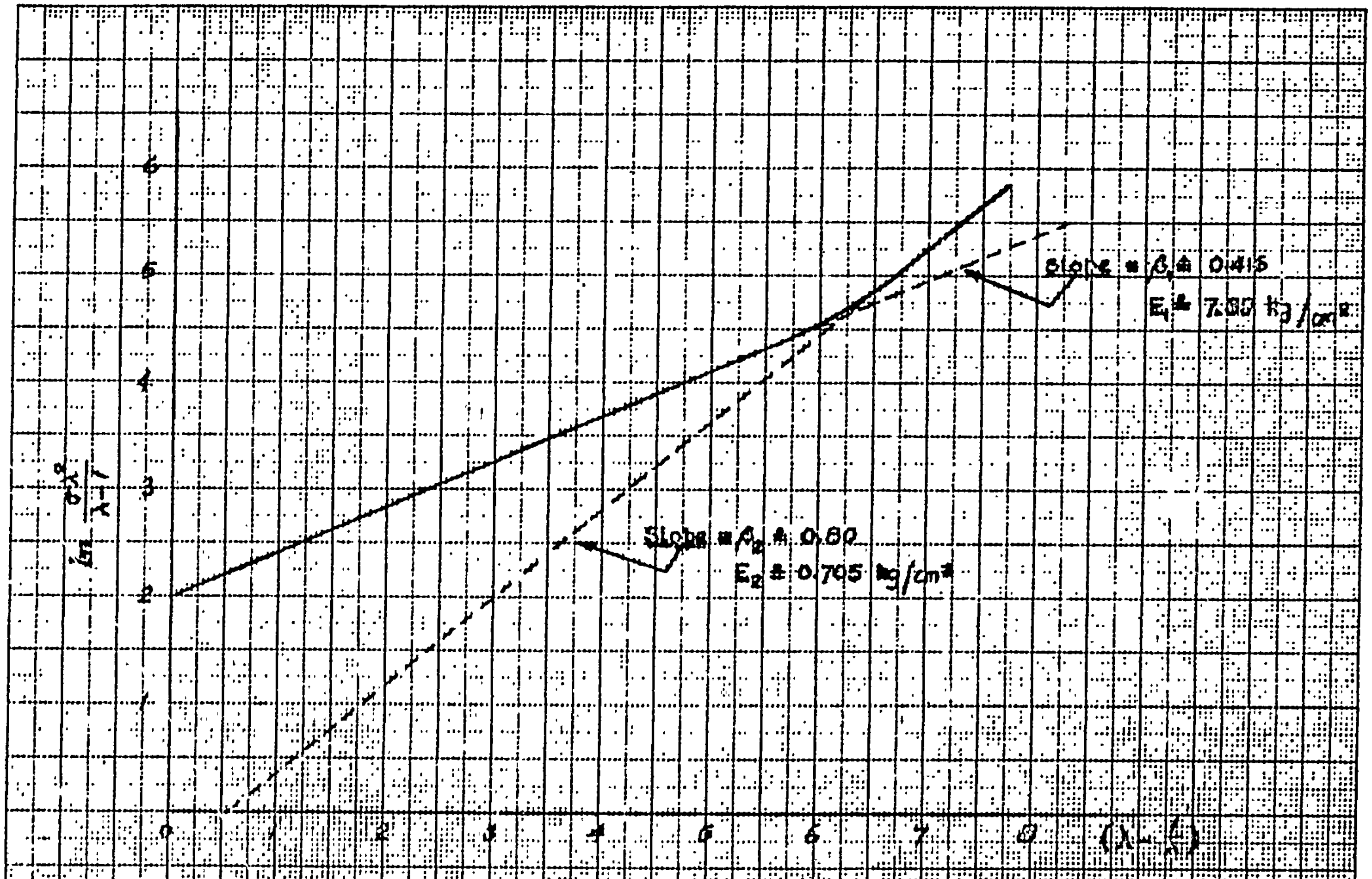

Fig. 4.2. Rectified stress-strain curve from Roth, Metz, Stiehler correlation (Reference 4.11).

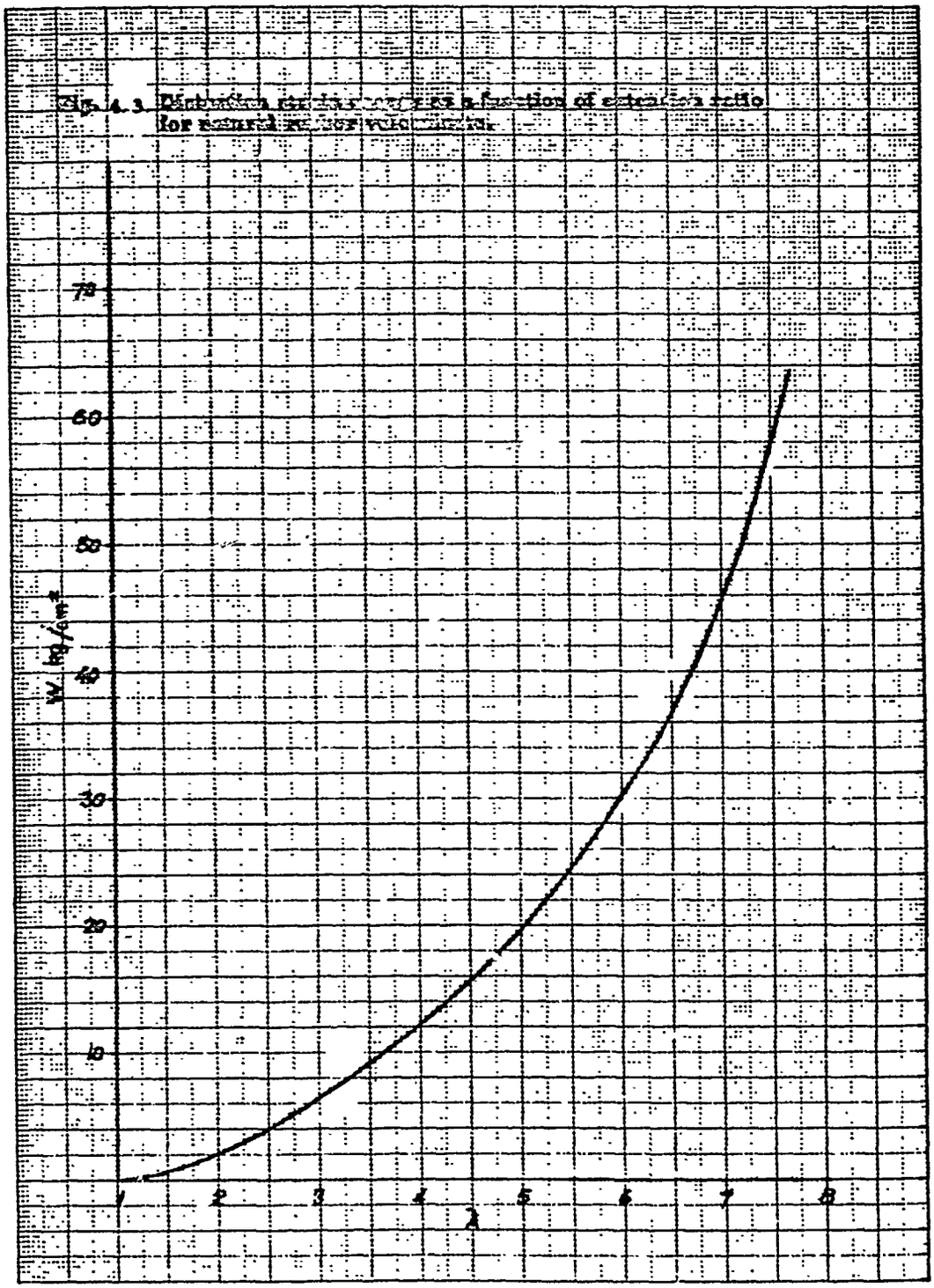

Fig. 4.3. Distribution [illegible] as a function of extension ratio for natural [illegible]

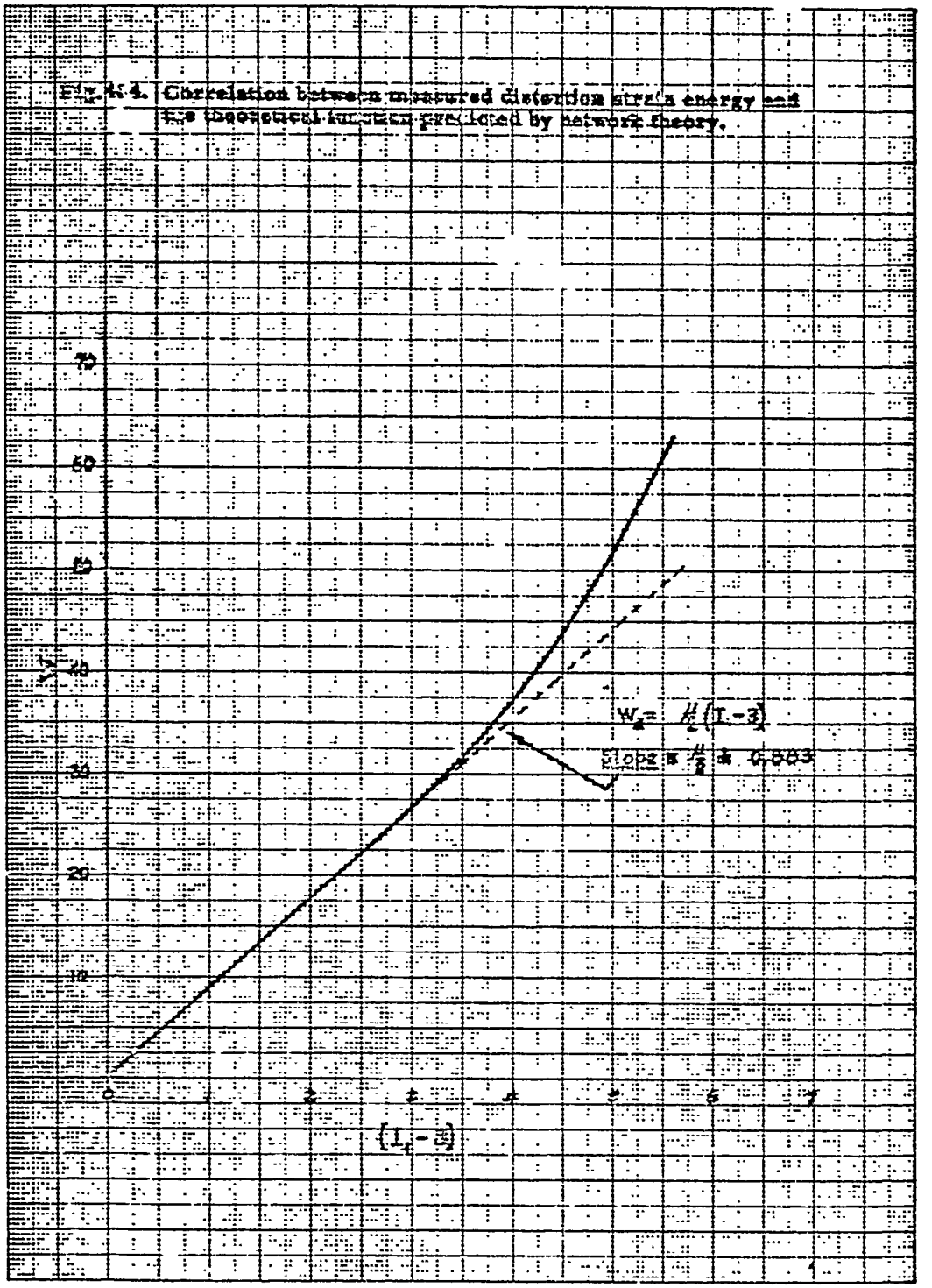

Fig. 4.4. Correlation between measured distortion strain energy and the theoretical values predicted by network theory.

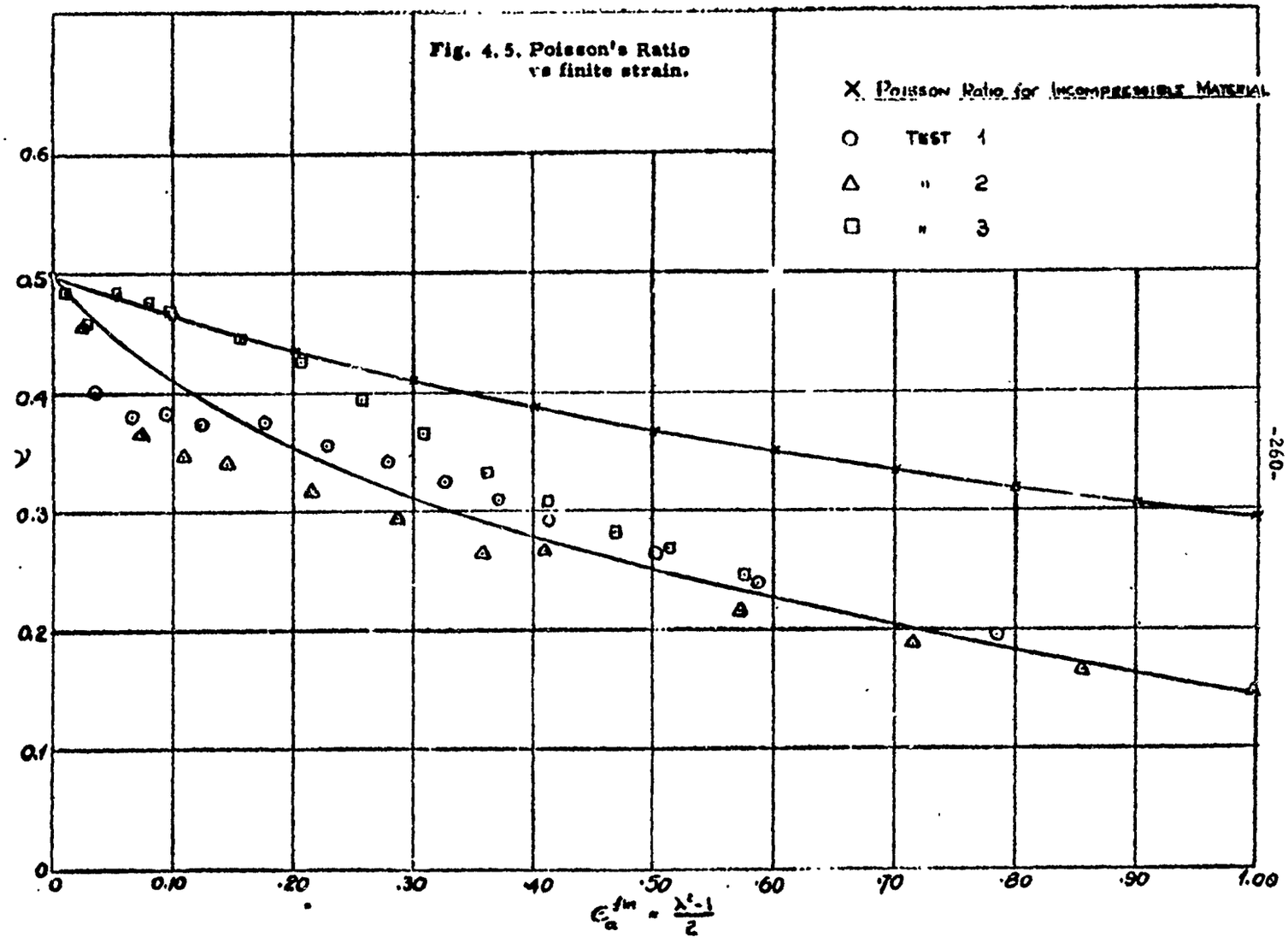

Fig. 4.5. Poisson's Ratio vs finite strain.

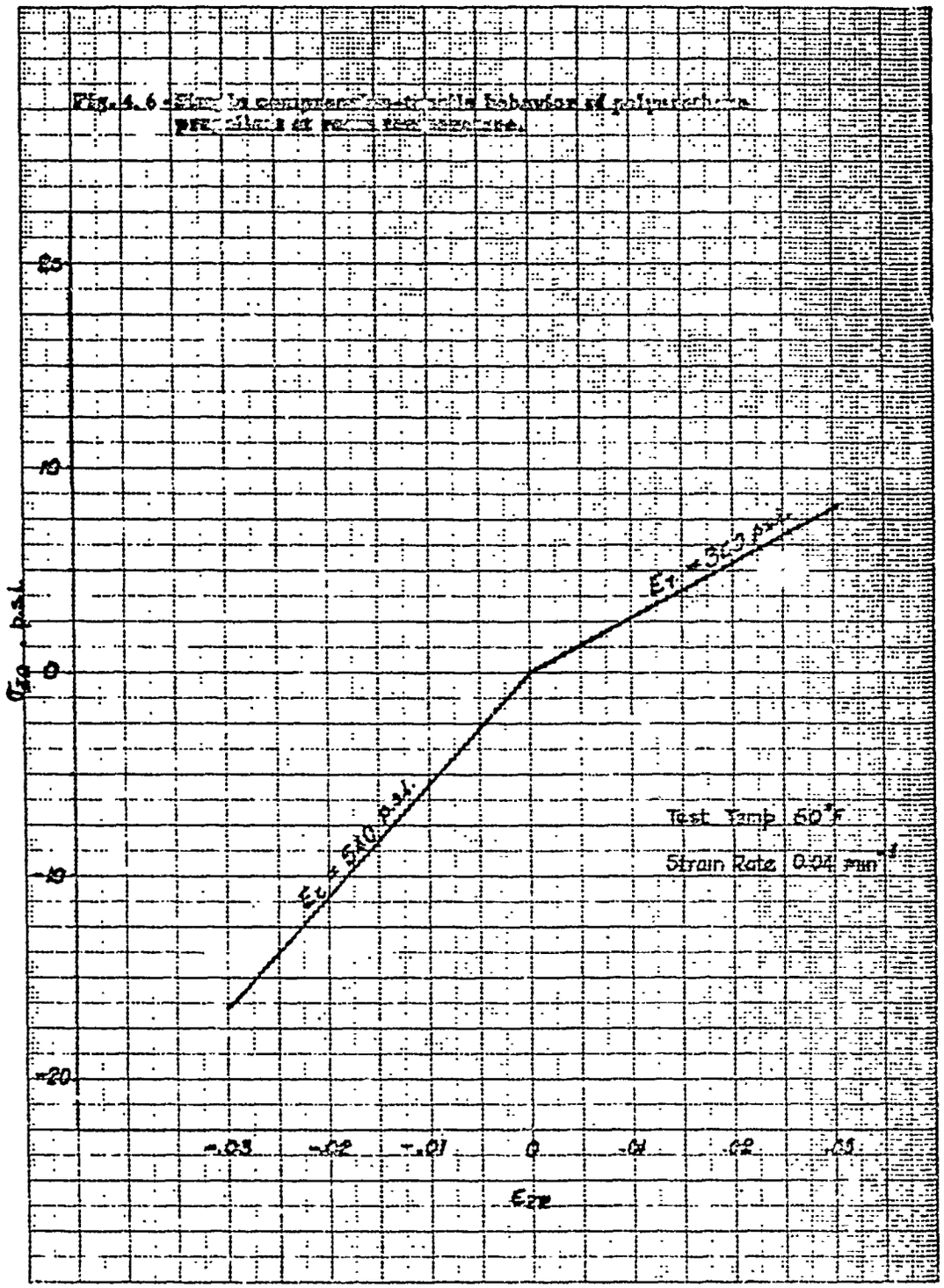

Fig. 4.6 - Stress-strain material behavior of polymer-base propellant at room temperature.

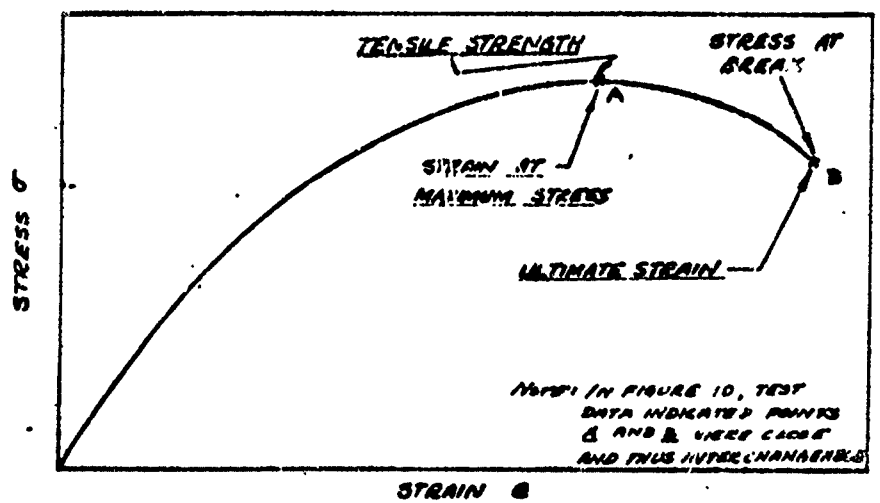

Fig.4.7- Typical Instron tensile curve.

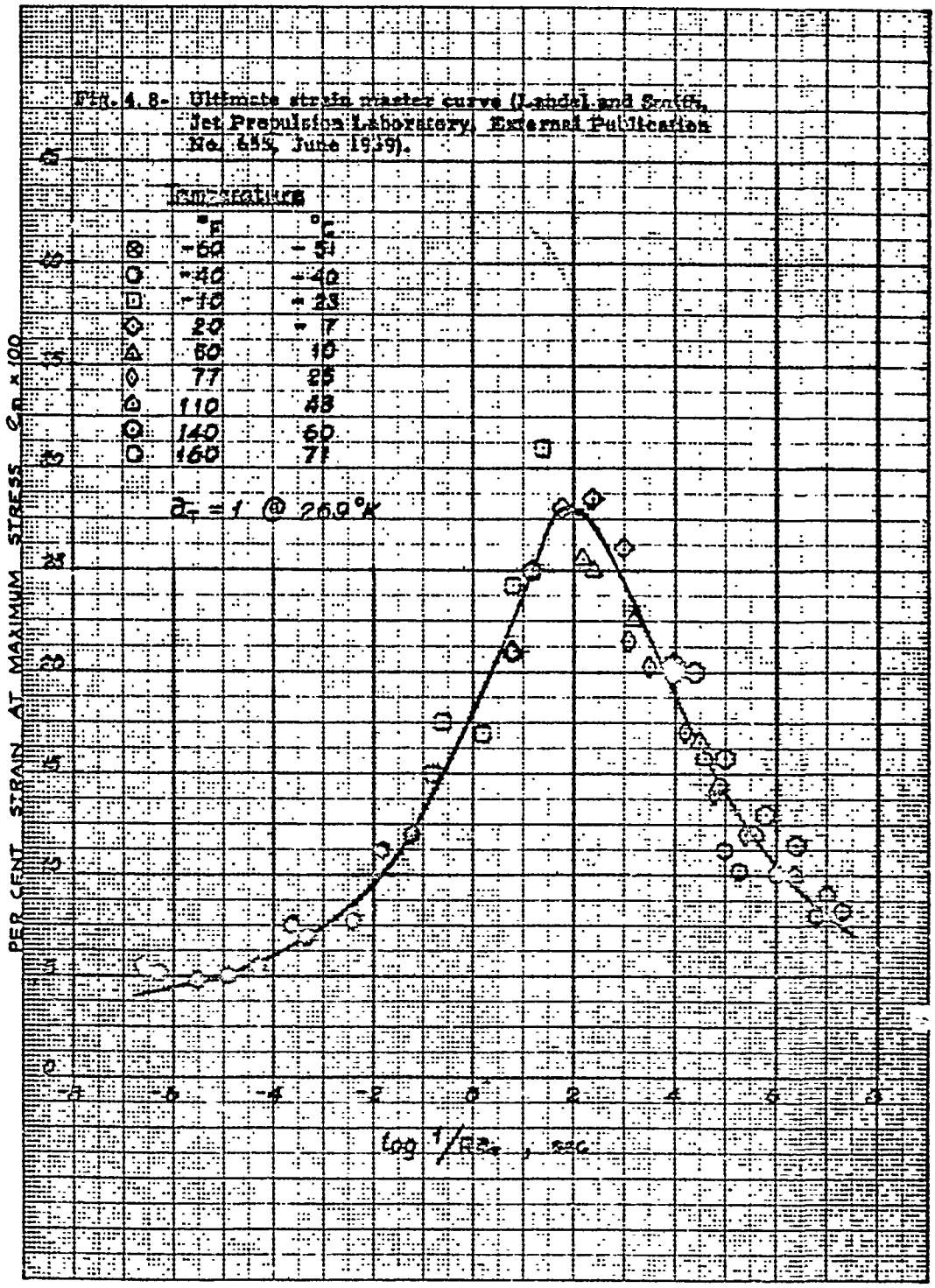

Fig. 4.8- Ultimate strain master curve (Landel and Smith, Jet Propulsion Laboratory, External Publication No. 455, June 1959).

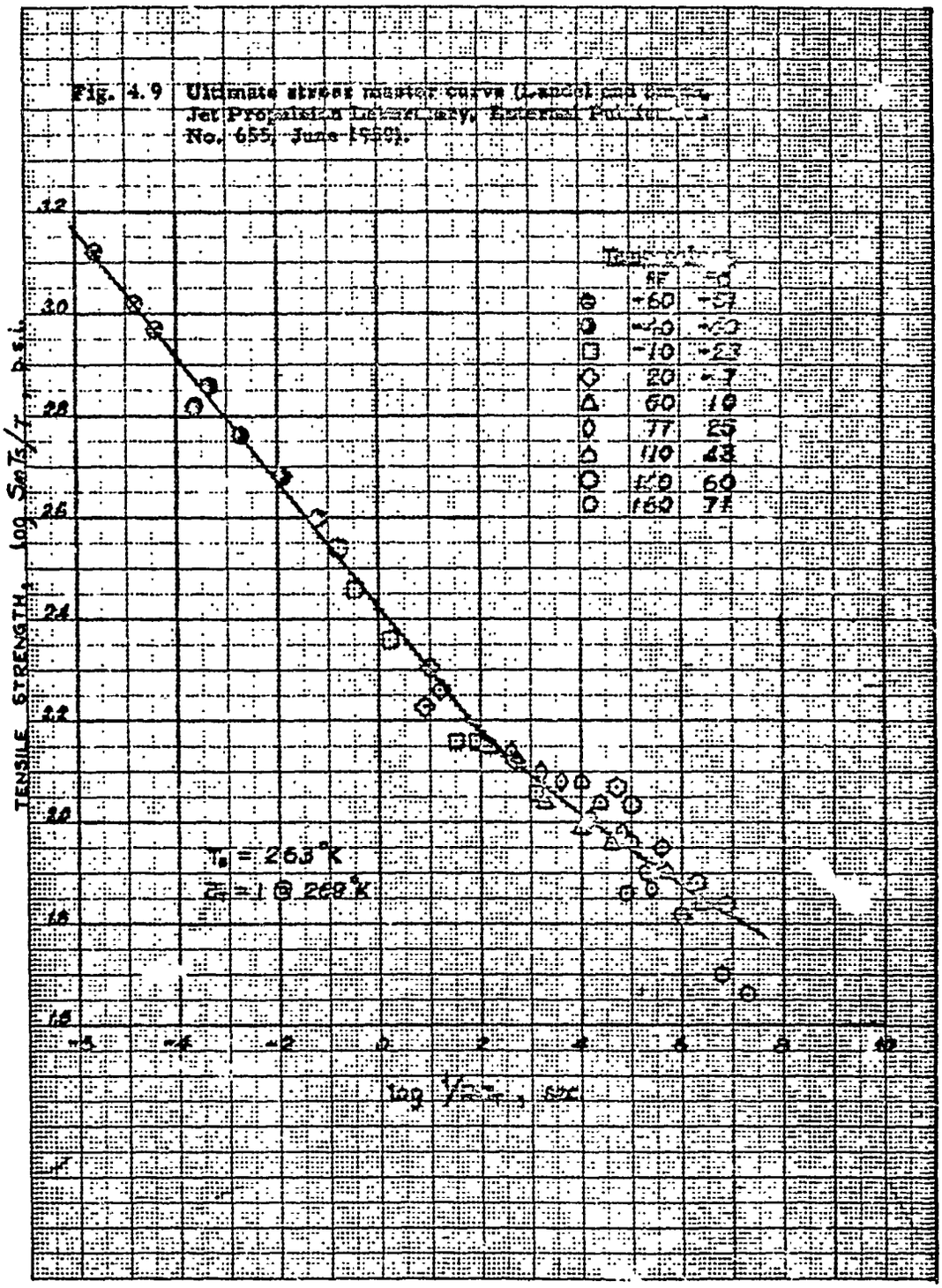

Fig. 4.9 Ultimate strength master curve (Lappel and [illegible] Jet Propulsion Laboratory, External Publication No. 655, June 1960).

Fig. 4.10 - Triaxial fracture data (Reference 20), for various compositions

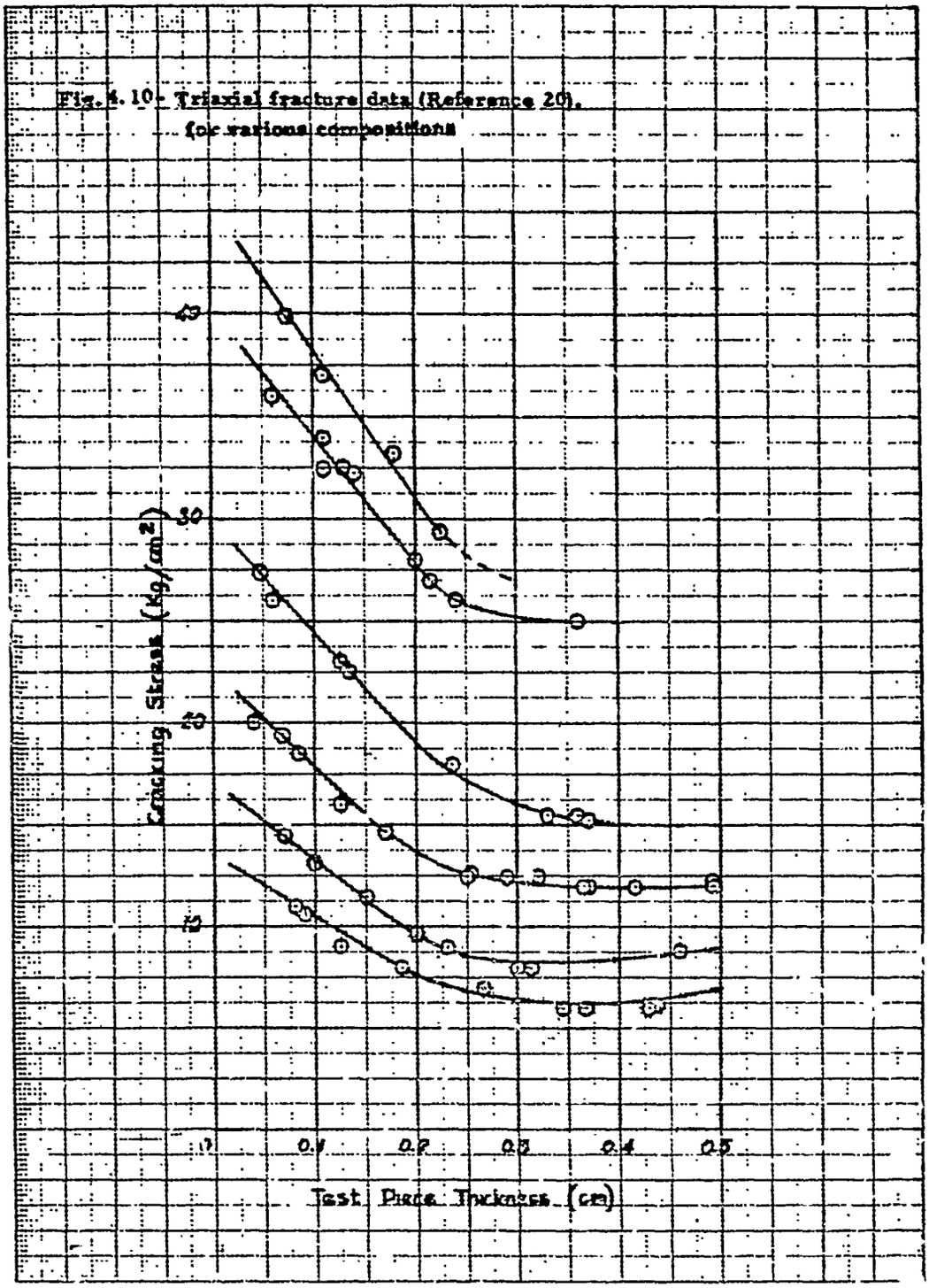

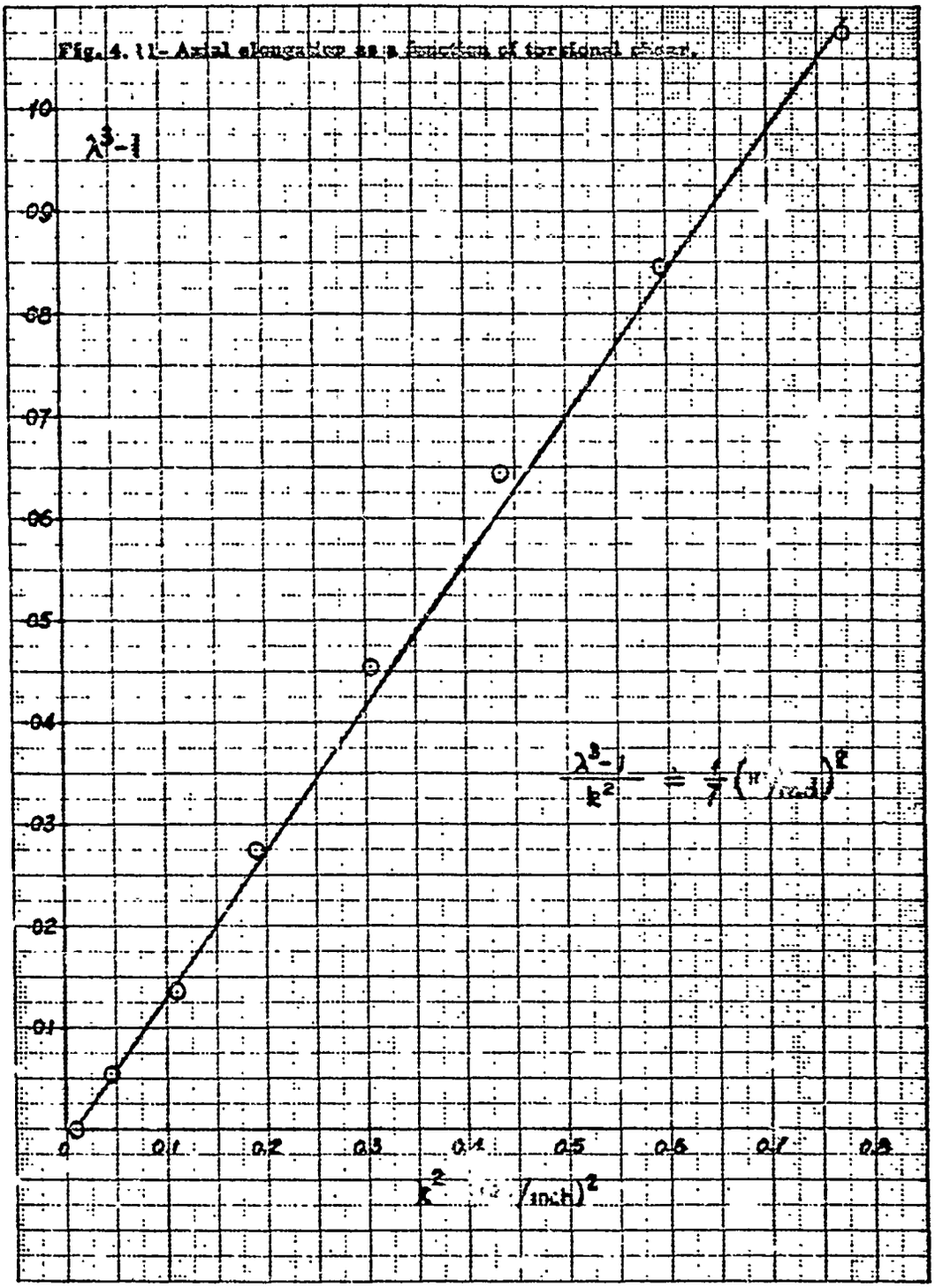

Fig. 4.11- Axial elongation as a function of torsional shear.

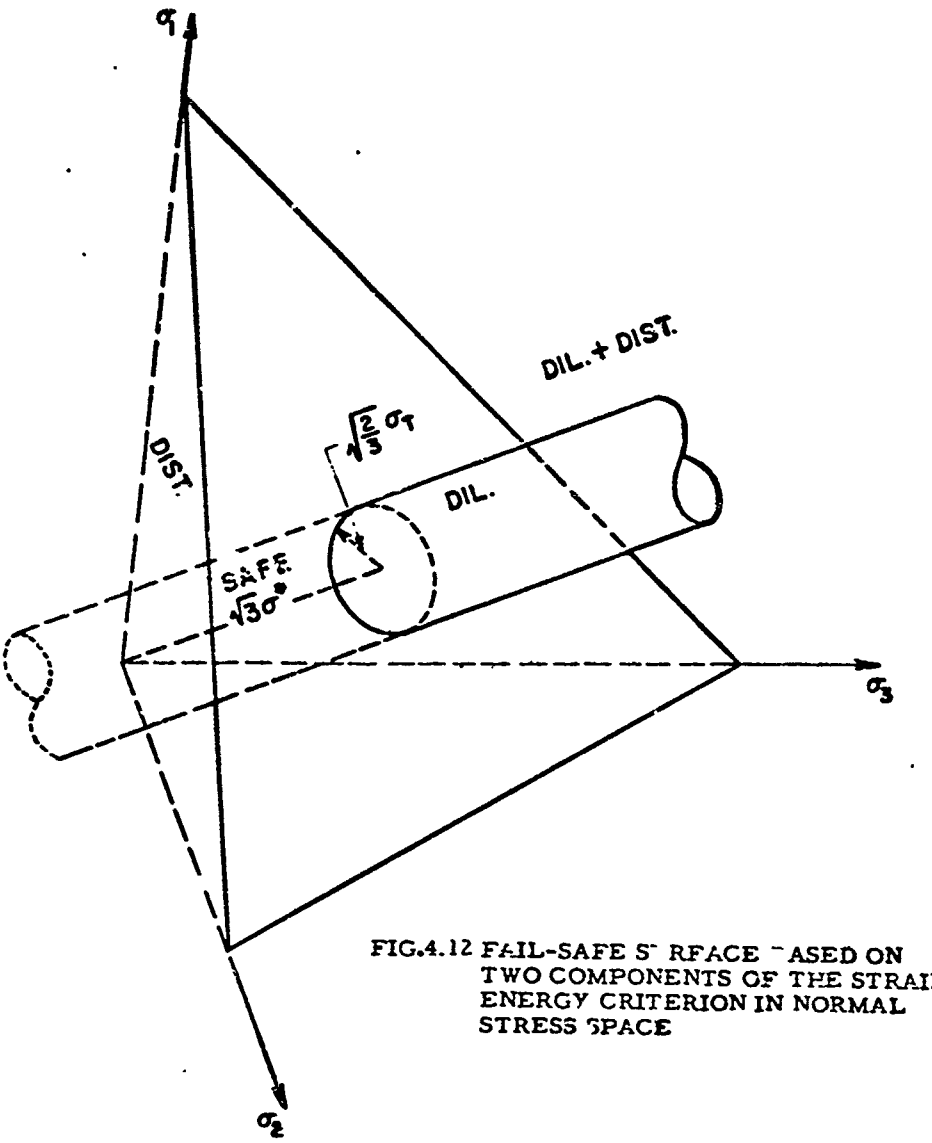

FIG.4.12 FAIL-SAFE SURFACE BASED ON TWO COMPONENTS OF THE STRAIN-ENERGY CRITERION IN NORMAL STRESS SPACE

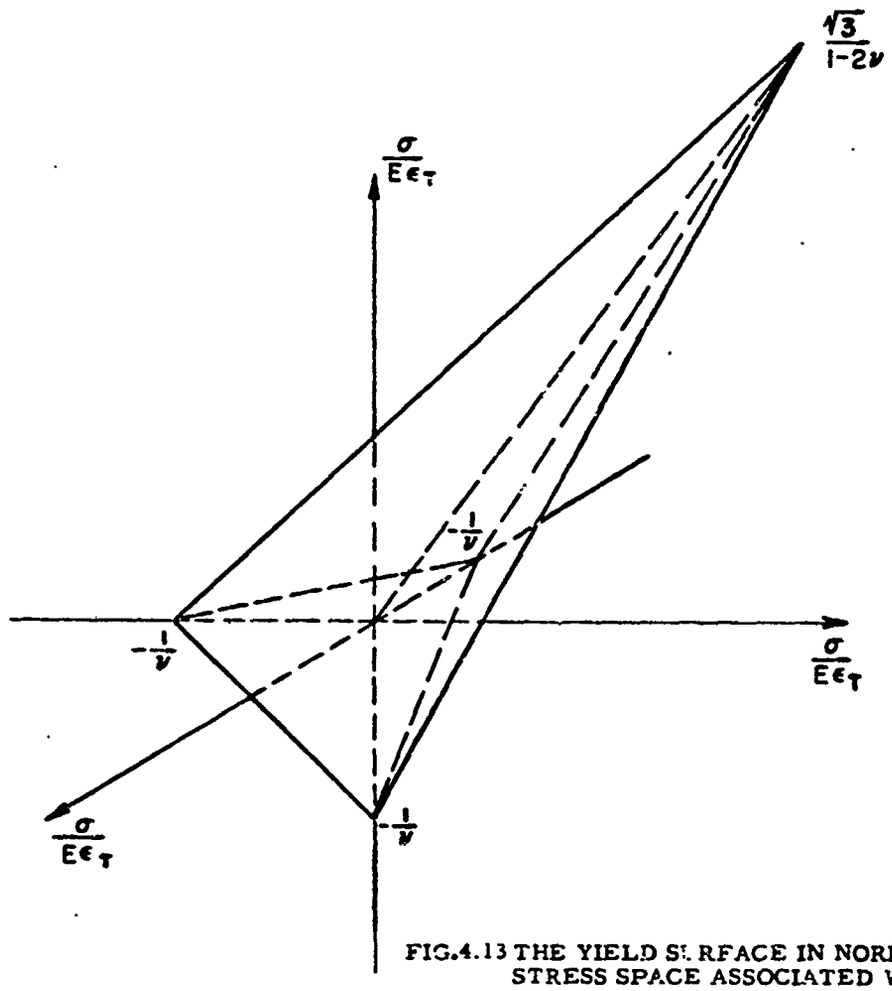

FIG.4.13 THE YIELD SURFACE IN NORMAL STRESS SPACE ASSOCIATED WITH THE MAXIMUM PRINCIPAL STRAIN FAILURE CRITERION

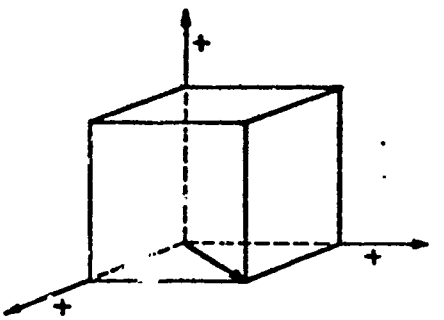

Fig. 4.14 - Biaxial tension

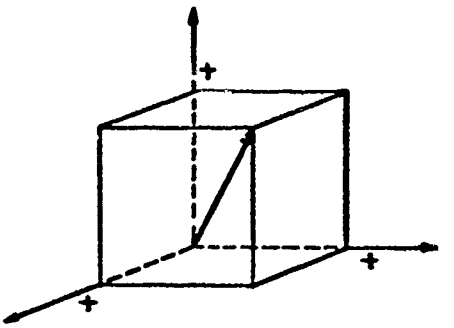

Fig. 4.15 - Hydrostatic tension

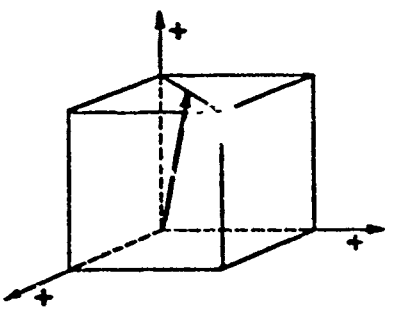

Fig. 4.16 - Parallel-plate tension

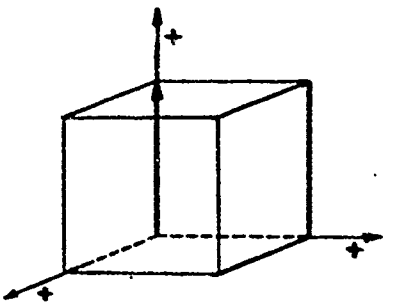

Fig. 4.17 - Simple tension

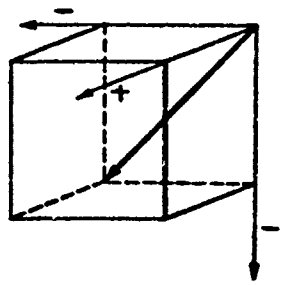

Fig. 4.18 - Biaxial compression

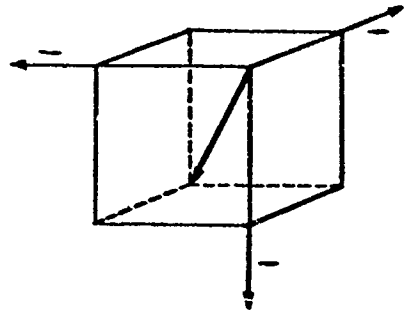

Fig. 4.19 - Hydrostatic compression

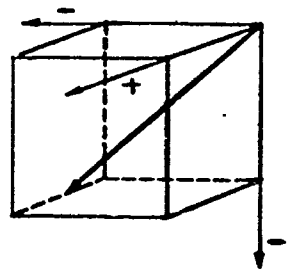

Fig. 4.20- Simple tension, hydrostatic compression, superimposed

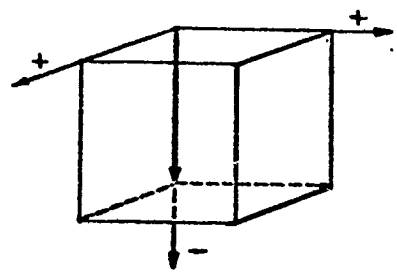

Fig. 4.21- Simple compression

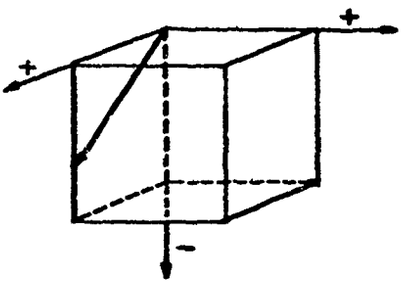

Fig. 4.22- Mixed tension - compression

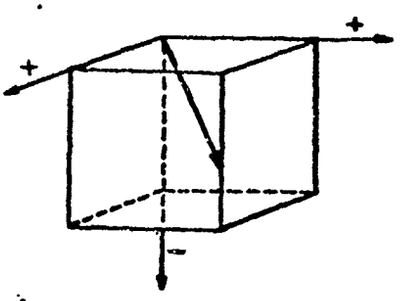

Fig. 4.23- Torsion and stretch combined

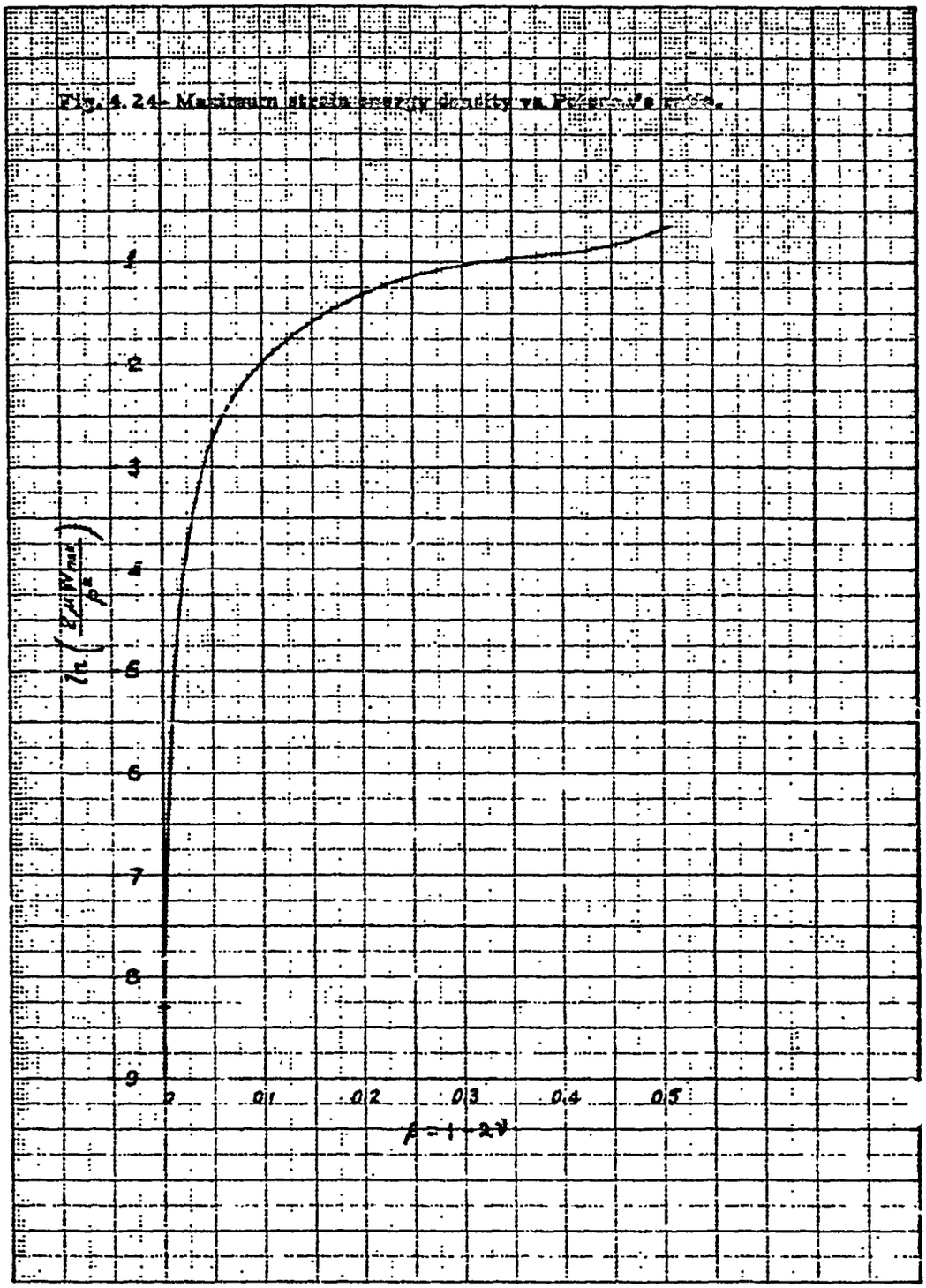

Fig. 4.24- Maximum strain energy density vs Poisson's ratio.

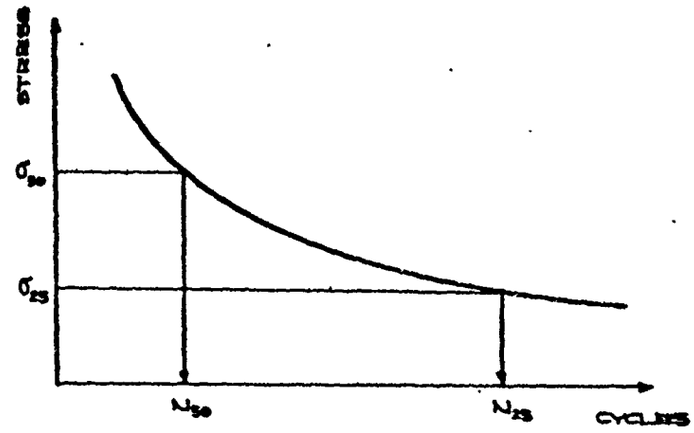

FIG. 4.25. S-N FATIGUE CURVE

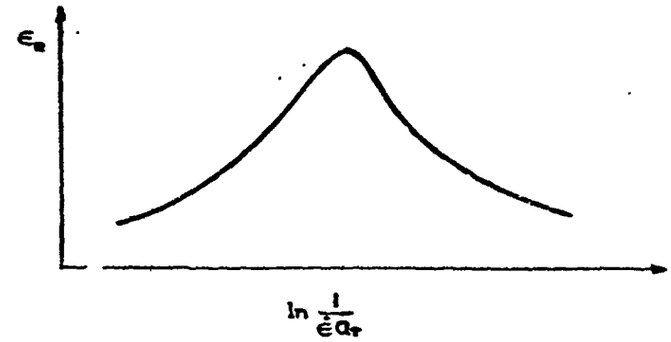

FIG. 4.26. SMITH FAILURE CURVE FOR POLYMERS
REF : JPL MEMORANDUM NO. 20-178

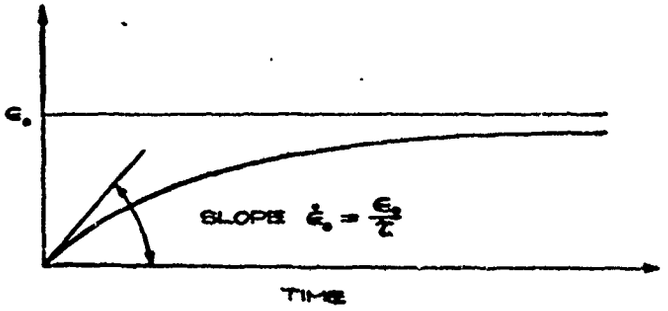

FIG. 4.27 CREEP CURVE

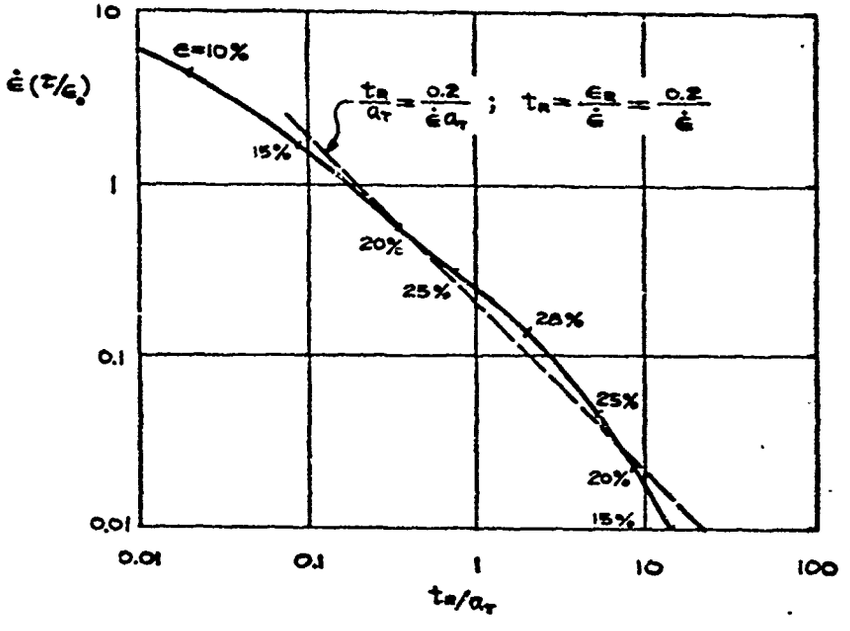

FIG. 4.28. MODIFIED SMITH CURVE

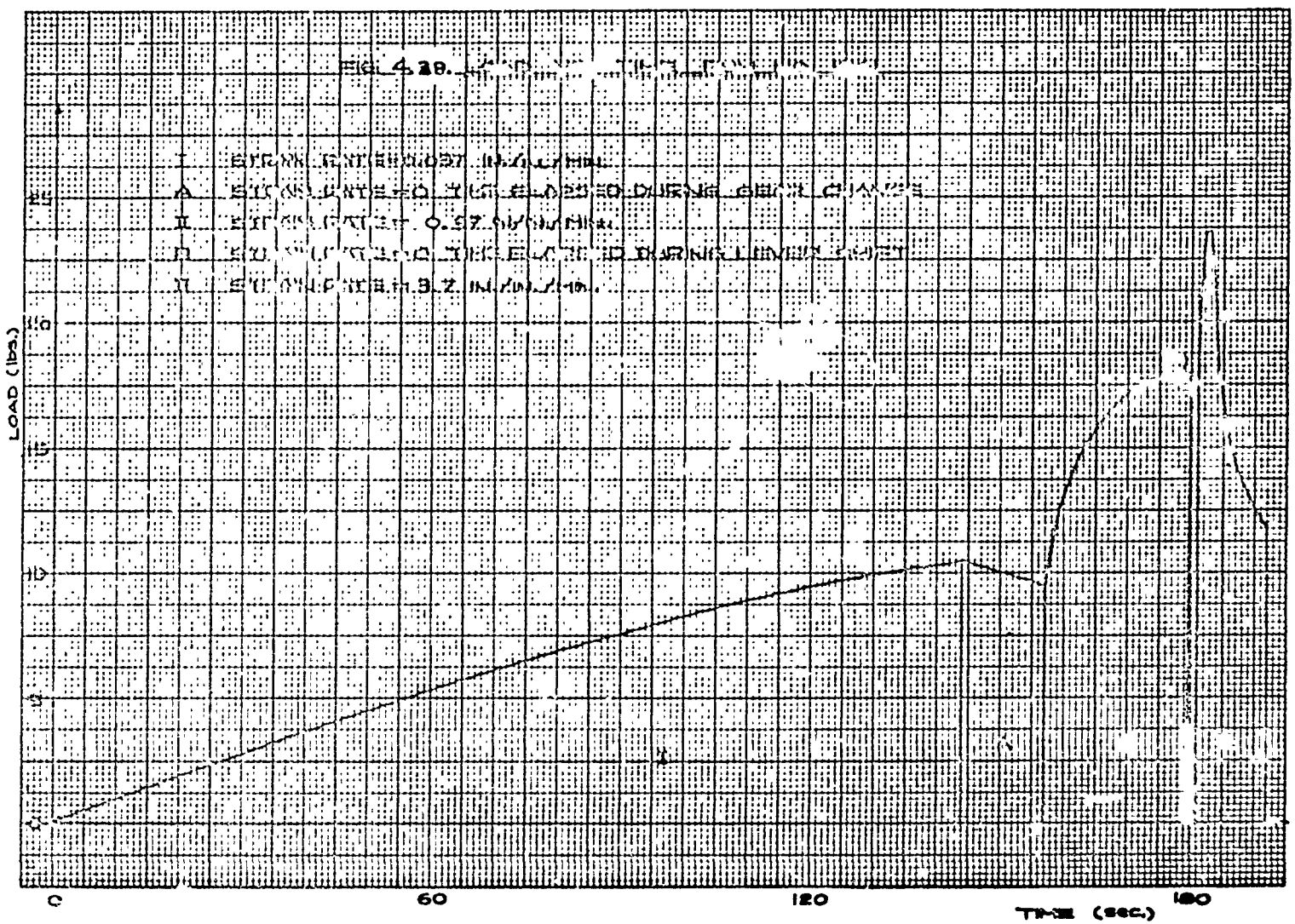
LOAD (lbs.)
0
60
120
180
TIME (sec.)

APPENDICES

I. Stress Analysis of a Thin Clamped Disk

II. Crack Propagation in Viscoelastic Media

III. Large Plane Strain Analysis for Distortion Energy in a Hollow Tube

APPENDIX I

Stress Analysis of a Thin Clamped Disk

In the course of analyzing failure characteristics of propellant specimens, it was indicated that one could test under essentially hydrostatic tension conditions by cementing a thin disk, or poker chip, of the material between two rigid (steel) supports and exerting tension in a direction perpendicular to the faces. Under such loading, the center of the specimen would be subjected to a three-dimensional tensile stress. The elementary analysis of the problem, assuming the disk radius is infinite such that plane strain conditions hold, leads to the result that the radial and circumferential stresses are equal and, for an isotropic homogeneous medium with Poisson ratio, ν, proportional to the applied axial stress σ_z.

$$\sigma_r = \sigma_\theta = \frac{\nu}{1-\nu}\,\sigma_z \qquad (1)$$

It may be noted that for an incompressible material not only is the stress state triaxial, but it is also hydrostatic leading to there being no shear distortion in the specimen.

Coupon tests have been employed by Gent and Lindley* in their experiments upon rubber and by Lehrer and Schwalzbart** in metals. The purpose of the following analysis is to calculate the stress distribution in a compressible thin disk of finite radius.

Gent and Lindley were concerned with displacements and their analysis employed what was equivalent to a minimum potential energy solution to predict deformations and an apparent modulus. However, for their approximation, a variational procedure was not used because the only free constant in their analysis, the amplitude of the assumed parabolic deformation or bulge, was fixed by the condition of incompressibility. While their analysis could be extended by introducing a higher order deformation shape and a provision for compressibility, it does not seem warranted at this time because our current interest is concerned with stresses.

---

* "Internal Rupture of Bonded Rubber Cylinder in Tension", Proceedings Royal Society, A. Vol. 249, p. 195, 1959.

** "Static and Fatigue Strength of Metals Subjected to Traixial Stresses", Institute of the Aeronautical Sciences, Paper No. 60-12, January 1960.

Complementary energy analysis.- The stress analysis will be carried out using the minimum complementary energy principle for a disk of thickness 2h and unit radius. The faces $z = \pm h$ are assumed to be rigidly bonded to much stiffer supporting plates. We may therefore formulate the problem, assuming circumferential symmetry, as requiring the satisfaction of the field equations of equilibrium

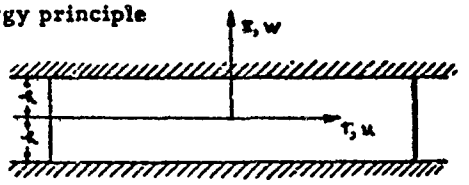

$$\frac{\partial \sigma_r}{\partial r} + \frac{\sigma_r - \sigma_\theta}{r} + \frac{\partial \tau_{rz}}{\partial z} = 0 \tag{2}$$

$$\frac{\partial \tau_{rz}}{\partial r} + \frac{\tau_{rz}}{r} + \frac{\partial \sigma_z}{\partial z} = 0 \tag{3}$$

and compatibility

$$\left(\frac{\partial^2}{\partial r^2} + \frac{1}{r}\frac{\partial}{\partial r} + \frac{\partial^2}{\partial z^2}\right)\sigma_r - \frac{2(\sigma_r - \sigma_\theta)}{r^2} + \frac{1}{1+\nu}\frac{\partial^2 \Theta}{\partial r^2} = 0 \tag{4}$$

$$\left(\frac{\partial^2}{\partial r^2} + \frac{1}{r}\frac{\partial}{\partial r} + \frac{\partial^2}{\partial z^2}\right)\sigma_\theta + \frac{2(\sigma_r - \sigma_\theta)}{r^2} + \frac{1}{1+\nu}\frac{\partial^2 \Theta}{r\partial r} = 0 \tag{5}$$

$$\left(\frac{\partial^2}{\partial r^2} + \frac{1}{r}\frac{\partial}{\partial r} + \frac{\partial^2}{\partial z^2}\right)\sigma_z + \frac{1}{1+\nu}\frac{\partial^2 \Theta}{\partial z^2} = 0 \tag{6}$$

$$\left(\frac{\partial^2}{\partial r^2} + \frac{1}{r}\frac{\partial}{\partial r} + \frac{\partial^2}{\partial z^2}\right)\tau_{rz} - \frac{\tau_r}{r^2} + \frac{1}{1+\nu}\frac{\partial^2 \Theta}{\partial r \partial z} = 0 \tag{7}$$

where $\Theta = \sigma_r + \sigma_\theta + \sigma_z$. The boundary conditions are on the faces

$$u(r, \theta, \pm h) = v(r, \theta, \pm h) \tag{8}$$

$$w(r, \theta, \pm h) = \pm w_0 \tag{9}$$

and on the unloaded circumference

$$\sigma_r(1, \theta, z) = \tau_{rz}(1, \theta, z) = 0 \tag{10}$$

The elasticity solution to this problem is a formidable one which is the reason for using an energy approach. The theorem of minimum complementary energy requires* that a proposed stress state is admissible if

a) it satisfies the stress equations of equilibrium, and

b) the boundary conditions on that part of the boundary where stresses are prescribed.

Inspection of (2)-(7), and (8)-(10) indicates by implication that the compatibility equations may not necessarily be satisfied, nor may the displacement boundary conditions (8) and (9). The theorem however guarantees that if there is some arbitrariness in the proposed stress state, it may be adjusted by minimizing the complementary energy

$$V^* = \int_{-\ell}^{\ell}\int_{0}^{2\pi}\int_{0}^{1}\left[\frac{1}{2E}\left\{\sigma_r^2+\sigma_\theta^2+\sigma_z^2\right\} - \frac{\nu}{E}\left\{\sigma_r\sigma_\theta+\sigma_\theta\sigma_z+\sigma_z\sigma_r\right\}+\frac{1}{2G}\tau_{rz}^2\right] r\,dr\,d\theta\,dz \qquad (11)$$
$$- 2\int_{0}^{2\pi}\int_{0}^{1}\sigma_z(r,\ell)\,w_o\,r\,dr\,d\theta$$

to give the best possible averaged satisfaction of the compatibility and displacement boundary conditions.

The heart of the problem lies in the initial choice of the admissible functions which is accomplished mainly by intuition and experience. Without any rationalization at this time, consider the following set which was chosen for reasonable simplicity in the subsequent algebra required.

$$\sigma_r = \frac{2\nu}{1-\nu} A\,(1-r^n)\cosh\sqrt{\frac{2\nu}{1-\nu}}\,z \qquad (12)$$

$$\sigma_\theta = \frac{2\nu}{1-\nu} A\left[1-(n+1)r^n+r^{p+1}-r^2\right]\cosh\sqrt{\frac{2\nu}{1-\nu}}\,z \qquad (13)$$

$$\sigma_z = \sigma_o + \left[1-\frac{p+1}{2}r^{p-1}\right]\left[2A\cosh\sqrt{\frac{2\nu}{1-\nu}}\,z - \sigma_o\right] \qquad (14)$$

$$\tau_{rz} = -A\left[r-r^p\right]\sqrt{\frac{2\nu}{1-\nu}}\sinh\sqrt{\frac{2\nu}{1-\nu}}\,z \qquad (15)$$

It will be found upon substitution into (2) and (3) that the equilibrium equations are satisfied, whereas insertion of $r = 1$ into (12) and (15) satisfies (10). The function set is therefore admissible, and furthermore contains a degree of arbitrariness represented by the, at present, unknown constants σ_o, A, p, and n. These latter constants will be determined by minimizing V*, e.g. $\partial V^*/\partial\sigma_o = 0$, etc.

---

* See Sokolnikoff, Mathematical Theory of Elasticity, McGraw Hill, 1956.

In passing it may be noted that the exponents n and p must exceed 0 and 1 respectively in order that infinite stresses are not introduced at the origin. Also the set has been chosen in such a way that at the origin r = z = 0,

$$\sigma_r = \sigma_\theta = \frac{\nu}{1-\nu}\sigma_z \tag{1}$$

to yield the desired limit as the disk thickness approaches zero, or, what is the same, the radius of the disk becomes infinitely large. Finally σ_0, although unknown, may be identified as the average tensile stress acting on the face to cause the deformation w_0.

For convenience, we define

$$\mu^2 = \frac{2\nu}{1-\nu} \tag{16}$$

and proceed to insert (12)-(15) into (11) to obtain the complementary energy as a function of the parameters, $V^* = V^*(A, \sigma_0, n, p)$. After the intergration and algebraic reduction, there results

$$\frac{E}{\pi}V^* = (s_1 + s_2 - 2\nu s_4)t_1 + s_3 t_2 - 2\nu s_5 t_3 + 2(1+\nu)s_6 t_4 + \sigma_0^2 h - 2E w_0 \sigma_0 + \mu\nu A \sigma_0 \left(\frac{p-1}{p+3}\right)\sinh \mu h \tag{17}$$

Where the following notation has been employed

$$s_1 = \frac{n^2}{2(n+1)(n+2)} \tag{18}$$

$$s_2 = 2(n+1)\left[\frac{n(n+6)}{4(n+2)(n+4)} - \frac{1}{n+p+3}\right] + \frac{p+15}{6(p+3)} - \frac{3(p+1)}{2(p+2)(p+5)} \tag{19}$$

$$s_3 = \frac{(p-1)^2}{2p} \tag{20}$$

$$s_4 = -\frac{n(p-1)(n+p+7)}{4(p+3)(n+p+3)(n+4)} \tag{21}$$

$$s_5 = \frac{n(p-1)}{p+n+1} \tag{22}$$

$$s_6 = \frac{(p-1)^2}{4(p+3)(p+1)} \tag{23}$$

$$t_1 = \frac{\mu^3 A^2}{2}\left[\sinh 2\mu h + 2\mu h\right] \tag{24}$$

$$t_2 = \frac{A^2}{2\mu}\left[\sinh 2\mu h + 2\mu h\right] - \frac{2\sigma_0 A}{\mu}\sinh \mu h + \frac{\sigma_0^2 h}{2} \tag{25}$$

$$t_3 = \frac{\mu A^2}{2}\left[\sinh 2\mu h + 2\mu h\right] - \sigma_0 A \mu \sinh \mu h \qquad (26)$$

$$t_4 = \frac{\mu A^2}{2}\left[\sinh 2\mu h + 2\mu h\right] \qquad (27)$$

The minimizing condition $\partial V^*/\partial A = 0$ leads to

$$A = \frac{\left[2S_3 - 2\nu S_5 \mu^2 - \nu \mu^2 \frac{p-1}{p+3}\right]\sigma_0 \sinh \mu h}{\left[(S_1+S_2-2\nu S_4)\mu^4 + S_3 - 2\nu\mu^2 S_5 + 2(1+\nu)\mu^2 S_6\right]\left[\sinh 2\mu h + 2\mu h\right] - 8(1+\nu)\mu^3 h S_6} \qquad (28)$$

while $\partial V^*/\partial \sigma = 0$ in conjunction with (28) gives

$$\sigma_0 = \frac{\frac{E w_0}{h}}{1 + \frac{S_8}{2} - \frac{\left[2S_3 - (2S_5 + \frac{p-1}{p+3})\nu\mu^2\right]^2 \sinh^2 \mu h}{2\mu h\left[\{(S_1+S_2-2\nu S_4)\mu^4 + S_3 - 2\nu\mu^2 S_5 + 2(1+\nu)\mu^2 S_6\}\{\sinh 2\mu h + 2\mu h\} - 8\mu^3 h(1+\nu)S_6\right]}} \qquad (29)$$

σ_0 can then be inserted into (28) to determine $A = A(w_0)$. With A and σ_0 known as functions of (n, p, w_0), they can be inserted into (17) to find

$$V^* = V^*(n, p; w_0) \qquad (30)$$

In principle, therefore, one could add the additional minimizing conditions $\partial V^*/\partial n = 0$ and $\partial V^*/\partial p = 0$ and find finally n and p as functions of the applied deformation w_0 and of course the thickness parameter h. Hence, all the constants A, σ_0, n, and p are known in terms of w_0 and h can be placed back into (12)-(15) to give the finall approximate stress distribution.

From the algebraic standpoint, however, it proves simpler to try various values of n_i and p_j in (30) and compute the corresponding value of V*. There will be some pairs that will give the algebraic minimum by this trial and error procedure which is equivalent to the minimization condition.

At this stage in the analysis, it is worth re-examining the necessity for finding this stress distribution with due consideration to the computational work involved. At least one solution is now available, but it may be worth investigating other function sets to see if they may be computationally simpler. Furthermore, it is recommended that any computations be first carried out for an incompressible medium, $\nu = \frac{1}{2}$, $\nu\mu^2 = 1$. If additional work on this solution or variations of it are thought warranted, it will be reported at a later time. The only qualitative statement which can be made at this time is that the true values of n, p will probably be fairly large corresponding to a stress distribution fairly close to (1) over a large part of the central portion of the disk. One major limitation of the technique is that both n and p will depend upon the width/thickness ratio of the sample, so that a parameter study of the latter ratio would entail an iteration of the computation of n and p.

APPENDIX II

Crack Propagation in Viscoelastic Media

In the body of the report, the stress distribution near a small crack in a large thin sheet subjected to a uniform tensile stress was discussed. Further, it was pointed out that the viscoelastic and elastic stress distributions are the same for this loading, thus leading to the possibility of computing the viscoelastic strains and displacements from the basic elastic information. The purpose of the following analysis is to use this information to predict crack propagation characteristics in a viscoelastic medium.

From the basic solution* the biaxial stress distribution in the plate strip subjected to a tension σ_o is

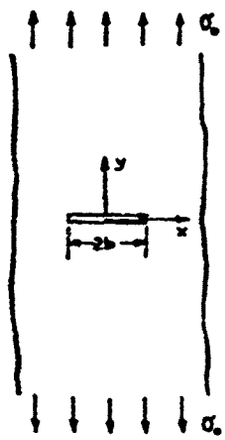

FIGURE 2

$$\sigma_x(x,0) = \frac{\sigma_o b^2}{\sqrt{x^2-b^2}\left[x+\sqrt{x^2-b^2}\right]} \quad ; \quad x>b \qquad (1\text{-a})$$

$$= \sigma_o\left[\sqrt{\frac{1}{2\frac{\epsilon}{b}}} - 1 + O\left\{\left(\frac{\epsilon}{b}\right)^{\frac{1}{2}}\right\} + \cdots\right] \quad ; \quad x=b+\epsilon \qquad (1\text{-b})$$

$$\sigma_y(x,0) = \sigma_o\left[1+\frac{b^2}{\sqrt{x^2-b^2}\left[x+\sqrt{x^2-b^2}\right]}\right] \quad ; \quad x>b \qquad (2\text{-a})$$

$$= \sigma_o\left[\sqrt{\frac{1}{2\frac{\epsilon}{b}}} + O\left\{\left(\frac{\epsilon}{b}\right)^{\frac{1}{2}}\right\} + \cdots\right] \quad ; \quad x=b+\epsilon \qquad (2\text{-b})$$

where it is clear that the stress becomes infinite as the point of the crack is approached. In order to circumvent the necessity for conducting a large strain, elastoplastic solution, it will arbitrarily be assumed that the stress may build up to a specified value at a distance δ from the crack tip and remain constant throughout the interval $0 \leq x-b \leq \delta$ until an ultimate one-dimensional strain ϵ^* is reached.

---

* D. D. Ang and M. L. Williams: Combined Stresses in an Orthotropic Plate Having a Finite Crack. GALCIT SM 60-1, California Institute of Technology, January 1960 (rev. September 1960).

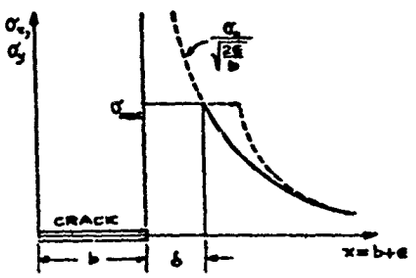

FIGURE b

It should be observed that the elastic solution is no longer correct, because the specimen, by the equations of equilibrium, is presumed to be absorbing the stress indicated by the dashed line. Thus the load represented by integrating the stress between x = b and x = b + δ is not accounted for when the truncation is made. Therefore the actual stress distribution would be more like the dotted line, with the additional area accomplishing the necessary force balance. On the other hand, because this (dotted) distribution cannot easily be calculated, and because it is desirable to still have the force balance, the analysis will be carried out using the modified truncated stress distribution shown in Figure c on which areas A_1 and A_2 are equal. If the existence of such quantities as ϵ^* and δ can be established by experiment, then the following analysis could lead to useful results.

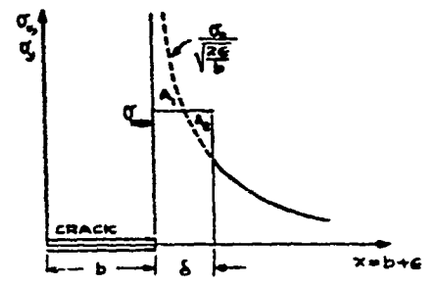

FIGURE c

Visualize then, the conditions along the line of crack prolongation, and assume that the internal forces along the shear free line are carried, for simplicity, by a series of discrete Voigt elements averaged over the characteristic length . The mechanism postulated is that each element will strain as a result of stresses (σ_x and σ_y) which are constant over the length δ assigned to each element as shown in Figure d. The values of these stresses are determined from equations (1) and (2) and the equilibrium condition discussed earlier. Namely we assume that for a crack width 2b, the stresses acting on element (n) are the average values:

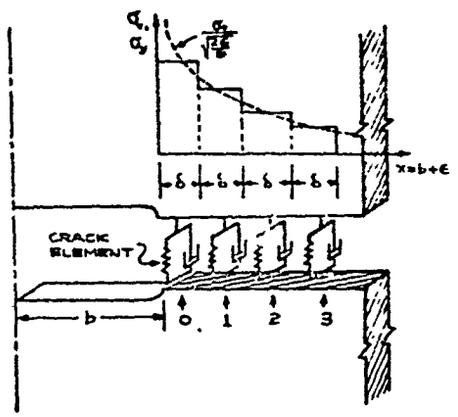

FIGURE d

$$\frac{\sigma_{nx}}{\sigma_o}=\frac{1}{\delta}\int_{b+n\delta}^{b+(n+1)\delta}\frac{\sigma(x)}{\sigma_o}dx = -\frac{b^2}{\delta}\int_{b+n\delta}^{b+(n+1)\delta}\frac{dx}{\sqrt{x^2-b^2}\left[x+\sqrt{x^2-b^2}\right]}$$

$$\simeq\frac{2}{\sqrt{2\delta/b}}\left[(n+1)^{\frac{1}{2}}-n^{\frac{1}{2}}\right]-1+\frac{1}{4}\sqrt{\frac{2\delta}{b}}\left[(n+1)^{\frac{3}{2}}-n^{\frac{3}{2}}\right]+\frac{2\delta/b}{2}\left[(n+1)^2-n^2\right]+\cdots \quad (3\text{-a})$$

$$\frac{\sigma_{ny}}{\sigma_o}=\frac{1}{\delta}\int_{b+n\delta}^{b+(n+1)\delta}\frac{\sigma(x)}{\sigma_o}dx = \frac{1}{\delta}\int_{b+n\delta}^{b+(n+1)\delta}\left[1+\frac{b^2}{\sqrt{x^2-b^2}\left[x+\sqrt{x^2-b^2}\right]}\right]dx$$

$$=\frac{2}{\sqrt{2\delta/b}}\left[(n+1)^{\frac{1}{2}}-n^{\frac{1}{2}}\right]+\frac{1}{4}\sqrt{\frac{2\delta}{b}}\left[(n+1)^{\frac{3}{2}}-n^{\frac{3}{2}}\right]+\frac{2\delta/b}{2}\left[(n+1)^2-n^2\right]+\cdots \quad (3\text{-b})$$

After the strain in the first element reaches ϵ^*, it will break and the stress distribution will shift by one δ width; i.e. the stress which had been acting on the element n is now acting on element $n+1$, where the effective crack length to be used is $2(b+\delta)$. After m translations, or after element $(m-1)$ breaks, one has

$$\frac{\sigma_{ny}^{(m)}}{\sigma_o}=\frac{2}{\sqrt{2\delta/(b+m\delta)}}\left[(n-m+1)^{\frac{1}{2}}-(n-m)^{\frac{1}{2}}\right]+\frac{1}{4}\sqrt{\frac{2\delta}{b+m\delta}}\left[(n-m+1)^{\frac{3}{2}}-(n-m)^{\frac{3}{2}}\right]+\cdots \quad (4\text{-a})$$

$$=\frac{\sigma_{nx}^{(m)}}{\sigma_o}+1$$

To reiterate, $\sigma_{ny}^{(m)}$ is the average stress acting on element (n) before element (m) breaks, but after element (m-1) has parted. Thus, the stress at the crack tip is given approximately by

$$\sigma_{my}^{(m)}\cong\frac{2\sigma_o}{\sqrt{\frac{2\delta}{b+m\delta}}}\cong\sigma_{mx}^{(m)}+\sigma_o \quad (4\text{-b})$$

It is clear that if δ is assumed to be a fixed characteristic dimension, the stress acting on the element at the crack tip is not limited, but increases with crack length. However, in the initial stages of crack growth ($m\delta \ll b$) the stress is practically constant as seen from equation (4-b).

Since we now have the two-dimensional stresses as a function of crack position, the time dependent strain in each element can be found from the plane stress, stress-strain equation. For an elastic material, we have

$$\epsilon_y=\frac{1}{E}(\sigma_y-\nu\sigma_x) \quad (5)$$

For simplicity, we will assume an incompressible medium ($\nu = \frac{1}{2}$). The viscoelastic strain is obtained in the usual manner by replacing E by its equivalent differential operator, which for a Voigt model is*

$$E \rightarrow E_v\left(\tau\frac{d}{dt}+1\right) \tag{6}$$

where

E_v = modulus of the spring in parallel with a dashpot with viscosity η

$\tau = \eta/E_v$ = retardation time of model

Insertion of (6) into (5) yields the viscoelastic stress-strain equation which applies to each element

$$\begin{aligned}\tau\frac{d\epsilon_y}{dt}+\epsilon_y &= \frac{1}{E_v}\left[\sigma_y-\tfrac{1}{2}\sigma_o\right]\\ &= \frac{1}{2E_v}\left[\sigma_y+\sigma_o\right]\end{aligned} \tag{7}$$

In terms of the notation used in equation (4), equation (7) becomes

$$\tau\frac{d\epsilon_n^{(m)}}{dt}+\epsilon_n^{(m)} = \frac{\sigma_o}{2E_v}\left[\frac{\sigma_{ny}^{(m)}}{\sigma_o}+1\right] \tag{8}$$

where $\epsilon_n^{(m)}$ is the strain in element (n) before element (m) breaks, but after element (m-1) has parted. If we denote the time at which element (m) breaks by t_m, then equation (8) applies to the time interval $t_{m-1} \leq t \leq t_m$. In this time interval the right hand side of (8) is constant so that we can integrate it for the strain:

$$\epsilon_n^{(m)}(t) = \frac{\sigma_o}{2E_v}\left[\frac{\sigma_{ny}^{(m)}}{\sigma_o}+1\right]+\left[\epsilon_n^{(m-1)b}-\frac{\sigma_o}{2E_v}\left(\frac{\sigma_{ny}^{(m)}}{\sigma_o}+1\right)\right]e^{-\frac{t-t_{m-1}}{\tau}} \qquad t_{m-1}\leq t\leq t_m \tag{9}$$

where $\epsilon_n^{(m-1)b}$ is defined as the strain existing in element (n) at the time element (m-1) breaks, which is t_{m-1}. If we set $t = t_{m-1}$ in equation (9), the initial condition

$$\epsilon_n^{(m)}(t_{m-1}) = \epsilon_n^{(m-1)b}$$

is satisfied. Letting $t \rightarrow \infty$, we have

$$\begin{aligned}\epsilon_n^{(m)}(\infty) \equiv \epsilon_{ne}^{(m)} = \frac{\sigma_o}{2E_v}\left[\frac{\sigma_{ny}^{(m)}}{\sigma_o}+1\right] = \frac{\sigma_o}{E_v}\Bigg[&\frac{1}{\sqrt{\frac{2\delta}{b+m\delta}}}\left\{(n-m+1)^{\frac{1}{2}}-(n-m)^{\frac{1}{2}}\right\}\\ &+\frac{1}{2}+\frac{1}{8}\sqrt{\frac{2\delta}{b+m\delta}}\left\{(n-m+1)^{\frac{3}{2}}-(n-m)^{\frac{3}{2}}\right\}+\cdots\Bigg]\end{aligned} \tag{10}$$

---

* See the comments in the text regarding the use of an approximate compliance representation (4. 4. 33) for greater generality, but with increased algebraic complexity.

which is the long-time or equilibrium strain that would result if element (m) did not break. It is seen from equation (10) that this is a known value if the crack position is given. Therefore as a matter of convenience we shall write (9) as

$$\epsilon_n^{(m)} = \epsilon_{ne}^{(m)} + \left[\epsilon_n^{(m-1)b} - \epsilon_{ne}^{(m)}\right] e^{-\frac{t-t_{m-1}}{\tau}} \qquad t_{m-1} \le t \le t_m \tag{11-a}$$

and the strain at the time when element (m) breaks

$$\epsilon_n^{(m)b} = \epsilon_{ne}^{(m)} + \left[\epsilon_n^{(m-1)b} - \epsilon_{ne}^{(m)}\right] e^{-\frac{t_m-t_{m-1}}{\tau}} \tag{11-b}$$

This expression can now be used to calculate the time at which each element breaks and hence will give the crack velocity as a function of time.

Consider first the strain in element zero for $0 \le t \le t_0$, so that $n = m = 0$ and

$$\epsilon_o^{(o)} = \epsilon_{oe}^{(o)} + \left[\epsilon_o^{(-1)b} - \epsilon_{oe}^{(o)}\right] e^{-\frac{t-t_{-1}}{\tau}}$$

in which we must define $t_{-1} = 0$, $\epsilon_o^{(-1)b} = 0$ to satisfy the initial condition that the material is unstrained at $t = 0$. Hence,

$$\epsilon_o^{(o)} = \epsilon_{oe}^{(o)}\left[1 - e^{-\frac{t}{\tau}}\right]$$

Element (0) breaks at $t = t_0$ when $\epsilon_o^{(0)}(t_0) = \epsilon_o^{(0)b} = \epsilon^*$,

$$\epsilon^* = \epsilon_o^{(o)b} = \epsilon_{oe}^{(o)}\left[1 - e^{-\frac{t_o}{\tau}}\right] \tag{12}$$

Solving for t_o,

$$\frac{t_o}{\tau} = -\ln\left[1 - \frac{\epsilon^*}{\epsilon_{oe}^{(o)}}\right] \tag{13}$$

which is the time that elapses before the crack starts to run. From equation (10)

$$\epsilon_{oe}^{(o)} = \frac{\sigma_o}{2E_v}\left[\frac{\sigma_{oy}^{(o)}}{\sigma_o} + 1\right]$$

$$= \frac{\sigma_o}{E_v}\left[\frac{1}{\sqrt{2\delta/b}} + \frac{1}{2} + \frac{1}{8}\sqrt{\frac{2\delta}{b}} + \cdots\right]$$

assuming $\left(\frac{\delta}{b}\right) \ll 1$

$$\frac{t_o}{\tau} \approx -\ln\left[1 - \frac{\epsilon^*\sqrt{\frac{2\delta}{b}}}{\sigma_o/E_v}\right] \tag{14}$$

Equation (11) gives the strain in the next element at $t = t_1$ as

$$\epsilon_1^{(n)b} = \epsilon_{1e}^{(n)} + \left[\epsilon_1^{(\omega)b} - \epsilon_{1e}^{(n)}\right] e^{-\frac{t_1 - t_2}{\tau}} = \epsilon^* \qquad (15)$$

In order to find t_1, $\epsilon_1^{(0)b}$ must be determined from (11-b) and (12)

$$\epsilon_1^{(\omega)b} = \epsilon_{1e}^{(\omega)}\left[1 - e^{-\frac{t_2}{\tau}}\right] = \frac{\epsilon_{1e}^{(\omega)}}{\epsilon_{oe}^{(\omega)}}\epsilon^*$$

Inserting this expression in (15) and solving for t_1,

$$\frac{t_1}{\tau} = \frac{t_2}{\tau} - \ln\left[\frac{\epsilon^* - \epsilon_{1e}^{(n)}}{(\epsilon_{1e}^{(n)}/\epsilon_{oe}^{(\omega)})\epsilon^* - \epsilon_{1e}^{(n)}}\right] = \frac{t_2}{\tau} + \ln\left[1 + \frac{\epsilon^*\left\{1 - (\epsilon_{1e}^{(\omega)}/\epsilon_{oe}^{(\omega)})\right\}}{\epsilon_{1e}^{(n)} - \epsilon^*}\right] \qquad (16)$$

It is observed that all of the strains appearing are equilibrium values and are thus known from equation (10). By assuming that the strain ϵ^* at which the element breaks is much smaller than the equilibrium strain $\epsilon_{1e}^{(1)}$, or equivalently that the retardation time τ is much larger than the time interval $t_1 - t_o$, equation (16) simplifies to

$$\frac{t_1}{\tau} \cong \frac{t_o}{\tau} + \frac{\epsilon^*}{\epsilon_{1e}^{(n)}}\left[1 - \frac{\epsilon_{1e}^{(\omega)}}{\epsilon_{oe}^{(\omega)}}\right]$$

Using (10) and assuming $\frac{\delta}{b} \ll 1$, it is found that

$$\frac{t_1}{\tau} = \frac{t_o}{\tau} + \frac{\epsilon^*\sqrt{2\delta/b}\,(2-\sqrt{2})}{(\sigma_o/E_v)} \qquad (17)$$

The initial velocity of crack propagation is given by

$$v_i = \frac{\delta}{t_1 - t_o} = \frac{\delta/\tau}{(t_1 - t_o)/\tau}$$

and from (17) is approximately

$$v_i \cong \frac{(\sigma_o/E_v)\sqrt{b\delta}}{\tau\epsilon^* 2\,(\sqrt{2}-1)} \qquad (18)$$

As a rough means of estimating δ, consider McCullough's preliminary data* shown in the figure in the region of constant stress, from which $V \cong 2 \times 10^{-3}$ in/sec, $\sigma_o = 20$ psi, $b = 0.2$ inches. Using typical room temperature properties gives $\delta \cong 10^{-3}$ inches, which does not seem to be an unreasonable magnitude and may be thought of as a characteristic strand diameter. Note, as hypothesized $\delta/b \ll 1$.

---

* J. McCullough: Studies on Velocity of Crack Propagation. Internal Report to Chemistry Department, Thiokol Chemical Corporation, Redstone Division, Huntsville, Alabama, September 1959.

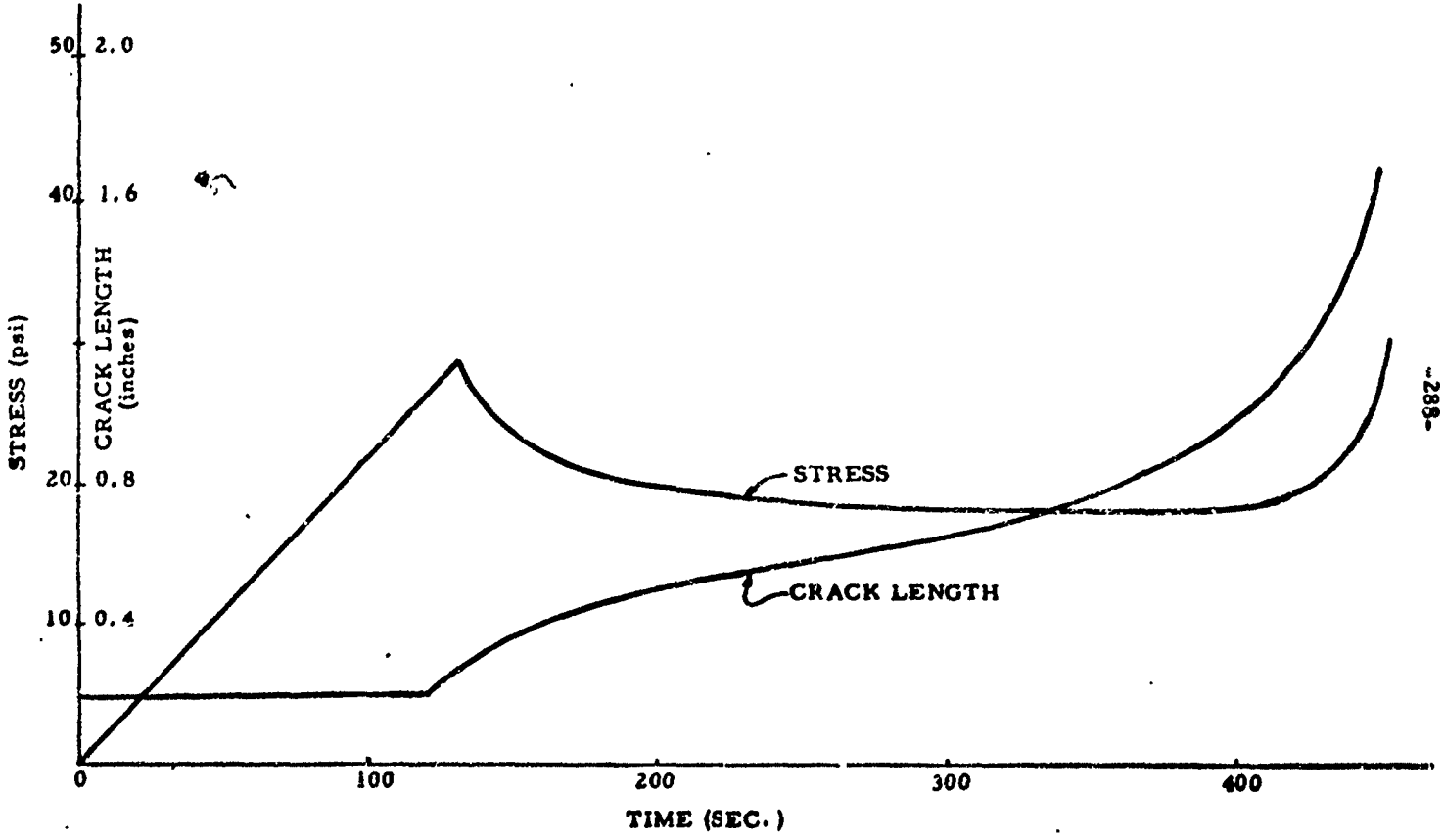

Appendix II - Typical data for crack growth in simulated propellant material.

Calculation of crack tip velocity as a function of tip location. -

With these results appearing reasonable, it is appropriate to extend the analysis and obtain an expression for crack tip velocity as a function of crack growth. To do this, the expression (11-b) for $\epsilon_n^{(m)b}$ must first be expanded so that all of the strains which appear on the right hand side are the known equilibrium values. It is seen from (11-b) that $\epsilon_n^{(m-1)b}$ must be replaced by a function of equilibrium strains. If we write

$$\epsilon_n^{(m-1)b} = \epsilon_{ne}^{(m-1)} + [\epsilon_n^{(m-2)b} - \epsilon_{ne}^{(m-1)}] e^{-\frac{t_{m-1}-t_{m-2}}{\tau}}$$

it is seen that $\epsilon_n^{(m-1)b}$ is in terms of equilibrium strains and $\epsilon_n^{(m-2)b}$. Continuing this process until the only non-equilibrium strain in the expression for $\epsilon_n^{(m-1)b}$ is $\epsilon_n^{-1b} \equiv 0$, we obtain the desired expression for $\epsilon_n^{(m-1)b}$. Substitution of this result into (11-b) leads to the representation

$$\epsilon_n^{(m)b} = \epsilon_{ne}^{(m)} + \sum_{j=0}^{m} [\epsilon_{ne}^{(j-1)} - \epsilon_{ne}^{(j)}] e^{-\frac{t_m - t_{j-1}}{\tau}} \qquad (19)$$

where, as before, we have defined $\epsilon_{ne}^{-1} = t_{-1} = 0$. Noting that $\epsilon_m^{(m)b}$ is the strain in element (m) just when element (m) breaks, and is therefore ϵ^*,

$$\epsilon_m^{(m)b} = \epsilon^* = \epsilon_{me}^{(m)} + \sum_{j=0}^{m} [\epsilon_{me}^{(j-1)} - \epsilon_{me}^{(j)}] e^{-\frac{t_m - t_{j-1}}{\tau}} \qquad (20)$$

Since all of the strains in this equation are known, as given by (10), equation (20) can be used to solve explicitly for crack tip velocity

$$V_m = \frac{\delta}{t_m - t_{m-1}} = \frac{\delta/\tau}{(t_m - t_{m-1})/\tau}$$

in which V_m is the velocity when the tip is at element (m). It will be convenient to rewrite (20) in the following form

$$\epsilon^* = \sum_{j=0}^{m} \epsilon_{me}^{(j)} \alpha_j e^{-\frac{t_m - t_j}{\tau}} \qquad m = 0, 1, 2, \cdots \qquad (21)$$

where we have defined

$$\alpha_m \equiv 1 - e^{-\frac{t_m - t_{m-1}}{\tau}}$$

To illustrate the significance of (21), it is expanded for m = 0, 1, 2:

$$m=0: \quad \epsilon^* = \epsilon_{oo}^{(o)}\left[1-e^{-\frac{\tau_o}{\tau}}\right] \tag{22-a}$$

$$m=1: \quad \epsilon^* = \epsilon_{1o}^{(o)}\left[1-e^{-\frac{\tau_o}{\tau}}\right]e^{-\frac{\tau_1-\tau_o}{\tau}} + \epsilon_{1o}^{(1)}\left[1-e^{-\frac{\tau_1-\tau_o}{\tau}}\right] \tag{22-b}$$

$$m=2: \quad \epsilon^* = \epsilon_{2o}^{(o)}\left[1-e^{-\frac{\tau_o}{\tau}}\right]e^{-\frac{\tau_2-\tau_o}{\tau}} + \epsilon_{2o}^{(1)}\left[1-e^{-\frac{\tau_1-\tau_o}{\tau}}\right]e^{-\frac{\tau_2-\tau_1}{\tau}} + \epsilon_{2o}^{(2)}\left[1-e^{-\frac{\tau_2-\tau_1}{\tau}}\right] \tag{22-c}$$

It is clear that if $(\tau_m-\tau_o)\ll\tau$, the exponential terms which multiply α_m can be taken as unity so that (21) becomes

$$\epsilon^* \cong \sum_{j=o}^{m} \epsilon_{mo}^{(j)}\alpha_j \tag{23}$$

Utilizing (22-a) for ϵ^*, we can rewrite (23) as

$$\frac{w_m}{w_o} = 1 - \sum_{j=o}^{m-1} \frac{\epsilon_{mo}^{(j)}}{\epsilon_{jo}^{(j)}}\frac{w_j}{w_o} \tag{24}$$

where it was convenient to define

$$\frac{w_m}{w_o} \equiv \frac{\epsilon_{mo}^{(m)}}{\epsilon_{oo}^{(m)}}\frac{\alpha_m}{\alpha_o}$$

If it is further assumed that only the first term in the equilibrium strain (10) need be considered (i.e. that the strain resulting from the leading term in the stresses (1-b) and (2-b) provides the main contribution to failure) then from (10)

$$\epsilon_{mo}^{(j)} \cong \frac{\sigma_o}{E\sqrt{2b}}\left[(m-j+1)^{\frac{1}{2}}-(m-j)^{\frac{1}{2}}\right] \tag{25-a}$$

and

$$\epsilon_{mo}^{(m)} \cong \frac{\sigma_o}{E\sqrt{2b}} \tag{25-b}$$

Substituting (25) into (24) gives the recurrence expression for $\frac{w_m}{w_o}$:

$$\frac{w_m}{w_o} = 1 - \sum_{j=o}^{m-1}\left[(m-j+1)^{\frac{1}{2}}-(m-j)^{\frac{1}{2}}\right]\frac{w_j}{w_o} \tag{26}$$

Calculations give, for example

$$\frac{w_o}{w_m} = 1,\ 1.71,\ 2.27,\ 2.75,\ \cdots \quad \text{for } m=0,1,2,3,\cdots$$

It can be deduced that

$$\frac{w_m}{w_o} \cong \frac{2}{\pi\sqrt{m}} \qquad \text{for } m \geq 4 \tag{27}$$

Under the assumption that $\frac{t_m}{\tau} \ll 1$,

$$\alpha_m \cong \frac{t_m - t_{m-1}}{\tau}$$

so that

$$\frac{w_m}{w_0} = \frac{\epsilon_{rr}^{(m)} \alpha_m}{\epsilon_{rr}^{(0)} \alpha_0} \cong \frac{\sigma_0 \sqrt{b}\sqrt{1+m\delta/b}}{E_v \epsilon^* \sqrt{2}\sqrt{\delta}} \frac{t_m - t_{m-1}}{\tau}$$

$$= \frac{\sigma_0 \sqrt{1+m\delta/b}}{E_v \epsilon^* \sqrt{2}} \frac{\sqrt{\delta b}}{\tau V_m} \qquad (28)$$

Solving for V_m and using (27) we find

$$V_m \cong \frac{\pi}{2\sqrt{2}} \frac{\sigma_0/E_v}{\epsilon^*} \frac{b}{\tau} \sqrt{\frac{m\delta}{b}\left(1+\frac{m\delta}{b}\right)} \quad ; \qquad m \geq 4 \qquad (29)$$

showing that the velocity increases without bound as the crack grows which is impossible because free running cracks are known to be limited by speeds of the order of half the shear wave speed. However such a result is not surprising since inertia has not been included in the formulation. Nevertheless, (29) may provide a reasonable approximation to the crack tip speed if it is sufficiently less than the shear wave speed.

Passing to the continuous form by letting $m\delta = s$, in which s is the distance the crack tip has traveled, we have

$$V = \frac{ds}{dt} \cong \frac{\pi}{2\sqrt{2}} \frac{\sigma_0/E_v}{\epsilon^*} \frac{b}{\tau} \sqrt{\frac{s}{b}\left(1+\frac{s}{b}\right)} \quad ; \qquad s \geq 4\delta \qquad (30\text{-a})$$

which shows

$$V \propto \sqrt{\frac{s}{b}} \quad ; \qquad \frac{4\delta}{b} \leq \frac{s}{b} \ll 1 \qquad (30\text{-b})$$

$$V \propto \frac{s}{b} \quad ; \qquad \frac{s}{b} \gg 1 \qquad (30\text{-c})$$

The initial behavior indicated in (30-b) results from the increasing amount of strain which accumulates in the elements ahead of the crack as it propagates. This increase in velocity when $s \ll b$ occurs while the stress at the crack tip remains essentially constant as seen from equation (4-b). However, the fact that the stress is proportional to $\sqrt{s}$ for $s \gg 1$ accounts for the more rapid increase in velocity shown by (30-c)

The time dependence of crack growth can be determined from (30-a) by integration:

$$\sqrt{1+\frac{s}{b}}+\sqrt{\frac{s}{b}} \cong e^{\frac{\pi}{4\sqrt{2}}\frac{\sigma_o/E_v}{\epsilon^*}\frac{t}{\tau}} \qquad (31\text{-a})$$

so that

$$\frac{s}{b} \cong \left[\frac{\pi}{4\sqrt{2}}\frac{\sigma_o/E_v}{\epsilon^*}\frac{t}{\tau}\right]^2 \quad ; \quad \frac{4\delta}{b} \leq \frac{s}{b} \leq 1 \qquad (31\text{-b})$$

$$\frac{s}{b} \cong \frac{1}{4}e^{\frac{\pi}{2\sqrt{2}}\frac{\sigma_o/E_v}{\epsilon^*}\frac{t}{\tau}} \quad ; \quad \frac{s}{b} \gg 1 \qquad (31\text{-c})$$

Remarks.

The proposed phenomenological model is by no means unique, with it being possible to include a more complicated material representation instead of the incompressible Voigt model used here. Also it should be possible to introduce a more sophisticated fracture criterion if necessary, based not upon maximum strain, but perhaps octahedral strain as a function of strain rate and cumulative damage. Further, for ease in manipulation, the discrete element formulation might be replaced by a continuous material formulation. Finally, a basic investigation might be conducted to ascertain the physical significance of the characteristic strand diameter, δ, incorporated in the analysis.

APPENDIX III

Large Plane Strain Analysis for Distortion Energy in a Hollow Tube

The strain transformation in cylindrical coordinates is given by

$$\bar{r} = \bar{r}(r) \; ; \quad \bar{\theta} = \theta \; ; \quad \bar{z} = z \tag{1}$$

Here the superscript bar indicates the deformed or Eulerian coordinate. The Jacobian of the transformation is given by

$$\begin{vmatrix} d\bar{r} \\ \bar{r}d\bar{\theta} \\ d\bar{z} \end{vmatrix} = \begin{vmatrix} \frac{d\bar{r}}{dr} & 0 & 0 \\ 0 & \frac{\bar{r}}{r} & 0 \\ 0 & 0 & 1 \end{vmatrix} \begin{vmatrix} dr \\ rd\theta \\ dz \end{vmatrix} \tag{2}$$

Incompressibility demands that

$$\frac{d\bar{r}}{dr} \times \frac{\bar{r}}{r} \times 1 = 1 \tag{3}$$

$$\bar{r}^2 = r^2 + \bar{a}^2 - a^2 = \lambda^2 r^2 \tag{4}$$

$$\lambda^2 = 1 + \frac{\bar{a}^2 - a^2}{r^2} \tag{5}$$

$$\frac{d\bar{r}}{dr} = \frac{1}{\lambda}$$

Substitution into (2) yields

$$\frac{\bar{\sigma}_r}{\mu} = \frac{1}{\lambda^2} + \bar{k} \tag{6}$$

$$\frac{\bar{\sigma}_\theta}{\mu} = \lambda^2 + \bar{k} \tag{7}$$

The equilibrium equation is cast in Eulerian coordinates

$$\frac{\bar{\sigma}_\theta - \bar{\sigma}_r}{\bar{r}} = \frac{d\bar{\sigma}_r}{d\bar{r}} \tag{8}$$

Substituting (6) and (7) yields after integration

$$\bar{k} = c - \ln\lambda - \frac{1}{2\lambda^2} \tag{9}$$

$$\frac{\bar{\sigma}_r}{\mu} = c - \ln\lambda + \frac{1}{2\lambda^2} \tag{10}$$

At the inner surface, radius a

$$\lambda_a = \frac{\bar{a}}{a} \tag{11}$$

$$-\frac{p}{\mu} = c - \ln\lambda_a + \frac{1}{2\lambda_a^2} \tag{12}$$

At the propellant-case interface, the radial stress (r=b) is taken to be $-p_i$

$$-\frac{p_i}{\mu} = c - \ln\lambda_b + \frac{1}{2\lambda_b^2} \tag{13}$$

$$\lambda_b^2 = 1 + m(\lambda_a^2 - 1) \tag{14}$$

where again

$$m = \frac{a^2}{b^2} \tag{15}$$

$$\frac{p - p_i}{\mu} = \frac{1}{2\lambda_b^2} - \frac{1}{2\lambda_a^2} + \ln\frac{\lambda_a}{\lambda_b} \tag{16}$$

The strain energy is easily seen to be a maximum at a, so that

$$W_a = \frac{\mu}{2}(I_{1a} - 3) = \frac{\mu}{2}\left(\lambda_a^2 + \frac{1}{\lambda_a^2} - 2\right) \tag{17}$$

The interfacial pressure is determined by matching with the case. We have, using a prime to indicate properties in the metal

$$\sigma_r = A - \frac{B}{r^2} \tag{18}$$

$$\frac{u}{r} = A\frac{1-2\nu'}{2\mu'} + \frac{1}{r^2}\frac{B}{2\mu'} \tag{19}$$

At r = b, we have

$$-P_i = A - \frac{B}{b^2} \tag{20}$$

$$\frac{\lambda_b^2 - 1}{2} = \left(\frac{u}{r}\right)_b = \frac{A(1-2\nu')}{2\mu'} + \frac{B}{2\mu' b^2} \tag{21}$$

Note that we equate $(u/r)_b$ to the finite (Murnaghan strain) to be consistent with large strain theory, even though we use small strain theory in the case. At the outer surface of the case, the pressure is assumed to be zero, so that

$$B = Ac^2 \tag{22}$$

Solution is expedited by defining, as before

$$\phi = \frac{\mu}{\mu'}\left(1 + \frac{2-2\nu'}{\delta}\right) \tag{23}$$

so that

$$\lambda_b^2 - 1 = \frac{P_i}{\mu}\phi \tag{24}$$

Substitution into (6) yields

$$\frac{p}{\mu} = \frac{1}{2\lambda_b^2} - \frac{1}{2\lambda_a^2} + \ell n \frac{\lambda_a}{\lambda_b} + \frac{\lambda_b^2 - 1}{\phi} \tag{25}$$

and with (14), there results

$$\frac{2p}{\mu} = \frac{1}{1+m(\lambda_a^2-1)} - \frac{1}{\lambda_a^2} + \ell n \frac{\lambda_a^2}{1+m(\lambda_a^2-1)} + \frac{2}{\phi} m(\lambda_a^2 - 1) \tag{26}$$

Since λ_a will be approximately 4 near the yield, (6) is easily approximated by

$$\frac{p}{\mu} = \frac{m}{\phi}(\lambda_a^2 - 1) \qquad \text{using } m = a/b \tag{27}$$

and the strain energy becomes

$$W = \frac{p^2\phi^2}{2mp\phi + 2\mu m^2} \tag{28}$$

This expression is to be compared with (4.5.48) for $\nu' = \frac{1}{2}$

$$W_{max.} = \frac{p^2\phi^2}{2\mu\left[\phi + m(1-\phi)\right]^2} \approx \frac{p^2\phi^2}{2\mu m^2} \tag{29}$$

for small ϕ. Thus, in small strain theory, the energy increases quadratically with pressure, whereas the dependence becomes linear in the large strain theory, i.e.

$$W \approx \frac{p\phi}{2m} \tag{30}$$